NASA CR-
ERIM 119300-10-F

NASA

Final Report

INVESTIGATION OF LANDSAT FOLLOW-ON THEMATIC MAPPER SPATIAL, RADIOMETRIC AND SPECTRAL RESOLUTION

JAMES P. MORGENSTERN, RICHARD F. NALEPKA,
EDWARD R. KENT and JON D. ERICKSON
Infrared and Optics Division

JUNE 1976

(E77-10057) INVESTIGATION OF LANDSAT FOLLOW-ON THEMATIC MAPPER SPATIAL, RADIOMETRIC AND SPECTRAL RESOLUTION Final Report, Nov. 1975 - Apr. 1976 (Environmental Research Inst. of Michigan) 228 p HC A11/MF G3/43

N77-14556
MF A01
Unclas
00057

Prepared for

NATIONAL AERONAUTICS AND SPACE ADMINISTRATION

Johnson Space Center
Houston, Texas 77058
Contract No. NAS9-14819

ENVIRONMENTAL
RESEARCH INSTITUTE OF MICHIGAN
FORMERLY WILLOW RUN LABORATORIES, THE UNIVERSITY OF MICHIGAN
BOX 618 • ANN ARBOR • MICHIGAN 48107

NOTICE

Sponsorship. The work reported herein was conducted by the Environmental Research Institute of Michigan under Contract NAS9-14819 for the National Aeronautics and Space Administration, Johnson Space Center, Houston, Texas 77058. Mr. M. Jay Harnage was Project Manager. Contracts and grants to the Institute for the support of sponsored research are administered through the Office of Contracts Administration.

Other Final Reports. This is one of two final reports on this contract.

Disclaimers. This report was prepared as an account of Government-sponsored work. Neither the United States, nor the National Aeronautics and Space Administration (NASA), nor any person acting on behalf of NASA:

(A) Makes any warranty expressed or implied, with respect to the accuracy, completeness, or usefulness of the information contained in this report, or that the use of any information, apparatus, method, or process disclosed in this report may not infringe privately owned rights; or

(B) Assumes any liabilities with respect to the use of, or for damages resulting from the use of any information, apparatus, method, or process disclosed in this report.

As used above, "person acting on behalf of NASA" includes any employee or contractor of NASA, or employee of such contract, to the extent that such employee or contractor of NASA or employee of such contractor prepares, disseminates, or provides access to any information pursuant to his employment or contract with NASA, or his employment with such contractor.

Availability Notice. Request for copies of this report should be referred to:

National Aeronautics and Space Administration
Scientific and Technical Information Facility
P.O. Box 33
College Park, Maryland 20740

Final Disposition. After this document has served its purpose, it may be destroyed. Please do not return it to the Environmental Research Institute of Michigan.

TECHNICAL REPORT STANDARD TITLE PAGE

1. Report No. NASA-CR ERIM No. 119300-10-F	2. Government Accession No.	3. Recipient's Catalog No.

4. Title and Subtitle

Investigation of Landsat Follow-on Thematic Mapper Spatial, Radiometric and Spectral Resolution

5. Report Date April 1976

6. Performing Organization Code

7. Author(s) James P. Morgenstern, Richard F. Nalepka, Edward R. Kent and Jon D. Erickson

8. Performing Organization Report No. 119300-10-F

9. Performing Organization Name and Address

Environmental Research Institute of Michigan
P.O. Box 618
Ann Arbor, Michigan 48107

10. Work Unit No.

11. Contract or Grant No. NAS9-14819

12. Sponsoring Agency Name and Address

National Aeronautics and Space Administration
Johnson Space Center
Experiments Procurement Section
Houston, Texas 77058

13. Type of Report and Period Covered Final report for period Nov 75 through Apr 76

14. Sponsoring Agency Code

15. Supplementary Notes

16. Abstract

Data simulating expected Landsat Follow-on Thematic Mapper (TM) data was generated from aircraft multispectral scanner data and analyzed to provide additional evidence for the definition of the system parameters; spatial resolution, radiometric sensitivity, and spectral band selection. The study involved analysis of the above parameters for both crop classification and crop mensuration accuracy with emphasis placed on the crop mensuration problem. Fine resolution M7 multispectral scanner data collected during the Corn Blight Watch Experiment in 1971 served as the basis for the study. Different locations and times of year were studied.

Definite improvement using 30-40 meter spatial resolution over present Landsat-1 resolution and over 50-60 meter resolution was observed, using crop area mensuration as the measure. Simulation studies carried out to extrapolate the empirical results to a range of field size distributions confirmed this effect, showing the improvement to be most pronounced for field sizes of 1-4 hectares (the average field sizes found in most of Western Europe and India, for example).

The radiometric sensitivity study showed significant degradation of crop classification accuracy immediately upon relaxation from the nominally specified values of 0.5% noise equivalent reflectance. This was especially the case for data which were spectrally similar such as that collected early in the growing season and also when attempting to accomplish crop stress detection. Radiometric sensitivity of twice the noise specification produced the same decrease in field center classification accuracy as decreasing spatial resolution from 30-50 meters did for area mensuration accuracy.

Spectrally, all of the 6 proposed TM spectral bands were shown to be of importance at some time during the growing season and together to provide performance as good as the 6 optimum bands of the M7 at each time. Distinct problems occurred in using (with other bands) a thermal band whose spatial resolution is 3 to 4 times that in the other bands even when oversampled. It is recommended that, if possible, the spatial resolution and sampling rate of the thermal band be set equal to that of the other bands. The 0.72-0.92 μm band was important for detection of crop stress condition.

17. Key Words		18. Distribution Statement
Design Specifications	Agricultural Field Sizes	Initial distribution is indicated at the end of this document.
Spatial Resolution	Crop Mensuration	
Thematic Mapper	Boundary Elements	
Radiometric Sensitivity	Time in Growing Season	
Spectral Band Location	Coarse Thermal Band	
	Machine Processing	

19. Security Classif. (of this report)	20. Security Classif. (of this page)	21. No. of Pages	22. Price
Unclassified	Unclassified	230	

PREFACE

This final report presents results of an investigation carried out at the Environmental Research Institute of Michigan (ERIM) to provide additional evidence for the definition of Landsat Follow-on Thematic Mapper multispectral scanner system parameters. The research covered in this report was performed under NASA Contract NAS9-14819 during the period November 1975 through April 1976. Mr. M. Jay Harnage of the NASA Earth Resource Program Office was technical monitor for this contract.

The work was performed in the Infrared and Optics Division of ERIM, directed by Mr. R.R. Legault, by the Multispectral Analysis Section (MAS). Dr. Jon D. Erickson was the Principal Investigator for this study. The authors wish to acknowledge the contribution of Mr. P.F. Lambeck to the accurate simulation of spatial resolution and the able assistance provided by Mr. D.L'Heureux and Mrs. A. Metzger of the MAS staff. The authors also want to thank Mr. R. Legault and Dr. W.A. Malila for their suggestions during the execution of the contract, and also Mrs. E. Hugg, Ms. D. Dickerson, and Ms. J. Solosky for their secretarial assistance.

CONTENTS

CONTENTS (CONT.)

FIGURES

FIGURES (CONT.)

FIGURES (CONT.)

FIGURES (CONT.)

TABLES

TABLES (CONT.)

EXECUTIVE SUMMARY

The principle is well established of determining the specifications for a new system so that the system's performance maximizes economic benefits for its projected users. Empirical evidence of the performance attainable with various possible configurations of a system, in general, provides the most convincing case for a particular set of specifications. The investigation summarized here adopts the above viewpoint and concentrates on system performance (cost-benefit analysis was not addressed). However, it is important to understand that all the impacts of a new technology, such as the subject here, cannot be anticipated or measured (pro and con) in advance to obtain net benefits. The second generation earth resources satellite multispectral scanner (MSS) called Thematic Mapper (TM) to be carried on Landsat Follow-on missions in the decade of the 1980's is sufficiently advanced over the multispectral scanner of the first three Landsat's to be considered a new technology for quasi-operational as well as research applications.

The objective of this investigation was to provide additional empirical evidence for the definition of system specifications for the TM and other future space MSS sensor systems. Specific TM parameters addressed were spatial resolution, radiometric sensitivity, and to a lesser degree spectral bandwidths and locations. The study used selected available narrow spectral band, fine spatial resolution, low noise aircraft MSS data as the basis for simulating spacecraft TM data of various spatial resolutions, radiometric sensitivities, and sets of spectral bands. The simulated TM data (more realistic than previous studies have used) were classified using automatic information classification techniques of proven capability. We emphasize that the results of this study apply to automatic information extraction techniques. At present, such computer classification techniques are predominantly of the spectral rather than spatial discrimination type, using mainly supervised pattern recognition. Results from manual image interpretation can only be inferred. For this study,

the agricultural crop inventory application, which probably offers the greatest economic benefit opportunity for the TM, was addressed using data from the ERIM M7 multispectral scanner collected during the 1971 Corn Blight Watch Experiment. Data from two different locations and with one area covered at three times of year were included in the study. The simulation of the specified TM bands was carried out as shown in Table ES-1, below.

TABLE ES-1. SIMULATION OF TM BANDS

RECOMMENDED TM BANDS	SIMULATED BANDS VIA M-7
0.45-0.52 μm	(0.46-0.49 μm) + (0.48-0.51 μm)
0.52-0.60 μm	(0.52-0.57 μm) + (0.54-0.60 μm)
0.63-0.69 μm	0.61-0.70 μm
0.74-0.80 μm	0.72-0.92 μm
0.80-0.91 μm	
1.55-1.75 μm	1.5-1.8 μm
10.4-12.5 μm	9.3-11.7 μm

Of foremost importance in priority of parameter specification is spectral band placement, width, and number of bands of the same resolution which offers the spectral sensing of unique attributes of the classes of interest against their backgrounds, assuming some reasonable radiometric sensitivity and spatial resolution are provided. Earlier efforts had placed this spectral parameter set on reasonably solid ground so our efforts were directed mainly at defining spatial resolution and radiometric sensitivity parameters, those being next in order of priority. Some additional study of the spectral band question was also undertaken. Therefore, the study was organized into two primary tasks and a third task of lesser effort.

The objective of the first task was to provide empirical evidence for spatial resolution (which is the most costly parameter to improve) as a function of location, time of observation in growing season, and field size. This evidence was obtained from simulations of 30,40,50,60, and 90-meter TM spatial resolution (with the thermal band at the same resolution and sampling rate). These simulated data, which included simulation of the nominally specified TM spectral bands and radiometric sensitivity (noise), were classified and analyzed by the criteria of acreage mensuration (proportion estimation), field center classification accuracy, and boundary element analysis. In addition, mensuration as a function of field size and spatial resolution was addressed through a type of simulation of a scene which allowed evaluation of performance for other field size distributions than the ones in our corn belt scenes -- an important step. Comparisons of performance of our simulations of 90-meter TM data to Landsat-1 or -2 MSS, which have the same spatial resolution, are only approximately accomplished because the spectral bands, radiometric sensitivities, and sampling rates are somewhat different for the two systems. Corn and soybeans were the major economic crops in a four-class mensuration.

A separate evaluation was made of the utility of a thermal band with spatial resolution of 120 meters (not 30 or 40 meters as the other bands) for crop mensuration assuming an appropriate near-midday overpass and otherwise nominal noise and spectral specifications. It was recognized that so using a thermal band does not always give a useful discriminant but the importance of the crop mensuration problem made the evaluation worthwhile in our view for those times when it could be used.

The objective of the second task was to provide empirical evidence for radiometric sensitivity which may be very important for machine processing. This evidence was obtained from simulations of field center classification accuracy for noise levels of 0.5s,1.0s,1.3s,1.6s,2s,3s,6s, 10s,and 20s where s is, by spectral band, the nominal noise equivalent

reflectance/temperature differences NE$\Delta\rho/\Delta T$ (for the bands in the reflectance region the nominal percent NE$\Delta\rho$ for bands of increasing wavelengths were 0.5,0.5,0.5,0.5,1.0, while, for the thermal band, the nominal NEΔT was 0.5°K). These cases were analyzed for both 30-meter and 40-meter spatial resolutions for the nominal spectral bands for both locations, 3 times of year at one location and 2 blight stress levels. A range of discrimination difficulty was thus tested, including the more difficult early season and crop condition discriminations as well as the more optimum late season ones.

Another objective based on the two tasks outlined above was to provide empirical bases for trade-off decisions which may need to be made in designing the Thematic Mapper. That is, field center classification performance as a function of resolution and sensitivity was studied to determine the priorities and magnitude of changes involved in worsening the spatial resolution and/or sensitivity to meet cost/technology constraints, while minimizing resultant decreases in classification accuracy. Spatial resolution needs affect the number of detectors required (and also cost) as an inverse fourth power and radiometric sensitivity as an inverse square. Therefore, if performance is affected equally by an equal percentage change in either parameter (spatial resolution or radiometric sensitivity) it is preferable to allow spatial resolution to worsen before radiometric sensitivity.

The objective of the third task was to provide empirical evidence on the spectral bands. This evidence was obtained by selection of the six optimum bands out of the twelve M7 bands which cover the spectrum from .45μm to 2.5μm plus thermal infrared at each time of the growing season and for two blight stress levels using signatures from the 30-meter data. Some rank orderings were also carried out to determine the relative importance of each band in optimum subsets. The criterion for finding the optimum six and the rank ordering was by minimizing the metric, average pairwise probability of misclassification averaged over all pairs of

signatures of dissimilar classes. Comparison of simulation classifier results for field center classification accuracy between the optimum bands and TM bands would also provide evidence of the adequacy of the TM specified bands for the cases studied.

Some clarifications are in order. In the spatial resolution study we have used a common training and testing area since we did not wish to confound selection between sensor parameters with questions of representativeness of training. As a consequence, absolute levels of performance achieved in this study will not necessarily extrapolate to operational use. Similarly, due to the simulation of coarser resolution TM data with finer resolution aircraft data where we knew and used the location of objects, effects reducing performance due to problems of uncertainty in locating fields for training which may arise in operational use have not been included.

Effects of the atmosphere and other sources of variability affecting the operational ability to accomplish signature extension* must also be considered in the approach to such a study. Our philosophy was to assume that sufficient solutions will be found so that the specification of the TM system design should not consider such effects. This assumption was based on our experience with the development of signature extension algorithms.

Our understanding of such noise limitations as imposed by atmospheric variations is that sufficient measurements or theories do not now exist to accurately define the spatial or time distribution of the minimum or average noise which would provide a natural limit to sensitivity. Thus we

---

* Signature extension is defined as the capability to use signatures well beyond the local time and place at which they are derived and usually implies a partitioning of the scene into similar areas and an active modification of the signatures, the data or both to achieve satisfactory performance.

have not assumed a limitation here, but recommend that measurements of atmospheric noise to define these limitations be pursued.

The results for the three tasks are briefly summarized here. The principal measure of performance over an entire data set is the area mensuration (proportion estimation) accuracy over all pixels in the data set. Here the results for the four data sets, when examined as a function of spatial resolution were best at 30 meters, inferior at 60 meters, and very poor at 90 meter resolution. Figure ES-1 presents these results using relative proportion averaged over all classes as the measure (or error in relative proportion as also shown). The trend to improved proportion accuracy at finer spatial resolution depicted in Figure ES-1 is felt to be primarily as result of there being relatively fewer boundary pixels at the finer spatial resolutions. It is important to note the consistent trends in these results over all the data sets studied.

A further consideration in choosing one spatial resolution over another is to understand what results would be for different areas in the world. The results reported above were for field size distributions that are representative of the U.S. corn belt. However, many other parts of the world -- Western Europe, India, parts of Asia, etc.-- have field sizes which are smaller. The impact of spatial resolution on overall mensuration accuracy for such areas was studied using simulation techniques both to construct a series of appropriate scenes, where each scene was composed solely of fields of the same size and shape, and to evaluate expected mensuration accuracy for them, varying spatial resolution as a parameter. A sample of these analyses is presented in Figure ES-2. Field sizes of 1-4 hectares are typical of Western Europe, India, etc., while the range 6-10 hectares is typical of the corn belt sites studied. As can be seen, significant reductions in accuracy occur with coarsening resolution for the smaller fields (1-4 hectares). In general, for such fields the loss of accuracy was 4-6% between 30 and 40 meter resolution;

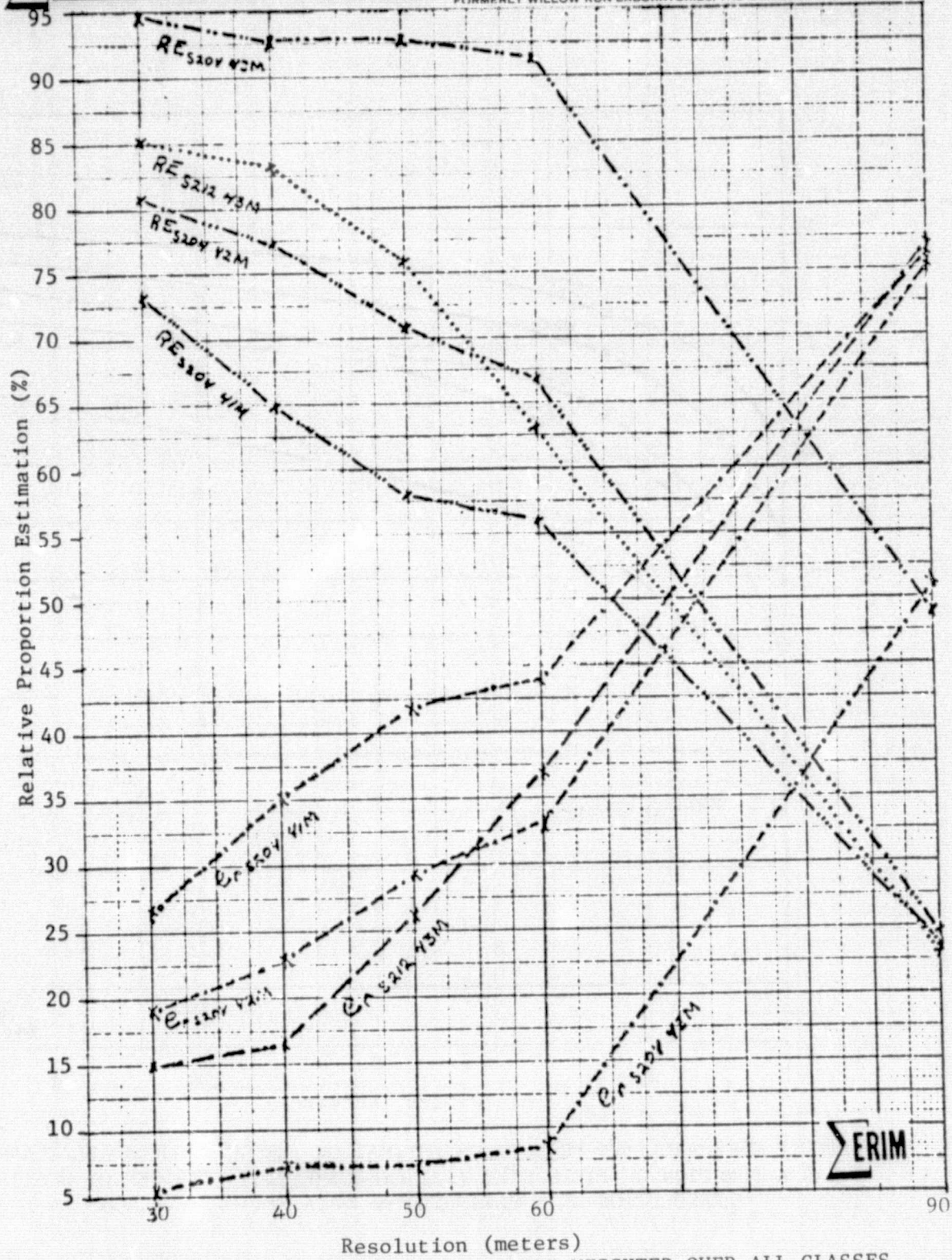

FIGURE ES-1. PROPORTION ESTIMATION WEIGHTED OVER ALL CLASSES

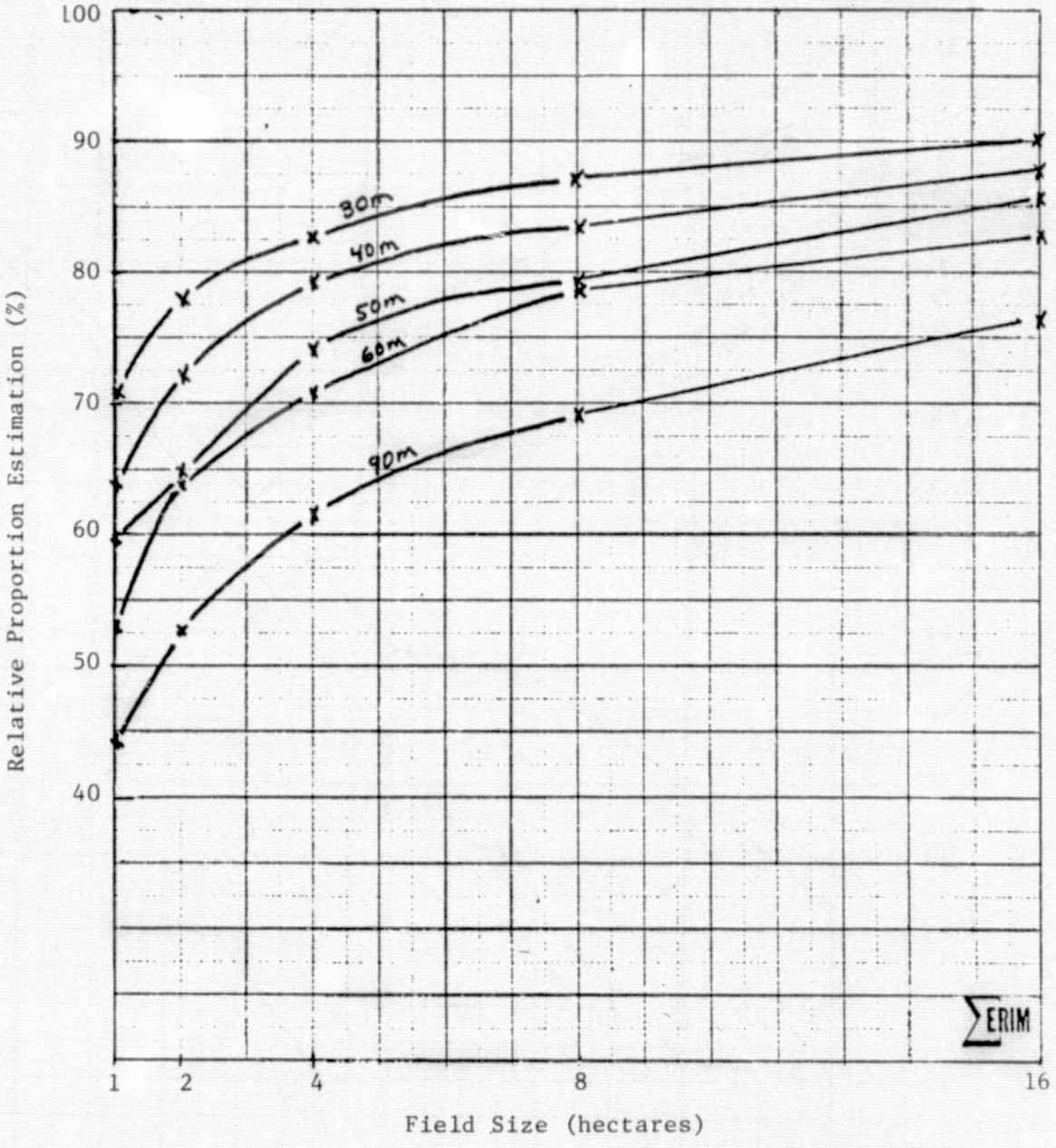

FIGURE ES-2. RELATIVE PROPORTION ESTIMATION (WEIGHTED OVER ALL CLASSES) AS A FUNCTION OF FIELD SIZE (2:1 ASPECT RATIO) WITH SENSOR SPATIAL RESOLUTION AS A PARAMETER -- DATA SET: S-204,43M

the decrease was 10-13% between 30 and 50 meter resolution. Even for 16 hectare fields (40 acres), a loss in mensuration accuracy of several percent is seen.

In the studies of radiometric sensitivity the results showed that classification accuracies decreased with increasing noise. The results, presented as a function of $NE\Delta\rho/\Delta T$ values simulated (nominally, 0.005 for all bands except the 1.5-1.8 μm band where $NE\Delta\rho = 0.010$ and the thermal where $NE\Delta T = 0.5°C$). An example of the radiometric results is displayed in Figure ES-3, where it can be seen that for the S204, July 12 (41M) data set, in which the major classes are spectrally similar, the effects of decreased sensitivity is immediately evident. Although the results for the S-204, August 12 (43M) data set are almost unchanged to twice the nominal noise case, further examination of this data set (Figure ES-4) shows that the recognition of corn, the key economic crop in the area, declines immediately with a small decrease in sensitivity. Furthermore, the correct detection of blight stressed corn was also seen to decrease significantly with immediate relaxation of sensitivity from the nominal point.

The TM is intended to provide quasi-operationally useful data for many users with different applications; however, the overriding criterion for the design of the system is that it must produce measurable dollar benefits greater than its cost. This criterion is appropriate to its quasi-operational mission and while not a research mission criterion it will also support research objectives. Such benefits accrue mainly from one source in current earth resources management: accurate mensuration statistics at all times throughout the growing season for the major trade crops (wheat, corn, soybeans, cotton, rice, etc). Further, we have taken as given that such measurements must be made both in the principal production areas of the world as well as the principal demand areas that are producers. This means the instrument must be as capable of collecting quality data over areas such as India or Western Europe

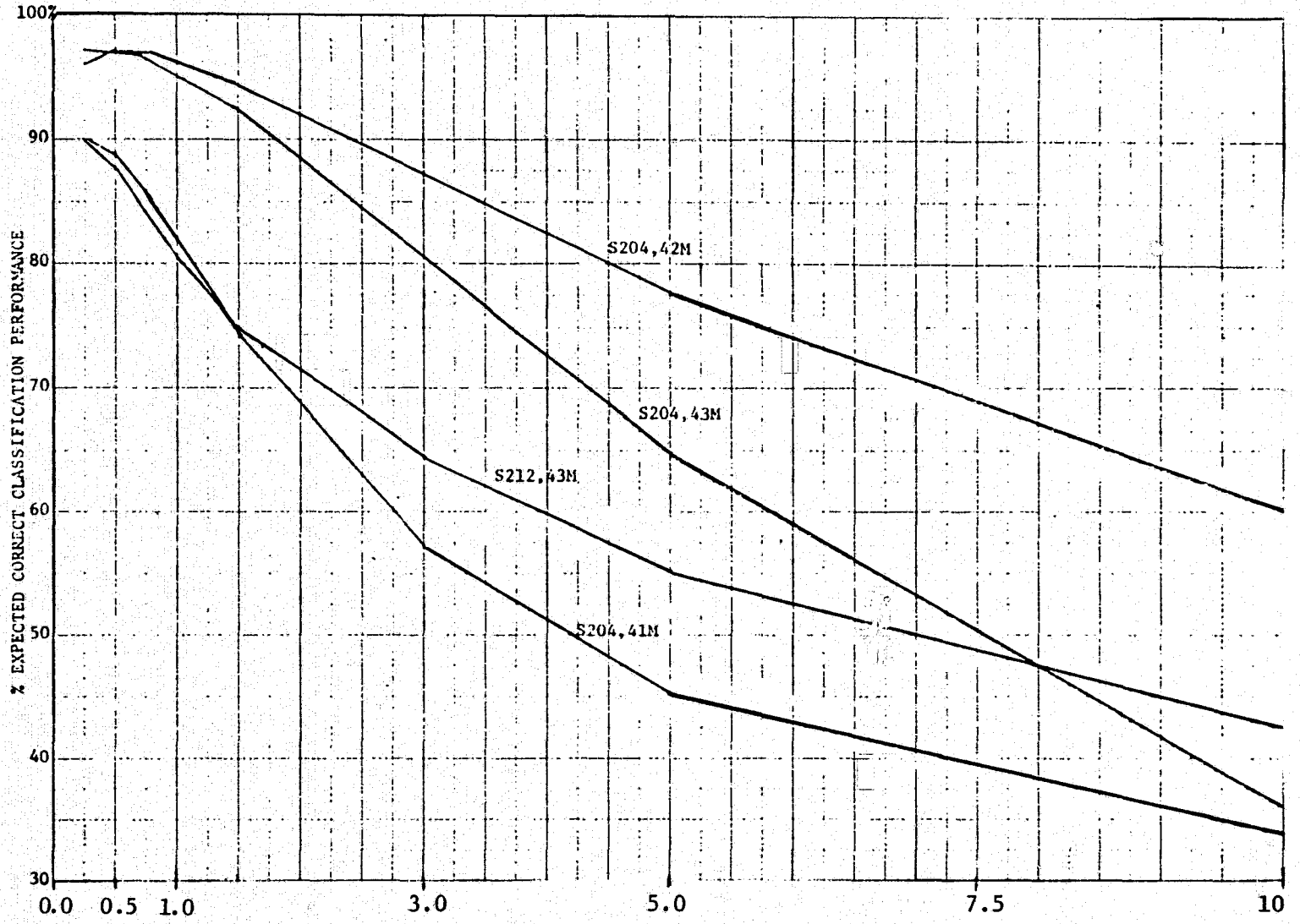

FIGURE ES-3. RADIOMETRIC SIMULATION -- 30 METER RESOLUTION -- PERFORMANCE OVER ALL CLASSES (All Available Fields in Scene Utilized in Training Procedure)

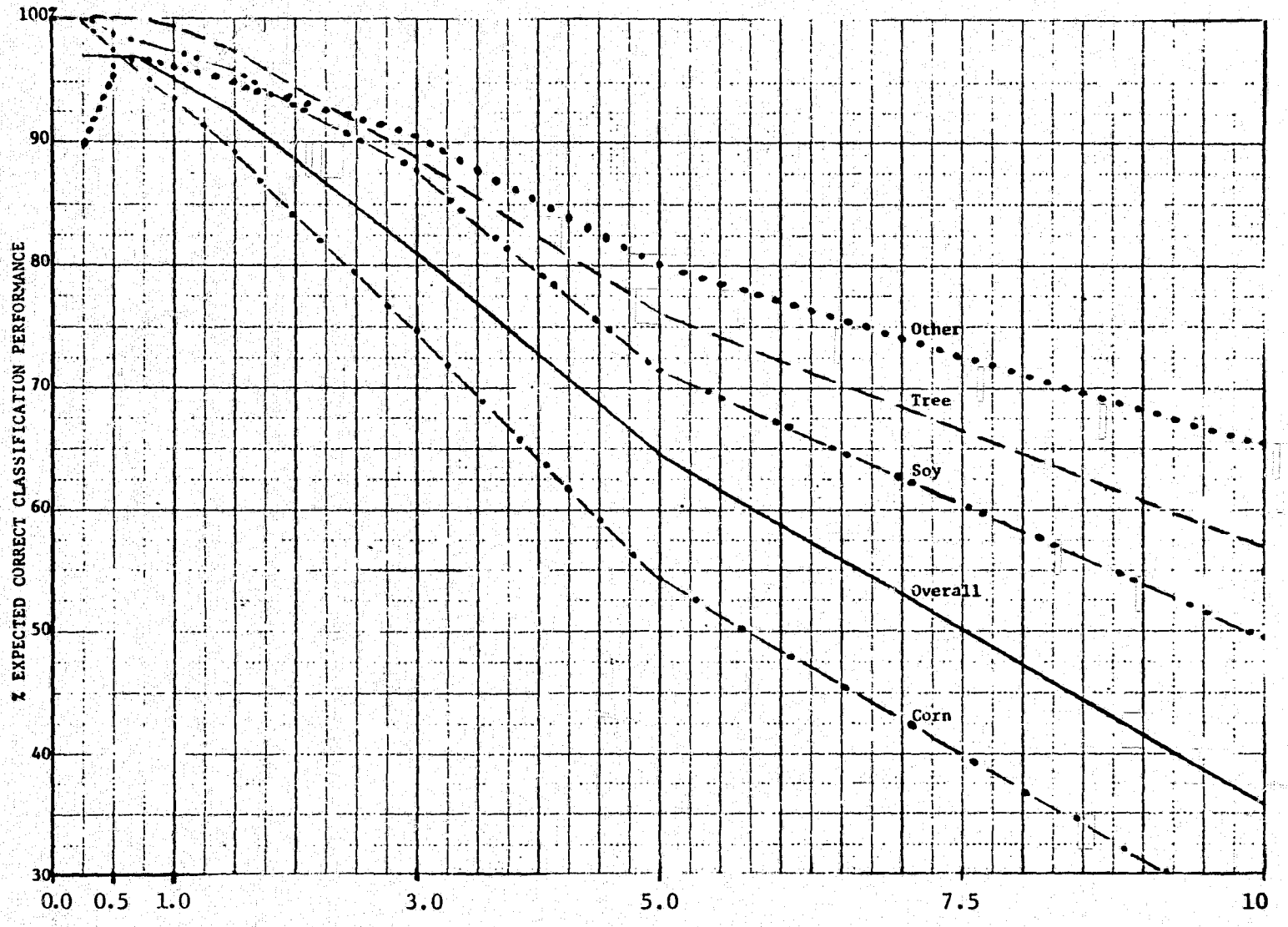

FIGURE ES-4. RADIOMETRIC SIMULATION -- Segment 204, August 13 (43M) -- 30 METER RESOLUTION (143 Fields in Scene Utilized in Training Procedure)

characterized by typically small fields (1-4 hectares) as well as over areas of predominantly larger (16-32 hectares) fields, e.g., Canada, U.S. wheat belt, U.S.S.R. The conclusions of this study were derived in light of the above.

Before summarizing the conclusions and recommendations it is important to note that our study is empirical and therefore limited to the evidence derivable from 3 times of year and two locations for four classes (except where simulation allowed generalizations). Our results are nevertheless supportable by theoretical arguments and the evidence is important and far reaching in its implications.

Conclusions Relating to Spatial Resolution and Radiometric Sensitivity are:

1. This study provides new but limited empirical evidence that 30-meter or 40-meter spatial resolution, and a TM system radiometric sensitivity of half-percent reflectance would provide significantly better performance in automatic information extraction for agricultural crop survey applications (particularly corn and soybeans) than coarser resolution or less sensitive systems such as Landsat-1, -2, and -C. Although direct comparisons to the current Landsat's were not made, the evidence for this conclusion is supportable by theoretical arguments.
2. We have shown additional empirical evidence for the priority of radiometric sensitivity at least equal to spatial resolution, if not higher.
3. Improvement in the area mensuration performance as spatial resolution increases in the range of 30-90 meters is shown to be largely due to the lesser proportion of boundary elements (where classifier performance is low) at finer resolution.
4. Improvement in performance with reduced noise levels in the range half-percent to one and a half-percent is more signifi-

cant earlier in the growing season and with more difficult discriminations. Both mensuration and field center performance are affected.

5. Thermal band resolution of 120 meters was shown to degrade performance (when it could be used with other bands) in crop surveys compared to thermal band resolution equal to the other bands.

Conclusions Relating to the Spectral Bands are:

1. The 6 TM spectral bands are confirmed by limited empirical evidence to be the best 6 bands for agricultural surveys of corn and soybeans, each band (including a fine resolution thermal band) being important at some time in the growing season. The TM set gives essentially the same performance as the various sets of 6 optimum aircraft scanner bands appropriate to each time. This means the 0.45-0.52 μm band should not be though of as a research band.
2. The 0.72-0.92 band is important for detection of crop stress conditions.
3. A 120-meter thermal band is not useful as a 30-meter thermal band in crop surveys.

Other Conclusions are:

1. Simulation of satellite or high altitude aircraft scanner performance using low altitude aircraft scanner data as an input is a powerful systems analysis technique.

Recommendations:

1. Thematic mapper should have the following specifications for crop inventory applications:

Spatial Resolution (all bands) 30 meters (42 microradians)

Spectral bands and radiometric sensitivities:

0.45-0.52μm at NEΔρ = .005

0.52-0.60μm at NEΔρ = .005

0.63-0.69μm at NEΔρ = .005

0.72-0.92μm at NEΔρ = .005

1.55-1.75μm at NEΔρ = .005 (perhaps 0.01)

10.4-12.4μm (perhaps broader) at NEΔT = 0.5°C

2. If tradeoffs need to be made, spatial resolution should be traded for radiometric sensitivity.
3. Additional effort should be made to achieve a finer thermal band resolution than 120 meters.
4. Additional investigations be made of:
   a. Classifier performance on boundary elements as a function of mixtures of classes to determine local bias.
   b. Spatial sampling effects giving types of boundary element mixtures as the spatial sampling changes.
   c. The incremental benefit and cost of incremental mensuration performance improvement in any specific application.
   d. The dynamic range and digital count vs spectral radiance (in the band) transfer characteristics of TM.
   e. Time effects such as frequency of coverage, time of day, etc.
   f. Other specific user applications.

It is also important to consider the effects of these recommendations on the users in addition to the expected performance improvement. To realize this benefit, timely and low cost (by comparison) means of automatic data processing must be available to extract the information. The data rate for the TM is nearly an order of magnitude greater than for the Landsat-1 MSS. Because of this, increased emphasis will need to be placed on user processing systems such as the NASA-sponsored

MIDAS, which offers accurate high throughput capabiltiy without a proportional increase in cost. Without such systems the users will be reluctant to operationally use the data except in a manual mode. Short turn-around time prior to receipt by the users of the data for processing will also be important.

1
INTRODUCTION

The Thematic Mapper (TM) multispectral scanner of the Landsat Follow-on program which is expected to be the basic design for earth resources multispectral scanners in the decade of the 1980's, has reached the design specification stage. This study was commissioned by NASA to provide additional evidence for TM design specifications as well as to provide bases for parameter tradeoffs in the design, if needed. The basis of the study was analysis of simulated TM data, the simulation being based on the preliminary TM specifications.

The data simulation was carried out using data acquired by a fine resolution aircraft scanner. Three principal parameters of the proposed TM sensor were studied: spatial resolution, radiometric sensitivity, and spectral band selection. Thus, data were simulated for a variety of spatial resolutions: 30, 40, 50, 60 meters and equivalent Landsat-1 resolution and also for a number of levels of radiometric sensitivity: one-half the nominal TM specification value, the nominal value (generally $NE\Delta\rho = 0.005$) and 1.3, 1.6, 2.0, 3.0, 6.0, 10.0, and 20.0 times the nominal noise value. The original 10 meter aircraft data was also used with its $NE\Delta\rho = 0.01$ unchanged.

A primary use of Landsat Follow-on will be to conduct large scale agricultural surveys to aid economists in forecasting supply and demand for the principal trading crops of the world. Thus, the data base used for this study was from agricultural sites, namely data acquired over the Indiana corn belt during the 1971 Corn Blight Watch Experiment. The data used here were collected at three times during the growing season, which permitted the study of TM parameters as a function of time. An additional feature of these data was the occurrence of crop stresses (corn leaf blight and drought) which enabled study of TM parameters as regards crop stress as well. The data had been collected by

the ERIM M-7 scanner which recorded 12 spectral bands; thus, studies were carried out to determine whether the preliminary specified spectral bands were adequate for the agricultural survey problem at different times as well as for the detection of crop stress.

2
BACKGROUND AND APPROACH

The proposed Landsat Follow-on satellites, the next generation in earth resources monitoring, has reached the design specification stage. The heart of the system is a second generation multispectral scanner, referred to as the Thematic Mapper (TM) and current NASA efforts are aimed at finalizing the technical specifications for the TM. The concept of a Thematic Mapper is as its name implies -- a sensor whose use would result in a mapping or description of the scene on the basis of the themes or subjects in the scene, utilizing largely automatic information extraction and image enhancement techniques to produce final data products.

A previous study [1] related performance errors in terms of probability of misclassification and acreage measurement errors to sensor parameters. This study extends the limited data base of the previous work with the same objectives, namely, to determine the relationship between sensor parameters and performance. Included in this study are such aspects as crop stress and analysis of results as a function of time of year of data collection. Additionally, this study addresses the question of performance versus field size.

2.1 BACKGROUND

Various previous studies have addressed advanced scanners and their applications [2,4]. Particular hardware aspects of TM have been addressed in point design studies by Hughes, Honeywell, and Te. The preliminary specifications for TM have been addressed by two technical study groups [5,6] and in a previous empirical study [1]. A benefits assessment of TM has also been made [7].

A number of issues have been raised including the number and placement of spectral bands, radiometric sensitivity, spatial resolution, dynamic range, sampling rate, and geometric accuracy as well as

the temporal frequency of observations, number of satellites, optimum orbit time, thermal band resolution and sampling, and atmospheric effects.

The current study was commissioned by NASA to provide additional evidence for the specification of spatial, spectral and radiometric parameters, and/or to provide the basis under which design tradeoffs between the three parameters might be made. Realistically, the parameters being studied (spatial, radiometric and spectral) are not independent attributes of the sensor but interact with each other and with other parts of the overall system in complex ways, and consequently their specification must be considered only within the context of the overall system. Furthermore, the criteria for design decisions should be based on user requirements for the system, within the constraints of keeping the system cost effective and avoiding the use of high-risk technology.

A fundamental viewpoint in studying alternative systems designs derives from the desire to achieve systems whose performances are such that they give benefits greater than their costs for some range of performances, benefits, and costs. Thus, design parameter tradeoff studies using performance as a measure must also relate in some way to using benefits and costs as measures. This assessment of costs or benefits was outside the scope of this study and is therefore not reported. A constraint is also placed by technology on the ranges of design parameters that may be achieved with acceptable technological risk.

For this study of the thermatic mapper, some of the sensor design parameters and their ranges under consideration were

Spatial Resolution (Angular)	α	milliradians corresponding to 30m-90m ground resolution
Radiometric Sensitivity	$\Delta\rho$	0.25-10.0%
Number of Spectral Bands	M	5-7

(Here resolution is specified as an angular quantity, for ease of incorporating it into a cost model. In general, this study will instead discuss resolution as the linear dimension of the instantaneous field of view. Thus, for example, 30 and 90 meter IFOVs correspond to .043 and .127 milliradian angular resolution, respectively.)

It can be shown that N, the total number of detectors in the focal plane (which is related to both spatial resolution and sensitivity) is equal to nM where n is the number of detectors in parallel in each band. This may be written in terms of the sensor design parameters as [2]

$$N \propto \frac{M}{\Delta\rho^2\alpha^4}$$

If cost is assumed to be proportional to N, then

$$C \propto \frac{M}{\Delta\rho^2\alpha^4}$$

and we have a relation between cost and values of the sensor design parameters $(\alpha,\Delta\rho,M)$. This is an example of one possible cost model, but the point for this discussion is that the model used imposes a fixed relation between the sensor design parameters. This study determines, through empirical simulation, values of performance for various discrete values of α and $\Delta\rho$. Tradeoffs between α and $\Delta\rho$ which give constant performance are necessary and this study provides evidence for these tradeoffs.

Ideally, we seek that set of sensor parameters which can be obtained for cost C_o and which maximizes performance $P = P(\alpha,\Delta\rho,M)$ for all $(\alpha,\Delta\rho,M)$ which satisfy the equation

$$C_o = K \frac{M}{\Delta\rho^2\alpha^4} .$$

In other words the sensor system given by the design parameters $(\alpha_o, \Delta\rho_o, M_o)$ (which maximize P and satisfy the cost equation) is the "best" performance system we can obtain for cost C. If we repeat this procedure for all costs C, we obtain a maximum performance (P_{max}) versus cost curve. Equivalently, we could obtain an E_{min} versus cost curve, where E_{min} is the minimum error.

Consider the curve of performance versus cost:

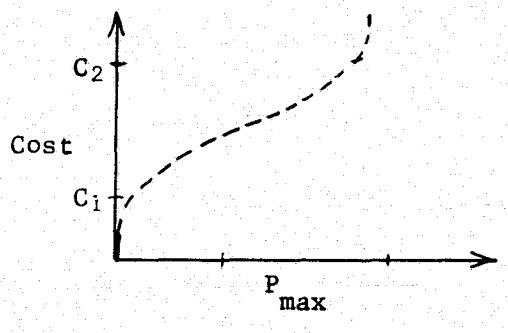

It seems reasonable that for some cost C_1, sensor systems costing less than C_1 produce nearly constant and poor performance. For systems costing between C_1 and C_2, performance improves rapidly. For systems costing more than C_2 little improvement in performance is achieved because of natural or technological limitations.

Now consider the curve of performance versus benefits:

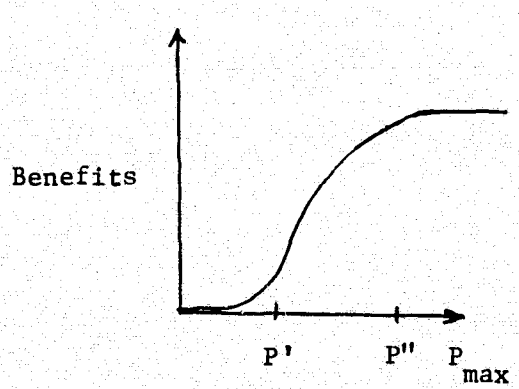

It seems reasonable that for some performance P', the benefit derived from systems whose performance is less than P' is essentially none. For systems with performance between P' and P", benefits improve rapidly. For systems with performance greater than P" little further increase in benefit is derived.

Finally, consider the combined curves of performance versus benefits and costs:

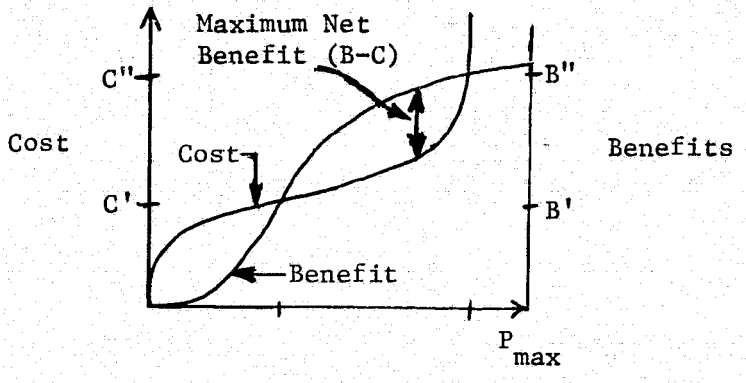

The region between B' and B" is where benefits exceed (are greater than) costs. The curves as drawn are not meant to be quantitative, but the general shapes are reasonable and are supported empirically. Such curves provide important insight into systems studies as managerial needs and tools as well as an understanding of the objective of such studies and the need for studying a range of performance short of that which is maximum as well as determining the "knee" near the maximum. We have assumed that the range of parameters being tested is in the region of performance where increased performance yields benefits that increase faster than do costs.

2.2 APPROACH

The basis for this study was to utilize data gathered using a fine resolution aircraft-mounted multispectral scanner to simulate, by spatially degrading the data, several different candidate spatial resolutions. Additionally, by artificially adding random noise effects to the data, several levels of radiometric sensitivity could be simulated and their effects studied. Also of importance was the identification of those spectral bands which were most important to accurate classification of the data.

For this study, data gathered during the 1971 Corn Blight Watch Experiment (CBWE) [8] was used, allowing the additional characteristic of crop stress to be factored into the analyses of thematic mapper parameters; i.e., what particular bands, if any, or what level of radiometric sensitivity are necessary to detect crop stresses. Four data sets were used from the CBWE. These were from two sites, each site one by ten miles in size, in northern and central Indiana, the data sets being collected at three different times in the growing season -- mid-July, early August and mid-August using the ERIM M-7 multispectral scanner. The data base is described in more detail in Appendix I.

As already mentioned, one dominant characteristic of the sites was the occurrence of Southern Corn Leaf Blight, a fungus which attacks corn plants. It appears in significant amounts only for one of the data sets being processed here, Segment 212, for mid-August. For this site and time, extensive ground truth existed which showed the vast majority of corn fields to be moderately affected by the blight, in various degrees, as would be expected. A few fields (5 in number) were found to be highly affected (rated at severity levels 4 on a 5 point blight scale). Previous work in 1971 [8] showed that, in general, three levels of corn blight could be detected: moderate (levels 0-3), fairly heavy (4) and most severe (5). Thus in this study two degrees of stress were available for inclusion in the analysis of TM parameters.

An overall view of the processing carried out for this study is given in Figure 1. The data were initially normalized for scan angle effects (mainly effects due to changing atmospheric path length as a function of scan angle) [9], which for aircraft scanners is significant, and the counts or number of quantization levels for a given change in scene reflectance were calculated for use in the radiometric sensitivity aspects of this study (this is covered in detail in Appendix I). The next stage was to simulate the TM data spatially, radiometrically and spectrally. The spectral simulation of TM data was carried out using the nearly equivalent M-7 bands, as shown in the table below. In performing the spatial simulations, the effects of

0.45-0.52 μm	(0.46-0.48 μm) + (0.48-0.51 μm)
0.52-0.60 μm	(0.52-0.57 μm) + (0.54-0.60 μm)
0.63-0.69 μm	0.61-0.70 μm
0.74-0.80 μm	0.72-0.92 μm
0.80-0.91 μm	
1.55-1.75 μm	1.5-1.8 μm
10.4-12.5 μm	9.3-11.7 μm

changes in pixel size for the aircraft data as a function of scan angle were accounted for; thus, we ensured that later analyses of mensuration accuracy would not be affected by this problem. Because of the desire to simulate the specified thematic mapper as closely as possible, care was taken at this stage to accurately simulate the expected point-spread functions* as based on the scanner modulation transfer function

* The point-spread function is the normalized diffraction pattern formed by a point object, and hence, is the spatial weighting function which defines the contribution of the radiation at any point on the ground to the scanner signal produced for a given pixel.

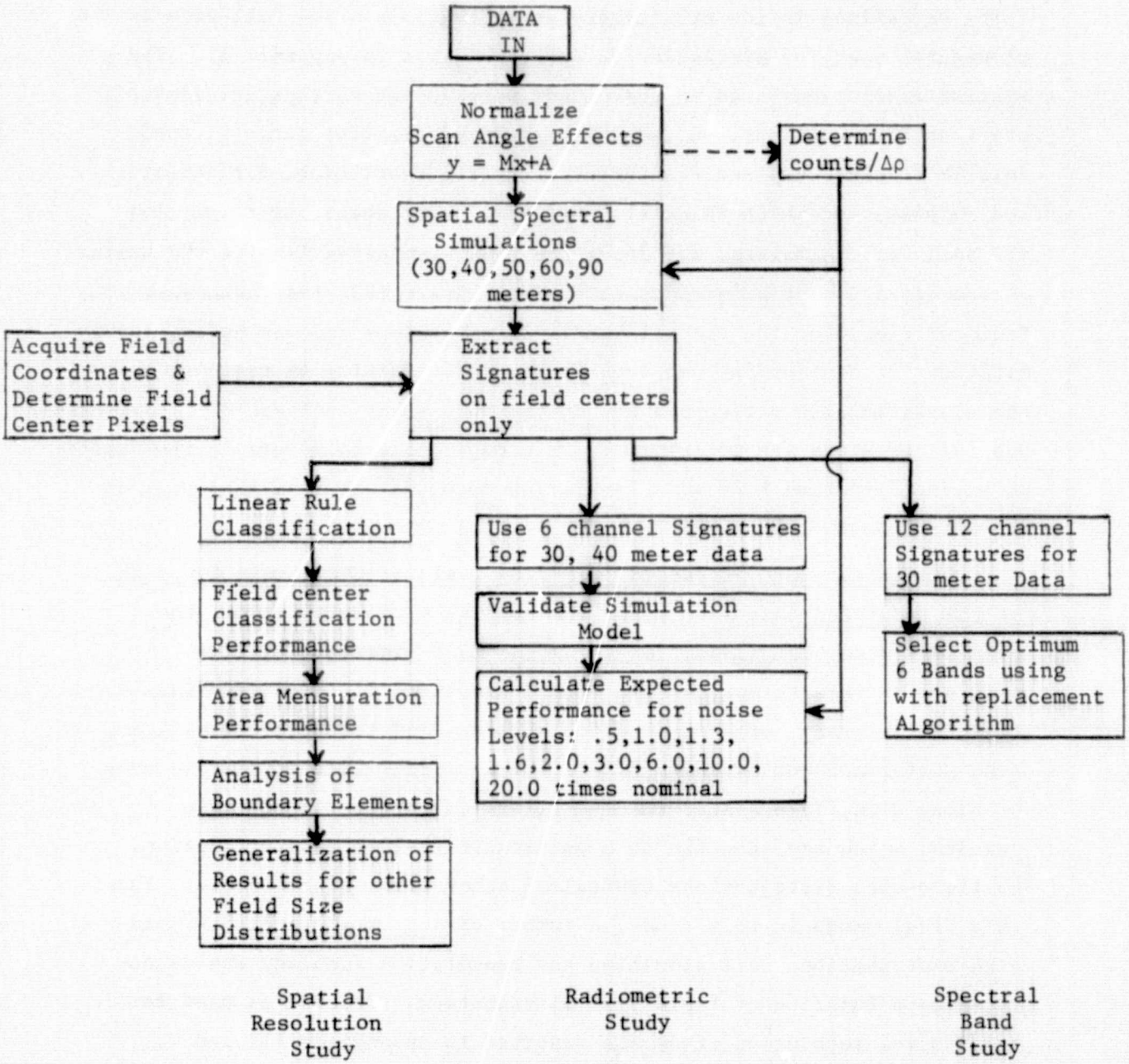

FIGURE 1. OVERALL STUDY FLOW (Data Base is 4 Aircraft-Acquired Data Sets)

(MTF) as defined in the preliminary specifications. The full details and procedures used for simulating TM data are given in Appendix II. The spatial resolutions used in this study were 10 meters (the original aircraft data resolution), 30, 40, 50, and 60 meters (the range of candidate TM resolutions) and equivalent Landsat-1 resolution, for comparison purposes for which 90 meters* was used. It should be noted that all bands were simulated as having the same resolution despite the nominal TM specification of a three or four times larger IFOV (instantaneous field of view) for the thermal band. This was done because having a very different resolution for one band created difficulties in training and in the classification procedures and in the subsequent analysis of the results. One further study was therefore carried out: this to determine the impact of having a thermal band with resolution much coarser than that used in the other bands.

Signatures were extracted only from field center pixels for each of the simulated data sets. For the spatial resolution study, the data sets were then classified using the ERIM linear classifier. Analysis of results was carried out by assessing field center classification accuracy, area mensuration accuracy and studying classification performance on boundary pixels. This latter is important because it, along with field center results, allows extrapolation of these results, which are specific to a particular field-size distribution, to field-size distributions typical of other areas of the world. Thus, as a final stage in this study, a number of scenes of specific field-size distributions were simulated and mensuration accuracy was calculated as a function of field size distribution. Procedures used for the spatial resolution study are reported in Appendices III and V.

* Following the definition of resolution as the number of meters of spacing between the half cycles which correspond to the 50% response on the system MTF [2],

The radiometric sensitivity study was carried out using the ERIM simulation classifier. Included was a validation of the model used, by comparison of simulation results to actual data classification results. Inputs to the radiometric sensitivity study were signature sets extracted from just the 30 and 40 meter simulated resolution. Full details on models, procedures and validation can be found in Appendix VI.

The spectral band study utilized signatures of 12 channels, the original 12 M-7 bands, extracted from the 30 meter simulated resolution data. The feature selection algorithm used as the performance criterion the average pairwise probability of misclassification between all pairs of signatures of different classes for all possible subsets of six channels. The optimum set was the one which minimized the metric used.

The reader is referred to Appendix IX which contains descriptions of the important computer algorithms used in this study.

2.3 TRAINING

Two training procedures were utilized during this study. In the first, the set of training fields used for each set of data were such that field signatures* could be extracted from them at the coarsest resolution (90 meters); that is, a common set of fields were used for each spatial resolution case of each time and segment. This meant that training was carried out over exactly the same ground areas for each of the studied resolutions. It was reasoned that this procedure would neutralize any effects in the classification results which would be attributable to the training procedure, leaving us with the

*The term "field signature" refers to the statistics (mean vector and covariance matrix) of a set of six or more pixels from the same field or contiguous homogeneous area on the ground. A minimum of six independent samples is necessary to produce a non-degenerate covariance matrix for six channel data.

knowledge that any observed changes in classification accuracy as a function of spatial resolution could be attributed solely to the effects of changing spatial resolution.

In the other procedure, the goal was different. Here the desire was to retain as much as possible the natural class variability and scene variability. Here, then, field signatures were extracted from all available fields in the scene at each resolution (a larger number at fine resolution than at coarse resolution), thus sampling the full range of variability as desired.

Field location was carried out using the fine (10 meter) spatial resolution data. This aspect of the study did not perfectly simulate or address the question of training on coarse resolution and/or noisy data. It has been our experience that the degree of difficulty encountered in location of fields which are not large will increase considerably for coarser resolution or poorer quality data. Thus the training procedures used here were able to estimate the training statistics more accurately than would have been the case had we used the spatially and radiometrically degraded data as inputs to the field location procedure for training. For this study we felt such accuracy in the estimation of training statistics was necessary, however it does mean that the coarser resolutions have had a significant advantage or favorable bias compared to a realistic handling of training area location in the actual coarse resolution data. A more detailed explanation of the training procedure is given in Appendix III.

3
RESULTS

To aid in understanding the results we first review the processing employed. In processing the data, in all the combinations of spatial resolutions, data sets and radiometric sensitivities, the general procedure followed was the same for each specific case studied: (a) training by extracting signatures from each training field using only field center pixels from that field, (b) classification using the ERIM best linear classifier [10] which employs a null test based on a 0.001 probability of rejection, and (c) analysis of the classification results, based on accuracy of pure (field center) pixel classification, on per class and overall mensuration accuracy, and also on the analysis of boundary pixel classification. In all cases the set of spectral bands used were the 6 simulated TM bands.

3.1 RESULTS FOR SPATIAL RESOLUTION STUDY*

As previously explained, the training procedure for this study primarily utilized only a few (15-20) common fields for each data set. Further, these same set of fields also defined the test fields for determining field center classification accuracy. In general, it is not a totally valid procedure to test solely on one's training data. However, here again we were most concerned with avoiding situations which might render the results ambiguous; we wanted to know with certainty that only resolution dependent effects would be observed in the results. Thus, we wanted the training data to be fully representative of the test data, and in fact to be representative of all the spectral variability in the scene. Therefore, in what follows one should not assume classification accuracies for the real TM when it becomes operational will be commensurate with the accuracies reported here.

* Detailed explanation of training procedures and the full tables of results obtained are in Appendices III and IV, respectively.

The analysis of classification results was broken up into analysis of field center pixels, mensuration accuracy and boundary pixel analysis. The field center results by their nature are not expected to display any significant change as a function of spatial resolution. The area mensuration results, on the other hand, are expected to be the predominant measure for this part of the study. Analysis of boundary pixels allows for the extrapolation of mensuration results to other field size distributions and thus allows for a generalization of the study's results.

3.1.1 ANALYSIS OF FIELD CENTER PIXELS

In the analysis of classification results we turn first to the accuracy obtained for field center (pure) pixels. Here we have set a situation where, at each resolution, training and testing were carried out over exactly the same areas on the ground. Thus it was expected that the classification accuracy as a function of spatial resolution would be constant and indeed, this analysis is carried out as a check on the training procedure.

We see in Figure 2, results obtained using the common field training procedure, that field center classification accuracy as a function of spatial resolution is not strictly constant as had been expected, but rather is constant or increases slightly over the range of 30 to 40 meters and then falls off significantly at 90 meter resolution. It is important to note that the results are fairly consistent between data sets. Also, analyses of classification accuracies for each of the classes showed the same general trends as those displayed in Figure 2.

There are basically two interacting mechanisms at work here to generate the non-constant results. The first causes the fall-off observed at the coarser resolution. At the coarser resolution, the signatures for the most part were calculated using very few pixels (10-20 pixels for the 90 meter data). The resulting covariance matrices thus

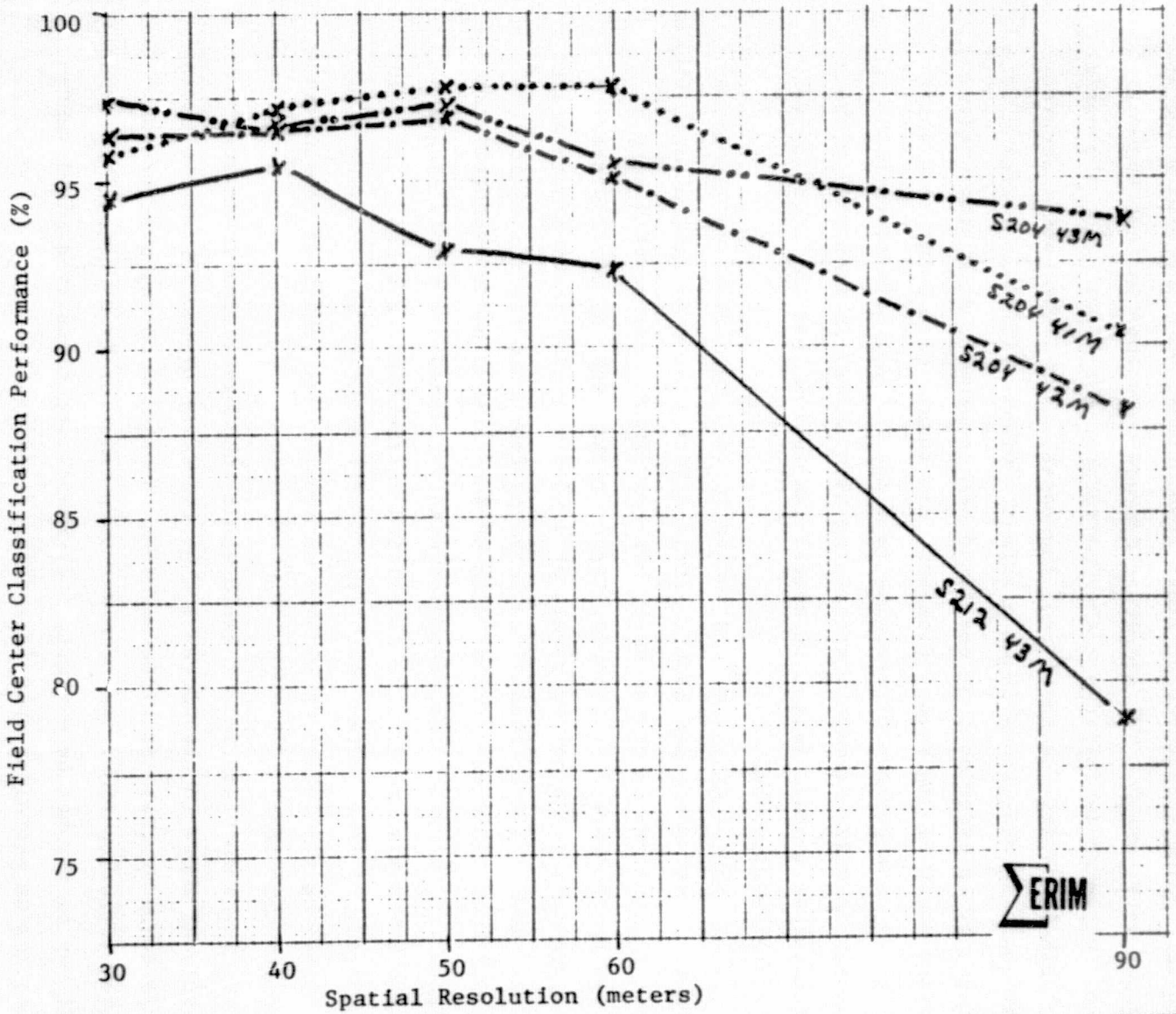

FIGURE 2. FIELD CENTER CLASSIFICATION RESULTS BY DATASET OVER ALL CLASSES AS A FUNCTION OF SPATIAL RESOLUTION -- (FIELD SIGNATURE TRAINING PROCEDURE)

represent hyper-ellipses with significantly smaller volume than the corresponding signatures at finer resolutions, an example of which is shown in Figure 3. The result of decreasing volume is that the null test employed is failed a higher portion of the time; i.e., the number of pixels called "unclassified" increases. Thus, the poorer accuracy at coarser resolutions is an artifact. Given sufficient training data then, it is expected that the field center results at coarser resolutions would be improved. Even so, this result does point to a valid effect: the process of training (and identifying sufficient pure pixels to well estimate the training signatures) is much more problematical at coarser (e.g., 90 meter) resolution than at finer (30-40 meter) resolutions.

The second effect of coarsening spatial resolution works counter to the first described above. It is a fact that many agricultural fields are not uniform in ground cover but contain inhomogeneities such as dead spots, bare soil patches, trees, rocks, etc. of small dimension. In general, field center pixels of equivalent size imaging such areas will clearly not be classified as being from that field's class. As pixel size increases, the effects of such areas, being averaged with larger and larger areas, is considerably reduced and pixels imaging such areas will tend to be classified as the field's class. Thus, in general, it is expected that field center accuracy will improve with increasing resolution up to some maximum value, and then remain essentially contstant.

The interpretation of small scale inhomogeneities in fields explored above focuses attention on the issue of scoring or evaluating field center classification results. Depending on the goal of the classification (location of class occurrence or crop productive acreage) it may or may not be correct, for example, to classify a pixel representing an anomalous spot in a wheat field as wheat.

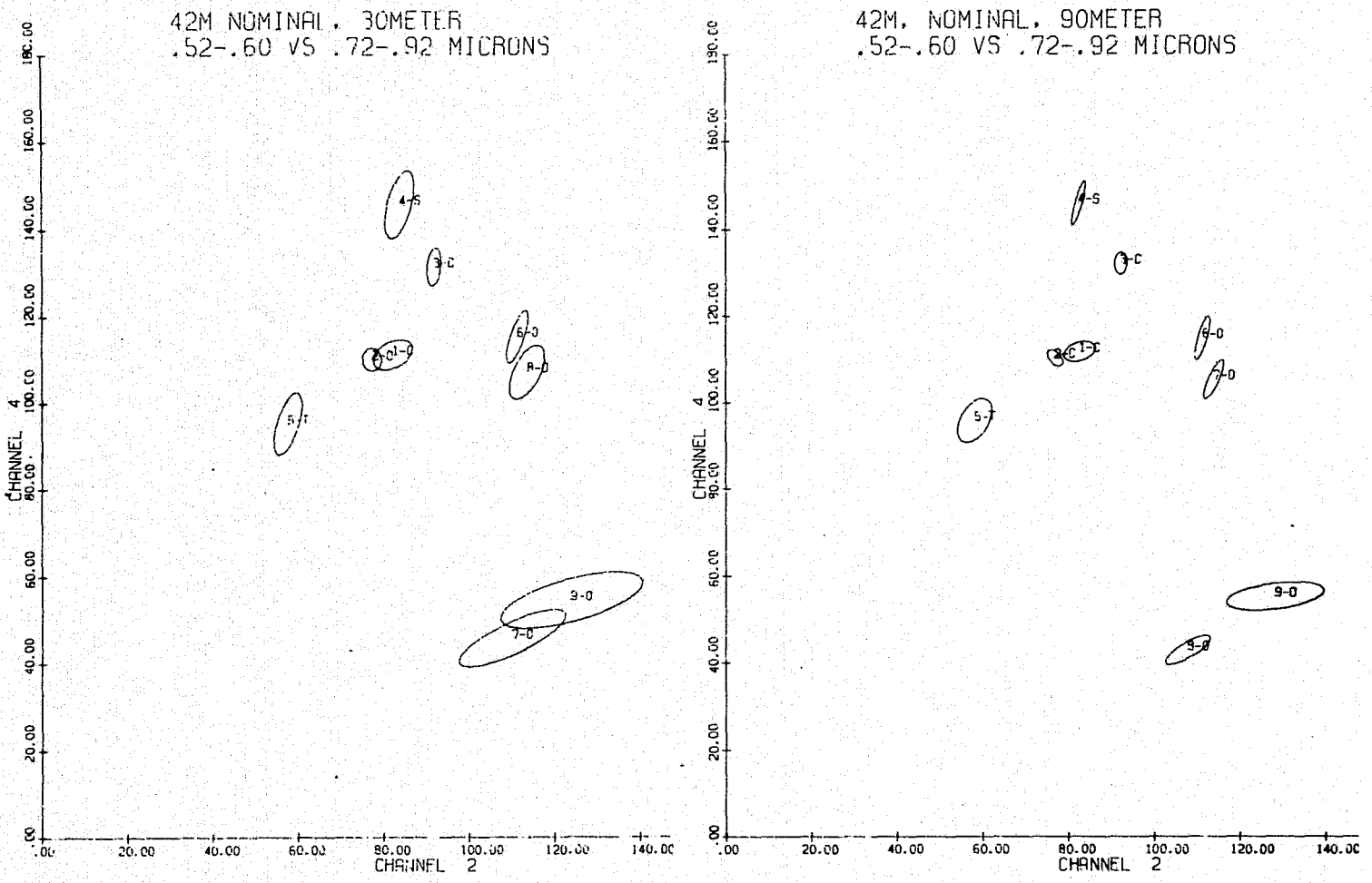

FIGURE 3. TWO-BAND ELLIPSE PLOTS OF TRAINING SIGNATURE SHOWING REDUCTION OF SIGNATURE VOLUME BETWEEN 30 and 90 METER DATA

For a sensor system aimed primarily at measuring acreage planted to a given crop, per field scoring would be the correct method of evaluation, i.e., eliminating effects of small scale anomalies within fields. Alternatively, for a sensor system designed primarily to measure productive acreage or yield, it is important to recognize only vigorous and productive samples of the crop. To evaluate parameters for this kind of system, the appropriate scoring method should be used. Unfortunately, the necessary detailed ground truth to properly evaluate results based on productive acreage was not available; the available ground truth was given only as acres planted, not productive acreage. The judgement was that increases in field center classification accuracy with coarsening spatial resolution were probably in some measure due to the method of evaluation used which compared number of pixels classified (or productive acreage) to acres planted to. None the less, the scoring method used was the best which could be employed under the circumstances and, in our judgement, has not led to erroneous conclusions.

Thus, we see that the effects in center field pixels are that accuracy generally increases with coarsening resolution -- up to the point where an insufficiency of training pixels results in an increase in "unclassified" pixels and, a subsequent decrease in accuracy. For the data sets examined, a maximum for classification accuracy is reached in the range 30-60 meters. However, it is judged that the differences in classification accuracy observed in this range are sufficiently small in most cases as to be in the realm of experimental error and are therefore probably not of significance. By experimental error we mean the scope of change which might result in the event that different training or scoring procedures would be used.

In conclusion, as was surmised at the beginning, field center classification accuracy of pure samples is largely unaffected by the

choice of resolution when a sufficient number of pixels are available for training. What is affected by resolution is the proportion of the scene which is field center (this is explored further in Section 3.1.3). Thus as resolution coarsens, less and less of the scene is described by the field center results and, additionally, the training procedures become much more problematical.

3.1.2 ANALYSIS OF AREA MENSURATION ACCURACY

As mentioned previously, area mensuration is the major criterion to be used in evaluating the effects of changing spatial resolutions. Area mensuration is essentially the combination of classification accuracy over field center and non-field center (boundary) pixels. With coarsening resolution the ratio of boundary to field center pixels increases and one may expect that, without compensating errors, the area mensuration accuracy will be affected.

The area mensuration results were calculated over all four classes in the scene: corn, soybeans, trees, and "other". Typically, what is calculated is the mean square error* over all classes and these results are presented in Figure 4 for the common field training procedure. (Complete tabular results are given in Appendix IV.) In Figure 4 the results appear constant over the range 30- to 40-meters, with the

---

* Mean square error is defined as:

$$E_{RMS} = \left(\frac{1}{n} \sum_{i=1}^{\text{Class}} (\hat{p}_i - p_i)^2 \right)^{1/2}$$

where

$\hat{p}_i$ is the estimated proportion of class i

p_i is the true proportion of class i

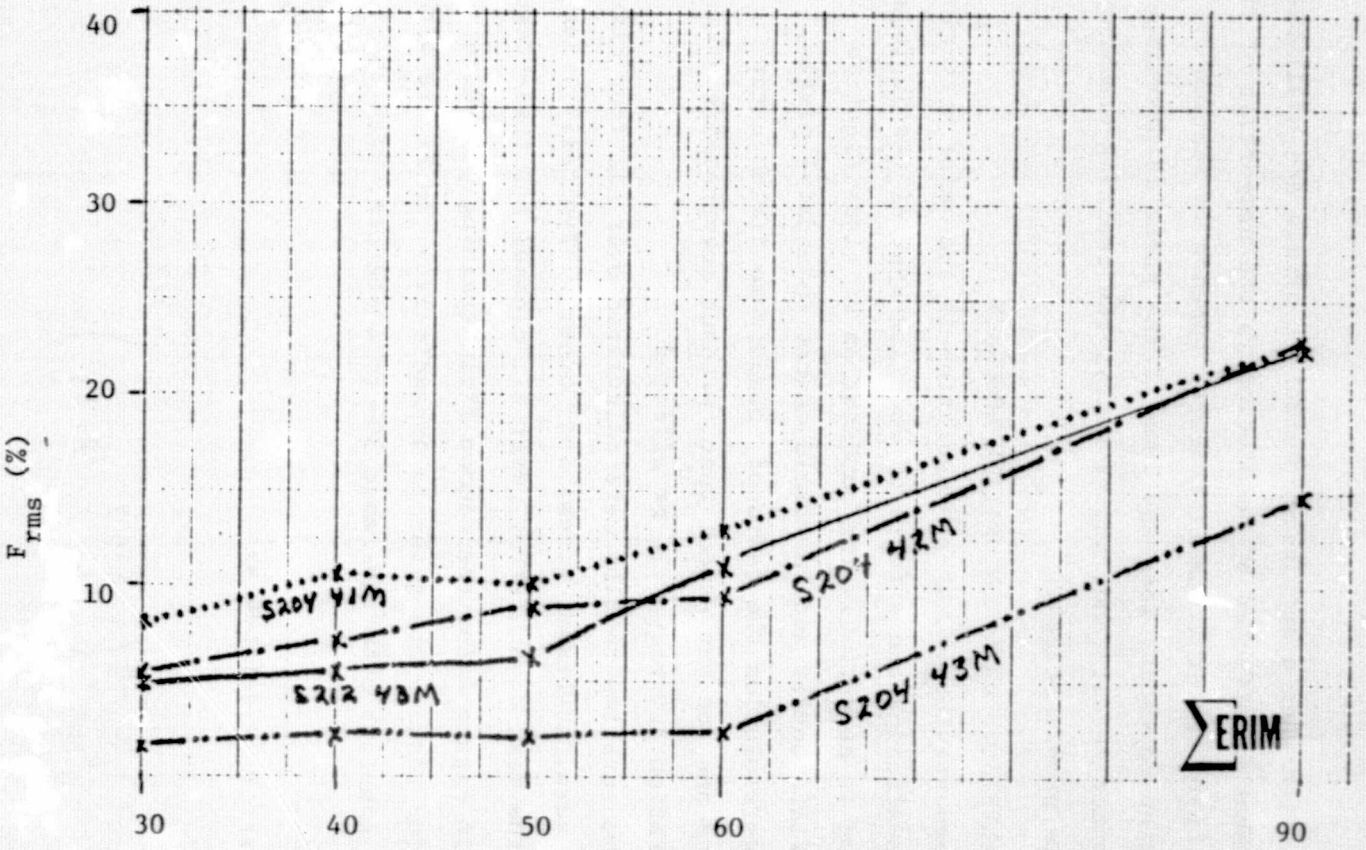

FIGURE 4. ROOT-MEAN-SQUARE-ERROR IN OVERALL PROPORTION ESTIMATIONS -- (FIELD SIGNATURE TRAINING PROCEDURE)

error rate then increasing as the spatial resolution approaches 90 meters. The rise in error at 90-meters resolution is understood in the same terms as for the field center results. At 90 meters, the large error is attributable to the increase in the number of unclassified pixels due to the reduced size of the signatures, as previously discussed.

While mean square error is a standard statistical measure, it is not a measure always intuitively understood for significant differences. As an alternative, the results were tabulated as shown in Fig. 5 where a different measure, relative proportion estimates and relative errors, are used; the formulas defining them are given on the figure.

Examining Figure 5 we see that the S-204, 13 Aug (43M) data set, which was gathered at a time of year which was close to optimal for spectral discriminability of the classes in the scene, shows no change in the range 30-60 meters. However, the other data sets show definite loss in accuracy with spatial resolution coarsening from 30 meters. The July 12 data (41M) in fact drops almost 10% in overall accuracy for each 10-meter increase in spatial resolution. For the other data sets, the decrease in accuracy for resolution 50-90 meters is also significant.

Another point to consider in interpreting the mensuration accuracy results is the bias introduced by the manner of training. At 90 meters, the training statistics accurately reflect a sizeable portion of all field center pixels in the scene. At successive finer spatial resolutions the proportion of field center pixels represented by the training statistics declines quickly. In other words, field center pixels at finer resolutions display much more within-class spectral variability than is evident in the training data. This results in an increase in field center classification errors. Thus, the bias introduced in the training process favors the coarser resolutions. This means that were this bias removed, the mensuration accu-

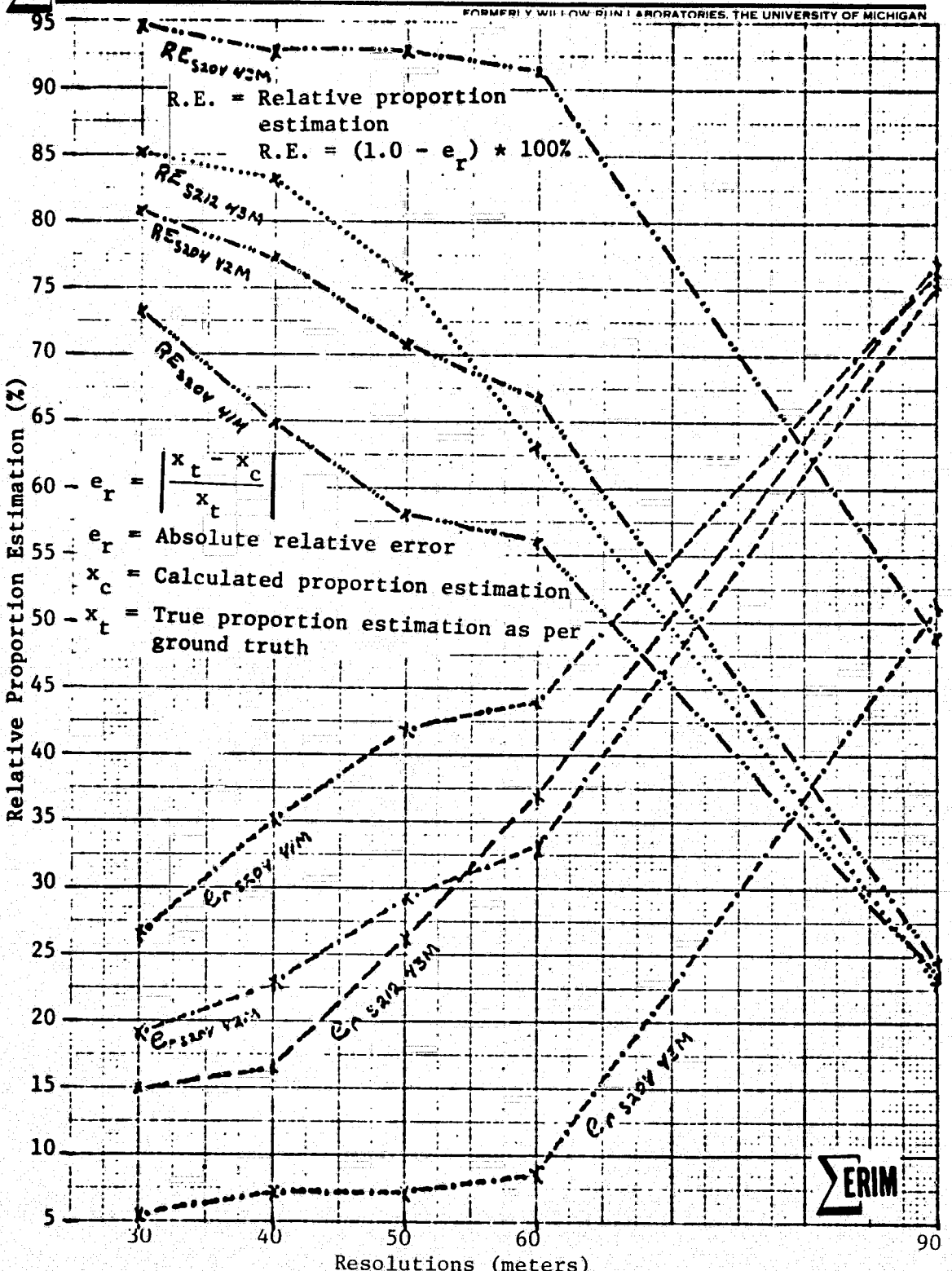

FIGURE 5. PROPORTION ESTIMATION WEIGHTED OVER ALL CLASSES

racies would be shown to increase more significantly with increasing spatial resolution. As evidence of this, we present the mensuration results achieved for the S-204, Aug. 13 data where the training procedure utilized all available fields at each resolution. Figure 6 compares these results as RMS errors to those previously presented for the common field training procedure. The differences observed at 30 and 40 meter spatial resolution show the bias inherent in the results achieved using the common field training procedure. Figures 4 and 5, therefore, include some bias and the truer, unbiased results would more strongly accent the maximums for mensuration accuracy attained at 30 and 40 meter spatial resolutions.

In conclusion, the mensuration results which are specific to the field size distributions and classes studied, indicate that the most accurate results accrue using 30 meter spatial resolution, and the loss of accuracy in going to 40 meter resolution, in some instances, can be significant. In all cases, significant decreases in accuracy occur for spatial resolutions in the 50 to 90 meter range.

3.1.3 GENERALIZATION OF SPATIAL RESOLUTION RESULTS TO OTHER FIELD SIZE DISTRIBUTIONS

Since all scenes consist of field center and boundary pixels, by understanding classification rates for these two groups of pixels the results obtained for the specific field size distributions studied can be generalized to any given field size distribution. Obviously, it is important to base design specifications on the range of scenes expected to be viewed by the Landsat Follow-on satellites, and not just on one specific instance.

Thus, one further analysis, this on the classification trends of boundary pixels, was undertaken. An attempt was made to find in the data as many examples as possible of two-class boundary pixels. Unfortunately, the number of such pixels found for each pair of classes was insufficient for any meaningful inferences to be drawn.

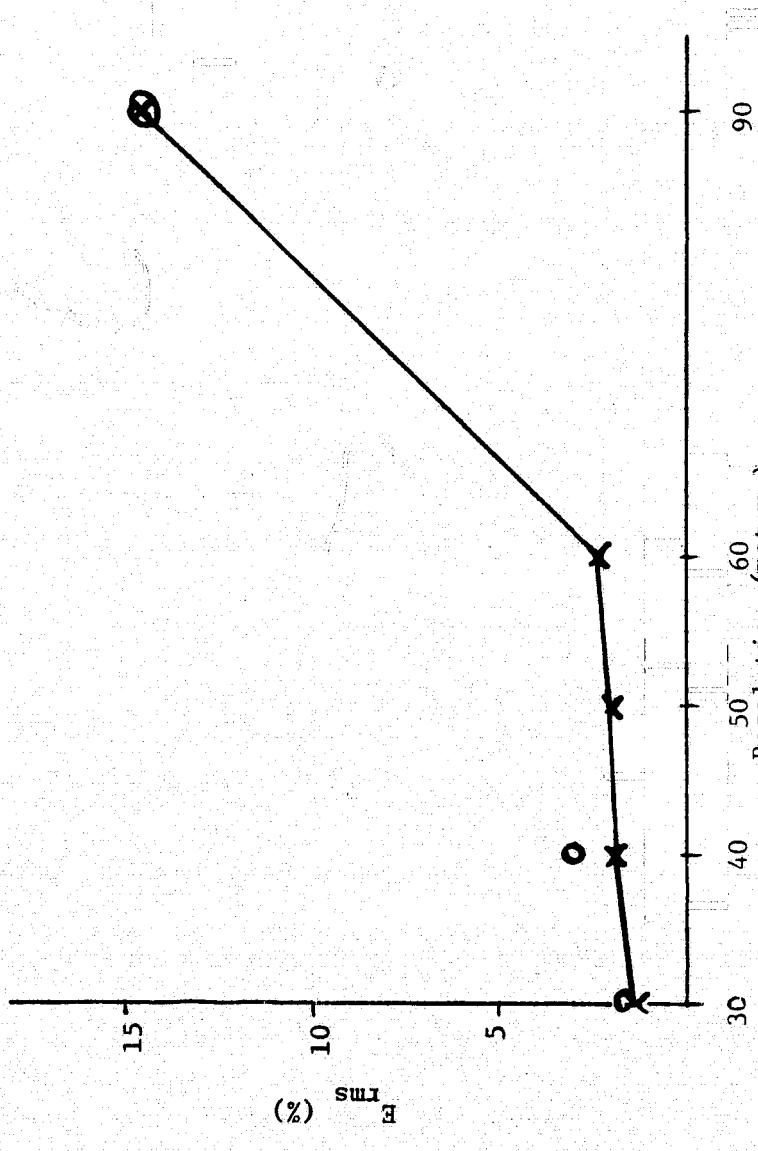

FIGURE 6. COMPARISON OF PROPORTION ESTIMATES BETWEEN TRAINING USING:

Instead, it was determined to carry out this part of the study using the ERIM simulation classifier which was modified to produce hundreds of two-class mixture pixels for each pair of classes for each exact mixture specified. Combining the output from this simulation, with the outputs from simulations carried out for field center pixels and a model which calculates the field center and boundary proportions of a specified scene (field size distribution and overall true proportion of classes within the scene), we were able to calculate expected mensuration accuracy as a function of field size distribution. The exact algorithm, and detailed procedures employed in arriving at the results discussed below are given in Appendix V, while tables of results are in Appendix VI. The results are discussed below, after a short explanation of the approach.

Briefly, a set of scenes were defined, each composed of the classes found in the Indiana sites in roughly the same proportions and containing, respectively, 1, 2, 4, 8 and 16 hectare fields only (2.5, 5, 10, 20, 40 acres) where each field was rectangular with aspect ratio 2:1 (this being approximately the average aspect ratio worldwide) [11]. Then each of these scenes was assumed to be scanned by instruments with resolutions of 30, 40, 50, 60 and 90 meters and with the scan plane being square to the field boundaries. (Such a scanning scheme, in general, will produce fewer boundary pixels than an oblique scan would.) The model further assumed that at no time were two fields of the same class located next to one another and that all boundary pixels were two-class boundaries. At fine resolutions and small fields, the proportion of 4-class mixtures is insignificant. We recognize that for coarse resolutions and larger field sizes, the number of 4-class mixtures is significant, however, this study did not attempt to analyze classification trends for 4-class mixtures and the effect upon the results reported is indeterminate.

The results of the calculation for proportion of field center pixels in each scene is given in Figure 7, where a marked reduction in such proportion with coarsening spatial resolution is seen. As a matter of fact, no 90-meter field center pixels are available from fields smaller than 1.6 hectares, for an aspect ratio of 2:1.

The basic classification probabilities were calculated for each of the four 30 meter data sets using the signatures from all available fields. Classification probabilities for simulated mixture pixels were calculated for numerous samples of pairwise combinations of corn, soybeans, trees and the "other" classes -- water, winter wheat, oats, hay, pasture and diverted. Mixtures of each combination of classes were simulated for porportions ranging from 0/1.0 to 1.0/0 in steps of size 0.1.

Examples of two particular outputs from the simulated boundary pixel classification are illustrated in Figures 8 and 9, showing results achieved for the pair corn-soybeans and the pair pasture and trees, respectively.

In Figure 8, we see the expected results of high classification accuracy for corn at high proportions of corn and the same effect for soybeans with a reduction in both as the 50-50 mixture is approached. In Figure 9, we have an example of a combination of classes (pasture and trees) whose mixture produces significant false corn classifications. Therefore, if many combinations of pasture and trees exist in the scene, the proportion of corn could be seriously overestimated. Additional samples of simulated boundary pixel classification are provided in Appendix V.

Using such data as input, expected area mensuration for each scene and each scanner resolution were calculated using Eq. (V.10) and the procedures given in Appendix V, and a measure of the accuracy, relative proportion estimation which was introduced earlier, was computed. For analysis, the weighted average over all classes was plotted, Figures 10-13.

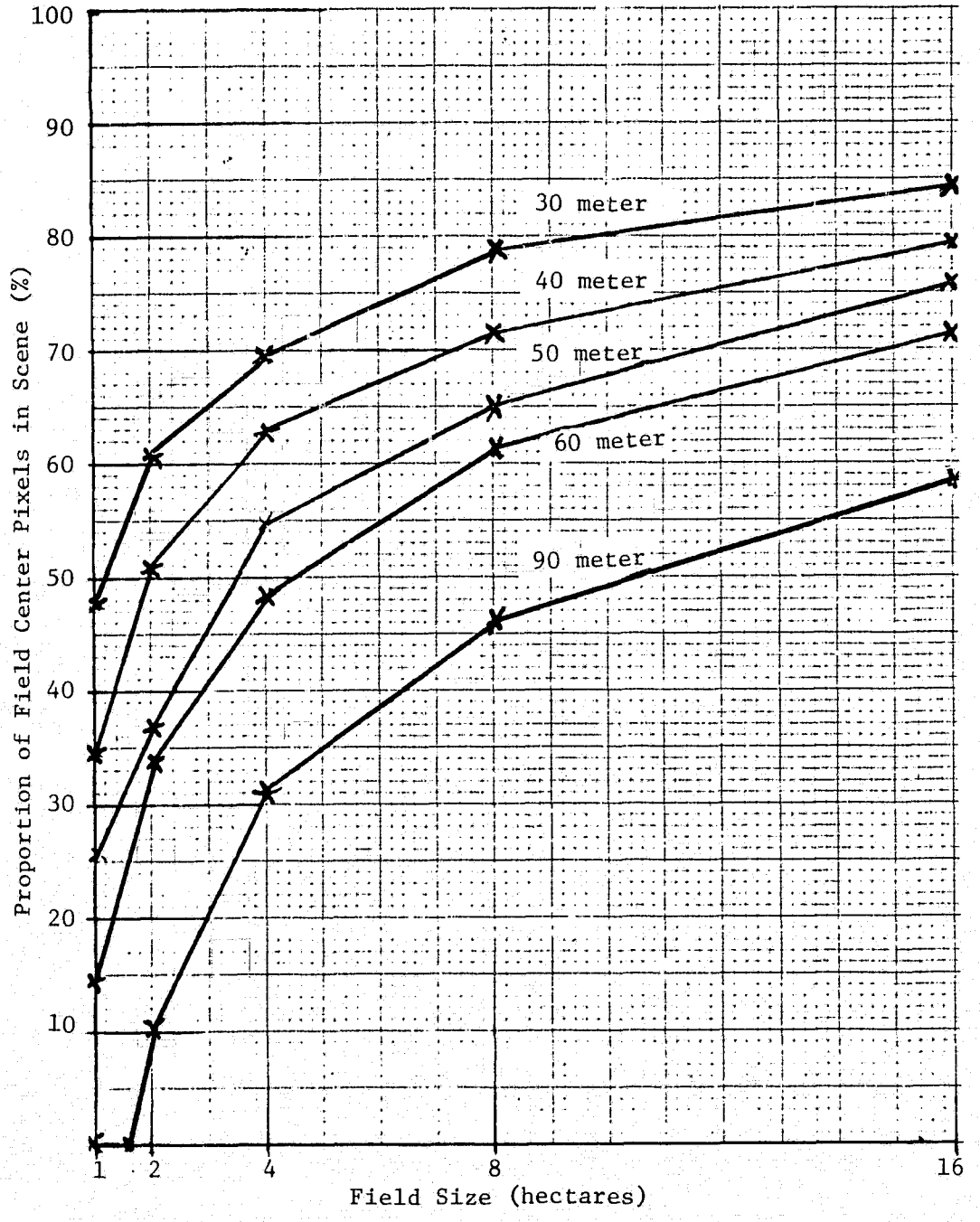

FIGURE 7. PROPORTION OF PIXELS IN SCENE WHICH ARE FIELD CENTER AS A FUNCTION OF FIELD SIZE (2:1 ASPECT RATIO) WITH SENSOR SPATIAL RESOLUTION AS A PARAMETER

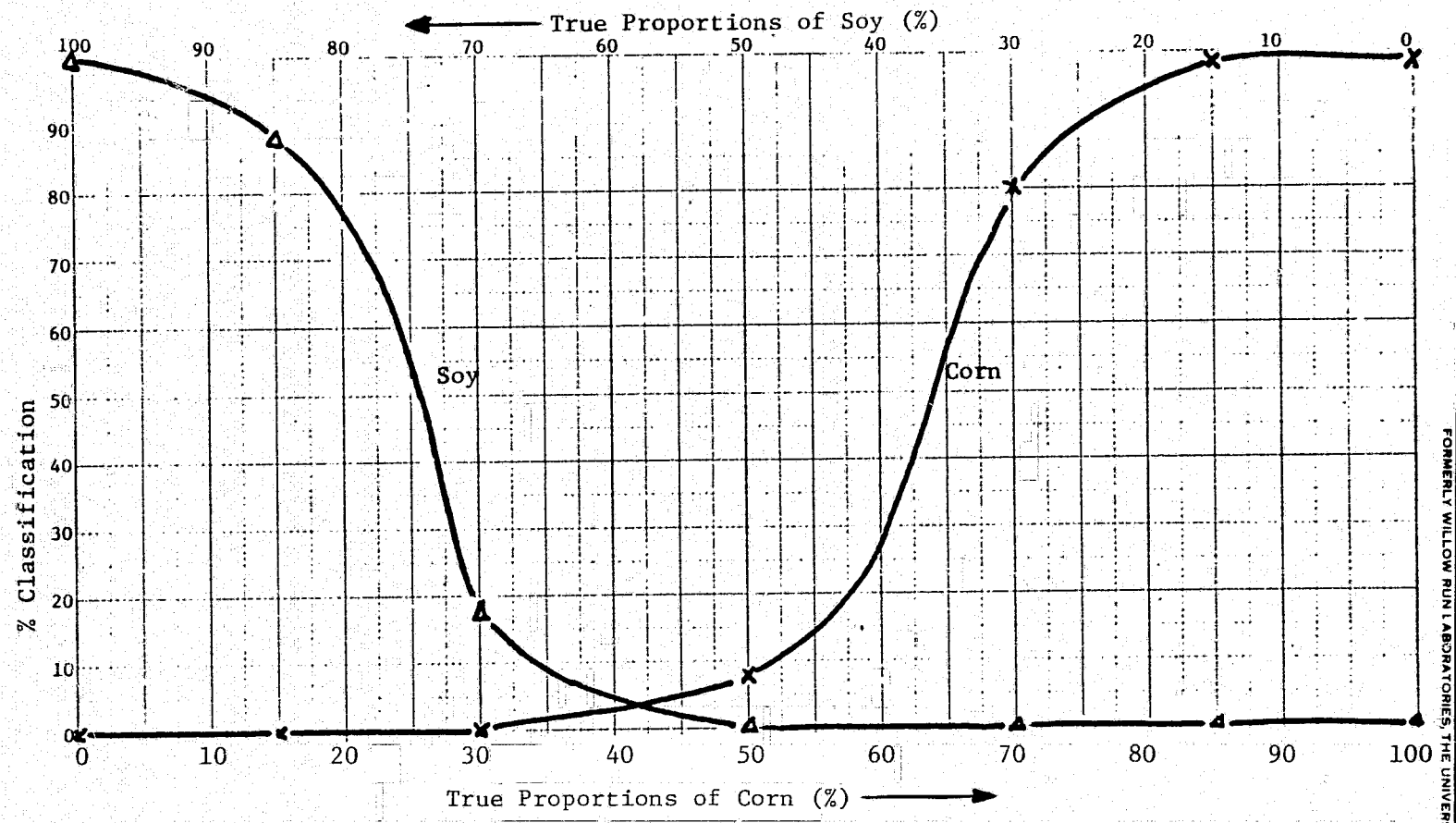

FIGURE 8. MIXTURE PIXEL CLASSIFICATION RESULTS (Corn-Soy Mixture)
Data Set: S-204, 43M

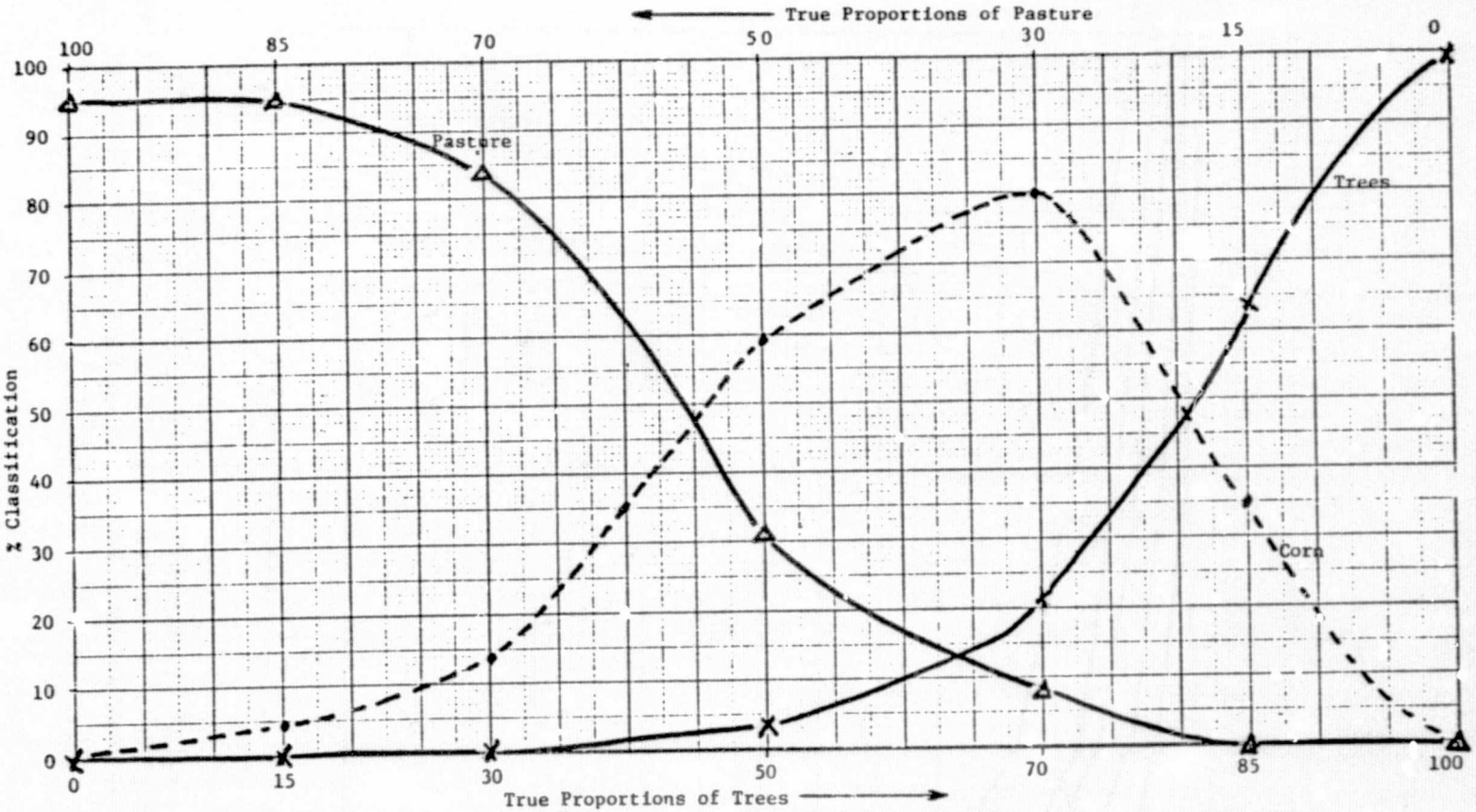

FIGURE 9. MIXTURE PIXEL CLASSIFICATION RESULTS (Pasture-Tree Mixture)
Data Set: S-204,43M

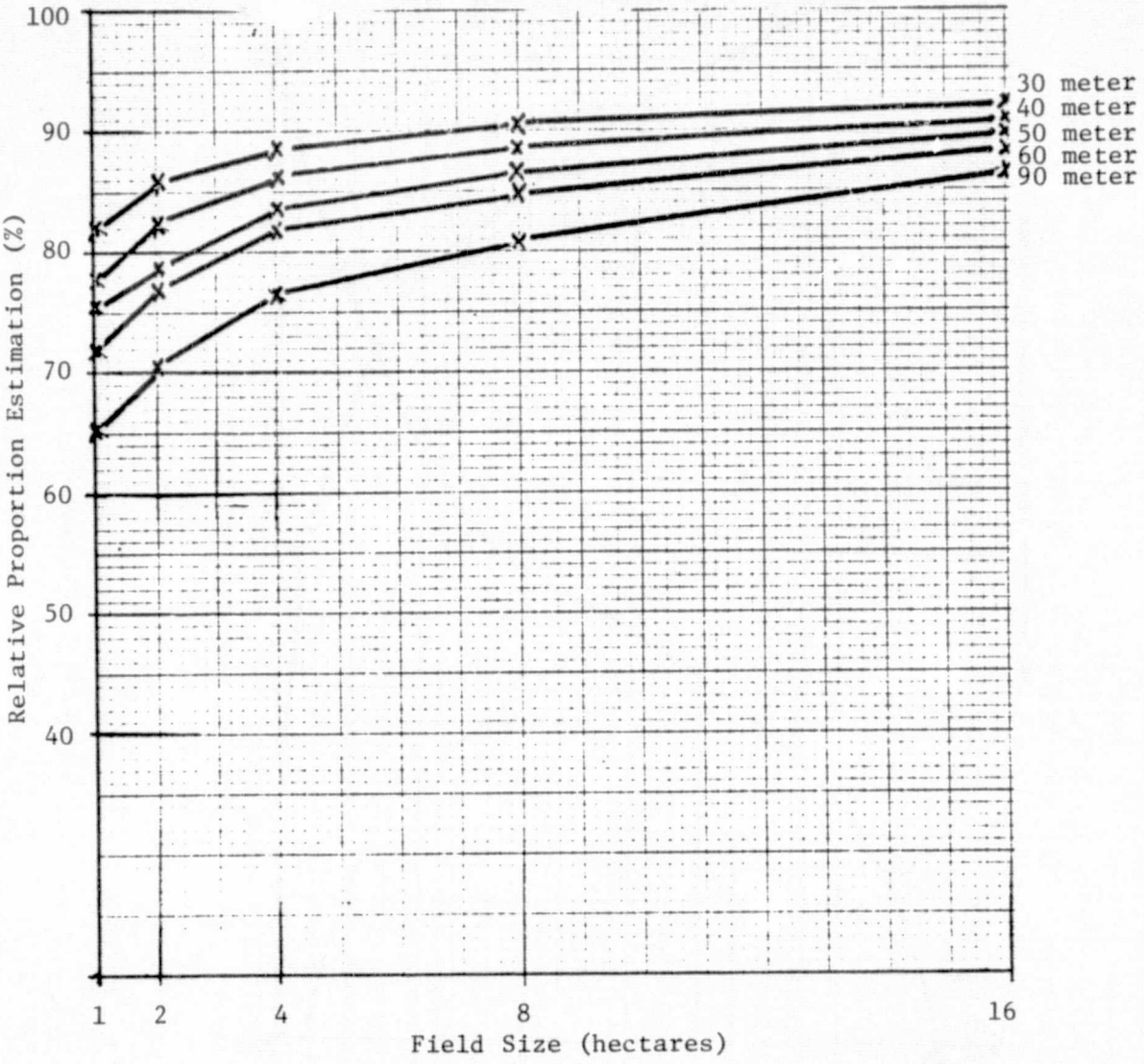

FIGURE 10. RELATIVE PROPORTION ESTIMATION (WEIGHTED OVER ALL CLASSES) AS A FUNCTION OF FIELD SIZE (2:1 ASPECT RATIO) WITH SENSOR SPATIAL RESOLUTION AS A PARAMETER -- DATA SET: S-204, 41M

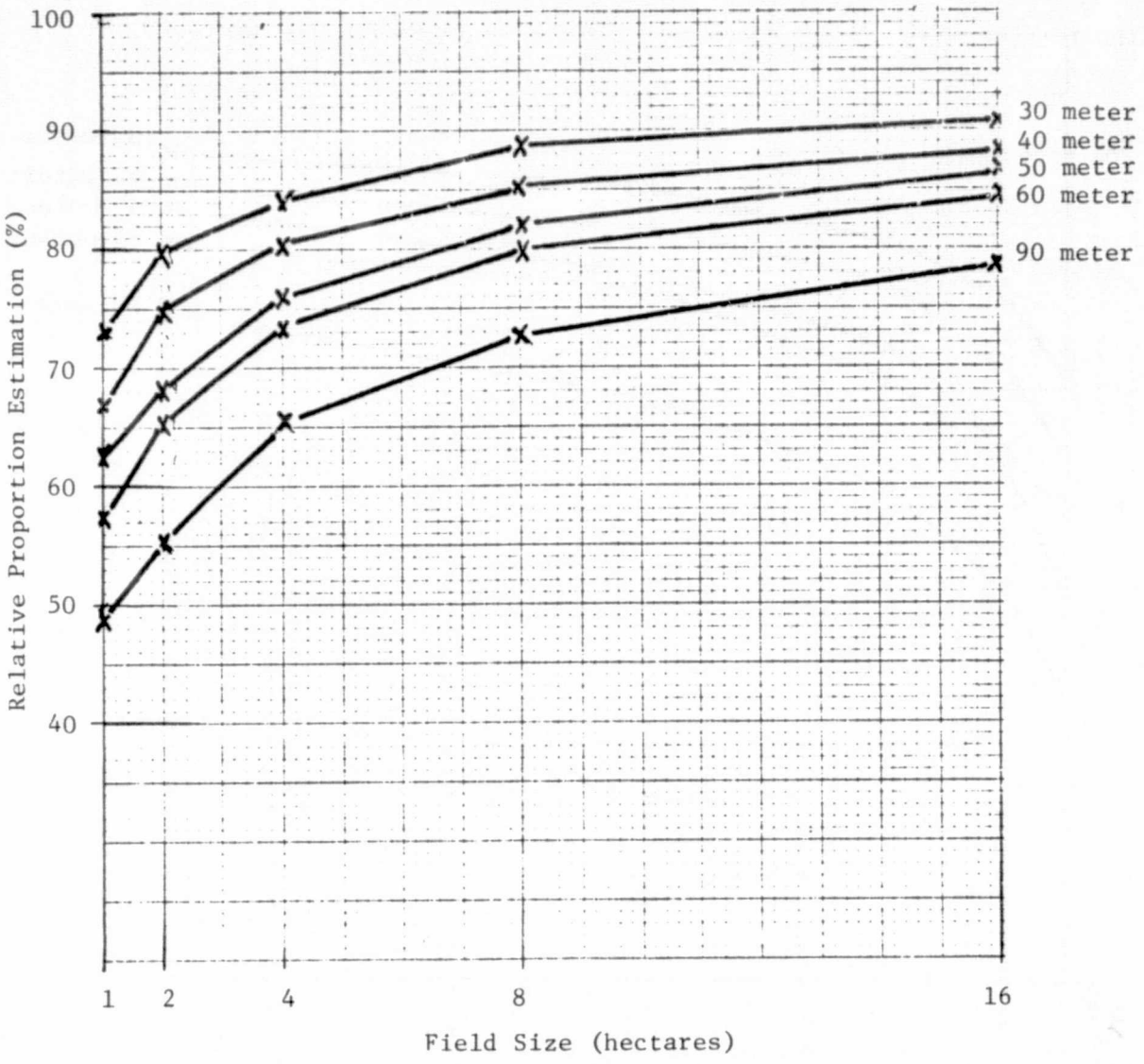

FIGURE 11. RELATIVE PROPORTION ESTIMATION (WEIGHTED OVER ALL CLASSES) AS A FUNCTION OF FIELD SIZE (2:1 ASPECT RATIO WITH SENSOR SPATIAL RESOLUTION AS A PARAMETER -- Data Set: S-204, 42M

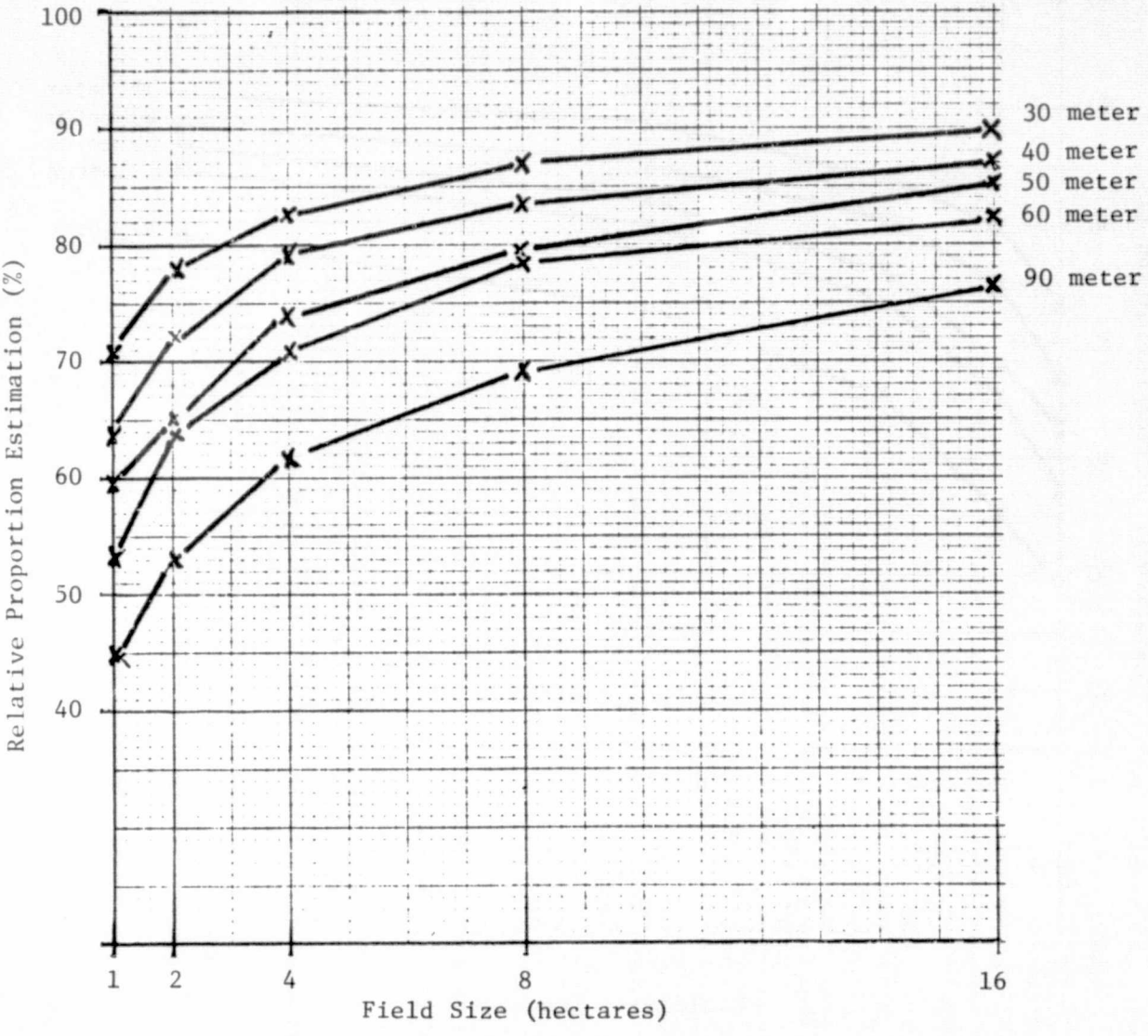

FIGURE 12. RELATIVE PROPORTION ESTIMATION (WEIGHTED OVER ALL CLASSES) AS A FUNCTION OF FIELD SIZE (2:1 ASPECT RATIO) WITH SENSOR SPATIAL RESOLUTION AS A PARAMETER -- DATA SET: S-204,43M

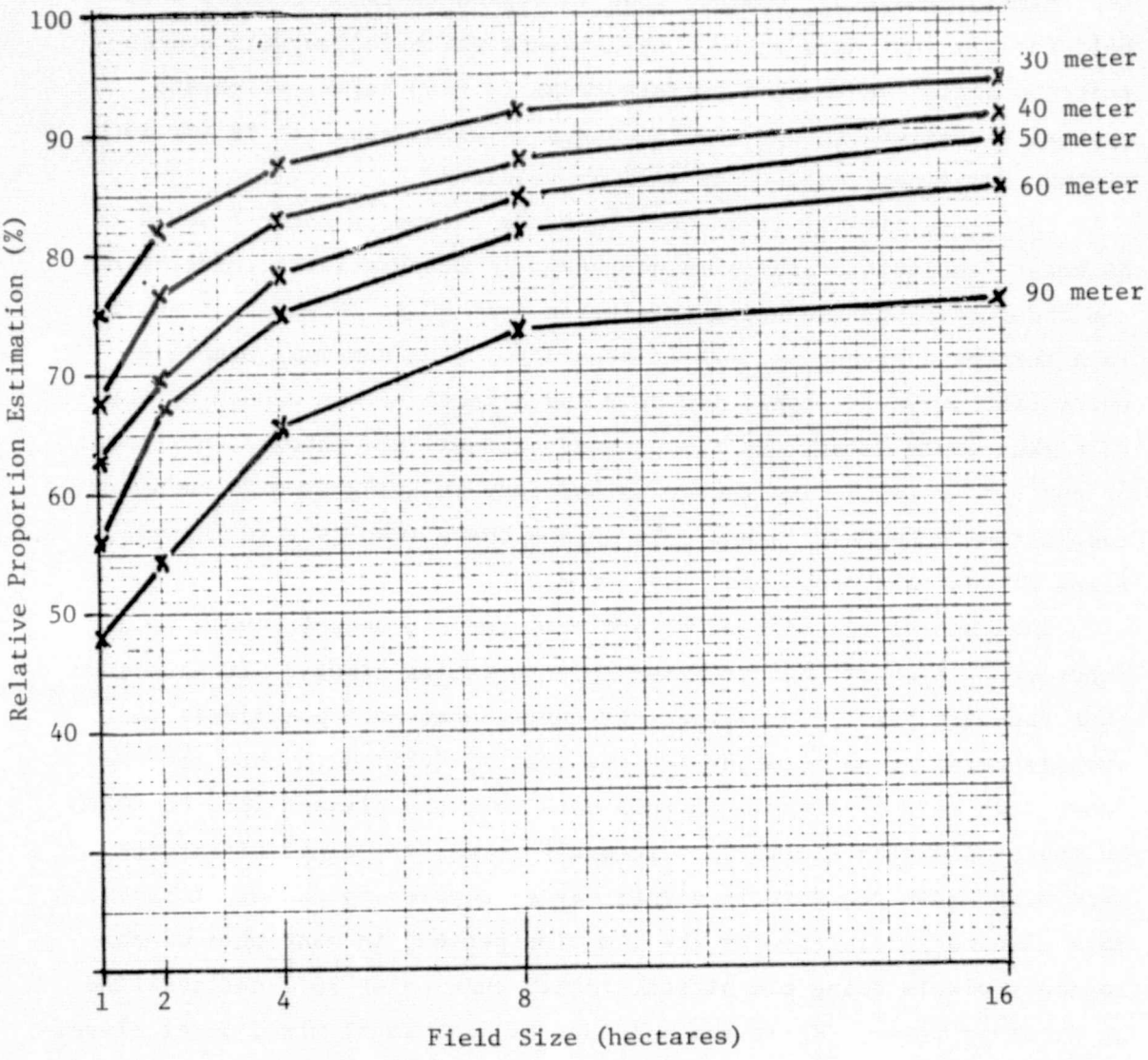

FIGURE 13. RELATIVE PROPORTION ESTIMATION (WEIGHTED OVER ALL CLASSES) AS A FUNCTION OF FIELD SIZE (2:1 ASPECT RATIO) WITH SENSOR SPATIAL RESOLUTION AS A PARAMETER -- DATA SET: S-212,43M

In general, the shapes of the curves for the four data sets are very similar and thus comments made in regard to these results will hold for all four data sets. The comments which follow will concentrate on fields in the 1-4 hectare range (2.5-10 acres) which are typical of Western Europe, India, parts of Asia, etc. It is for such fields that finer resolutions will be required.

For these fields, it is seen that the change in going from 30 to 40 meter resolution results in decreases in mensuration accuracies on the order of 4-6%. Changing resolution from 40 to 50 meters results in a further decrease of 5-7% in accuracy. (The somewhat anomalous points for 50-meter resolution at 2 and 8 hectares are caused by the fact that field dimensions (in both directions) are integral multiples of the resolution.) The change in accuracy in going from 30 to 90 meter resolution is between 15 and 25%. Again these results hold for all times of year and crop conditions studied.

Analysis of classification performance on boundary pixels as a function of time of year produced an interesting result. It was seen that boundary pixel classifications contributed more positively to overall mensuration accuracy for the July 12 (41M) data than for the other data sets studied. For this data set, the classes were found to be spectrally very similar, or in other terms, the class signatures were very close together in signal space compared to the other times. This closeness results, for the 41M time period, in many more of the boundary pixels being classified, rather than being left unclassified as at other times. While the accuracy of individual mixed pixel classifications may not be great, and errors of commission tend to be large but may be compensating, nevertheless the increased numbers of pixels classified as corn, soy, trees or other at this time tended to increase the overall mensuration accuracy not decrease it as at other times.

An accompanying trend for data characterized by spectrally similar classes, the tendency toward slightly less accuracy in field center

classifications, produced another intuitively unexpected result: mensuration accuracy increased as the proportion of boundary pixels increased for this case (Appendix VI, Table VI.2). Whether errors will usually compensate on the boundaries with some determinable bias which is a function of class mixtures is a question for which additional analysis is required before an answer can be given.

In conclusion we have shown a definite relationship between spatial resolution and accuracy in area mensuration. Spatial resolution of 30 meters is shown to increase accuracy generally by 4-6% for many field size distributions over that achieved with 40 meter resolution, independent of time of year.

The manner in which spatial resolution can be traded for radiometric sensitivity will be addressed in Section 4, after presentation of results for the radiometric sensitivity study.

3.2 RADIOMETRIC SENSITIVITY STUDY

Analysis of the effects of changing radiometric sensitivity on classification accuracy was accomplished using the ERIM simulation classifier; the models and procedures involved are fully described in Appendix VII. To briefly describe them, a set of signatures for a particular data set and resolution are used to define decision boundaries. The pixels in the "scene" are randomly generated from each of the distributions represented by these signatures and are classified. Different levels of radiometric sensitivity are simulated by adding corresponding amounts of noise to the covariance matrices of the signatures.

The simulation was run for all four data sets, for simulated spatial resolutions of 30 and 40 meters. For each of these, two signature sets were used, one acquired using the common field training procedure and the other acquired using the all-field training procedure.

The discussion here will focus only on results obtained from the latter, as it more realistically simulated the extent of spectral variation which would be expected in a real scene.

The nominally specified radiometric sensitivities* for TM were for one-half percent NE$\Delta\rho$ (noise equivalent reflectance) for the first four bands (i.e., those between 0.4 and 1.0 μm), one percent NE$\Delta\rho$ for the 1.55-1.75 near IR band and one-half degree Kelvin NEΔT for the thermal band. Other radiometric sensitivities studied were taken to be multiples of these base line values. For this study, then, simulations were carried out for the set of noise levels {0.5, 1.0, 1.3, 1.6, 2.0, 3.0, 6.0, 10.0, and 20.0} times the nominal case.

Inspection of Figure 14 (an example of the results presented more fully in Appendix VIII) shows that, generally speaking, correct classification rates decrease with increasing noise levels, as expected. The point at which the fall-off becomes significant varies between data sets and for classes within data sets. In general the figure shows that where spectral separability is least, for the July 12 (41M) data, the overall fall off is immediate from the half-nominal point, and falls significantly (7%) between the nominal and twice nominal cases. Even for the August 13 (43M) data, where it appears that the overall loss in accuracy between nominal and twice nominal noise levels is less than two percent, it is seen that the decrease in classification accuracy of corn (the dominant economic class in the scene) is almost 4%. This is much more serious.

The analysis of the effects of radiometric sensitivity on detection of corn blight was carried out for the S-212 data set. It is seen, in Figure 15, that accurate detection of highly blighted corn falls off dramatically from the half-nominal case. The fall off from

---

* As obtained from Dr. Lou Walter, TM Project Scientist, of Goddard Space Flight Center.

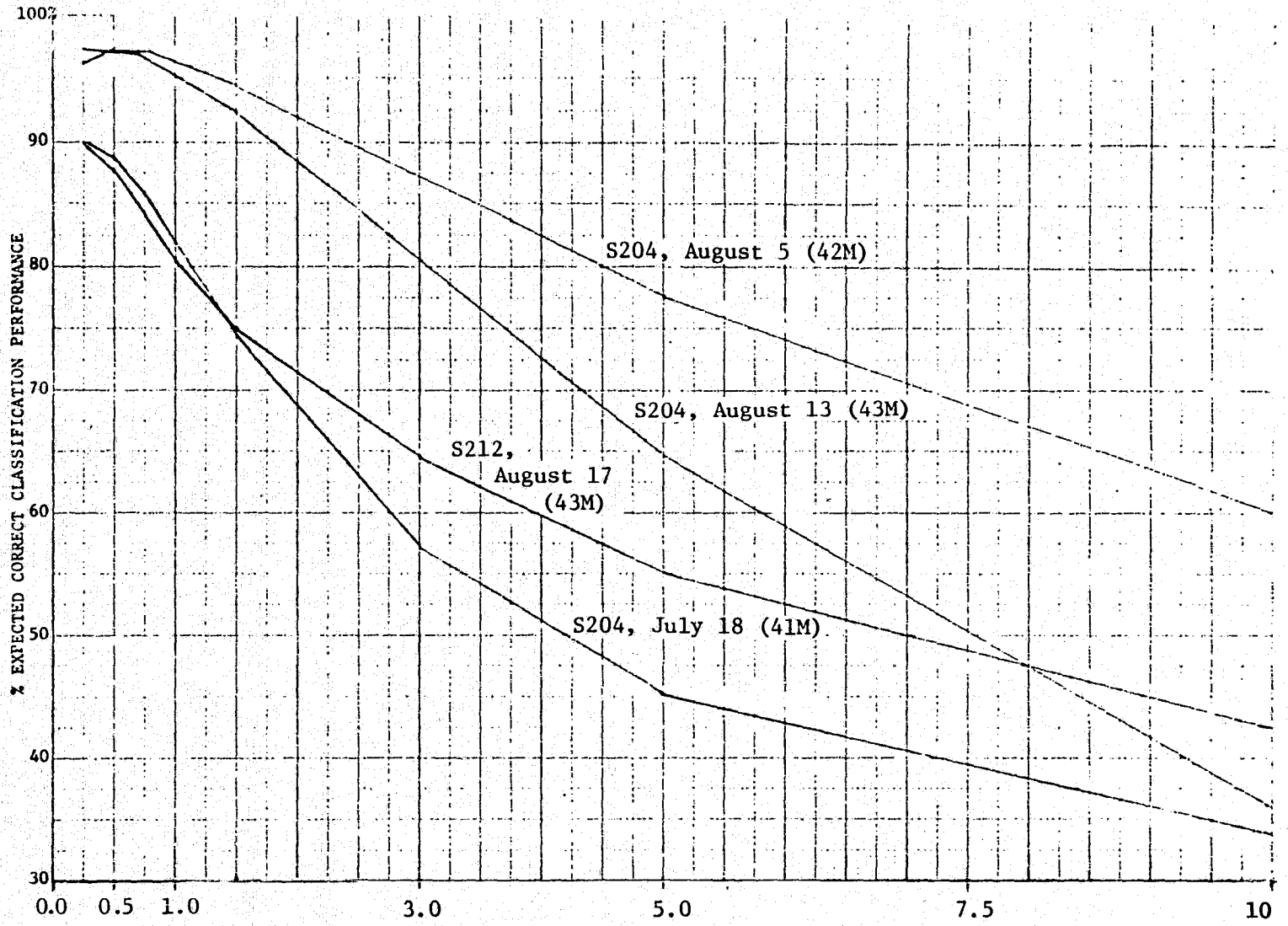

FIGURE 14. RADIOMETRIC SIMULATION -- 30 METER RESOLUTION -- PERFORMANCE OVER ALL CLASSES (All Available Fields In Common Scene Utilized In Training Procedure)

one-half nominal to nominal sensitivity results in a 9% decrease in accuracy, and a further fall off to twice the nominal degrades accuracy an additional 18%. Thus it is seen that discrimination of corn blight as an example of stressed crops requires fine radiometric sensitivity.

Thus for a situation of near optimum discriminability, serious degradation of results ensues from a change in radiometric sensitivity to twice the nominal. In cases where discrimination is not optimum or where crop stress such as corn blight is being assessed, severe degradation in accuracy follows with immediate relaxation from the nominally specified set of values.

Two unexpected effects can be seen in the results. The first, a decrease in "other" classifications for the half-nominal case in some instances is understood by noting there was an increase in "unclassified" pixels for this case -- due to the small volume of the signatures. The other, an increase in accuracy of the 40 meter data over that of the 30 meter data arises because the former did not include signatures from as much of the area as the latter, and hence considered less natural scene variability. Fewer confusion classes thus yield the marginally better results observed for 40 meter resolution.

The simulation results reported above showed how field center classification accuracy was affected by changes in radiometric sensitivity. These are very insightful results, but they do not directly compare with the expected mensuration accuracies. Mensuration accuracy is a complex function of many factors, only one of which is field center accuracy. For this effort, we have studied only a few examples and these are not sufficient to allow a full extrapolation of these field center classification results to mensuration accuracy. In general it is expected that a decrease in field center accuracy would

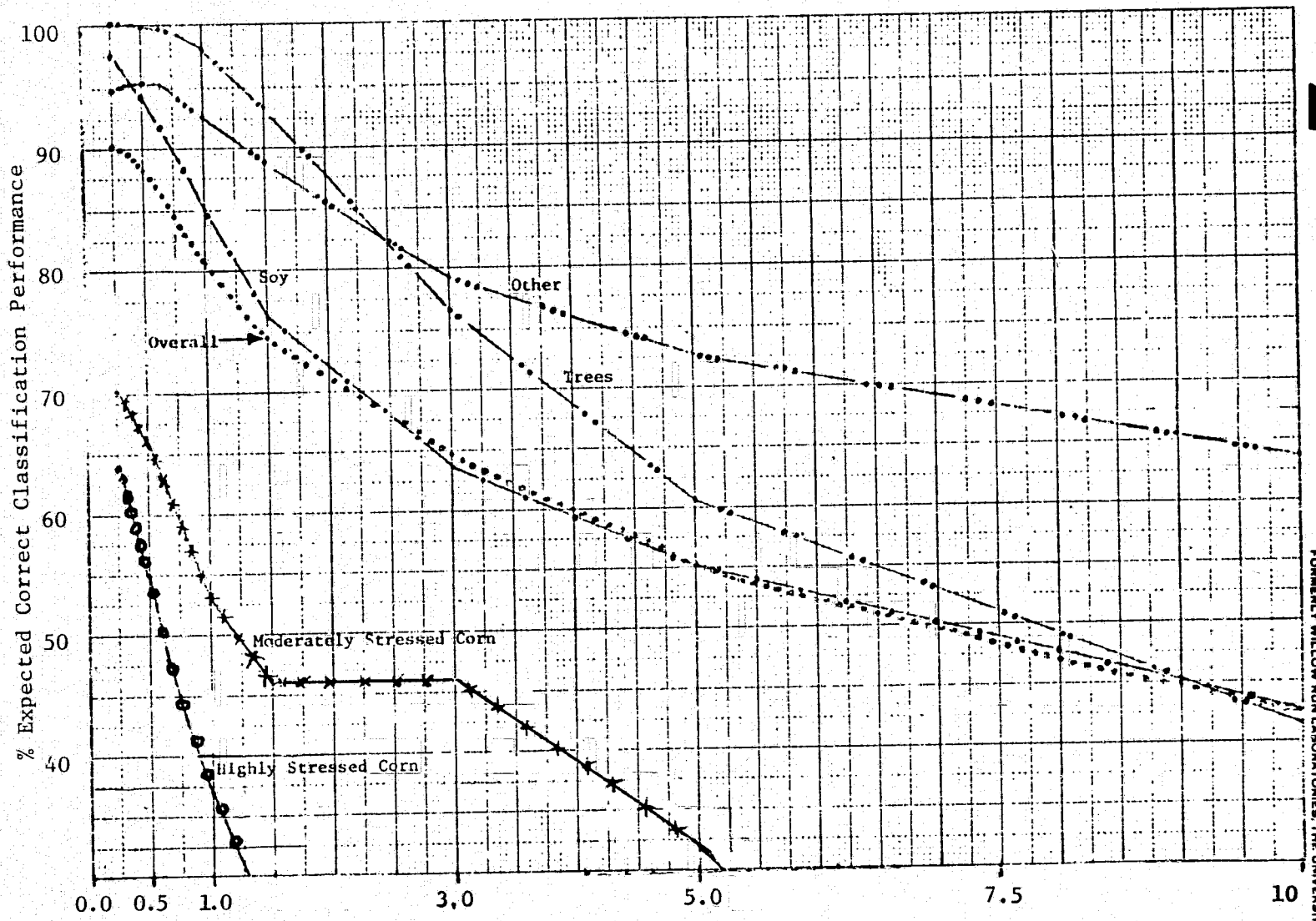

FIGURE 15. RADIOMETRIC SIMULATION -- Segment S212, August 17 (43M) -- 30 METER RESOLUTION (All Available Fields Used In Training Procedure)

result in a decrease in mensuration accuracy, although it does not follow that the two decreases would necessarily be of the same order. In fact, there can be cases which run counter to this intuition.

3.3 STUDY OF EFFECTS OF 120 METER THERMAL BAND RESOLUTION

Because of mirror size and hence Rayleigh limit (wavelength over diameter) considerations, it is expected that the resolution of the thermal band will be 120 meters -- three to four times that of the other bands. The spatial simulations which had been carried out to this point had assumed that all bands had the same resolution.

Thus, an investigation into the impact of using 120 meter resolution for the thermal band was undertaken to analyze the effects of a larger thermal band IFOV along with the 30 meter data. It is recognized that the thermal band is useful as a "temperature" mapper for some users and that the physical attribute sensed is not diagnostic in the same sense as what the reflective bands see, however we restricted ourselves here to the crop mensuration application under the assumption the thermal band will often offer information to aid discrimination if the time of overpass is not too far from local solar noon. The 30 meter data was used because this was considered the likeliest TM spatial resolution. In simulating the coarser resolution, sampling was done for each 30 meter pixel -- i.e., by oversampling the 120 meter resolution thermal band. A moving window averaging algorithm was employed such that the middle of the window coincided with the middle of each 30 meter pixel; the spatial weighting function used is shown in Figure 16. For each 30 meter pixel, a value for the 120 meter resolution thermal band was calculated using the values from the thermal channel of the surrounding 24 pixels, thus effectively simulating an oversampled thermal band. As part of the averaging process,

Scan Lines \ Scan Points					
	.25	.50	.50	.50	.25
	.50	1.0	1.0	1.0	.50
	.50	1.0	1.0	1.0	.50
	.50	1.0	1.0	1.0	.50
	.25	.50	.50	.50	.25

FIGURE 16. WEIGHTING FUNCTION (UNNORMALIZED) USED FOR SIMULATING 120 METER THERMAL BAND IFOV FOR 30 METER DATA (Grid of 25 pixels used to simulate 120 meter thermal IFOV)

sufficient Gaussian noise was added to the resultant thermal data so that the NEΔT stayed at .5^{o}K as specified.

The data prepared in this manner were the 30 meter spatial resolution data for mid-July (41M) S-204 gathered one hour before local solar noon and mid-August (43M) S-204 which had been gathered three hours before local solar noon. These two particular data sets were chosen because they represented, respectively, data where the thermal band helped the most and where it was insignificant. (A more complete discussion of the analysis of spectral band ranking is given in Section 3.4.)

For this particular study, training was carried out exactly as it had been done for the data with 30 meter IFOV in the thermal band, extracting signatures from exactly the same set of fields and pixels within those fields. This means that the pixels selected were field center for the five reflective bands but for the larger IFOV thermal band many if not most of these pixels were now mixtures. It would have been preferable to use only those pixels which were field center in all channels, but for the corn belt sites used in this study there

would have been essentially no field center pixels available for training. Thus, the coarser resolution of the thermal band forced the use of non-pure pixels (in one band) for training purposes.

What then results from such data? Tables 1 and 2 show the results of the 120m thermal IFOV data, for field center classification results and overall proportion estimates, and compares them to the comparable results from the data which had a 30 meter thermal band resolution. The thermal band had been the second best channel for the 41M data set, while its effectiveness had been negligible for the 43M data. Thus, we see in Table 1 that the field center results decline for the 41M data; the 43M results are slightly affected, which shows that not only does the larger IFOV thermal band not help separate classes, but using it increases the confusion between classes and decreases classification accuracy.

Comparison of results as a function of the overall area mensuration results is accomplished using Table 2. The 43M results show a slight increase in overall root-mean-square error using a 120 meter resolution for the thermal band, as was expected. The results for the July 12 (41M) data, however, are not as expected, showing improvement in mensuration accuracy for each of the four classes. This is felt to be an anomalous result attributable possibly to the training procedure that used pixels which were field center in all bands except the thermal band; here the substantially coarser resolution caused many of the pixels in this band to image areas which included other fields. Also, since at this time in the growing season the crops are all spectrally similar, the compensating classification errors improved the results, in this case. To reiterate, it would have been preferable to train only on pixels that imaged field center areas in all bands however it was not possible to train in such a manner for this data set.

The primary conclusions to be reached from this study, therefore, is that use of a thermal band with spatial resolution three or four times that in the other bands will impact the training in that it may

TABLE 1

FIELD CENTER CLASSIFICATION PERFORMANCE MATRICES
30 METER DATA WITH 120 METER THERMAL BAND

(NUMBERS IN PARENTHESES ARE RESULTS USING 30 METER THERMAL BAND)

S204 JULY 12 (41M)

	CORN	SOY	TREES	OTHER	UNCLASSIFIED
Corn	94 (96)	0	1 (1)	1	4 (3)
Soy	1.0	92 (96)	0	5 (2)	2 (2)
Trees	2.6 (1)	.3	95 (94)	.3 (1)	1.8 (4)
Other	0	.7	0	97.6 (98)	1.7 (2)

S204 AUGUST 13 (43M)

Corn	97.6 (98)	1 (1)	0	0	1.4 (1)
Soy	.3 (1)	95.2 (97)	.3	0	4.0 (2)
Trees	.6 (1)	.5	95 (95)	0	3.8 (4)
Other	.3	.5	0	97.2 (98)	2.0 (2)

TABLE 2

ESTIMATED PROPORTIONS OF CLASSES OVER THE ENTIRE SCENE
30 METER DATA WITH 120 METER THERMAL BAND IFOV

	CORN	SOY	TREES	TOTAL OTHER =	(OTHER & UNCLASSIFIED)	ERMS(%)
S204, JULY 12 (41M)	28.9	10.4	9.5	51.3	(26.6 + 24.7)	6.8
(With 30 meter thermal)	(26.8	10.0	8.8	54.3	(25.8 + 28.5)	7.9)
S204, AUGUST 13 (43M)	31.4	12.7	14.4	41.6	(11.9 + 29.7)	1.61
(With 30 meter thermal)	(32.2	12.6	14.1	41.0	(12.0 + 29.0)	1.4)
REAL	33	11	16	40		

not be possible to find pure samples of the classes of interest. It also impacts the classification and indicates that it might not be possible to utilize multivariate pattern recognition techniques using a larger IFOV thermal band in concert with the other TM bands. Thus, in using a thermal band with coarser resolution than the other bands, field center classification accuracy will be impaired as well as overall mensuration accuracy.

3.4 SPECTRAL BAND STUDY

The purpose of the spectral band study was to determine the adequacy of the specified TM bands for agricultural problems -- as a function of the time of year and for the detection of non-systemic crop stress such as corn blight.

The bands considered in the study were the twelve M-7 bands, which cover the spectrum from .45 μm to 2.5 μm plus the thermal infrared. The algorithm used to find the optimum 6 bands tested all possible combinations of 6 bands. The optimum set was the one which minimized the metric used: average pairwise probability of misclassification averaged over all pairs of signatures of dissimilar classes. The signature set used for each of the four data sets was that calculated from the 30 meter resolution data using all fields in the scene. Thus the selection of optimum bands was based on an exhaustive search algorithm using all the classes and sub-classes (spectral variation within each class) for the scene.

The processing outlined above was carried out, and the results are shown in Table 3. As a comparison between the optimum set and the set of TM bands, the ERIM simulation classifier was run for both sets of bands, using the signatures which had been used in selecting the optimum subset. These results are summarized in Table 3 also. To determine the relative importance of each band in the optimum subset, rank orderings were also carried out.

TABLE 3

OPTIMUM 6 BANDS FOR INDIANA CORN BELT DATA

DATA SET	OPTIMUM M-7 BANDS* (IN NUMERICAL ORDER)	OVERALL % CORRECT CLASSIFICATION OPTIMUM BANDS	OVERALL % CORRECT CLASSIFICATION FOR TM BANDS (2,4,7,8,10,12)**
S204, 41M (July 12)	4,7,8,9,11,12	89.9	88.0
S204, 42M (August 5)	2,4,7,8,11,12	92.6	92.6
S204, 43M (August 13)	1,4,7,8,9,10	96.4	96.8
S212, 43M (August 17)	2,4,8,9,10,11	93.5	93.0

** Band designations are:

1 = .46-.49	4 = .52-.57	7 = .61-.70	10 = 1.5-1.8
2 = .48-.51	5 = .54-.60	8 = .72-.92	11 = 2.0-2.6
3 = .50-.54	6 = .58-.65	9 = 1.0-1.4	12 = 9.3-11.7

** TM Bands 1 and 2 were simulated by combining M-7 Bands 1 and 2, and 4 and 5 respectively.

It is certainly encouraging to see the frequency with which TM bands are chosen as members of the optimum set. Three particular results are noted from all the analyses carried out. The first is that the thermal band is important early in the growing season. This result is consistent with experiments run during the Corn Blight Watch Experiment in 1971 [8]. In fact, the rank ordering of the set of TM bands for the July (41M) data shows that the thermal band is second in importance -- only the green band (0.52-0.57 μm) is more important for this time. One must bear in mind, however, the characteristic of the TM thermal band. While this study has used the same spatial resolution in all bands the spatial resolution of the thermal band in the Thematic Mapper is specified to be three to four times that of the other bands. A brief study carried out to determine the effects of coarser thermal resolution, detailed in the preceding section, ranked the larger IFOV thermal band fifth (Figure 17) and more importantly showed that its use did degrade recognition accuracy. This raises questions about the ultimate utility of a thermal band with coarser resolution when used in concert with other bands for processing agricultural data.

Analyses of spectral bands for detection of corn blight was carried out, using rank ordering of bands along with study of the spectral signatures. It was seen that the 0.72-0.92 μm band was the most important band for discriminating between blight levels of corn; the only other band which also aided in this discrimination was the 1.0-1.4 μm band, which was seen to be highly correlated (redundant) with the above band for stress discrimination.

An additional point is that the two M-7 near-IR bands (9 and 11) not included in the TM set are shown to be important. In particular, in ranking the set of optimum bands it was seen that Band 9 is second in importance of all bands for the July (41M) data set.

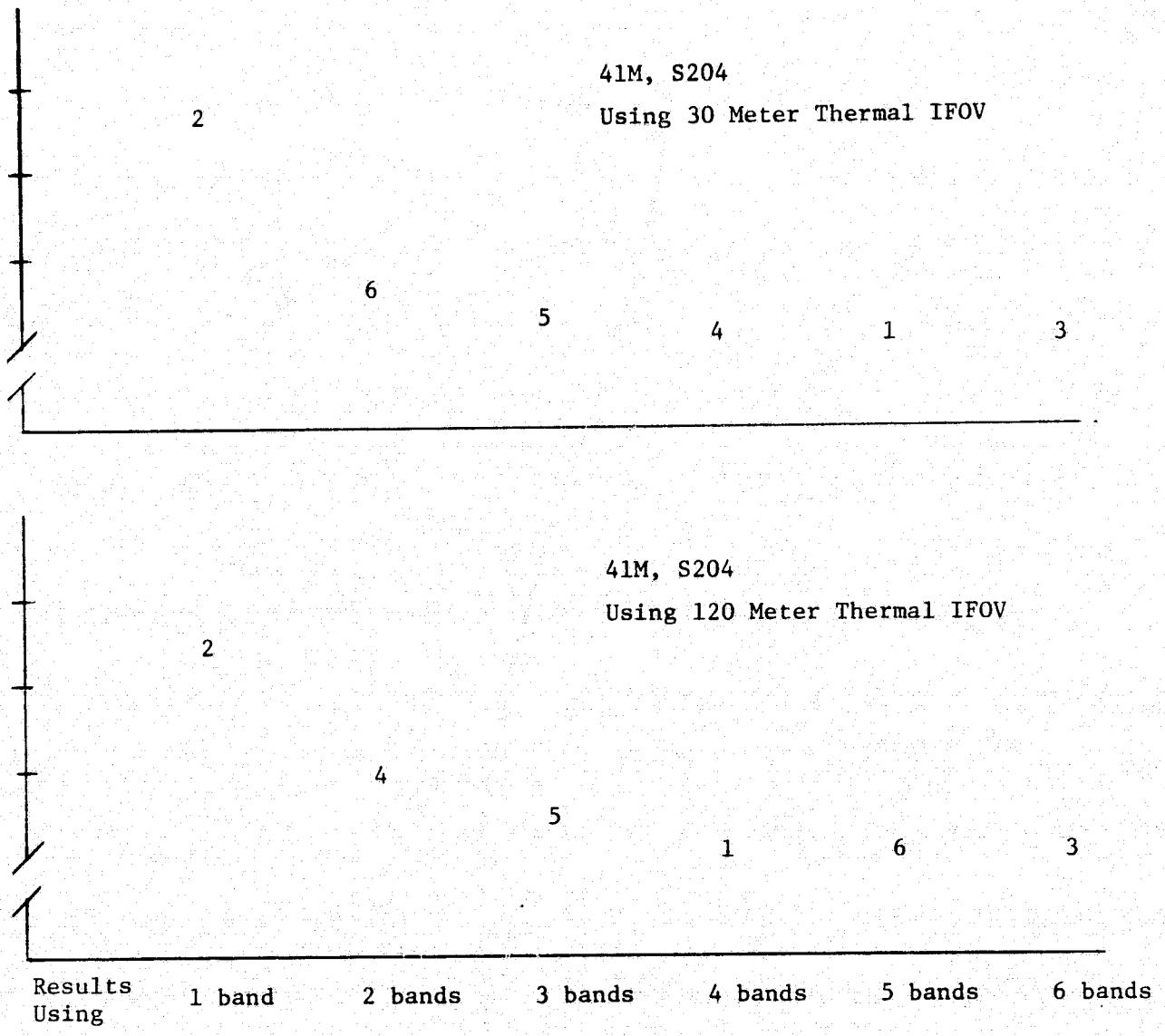

FIGURE 17. RANK ORDERING OF THEMATIC MAPPER BANDS, Thermal IFOV as a Parameter

Thus, the spectral study has three main conclusions. The first is that the thermal band is shown to be an important TM band for data gathered early in the growing season, but the use of a thermal band with spatial resolution seriously degraded from that of the other bands severely limits its utility when employed in multivariate analysis with other bands. Secondly, the TM bands are shown to be essentially as good at all times as each optimum set of bands for each time studied. Thirdly, TM band 0.72-0.92 μm was seen to be an important band for the detection of crop stress.

4
CONCLUSIONS AND RECOMMENDATIONS

The purpose of this section is to draw together all the analyses from the previous sections and provide recommendations on how the parameters of spatial and radiometric resolution might be traded off in the reality of designing the Thematic Mapper. However, in order to intelligently tradeoff parameter settings, there must be a clear goal as to what the Thematic Mapper is intended to be. Here we outline a philosophy for the TM which was followed for this analysis.

The overriding criterion for the TM is that it be cost effective -- the benefits accrued by it must outweigh its costs. The primary measurable dollar benefits for an earth resources satellite come from accurate crop mensuration and production forecasting of the world's primary market goods: wheat, corn, soybeans, cotton, and rice. The global picture of supply and demand for these goods requires that crop mensuration information be acquired for both prime areas of supply and areas of possible heavy demand that are also producers. This means that, in order to maximize benefits, the Thematic Mapper must be designed to be effective on fields in the 1-4 hectare range (2.5 to 10 acres) typical of Western Europe, and India, as well as the larger 16 and 32 hectare (40 and 80 acre) fields typical of the world's primary producing areas (U.S. wheat belt, Canada, USSR).

Another design consideration is that benefits accrue from early forecasts of crop production which requires accurate processing for data acquired at times of year which in all likelihood will not be optimum for spectral discriminability. It will also be important to monitor for crop stress during the growing season as this will also affect potential crop productivity. Both these considerations address the radiometric sensitivity requirement for the Thematic Mapper, as well as the selection of appropriate spectral bands.

An additional aspect is that, since the emphasis is on accurate crop mensuration, measures of productive acreage are desired rather than estimates of acreage planted to specific classes. For these former purposes, per-field classifiers may be deemed to be inadequate. This also implies a desire for finer resolution data, so as to make more accurate estimates of productive acreage.

Thus, the following assumes TM to be concerned with the crop mensuration problem at all points of the globe with data acquisition and processing for times early in the growing season, when spectral discriminability will not necessarily be optimum, as well as later in the season when discriminability may improve.

What then, is the recommended tradeoff philosophy, keeping in mind the above sensor goals? From an overall analysis of the results obtained from the various studies undertaken on this contract, the following observations emerge. All spatial resolution study results show definite improvement in mensuration accuracy for 30 meter and 40 meter resolution over that obtained at 50, 60, and 90 meters. The decrease in mensuration accuracy between 30 and 90 meters ranged between 15 and 25 percent. We conclude that TM will provide marked improvement over LANDSAT-1 or -2 type resolution for area mensuration performance in agricultural crop surveys if its spatial resolution is 30 or perhaps 40 meters. No benefit-cost estimate was part of the study to calibrate this differential performance improvement in terms of incremental benefit or cost, nevertheless, we are interested in understanding the differences between 30 and 40 meter resolution.

The simulation of scenes of different field sizes, not previously accomplished, shows that 30 meter data has 7-13% more field center pixels than 40 meter data for fields between 1-8 hectares (2.5-20 acres), and an increase of 5% even at the 16 hectare field size. In what follows we concentrate on results for fields in the 1-8 hectare range (2.5-20 acres).

For such fields we see that the change in going from 30m to 40m resolution is that significantly less of the scene is in pure pixels and this results, in general, in about a 4% decrease in area mensuration accuracy. (The decrease in going from 40 to 50 meters is another 5-7%.) These results appear to be independent of time of year and crop stress condition.

We conclude that there is a definite if not large improvement in performance going from 40 meters to 30 meters resolution.

In keeping 30 meter resolution but decreasing radiometric sensitivity to twice the nominal noise (generally NE$\Delta\rho$ = 1.0%) the decrease in field center classification accuracy varies from 5-10%, with a larger reduction with decreasing spectral discriminability between the classes (caused by time of year, crop stress, etc).

Conversion of the field center accuracy results from the radiometric sensitivity study to mensuration accuracy is not readily accomplished, nevertheless it seems that, if such a choice is necessary, one should choose to retain a finer value for radiometric sensitivity over one for spatial resolution. This judgement is based on the observed sizeable decreases for field center classification results seen for data including crop stress such as corn blight and also seen in data collected early in the growing season when radiometric sensitivity is reduced.

As regards spectral issues, our experience is that the utility of a thermal band with 120 meter resolution will be marginal when used in concert with finer resolution bands to carry out crop identification and mensuration assuming a late morning pass. However, the study has shown that a comparable resolution thermal band is a very important band for crop discrimination for times early in the growing season. A substantially coarser resolution thermal band reduces the discrimination possibilities for a crucial time of year. The coarser resolution in one band may introduce problems of registration and data

reconstruction if not oversampled to provide data at each time the other bands do. Although this aspect of the scanner (larger thermal IFOV) seems fixed, our recommendation is that every effort be made to bring the spatial resolution of the thermal band into line with the resolution of the other bands. In regard to the other bands, at each time of the growing season the TM set of bands were seen to be as effective as each best subset of M-7 bands for the times of year studied. Additionally, the 0.72-0.92 μm TM band was seen to be an important band for detection of crop stress conditions.

Before summarizing the conclusions and recommendations it is important to note that our study is empirical and therefore limited to the evidence derivable from 3 times of year and two locations for 4 classes (except where simulation allowed generalizations). Our results are nevertheless supportable by theoretical arguments and the evidence is important and far reaching in its implications.

Conclusions relating to spatial resolution and radiometric sensitivity:

1. Study results provide new but limited empirical evidence that a 30 meter or perhaps 40 meter spatial resolution and a TM system radiometric sensitivity of one-half percent reflectance would provide significantly better performance in automatic information extraction for agricultural crop survey applications (particularly corn and soybeans) than coarser resolution or less sensitive systems such as LANDSAT-1, -2, or -C. Although direct comparisons to the current LANDSATs were not made, the evidence for this conclusion is supportable by theoretical arguments.

2. Study results have shown additional empirical evidence for the priority of radiometric sensitivity at least equal to spatial resolution, if not higher.

3. Improvement in the area mensuration performance in the range 30-90 meters is shown to be largely due to the lesser proportion of boundary elements at finer resolutions where classifier performance is low and tends to decrease with coarser resolution as compared to field centers where classification accuracy is high.

4. Improvement in performance with reduced noise levels in the range one-half percent to one and one-half percent is more significant earlier in the growing season and with more difficult discriminations. Both mensuration and field center performance are affected.

5. Thermal band resolution of 120 meters was shown to degrade performance when it could be used with other bands in crop surveys compared to thermal band resolution equal to the other bands.

Conclusions relating to spectral bands:

1. The 6 TM spectral bands (we used a 0.72-0.80 + 0.80-0.92 combined band) are confirmed by our limited empirical evidence to be the best six bands for agricultural surveys of corn and soybeans, each band (including a fine resolution thermal band) being important at some time in the growing season and the set giving essentially the same performance as the various sets of 6 optimum aircraft scanner bands appropriate to each time. This means the 0.45-0.52 μm band should not be thought of as a research band.

2. The 0.72-0.92 band is important for detection of crop stress conditions.

3. A 120 meter thermal band is not as useful as a 30 meter thermal band in crop surveys.

Other conclusions:

1. Simulation of satellite or high altitude aircraft scanner performance using low altitude aircraft scanner data as an input is a powerful systems analysis technique.

Recommendations:

1. Thematic Mapper should have the following specifications for crop inventory applications:

Spatial Resolution (All Bands) 30 meters (42 microradians)
Spectral Bands and Radiometric Sensitivities:

0.45-0.52 μm at NEΔρ = .005
0.52-0.60 μm at NEΔρ = .005
0.63-0.69 μm at NEΔρ = .005
0.72-0.92 μm at NEΔρ = .005
1.55-1.75 μm at NEΔρ = .005 (perhaps 0.01)
10.4-12.4 μm (perhaps broader) at NEΔT = 0.5°K

2. If relaxation of the above is needed, relax spatial resolution before radiometric sensitivity.

3. Additional effort should be made to achieve a finer thermal band resolution than 120 meters.

4. Additional investigations be made of:

a. Classifier performance on boundary elements as a function of mixtures of classes to determine local bias.

b. Spatial sampling effects giving types of boundary element mixtures as the spatial sampling changes.

c. The incremental benefit and cost of incremental mensuration performance improvement in any specific application.

d. The dynamic range and digital count vs spectral radiance (in the band) transfer characteristics of TM.

e. Time effects such as frequency of coverage, time of day, etc.

f. Other specific user applications.

APPENDIX I

DATA BASE DESCRIPTION

The data being used for this study were gathered by the ERIM M7 aircraft-mounted multispectral scanner during the Corn Blight Watch Experiment (CBWE) of 1971. These data were selected in part because of the ready availability of the data, ERIM's past involvement in the CBWE and experience with the data and confidence in the quality of both the MSS data and the ground observations, and also because of the presence of crop stress which allowed evaluation of LANDSAT-D TM parameter specification with regard to this possible application.

I.1 CBWE DATA

These data were gathered over 30 segments in western Indiana from an altitude of 5000 ft every two weeks throughout the growing season. The major agricultural crops planted in these segments were corn and soybeans. The ground truth provided called out the size and contents of each field in the scene.

The characteristics of the M7 scanner are fully detailed in the references [12]. Briefly, it is an electromechanical line scanner with a period of 60 cycles (scans) per second and a nominal resolution of $2 \cdot 10^{-3}$ radians for the spectrometer although the subsequent recording and digitizing electronics degrade this to $5 \cdot 10^{-3}$ radians in the along-scan direction. The system is capable of recording information for up to 12 detectors; the 12 spectral bands of information which were recorded during the CBWE missions are listed below:

TABLE I.1

M7 SPECTRAL CHANNELS RECORDED DURING CBWE
(10% Response Points)

1.	0.46 - 0.49μm
2.	0.48 - 0.51μm
3.	0.50 - 0.54μm
4.	0.52 - 0.57μm
5.	0.54 - 0.60μm
6.	0.58 - 0.65μm
7.	0.61 - 0.70μm
8.	0.72 - 0.92μm
9.	1.0 - 1.4 μm
10.	1.5 - 1.8 μm
11.	2.0 - 2.6 μm
12.	9.3 - 11.7 μm

I.2 DATA PREPARATION

In order to conserve time and resources on this investigation, some of these data which were previously digitized and preprocessed were utilized. The segment designated 204 in northwestern Indiana, Fig I.1, was selected as the prime site for this investigation. Digitized data for this segment for the following missions were used: 41M, 12 July collected at 11:09 CST; 42M, 5 August collected at 9:41 CST; and 43M, 13 August collected at 9:28 CST. In addition, Segment 212 (midwestern Indiana) data for Mission 43M (collected 17 August at 10:19 CST) were used to provide results from another site with similar crops as well as being the only available data set where substantial instances of actual corn blight existed. Each of the study segments was approximately one-mile wide and ten-miles long.

Roughly 30% of each of the study segments were corn, 15% trees and 10% soybeans; the rest were pastures, farmsteads and lesser crops. Summary tables of each class, broken down by field size, are shown at the end of this appendix. Also shown are plots of field-size distributions and a comparison to the overall U.S. curve which shows the corn belt sites we used have substantially smaller field sizes than the U.S. average [7]. Certain temporal changes in the scene classes were observed, primarily for corn and soybeans. For the 12 July flight, corn stood 5-7 feet high and was a highly variable ground cover, ranging from 50-80%. Soybeans in that period exhibited a 30-50% ground cover. By mid-August both classes were assessed as 80-100% ground cover. As for the other classes, trees changed very little in this period, wheat and oats had been harvested before the 41M flight and thereafter were bare soil, stubble and pasture areas. The changes in hay fields, pastures, etc. were not determined.

The procedures by which the data had been digitized and preprocessed are covered in reference [13]. Briefly, because of the high scan rate used and relatively low forward velocity of the aircraft (1 meter/scan) there was considerable overlap (67%) between consecutive scan lines. Advantage could be taken of this overlap to reduce effects of high frequency noise.

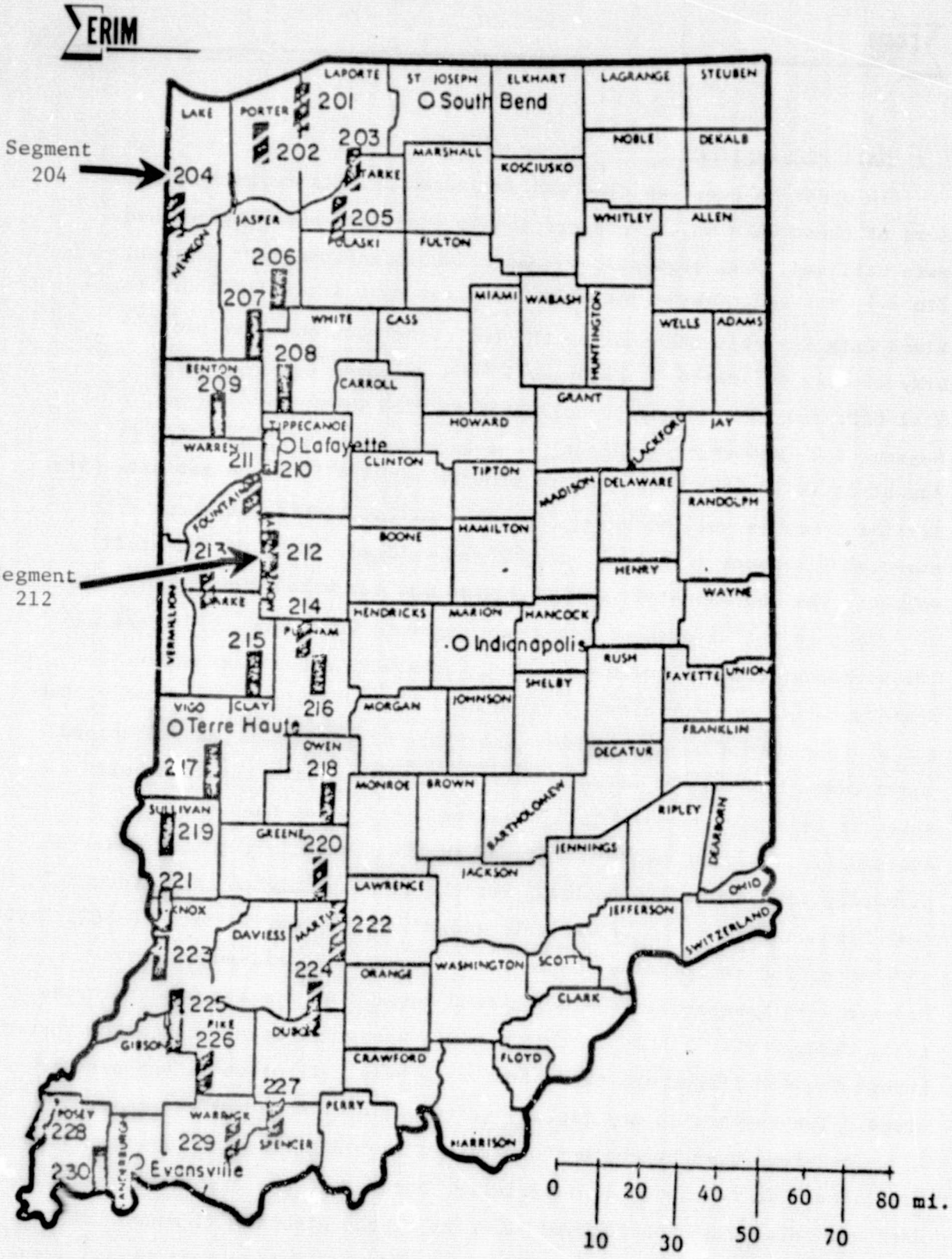

FIGURE I-1. CORN BLIGHT WATCH EXPERIMENT SEGMENT LOCATIONS

Thus, during digitization groups of eight consecutive scan lines were averaged together to yield one output line of data. So, for the combination of scanner resolution, altitude of data collection and digitization procedure, the output pixel dimensions were roughly 7.6 meters (along scan) by 10 meters (along track) at nadir.

To achieve reasonable area coverage, aircraft scanners must view relatively large total fields of view (60-90°) which can affect signal characteristics. For example, in scanning over this range of angles, the atmospheric path traversed by the target radiation varies considerably with the result that similar targets at different scan angles produce different apparent, spectral radiances. Therefore, prior to degrading the spatial resolution, a procedure to minimize this and other angle effects needs to be carried out. For this study, the average signal versus angle transformation [9] was implemented.

After this preparation, the data were ready for the spatial degradation procedures which are described in Appendix II.

I.3 CALCULATION OF COUNTS EQUIVALENT CHANGE IN REFLECTION

One initial analysis carried out on these data sets was to measure the number of counts or quantizing levels for each of the data sets which was equivalent to a 0.5% change in ground reflectance. The results of this analysis were used in simulating all the various levels of radiometric sensitivity studied during this project. The following paragraphs define the method used and the results.

The procedure for calculating the set of values of DE$\Delta\rho$ (Data Equivalent Change in Reflectance) is given here for visible and near-IR bands. The procedure for the thermal band is given later in this appendix. The general strategy employed was to establish reflectance versus data value transfer curves for each channel of aircraft data by using targets of known reflectance in the scene.

The various ground classes in the scene were examined and a review of published reflectance spectra was also undertaken to establish those classes which might be used to establish the transfer curves. In the end, only three "known" reflectances were used in determining the transfer curves. The quote marks around the word known are there because the the reflectances in each of these cases is not exactly known by in situ measurement at the time of data collection, but rather a good estimate with appropriate error bars was obtained. It is recognized that this procedure for determining the transfer curves is inexact and error prone, however, it was felt that this was the best strategy employable under the circumstances. Further on, it will be shown that the impact of any error made on the final set of $DE\Delta\rho$ is not sizeable.

The three classes used here were corn, concrete, and dark objects (i.e., zero or almost zero reflectors). The following discussion concerns itself only with the S-212 data set. The corn class pixels from eleven typical corn fields were clustered with controlling parameters for the cluster program set so as to form many "tight" clusters (clusters with small spread or volume). One cluster contained by far the most pixels and it was deemed representative of typical corn in the data set. Reflectance data for this class was taken from measurements made by Suits and Safir [14] of a corn field in Michigan on 25 August 71. The time of the measurement was thus 8 days later than the date of data acquisition for S-212. Because Michigan spring planting dates are approximately one or two weeks later than the dates for S-212, it was felt that maturity of the crop in the two areas were comparable. Furthermore, the average blight level in the S-212 corn fields was near 2 or 3 while the Michigan field measured was assessed as a blight level 3 field. Thus, again, the field conditions appear comparable. As a further reference, use was made of a family of corn curves in the NASA Earth Resources Spectral Information Systems library [15]. These proved useful in assessing error bars for the corn reflectance spectra.

For the concrete class, use was made of an interstate highway which appears in the S-212 data set. Clustering was carried out to determine mean signals for the concrete, again setting the cluster algorithm for small volume clusters. A problem here obviously is in the very narrow concrete roadbed causing many concrete-vegetation mixture pixels and also the likelihood that the radiation reflected from the concrete was affected by scattered radiation from other nearby classes. This was taken into account in determining error bars for this case. Concrete reflectance spectra were obtained from the Target Signatures Analysis Center library [16] maintained at ERIM.

The third class, dark objects, are assumed to represent zero reflected radiance from the ground and hence a zero reflector. Obviously they may not be exactly zero and hence a small error bar for reflectance is used for these data. The darkest objects are obtained by examining histograms of all pixels in the scene channel by channel and selecting the data value in each channel which is one more than the first empty histogram bin as one travels from the mean toward the small data values. Data values smaller than the chosen data value were examined and found to come from bad (excessively noisy or dropped) scan lines.

To digress for a moment, it should be explained why several other classes in the scene were not utilized. The scene contained two water bodies -- a small pond and a river. Because reflectance characteristics for water bodies such as these are highly variable according to the turbidity of the water and the characteristics of the pond or river bottom these were not used. Similarly, bare soil was found to be a class whose reflectance spectra are very dependent on the amount of moisture in the soil and the mineral characteristics of the top soil. Thus, it was felt that this class was also too variable to obtain accurate reflectance spectra for it. Dense tree stands or forests make up over 10% of the scene, but we were unable to locate satisfactory reflectance spectra for such forests at the specified time of year.

For the analysis at hand, for each channel of M7 data, the data value-per cent reflectance pairs were graphed along with the appropriate error bars for each of the three classes utilized. Then a best fit line was drawn (a strictly linear relationship being assumed), taking into account the biases noted. From these curves, the noise equivalent data value in quantizing levels was calculated for the appropriate change in reflectance for each of the M7 bands.

In the case of the thermal band, information regarding the two greybody thermal references in the scanner was used to determine the data value equivalent change in temperature in a straightforward manner by:

$$DE\Delta T = \left| \frac{V_{G1} - V_{G2}}{T_{G1} - T_{G2}} \right| \qquad (I.1)$$

where V is the average data values and T, the temperatures for the two references G1 and G2.

The final values derived are given in Table I.2. Note that the value for the 1.5-1.8μm band is based on an NEΔρ of .010 rather than .005 as used in the other bands. This change was made at the suggestion of L. Walter of GSFC as being a more realistic simulation of the final design. As one further note, the errors due to the causes cited above in the calculation of the DEΔρ values were examined to establish an upper bound on the possible error. The worst case, the .54-.60μm band, was identified and here the worst-case line yielded value of 0.93, which is an 11% change from the value in Table I.2. Thus, the maximum error which might have been introduced in the calculation of the DEΔρ values is only 11% and thus the actual errors in the values presented in Table I.2 are much less than this. Therefore, it is felt that errors in the estimation of DEΔρ due to the method employed are acceptable.

TABLE I.2 DATA-VALUE EQUIVALENT CHANGE IN REFLECTANCE

M-7 Chan	TM Chan	λ (μm)	Δρ at 15% (%)	DEΔρ S-212	DEΔρ S-204, 43M	DEΔρ S-204, 42M	DEΔρ S-204, 41M
1	> 1	.46-.49	0.5	4.8	2.6	.94	2.3
2		.48-.51	0.5	4.0	3.2	1.56	4.1
3		.50-.54	0.5	5.6	3.5	.81	2.2
4	> 2	.52-.57	0.5	6.1	3.9	1.48	4.7
5		.54-.60	0.5	5.3	3.3	.76	2.0
6		.58-.65	0.5	5.1	3.3	1.95	5.0
7	3	.61-.70	0.5	4.5	2.5	.93	2.3
8	{4,5}	.72-.92	0.5	3.5	2.3	.75	.91
9		1.0-1.4	0.5	2.1	2.2	1.21	1.28
10	6	1.5-1.8	1.0	6.3	1.9	3.69	3.61
11		2.0-2.6	0.5	7.8	2.7	1.46	0.89
12	7	9.3-11.7	.5°C ΔT	7.3	7.2	2.50	1.0

To calculate the DE$\Delta\rho$ values for Segment 204, 41M, 42M and 43M data sets, a slightly different procedure was used. Examination of the data set showed there was no large concrete reflector as there had been in Segment 212. Furthermore, the corn in S-204 was much healthier (blight levels 0 and 1) than was the case in S-212. Rather than base the DE$\Delta\rho$ calculations on only two data points (dark object and corn), a signature extension-like scheme was devised to extend the DE$\Delta\rho$ values from S212 to the S204 data set. First, the results were extended to the 43M data set, and then from there to the other two segment 204 data sets.

For the 43M data set, the procedure used was to first identify two reflectors which occurred in both scenes. The dark object reflectors were utilized as one of these. For the other, the mean of all the reflectors in the scene was used, reasoning that overall the two data sets displayed the same mix of ground classes and would therefore have almost the same average reflectance. For the former, dark object signals were evaluated for S-204 in the same manner as had been done for the S-212 data set. For the latter, an average overall of all pixels in the the scene was calculated in each channel for both S-212 and S-204.

Since, the transfer curves for the two data sets are given as:

$$D_{212} = \rho m_{212} + DO_{212} \tag{I.2}$$

and

$$D_{204} = \rho m_{204} + DO_{204} \tag{I.3}$$

where D is the data value, ρ reflectance, m the slope of the line and DO the dark object values. For $\rho = \bar{\rho}$, and solving for m_{204} this is:

$$m_{204} = m_{212} \frac{(\bar{D}_{204} - \bar{D}_{204})}{(\bar{D}_{212} - \bar{D}_{212})} \tag{I.4}$$

and finally the values of DE$\Delta\rho$ for segment 204, 43M are generated by

$$DE\Delta\rho_{204} = m_{204} * \Delta\rho \qquad (I.5)$$

The DE$\Delta\rho$ values for the 42M and 41M data sets were defined by first determining a set of classes in the scene whose reflectances were not expected to change during the time period in question (mid-July to mid-August). Three such classes, trees, water (rivers and canals), and roads were identified and 3-7 specific instances of each class were located on graymaps of the three data sets. Mean signals for each area of each class were calculated; for exact location of the water pixels and road pixels clustering techniques were used. In analyzing the results it became evident that the narrow county roads in the scene were too narrow to be used for this purpose -- most or all of the pixels seemed to be mixtures and it was impossible to determine which pixels were pure road pixels.

The mean signals between remaining corresponding areas of the 41 M and 43M (and then the 42M and 43M data sets) were analyzed, using regression techniques to determine transfer curves for data values between 41M and 43M (and then also, 42M and 43M). Then, if M is the slope of this latter transfer curve then for each channel i

$$DE\Delta\rho_{41M_i} = M_i \cdot DE\Delta\rho_{43M_i} \qquad (I.6)$$

and similarly for the 42M data. Thus, DE$\Delta\rho$ values for channels 1-11 for 14M and 42M were calculated. The values DEΔT for the thermal band (channel 12) were determined using the digitized data representing the two thermal calibration references in the scanner. All the data equivalent change in reflectance are given in Table I.2.

TABLE I.3 MISSION 43M SEGMENT 212 FIELD SIZE DISTRIBUTION

ACRES	1	2	3	4	5	6	7	8	9	10	11	12	13	14	15	16	17	18	19	20	21	22	23	24	25
Corn	1	1	2	6	4	7	4	5	2	10	4	8	2	1	9	2	4	5	7	17	1	2	1	2	6
Soybeans	-	1	2	-	2	-	3	2	5	3	2	2	-	3	3	2	2	4	-	8	1	1	1	1	2
Hay	-	-	1	2	2	2	1	-	4	2	1	-	1	3	3	1	-	4	1	2	-	1	-	-	-
Oats	-	2	1	4	2	-	-	2	-	2	1	1	1	-	2	-	-	-	-	2	-	2	-	-	-
Pasture	6	6	4	7	4	7	4	5	2	5	3	6	2	1	5	4	-	3	-	6	-	-	-	1	2
Winter Wheat	-	-	1	-	-	-	-	1	-	1	2	1	-	2	-	1	2	-	-	1	-	-	-	1	-
Gr Sorghum	-	-	-	2	1	-	-	-	-	-	-	-	1	-	-	1	-	-	-	-	-	-	-	-	-
Grass	-	-	-	1	-	-	-	-	-	-	-	-	-	-	-	-	-	-	-	-	-	-	-	-	-
Idle	-	2	1	3	1	-	-	-	-	1	-	-	-	-	-	-	-	-	-	-	-	-	-	-	-
Sudex	-	-	-	1	-	-	-	-	-	-	-	-	-	-	-	-	-	-	-	-	-	-	-	-	-
Row Crop	-	-	-	-	-	1	-	-	-	-	-	-	-	-	-	-	-	-	-	-	-	-	-	-	-
Diverted	-	1	2	-	1	-	1	1	-	3	1	1	-	-	-	-	1	-	-	-	1	-	-	-	-
Wood/Pasture	-	2	1	2	2	-	-	2	-	3	-	-	-	-	3	1	-	1	-	1	-	-	-	-	1
Woods	3	6	7	1	2	1	2	-	3	2	-	2	-	-	5	-	-	-	-	2	-	-	-	-	-
Non-Farm	16	25	12	8	7	1	-	1	-	1	-	-	-	-	-	-	-	-	-	-	-	-	-	-	-
Bare Soil	-	-	-	-	-	-	-	-	1	-	-	-	-	-	-	-	-	-	-	-	-	-	-	-	-
TOTAL	26	46	34	36	29	19	15	19	16	34	14	21	7	10	30	12	9	17	8	39	3	6	2	5	11

ACRES	26	27	28	29	30	31	32	33	34	35	36	37	38	39	40	41	42	43	44	45	46	47	48	49	50
Corn	2	-	1	-	2	1	-	-	-	1	-	1	3	-	1	-	-	1	1	1	-	-	-	-	1
Soybeans	-	1	-	-	2	1	1	-	3	-	-	-	-	1	-	-	-	-	-	-	-	-	-	-	-
Hay	-	-	-	-	-	-	-	-	-	-	-	-	-	-	1	-	-	-	-	-	-	-	-	-	-
Oats	-	1	-	-	-	-	-	-	-	-	-	-	-	1	-	-	-	-	-	-	-	-	-	-	-
Pasture	-	-	-	-	2	-	-	-	-	-	-	-	-	-	2	-	-	-	-	-	-	-	1	-	-
Winter Wheat	-	-	-	-	-	-	1	-	-	-	-	-	-	-	-	-	-	-	-	-	-	-	-	-	-
Gr Sorghum	-	-	-	-	-	-	-	-	-	-	-	-	-	-	-	-	-	-	-	-	-	-	-	-	-
Grass	-	-	-	-	-	-	-	-	-	-	-	-	-	-	-	-	-	-	-	-	-	-	-	-	-
Idle	-	-	-	-	-	-	-	-	-	-	-	-	-	-	-	-	-	-	-	-	-	-	-	-	-
Sudex	-	-	-	-	-	-	-	-	-	-	-	-	-	-	-	-	-	-	-	-	-	-	-	-	-
Row Crop	-	-	-	-	-	-	-	-	-	-	-	-	-	-	-	-	-	-	-	-	-	-	-	-	-
Diverted	-	-	-	1	-	-	-	-	-	-	-	-	-	-	-	-	-	-	-	-	-	-	-	-	-
Wood/Pasture	-	1	-	-	1	1	-	-	-	1	-	-	-	-	-	-	-	-	-	-	-	-	-	-	2
Woods	-	-	-	-	1	-	-	-	-	-	-	-	-	-	-	-	-	-	-	-	-	-	-	-	-
Non-Farm	-	-	-	-	-	-	-	-	-	-	-	-	-	-	-	-	-	-	-	-	-	-	-	-	-
Bare Soil	-	-	-	-	-	-	-	-	-	-	-	-	-	-	-	-	-	-	-	-	-	-	-	-	-
TOTAL	2	3	1	1	8	3	1	1	3	2	0	1	3	2	4	-	-	1	1	1	-	-	1	-	4

ACRES	55	57	60	65	70	75	78	80	94	100
Corn	1	1	-	1	-	-	1	-	-	-
Soybeans	-	-	-	-	-	1	-	-	-	-
Woods	-	-	1	-	-	-	-	1	1	1
Wood/Pasture	-	-	1	-	1	-	-	-	-	-
TOTAL	1	1	2	1	1	1	1	1	1	1

ERIM

TABLE I.4 MISSION 43M SEGMENT 204 FIELD SIZE DISTRIBUTION

ACRES	1	2	3	4	5	6	7	8	9	10	11	12	13	14	15	16	17	18	19	20	21	22	23	24	25
Corn	1	1	4	3	9	6	2	8	3	13	6	5	2	2	7	1	1	1	1	11	2	3	1	2	2
Soybeans	-	-	-	-	2	1	-	1	-	2	6	1	-	1	2	-	-	-	1	6	-	1	1	1	1
Hay	-	1	1	1	3	1	2	-	-	2	1	-	1	2	1	-	-	-	-	2	-	-	-	-	1
Oats	1	-	4	1	2	-	-	1	-	1	-	2	-	-	1	-	1	-	-	-	-	-	-	-	1
Pasture	-	-	2	2	1	3	1	2	-	4	-	1	-	1	-	-	-	-	-	-	-	-	-	-	-
Winter Wheat	-	-	-	-	-	-	1	1	1	3	1	-	-	-	1	-	-	1	-	1	-	-	-	-	-
Vegetable	-	-	-	1	-	-	-	-	-	-	-	-	-	-	1	-	-	-	-	1	-	-	-	-	-
Mix Grain	-	-	-	-	-	-	-	-	-	-	-	-	-	-	-	-	-	-	-	1	-	-	-	-	-
Idle	-	-	-	-	-	1	-	-	-	1	-	-	-	-	1	-	-	-	-	-	-	-	-	-	-
Rye	-	-	-	-	-	-	-	-	-	-	-	-	-	-	-	-	-	-	-	-	-	-	-	-	-
Diverted	-	3	2	3	3	2	5	4	-	2	2	1	-	1	2	1	2	1	1	-	-	1	1	1	1
Wood/Pasture	-	-	-	-	-	-	-	-	1	-	-	-	-	-	-	-	-	-	-	-	-	-	-	-	-
Woods	1	1	3	3	1	1	-	1	-	1	-	-	-	-	1	-	-	-	-	1	-	-	-	-	2
Non-Farm	3	3	4	9	5	2	-	1	2	3	-	-	-	1	-	-	-	-	-	1	-	-	-	-	-
Bare Soil	-	-	-	-	-	-	-	-	-	-	-	-	-	-	-	-	-	-	-	-	-	-	-	-	-
TOTAL	6	9	20	23	26	17	11	19	7	32	16	10	3	8	17	2	4	3	3	24	2	5	3	4	8

ACRES	26	27	28	29	30	31	32	33	34	35	36	37	38	39	40	41	42	43	44	45	46	47	48	49	50
Corn	2	3	1	1	11	-	1	-	3	1	2	2	1	-	6	-	-	-	-	2	-	-	-	-	4
Soybeans	-	-	2	1	1	-	1	-	-	1	-	-	1	-	1	-	-	-	-	-	-	-	-	-	-
Hay	-	-	-	-	2	-	1	-	-	-	-	-	-	-	-	-	-	-	-	-	-	-	-	-	-
Oats	-	-	-	1	2	-	-	-	-	-	-	-	-	-	-	-	-	-	-	-	-	-	-	-	-
Pasture	-	-	1	-	1	-	1	-	-	1	-	-	-	-	-	-	-	-	-	-	-	-	-	-	-
Winter Wheat	-	-	-	-	1	-	-	-	-	-	-	-	-	-	-	-	-	-	-	-	-	-	-	-	-
Vegetable	-	-	-	-	-	-	-	-	-	-	-	-	-	-	-	-	-	-	-	-	-	-	-	-	-
Mix Grain	-	-	-	-	-	-	-	-	-	-	-	-	-	-	-	-	-	-	-	-	-	-	-	-	-
Idle	-	-	-	-	-	-	-	-	-	-	-	-	-	-	-	-	-	-	-	-	-	-	-	-	-
Rye	-	-	-	-	-	-	-	-	-	-	-	-	-	1	-	-	-	-	-	-	-	-	-	-	-
Diverted	-	-	-	1	1	1	-	-	-	-	-	1	-	-	1	-	-	-	-	-	-	-	-	-	-
Wood/Pasture	-	-	-	-	-	-	-	-	-	-	-	-	-	-	-	-	-	-	-	-	-	-	-	-	1
Woods	-	-	-	-	3	-	-	-	-	-	-	-	-	-	-	-	-	-	1	1	-	-	-	-	-
Non-Farm	-	-	1	-	1	-	-	-	-	-	-	-	-	-	-	-	-	-	-	1	-	-	-	-	1
Bare Soil	-	-	-	-	-	-	-	-	-	-	-	-	-	-	-	-	-	-	-	-	-	-	-	-	-
TOTAL	2	3	5	4	23	1	4	-	3	3	2	3	2	1	8	-	-	-	1	4	-	-	-	-	6

ACRES	52	53	60	68	70	75	80	91	100	300
Corn	-	1	1	1	1	-	-	1	-	-
Soybeans	-	-	2	-	-	-	1	-	-	-
Winter Wheat	1	-	-	-	-	-	-	-	-	-
Woods	-	-	-	-	-	1	1	-	-	-
Non-Farm	-	-	-	-	-	-	-	-	1	1
TOTAL	1	1	3	1	1	1	2	1	1	1

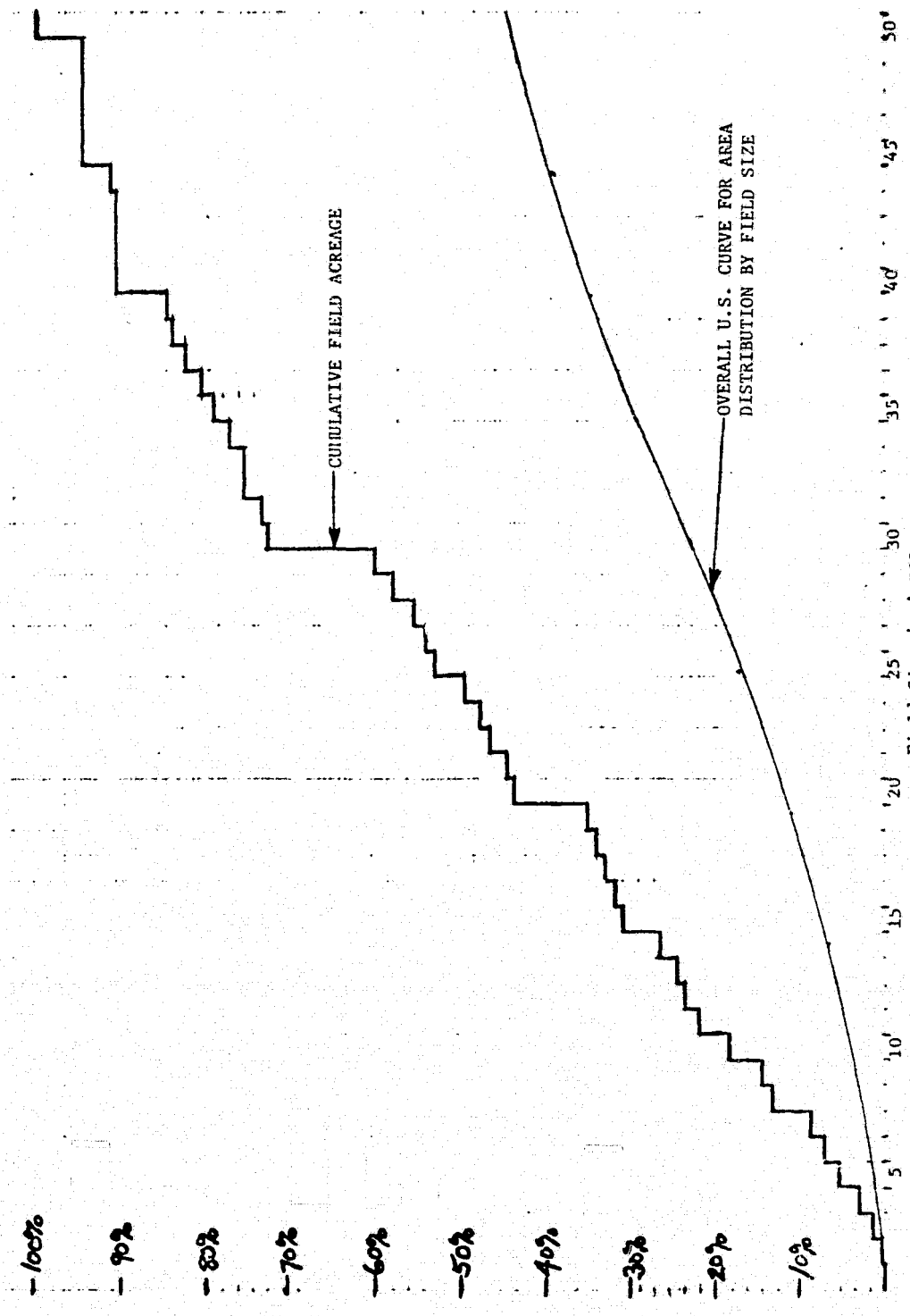

FIGURE I-2. FIELD SIZE DISTRIBUTION FOR SEGMENT 204 CUMULATIVE FIELD ACREAGE VS FIELD SIZE

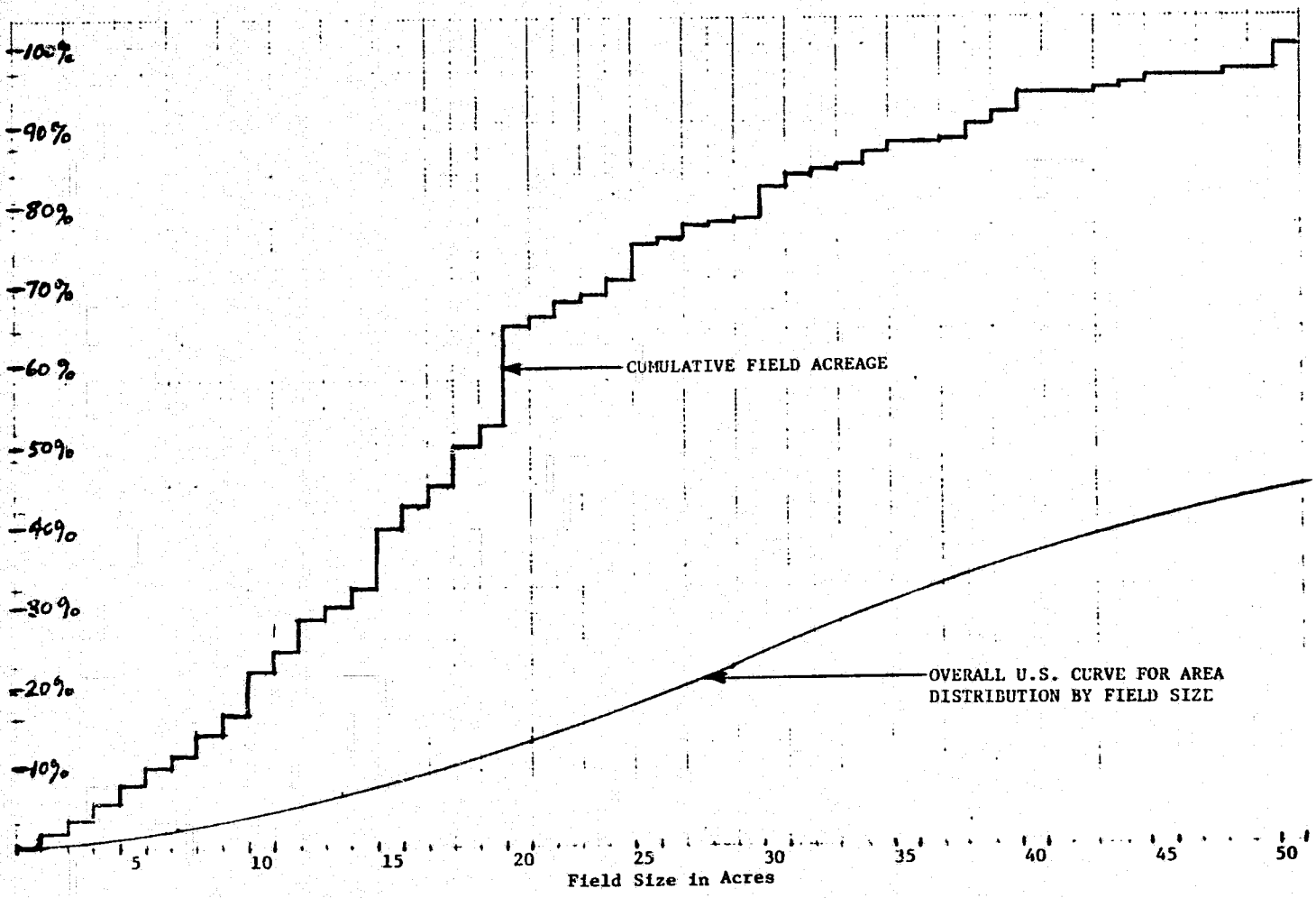

FIGURE I-3. FIELD SIZE DISTRIBUTION FOR SEGMENT 212 CUMULATIVE FIELD ACREAGE VS FIELD SIZE

result in a decrease in mensuration accuracy, although it does not follow that the two decreases would necessarily be of the same order. In fact, there can be cases which run counter to this intuition.

3.3 STUDY OF EFFECTS OF 120 METER THERMAL BAND RESOLUTION

Because of mirror size and hence Rayleigh limit (wavelength over diameter) considerations, it is expected that the resolution of the thermal band will be 120 meters -- three to four times that of the other bands. The spatial simulations which had been carried out to this point had assumed that all bands had the same resolution.

Thus, an investigation into the impact of using 120 meter resolution for the thermal band was undertaken to analyze the effects of a larger thermal band IFOV along with the 30 meter data. It is recognized that the thermal band is useful as a "temperature" mapper for some users and that the physical attribute sensed is not diagnostic in the same sense as what the reflective bands see, however we restricted ourselves here to the crop mensuration application under the assumption the thermal band will often offer information to aid discrimination if the time of overpass is not too far from local solar noon. The 30 meter data was used because this was considered the likeliest TM spatial resolution. In simulating the coarser resolution, sampling was done for each 30 meter pixel -- i.e., by oversampling the 120 meter resolution thermal band. A moving window averaging algorithm was employed such that the middle of the window coincided with the middle of each 30 meter pixel; the spatial weighting function used is shown in Figure 16. For each 30 meter pixel, a value for the 120 meter resolution thermal band was calculated using the values from the thermal channel of the surrounding 24 pixels, thus effectively simulating an oversampled thermal band. As part of the averaging process,

APPENDIX II

SIMULATION OF LANDSAT FOLLOW-ON DATA

The approach adopted for this study was to simulate, for each of the original four data sets, five different, coarser, spatial resolutions each at the nominally specified level of radiometric sensitivity. Also, a spectral simulation was required to more accurately simulate the proposed TM bands. Thus processing was carried out, Fig. II.1, to spatially degrade the M7 data and simulate the expected TM data. These data formed the basis for the analysis of spatial resolution and also for the spectral band study. Further degradation of these data sets were carried out for the radiometric simulation of the basic spatially degraded data.

In obtaining coarser spatial resolution by simple averaging techniques, both the noise content of the resultant data and the modulation transfer function (MTF) become unrealistic for simulating spacecraft sensors. Therefore, for this study, we endeavored to accurately simulate the expected Landsat Follow-on Thematic Mapper MTF and to include in our model the addition of uncorrelated Gaussian noise sufficient to generate a set of data exhibiting NE$\Delta\rho$ as nominally specified.

We adopted a linear systems approach to the mathematical modeling of the system MTF, for the combined optical and electronic systems and the atmospheric effects considered as part of the system. Each component of the system was modeled by a transfer function (the Fourier transform of the impulse response function for temporal components or of the point spread function for spatial components). Although the assumption of a linearly invariant system may not be strictly valid if the impulse response is dependent on the nadir scan angle (it is), the changes in this angle were assumed small and an approximately invariant system was modeled.

We begin discussing the simulation modeling of the atmosphere through which TM senses the earth. The radiant energy received by the optical system of the sensor is the sum of the radiant energy from the viewed

C-2

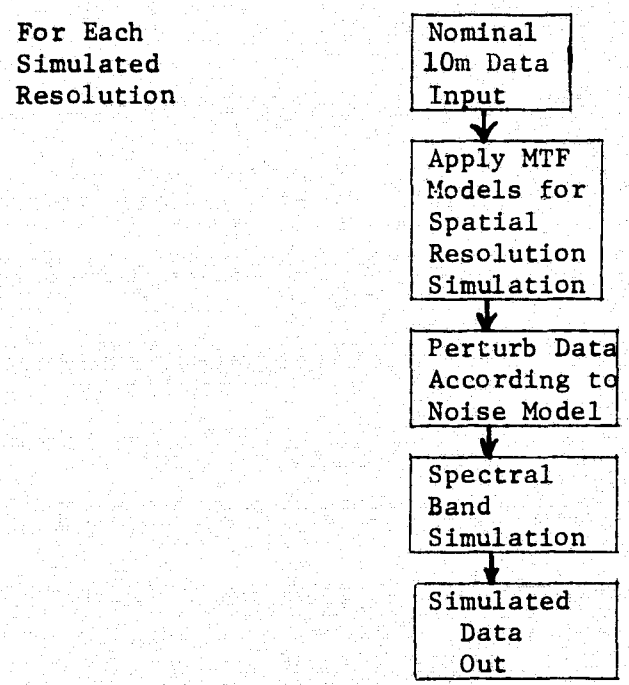

FIGURE II.1 PROCESSING FLOW FOR SIMULATING LANDSAT FOLLOW-ON TM DATA

ground scene transmitted through the atmosphere, radiant energy from the background scattered on the atmosphere (Rayleigh scattering and scattering by aerosols, dust and clouds), and radiant energy from the atmosphere itself (path, or veiling radiance). Another atmospheric effect is the turbulence blurring in the image.

The atmospheric scattering, absorption, and emission of radiation from the scene can be described by an integro-differential equation of radiative transfer [17]. Approximate radiative transfer solutions, such as described by Malila, et al [18] provide for the near ultraviolet, visible, and near infrared. LaRocca and Turner [19] describe solutions for the thermal infrared. Approximate solutions are needed because of computer-time limitations imposed by exact numerical calculations and approximate atmospheric radiation models are sufficient for sensor system simulation modeling because they are used only to estimate the magnitude of radiance for signal-to-noise ratio calculations. In most of these models, the polarizing effects of ground reflection and atmospheric scattering are normally neglected on the assumption that the effects is constant over the scene of interest for orbital scenes which subtend small angles. Coulson, et al [20] found the polarization of the incident radiation to be a maximum of 20% and Hasell, et al [12] measured scanner polarization of 20% as well. Thus, at most a 4% fluctuation is being ignored.

The transfer function T(f) for atmospheric turbulence has been given by Hufnagel and Stanley [21] as

$$T(f) = \exp[-5.82\pi^2\lambda^{-1/3} f^{5/3} S(A)/\cos\theta]$$

where λ is the spectral wavelength of the band center, f is the spatial frequency in cycles/radians, θ is the nadir scan angle, and S(A) is an empirical function whose numerical value versus sensor altitude A is represented in Fig. II.2. The transfer function is similar to a Gaussian

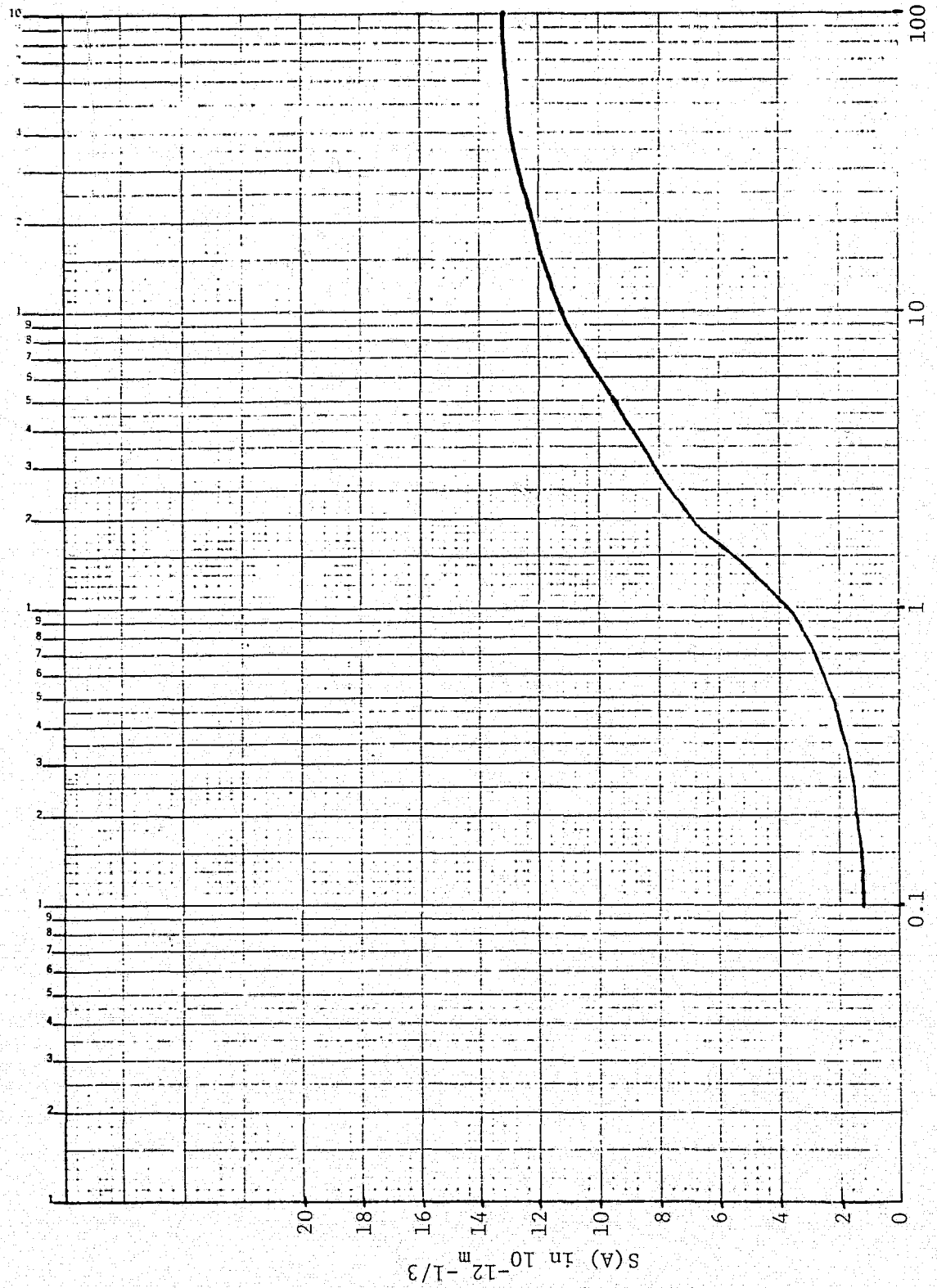

FIGURE II-2. S(A) An Empirical Function Vs. Sensor Altitude

curve, and the point spread function exhibits a similar shape. Because the atmospheric transfer function is real, its phase shift is zero.

As indicated in Section 2.2, a normalization for scan angle effects (primarily of the atmosphere) was the first step in processing. Simulation of other atmospheric effects was assumed to be convolved into the system MTF points we were given (see below) or were otherwise neglected. Differential atmospheric effects such as change in optical depth as a measure of haze differences have been shown to degrade classification accuracy in field centers [22]. We did not simulate this confounding effect. The effect of atmospheric noise contributions have been addressed [23] but have not been totally quantified and were therefore assumed to be included in the noise simulation.

II.1 DERIVATION OF WITHIN-SCAN AND ALONG-TRACK WEIGHTING FUNCTIONS FOR SMOOTHING AIRCRAFT SCANNER DATA TO SIMULATE DATA FROM THE LANDSAT FOLLOW-ON THEMATIC MAPPER*

A set of points on a target MTF curve for the Landsat Follow-on Thematic Mapper, which was hoped to be matched in the laboratory tests at GSFC, was specified to ERIM by Oscar Weinstein of GSFC. This MTF curve corresponded to the total end-to-end system response (within-scan) and was based on the observed performance of similar MSS systems with which GSFC had experience. For a system with a "30-meter" resolution, the data points for this MTF were the following:

Spatial Frequency (Half-Cycles/Meter)	Target MTF ("30-Meter" Resolution)
1/500	1.00
1/60	.75
1/45	.50
1/30	.35
1/15	.00

*Work on this section was performed by P.F. Lambeck.

An initial model for this system, tested at ERIM, was based on the following premises (for "30 meter" resolution): (1) a 30 meter IFOV, (2) integrate and dump for each 30 meters of scan, and (3) Gaussian optical blur to match the .35 value of the target MTF curve at 1/30 half cycles per meter. (Since the response characteristics of the detectors to be used were not known, and could be expected to cause either a boost or a reduction at any point on the system MTF curve, the alterations to the MTF to be caused by the detectors were ignored.)

Since the MTF for a system with a 30 meter IFOV and with integrate and dump for each 30 meters of scan is given by

$$|A(k)|_{\sqcap\sqcap} = \frac{\sin^2(k \times 15\pi M)}{(k \times 15\pi M)^2} \qquad \text{(II.1)}$$

with k = spatial frequency in half cycles per meter (M),

this portion of the initial model system already reduced the frequency response at k = 1/30 half cycles per meter to .405. To further reduce this response to the target value of .35, the MTF for the corresponding Gaussian blur would be given by

$$|A(k)|_{\Lambda} = e^{-\frac{(\sigma\pi k)^2}{2}} \qquad \text{(II.2)}$$

$$= \frac{.35}{.405} \quad \text{for } k = 1/30 \text{ half cycles per meter,}$$

with σ = the standard deviation for the spatial Gaussian blur.

From this equation σ was calculated and was found to be 5.16 meters. For the sake of using round numbers, σ = 5 meters was used for the initial model:

$$|A(k)|_{\sqcap\sqcap\Lambda} = \frac{\sin^2(k \times 15\pi M)}{(k \times 15\pi M)^2} \; e^{-\frac{(k \times 5\pi M)^2}{2}} \qquad \text{(II.3)}$$

This system MTF curve is plotted in Fig. II.3. The curve is a reasonable match to the target MTF values. The within-scan spatial weighting function corresponding to this MTF is plotted in Fig. II.4.

The along-track portion of this initial system MTF includes only the effects of the 30 meter IFOV and the Gaussian optical blur (i.e., it excludes the integrate and dump effect as well as the detector response, if this were defined). This along-track MTF is given by

$$|A(k)|_{\Pi\Lambda} = \left|\frac{\sin(k \times 15\pi M)}{(k \times 15\pi M)}\right| e^{-\frac{(k \times 5\pi M)^2}{2}} \qquad \text{(II.4)}$$

and is plotted in Fig. II.5. The along-track spatial weighting function corresponding to this MTF is plotted in Fig. II.6.

The spatial weighting function for the Gaussian optical blur used in this initial system model is plotted by itself in Fig. II.7. The 50% points of this function fall approximately 12 meters apart, while the 10% points are approximately 22 meters apart. The MTF for just this Gaussian blur component of the initial model, given by Eq. (II.2), is plotted for reference in Fig. II.8.

Conventionally the optical resolution of a scanner system is interpreted to be 1/k for the value of k at which the MTF curve has a value of .5 (with k defined in terms of half cycles per meter, as above)[2]. By this definition the initial system model specified above corresponds to a system with 36 meter resolution. (The target MTF corresponds then to a 45 meter resolution.) A second system model was developed at ERIM to simulate a scanner system with 30 meter resolution as conventionally defined.

For the second MSS system model it was decided to keep the Gaussian optical blur component as defined for the initial model. A choice was then considered whether (1) to retain the integrate and dump over each 30 meters of scan and adjust the IFOV within-scan (i.e., reduce the detector width) as required, or (2) to retain the IFOV within-scan as in the initial model and devise an appropriate filtering scheme (e.g., a two pole Butterworth

filter) to go with "instantaneous" sampling. Since an integrate and dump over 30 meters of scan and a 30 meter within-scan IFOV are mathematically equivalent components of the system MTF, either of these components together with the Gaussian optical blur from the initial model would lead to a partial system MTF as defined by Eq. (II.4) above (repeated here)

$$|A(k)|_{\sqcap\!\!\wedge} = \left|\frac{\sin(k \times 15\pi M)}{(k \times 15\pi M)}\right| e^{-\frac{(k \times 5\pi M)^2}{2}}$$

The MTF curve for this partial system (Fig. II.5) indicates a value of .553 at k = 1/30 half cycles per meter, hence the remaining component of the second system model must have an MTF value of approximately .9 at this spatial frequency.

For the first option the within-scan IFOV would have to be reduced to 15 meters, as indicated by Fig. II.5 which plots the MTF curve corresponding to this IFOV. Note that the curve has a value of .9 at k = 1/30 half cycles per meter.

For the second option, the MTF for a Butterworth filter with n poles is given by

$$|A(k)|_B = \left[1 + \left(\frac{k}{k_c}\right)^{2n}\right]^{-1/2} \qquad \text{(II.5)}$$

with k_c = the cutoff frequency for the filter.

If a two pole filter is chosen, then at k = 1/30 half cycles per meter

$$\left[1 + \left(\frac{1}{k_c \times 30M}\right)^4\right]^{-1/2} = .9 \qquad \text{(II.6)}$$

This produces the result k_c = 1/20.6 half cycles per meter. The MTF for this filter is then specified by

$$|A(k)|_{B_2} = [1 + (k \times 20.6M)^4]^{-1/2} \qquad \text{(II.7)}$$

and is plotted in Fig. II.10) The spatial weighting function for this filter is given by

$$H(x)_{B_2} = \pi k_c \sqrt{2}\ e^{-\frac{\pi k_c x}{\sqrt{2}}} \sin \frac{\pi k_c x}{\sqrt{2}} \qquad \text{(II.8)}$$

and is plotted in Fig. II.11.

Note that the area enclosed under the MTF curve for this two pole Butterworth filter (Fig.II.10) is less than the area enclosed under the MTF curve for the 15 meter IFOV (Fig.II.9). Since the noise throughput of a MSS system is related to the area enclosed under the system MTF curve, it appears that the Butterworth filter approach would lead to a better signal to noise ratio than would the reduced IFOV. In fact this Butterworth filter approach was that chosen for the second system model.

The within-scan MTF for the second system model is given by

$$|A(k)|_{\sqcap\!\wedge\, B_2} = \left|\frac{\sin(k \times 15\pi M)}{(k \times 15\pi M)}\right| e^{-\frac{(k \times 5\pi M)^2}{2}} [1 + (k \times 20.6M)^4]^{-1/2} \qquad \text{(II.9)}$$

and is plotted in Fig. II.12. The within-scan spatial weighting function corresponding to this MTF is plotted in Fig.II.13, Note that this weighting function is now asymmetric. This asymmetry arises because the response of the Butterworth filter to any signal input is delayed in time by an amount

which is variable according to each frequency present in the signal. However, a fixed delay in the response of the filter can be defined, relative to which the remaining variations in the response delay are small.

The phase shift ($\Delta\phi$) in the within-scan response of the second system model is plotted vs. spatial frequency (k) in Fig.II.14. This plot has been adjusted to take into account the apparent fixed delay in the response, as indicated by the horizontal asymptote of the curve as k approaches zero (see discussion below). There is an additional 180 degree phase shift which starts as k becomes greater than 1/15 half cycles per meter, which is not plotted. The phase shift can be related to a spatial delay or misregistration (Δx) in detecting a given spatial frequency according to the following formula

$$\Delta x = \frac{\Delta\phi}{k \times 180^{o}} \qquad \text{(II.10)}$$

Since $\Delta\phi/k$ is the slope of a line drawn through the origin to a given point on the curve, the maximum relative misregistration within the spatial frequency range $0 \leq k \leq 1/15$ half cycles per meter can be determined from the slope of a line, drawn through the origin, which is tangential to the peak of the curve. This produces the result

$$\Delta x_{max} = 1.07 \text{ meters} \quad @\ k = 1/24 \text{ half cycles per meter} \qquad \text{(II.11)}$$

for $0 \leq k \leq 1/15$ half cycles per meter.

For a system with 30 meter resolution, a maximum misregistration of 1.07 meters for some spatial frequencies is probably not critical.

The horizontal asymptote to the phase shift curve (Fig.II.14) is caused by defining the center of the effective field of view of the system (within-scan) to be at the horizontal centroid of the spatial weighting function (i.e., there is equal area enclosed beneath the curve to the left

and to the right of the "center"). In Fig.II.13, the within-scan spatial weighting function has been centered according to this convention. This causes the edge response of the system (the integral of the spatial weighting function or impulse response) to reach the 50% level when the effective field of view is "centered" on the edge (see Fig.II.15). Note that this edge response overshoots by only 1.5% and goes from 10% response to 90% response within less than 30 meters (a fairly sharp response).

If the signals recorded by this second system model, with 30 meter resolution, were digitized at the rate of one sample for every 30 meters of scan, the portion of the within-scan MTF curve (Fig. II.12) for $k > 1/30$ half cycles per meter would be accordion-folded back and forth between $k = 1/30$ half cycles per meter and $k = 0$ half cycles per meter, so that spatial frequencies greater than half the sample rate would masquerade as frequencies between zero and half the sample rate, accordingly. This masquerading effect is called aliasing. Since, for a 30 meter resolution system, by conventional definition the MTF at half a sample rate of once every 30 meters would be equal to .5, some aliasing at this sample rate is guaranteed. The amount of aliasing could be reduced somewhat by using more poles in the Butterworth filter, leading to a more rapid cutoff and a lower and lower cutoff frequency (asymptotic to half the sampling rate as more and more poles are added to the filter) via the design procedure outlined in Eqs. (II.5,II.6, and II.7). Another option would be to increase the sample rate, say by a factor of 2, so that the aliasing effect would become negligible. Such an approach would be mandatory should it be required to completely reconstruct the recorded digital signal in analog form. However, it is believed that the amount of terrestrial scenic content in the spatial frequency range between 1/30 half cycles per meter and 1/15 half cycles per meter is probably of major consequence only to the most demanding uses of the data (e.g., trying to resolve, locate, and analyze isolated features on the order of 30 meters by 30 meters in size). In fact, it is

not an uncommon procedure to try to reduce the amount of number crunching involved in classifying or displaying a large multispectral scene by processing only every other pixel from every other scan line. Digitizing an analog signal with 30 meter resolution by taking one sample for every 30 meters is in a sense equivalent to digitizing only every other sample from every other scan line that would have been required to fully represent the pre-digitized data in analog form.

The final TM system model adopted for the simulation to be performed at ERIM was the second model discussed above, which is described by Eqs. (II.4, II.9, II.10), and by Figs. II.5-8 and II-10-15. Although the response of the detectors was unknown (and hence omitted) and the remaining components of the system were based on educated guesses, it is believed that the model is sufficiently realistic to provide a useful and valid simulation. It should be noted that the effective resolution of the system, by conventional definition, when used to simulate 30 meter resolution, is 30 meters in the within-scan direction but is only 28 meters in the along-track direction. Although the model could have been adjusted to produce the same exact resolution (by conventional definition) in both directions (e.g., by assuming a rectangular rather than square IFOV), this was judged not to be of major importance, since it is expected that the real system will probably not have a more equally matched resolution in both directions than the model.

The application of the model in smoothing aircraft data for the simulation, and the effective sampling rate for the model are to some degree dependent on the sample spacing in the aircraft data. Although a simulated LANDSAT-D sampling rate of one sample for every 30 meters was the goal (for 30 meter resolution), the necessity of replacing every n by m aircraft samples by one simulated Landsat Follow-on sample constrained the resultant simulated sampling rate to be slightly different from the goal.

Since the aircraft data contained one sample value for every 7.6 meters within-scan and one for every 10 meters along-track, the following effective sampling rates were obtained for each of the four resolutions simulated:

Resolution (meters)	Number of Aircraft Pixels Replaced Per Sample		Effective Sampling Rate (per meter)	
	Within-Scan	Along-Track	Within-Scan	Along-Track
30	4	3	1/30.4	1/30
40	5	4	1/38.0	1/40
50	7	5	1/53.2	1/50
60	8	6	1/60.8	1/60
90	12	9	1/91.2	1/90

These variations in the effective sampling rates from those rates intended are judged to cause an insignificant change in the information content of the simulated TM data.

To digress for a moment, the 90m simulation was carried out to provide a Landsat-1 like resolution data set so that results for finer resolution data could be compared to Landsat-1. The basis for calling Landsat-1 data 90m was that, according to Oscar Weinstein of GSFC, the Modulation Transfer Function for Landsat-1 and that proposed for Landsat Follow-on TM are similar in shape but that the curve for Landsat-1 has a response of .42 at 1/80 half cycles per meter. Examination of the MTF curve showed that the corresponding frequency at the .50 response point was 1/90 half cycles per meter. Therefore, by the accepted definition of resolution, the Landsat-1 system, in operation, has a resolution of 90 meters.

The smoothing of the aircraft data for the simulation, according to the spatial weighting functions chosen (Figs. II.6 and II.13), was accomplished by adjusting the horizontal scale of the within-scan and along-track weighting curves to match each desired resolution, and then reading values from the curves at 7.6 meter intervals (within-scan) and at 10 meter intervals

(along-track), respectively, to determine the discrete weighting factors to be applied to each aircraft pixel. These weighting factors were then multiplied by a normalization factor to make this sum equal to unity. The resulting weights are listed below, separately for the within-scan and along-track weightings.

TABLE II.1

WEIGHTING FACTORS

Resolution (meters)	Weighting Factors (within-scan)												
30	.068	.164	.233	.248	.193	.093							
40	.022	.062	.120	.160	.180	.176	.158	.085	.036				
50	.033	.076	.118	.148	.164	.163	.133	.095	.051	.018			
60	.022	.045	.069	.092	.109	.120	.124	.120	.107	.083	.058	.035	.016
90	.008	.016	.022	.034	.043	.051	.063	.070	.075.	.079	.082	.083	
	.080	.076	.061	.050	.039	.031	.018	.012	.006				

Resolution (meters)	Weighting Factors (along-track)											
30	.060	.278	.325	.278	.060							
40	.058	.194	.248	.248	.194	.058						
50	.057	.147	.195	.202	.195	.147	.057					
60	.046	.115	.163	.176	.176	.163	.115	.046				
90	.009	.037	.070	.097	.111	.116	.117	.116	.111	.097	.070	.037
		.009										

Weighting factors corresponding to values from the weighting curves which were less than 10% of the peak value from the curves were not used, so that the number of pixels to be weighted and summed to generate each simulated Landsat Follow-on TM pixel could be minimized. The weight applied to each aircraft pixel in each sum was then the product of the appropriate within-scan and along-track weighting factors. These simplifications in the weighting or smoothing procedure are believed not to affect significantly the accuracy of the Landsat Follow-on TM simulation.

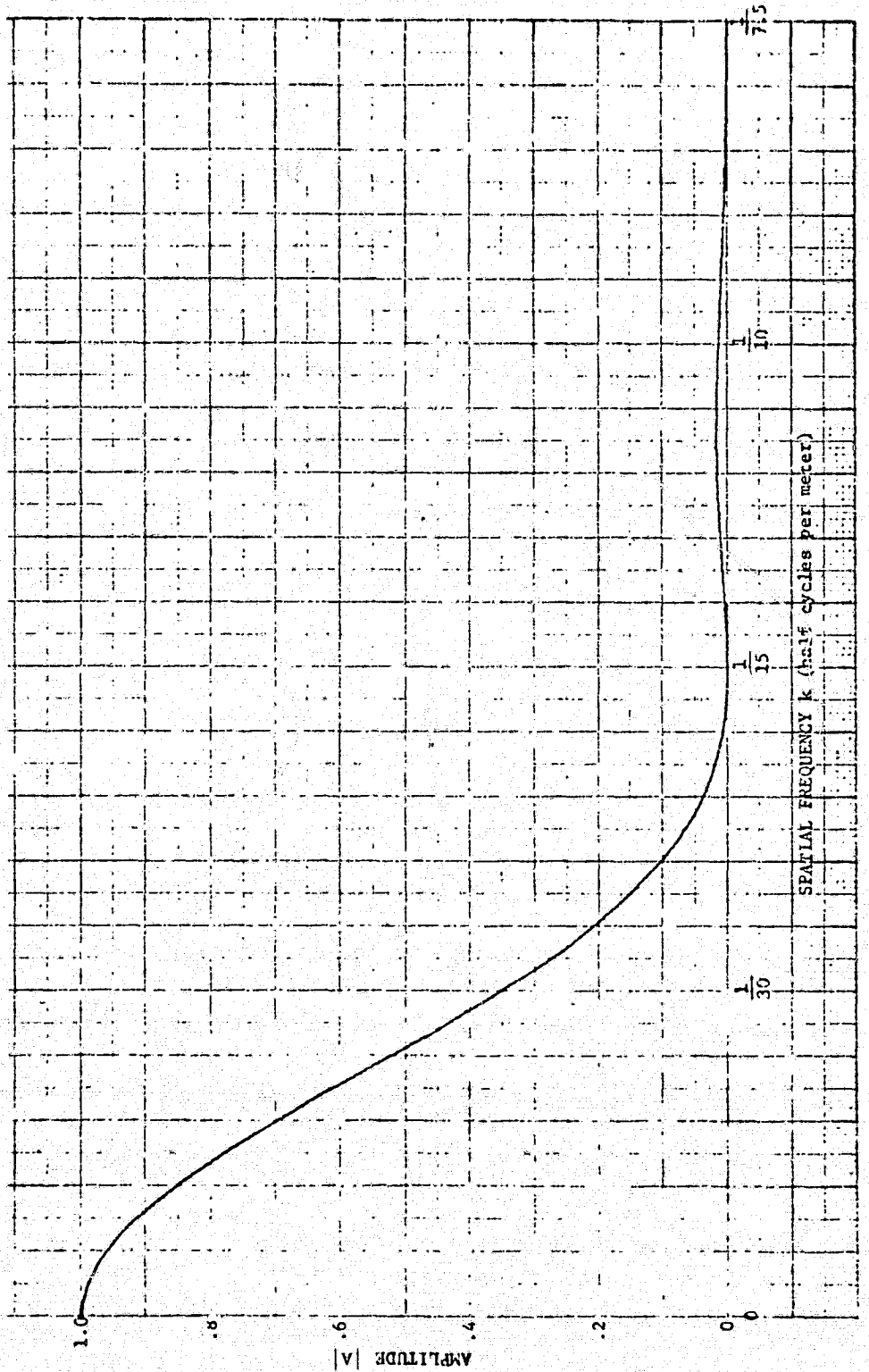

FIGURE II-3. INITIAL LANDSAT FOLLOW-ON TM SIMULATION WITHIN-SCAN MODULATION TRANSFER FUNCTION "30 METER" RESOLUTION.

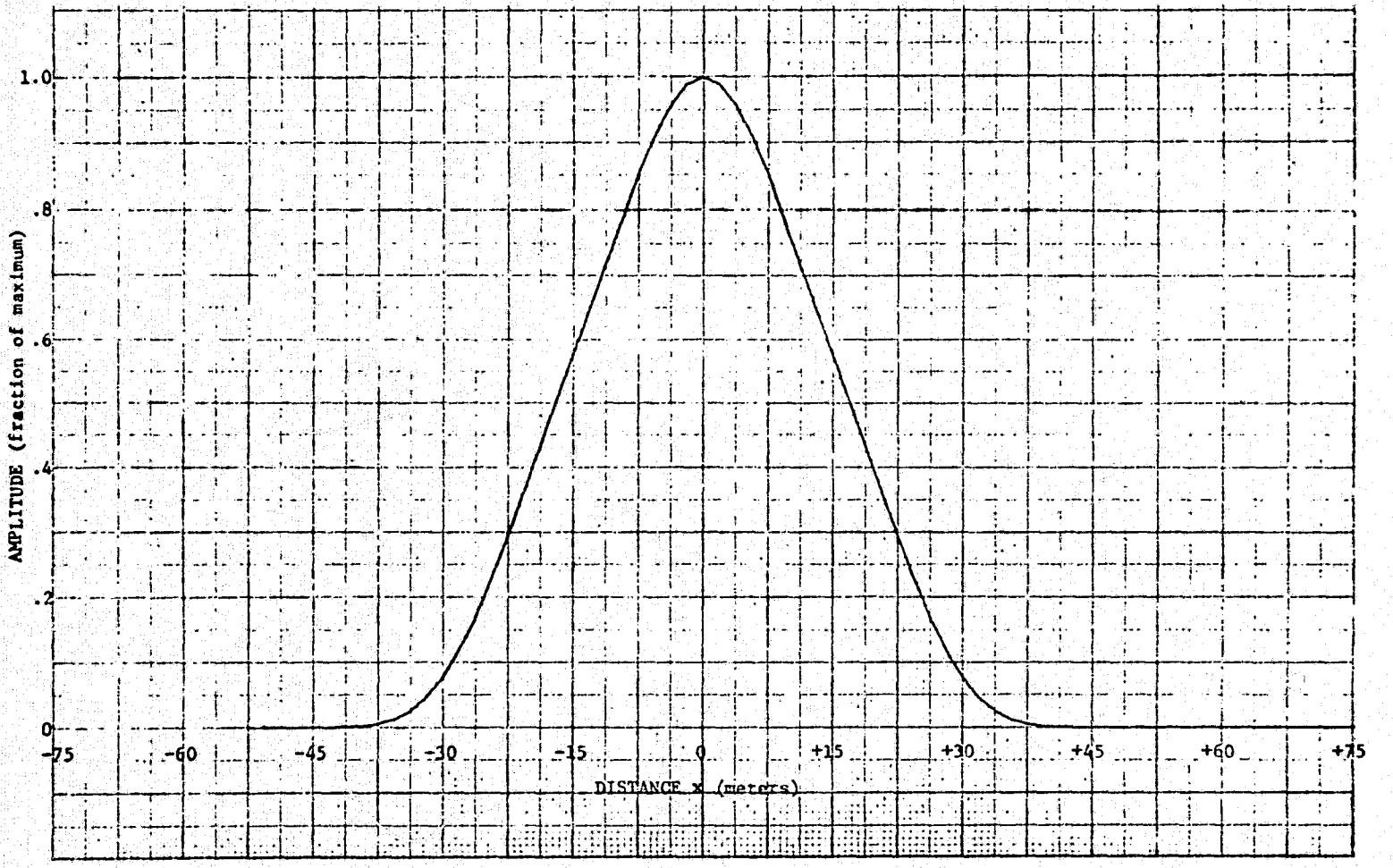

FIGURE II-4 INITIAL LANDSAT FOLLOW-ON TM SIMULATION WITHIN-SCAN SPATIAL WEIGHTING FUNCTION "30 METER" RESOLUTION

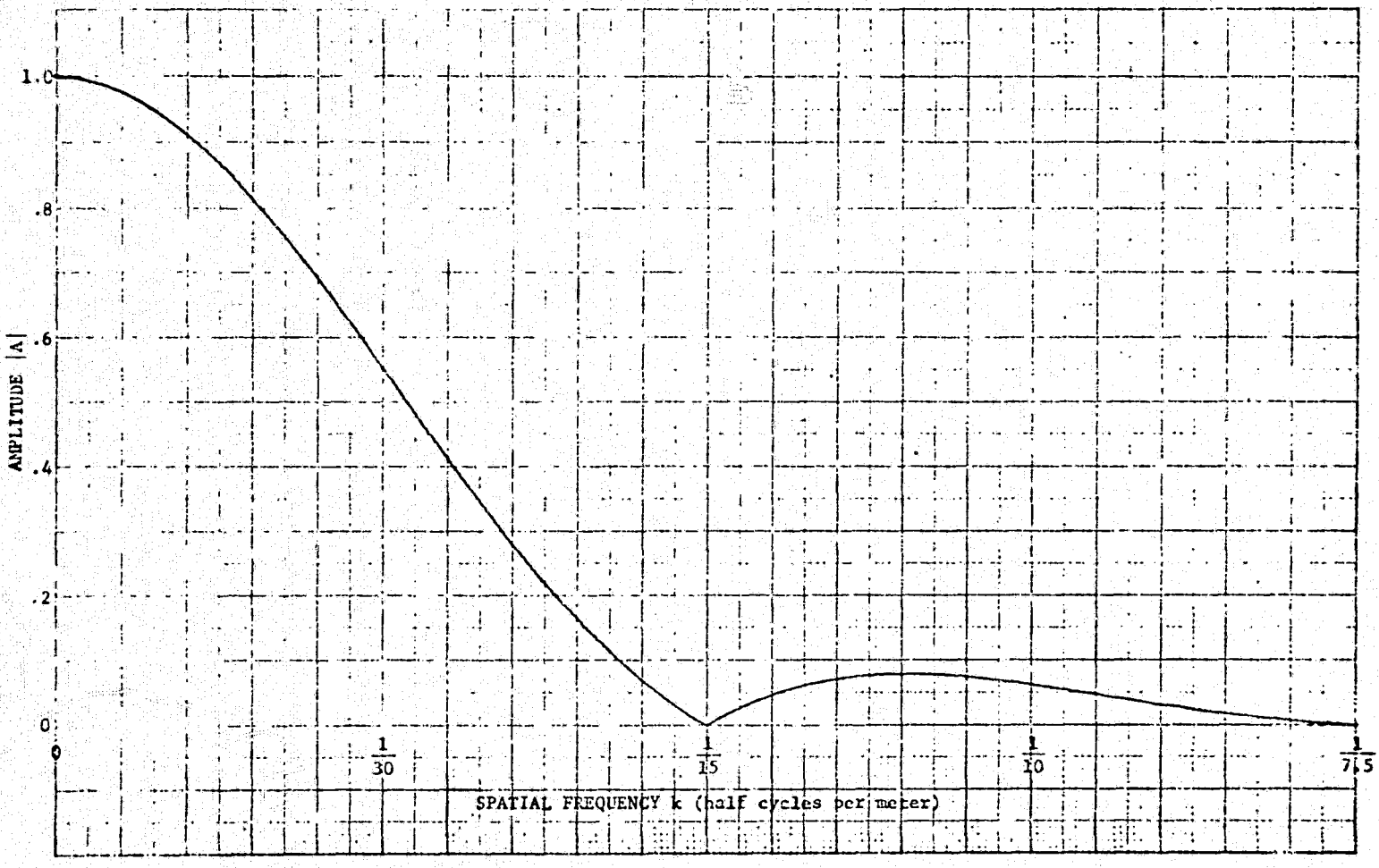

FIGURE II-5 INITIAL AND FINAL LANDSAT FOLLOW-ON TM SIMULATION ALONG-TRACK MODULATION TRANSFER FUNCTION "30 METER" RESOLUTION

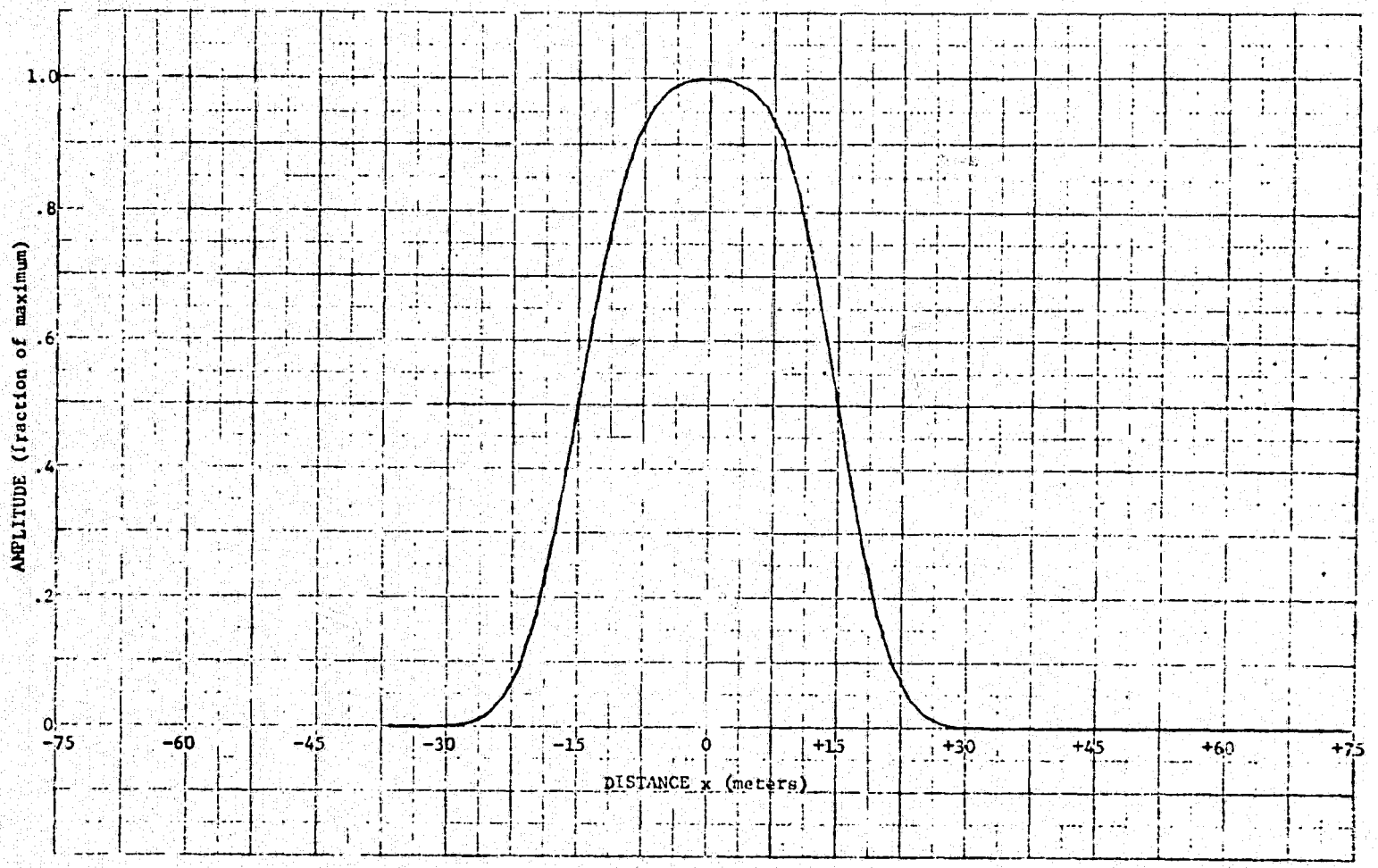

FIGURE II-6 INITIAL AND FINAL LANDSAT FOLLOW-ON TM SIMULATION ALONG-TRACK SPATIAL WEIGHTING FUNCTION "30 METER" RESOLUTION

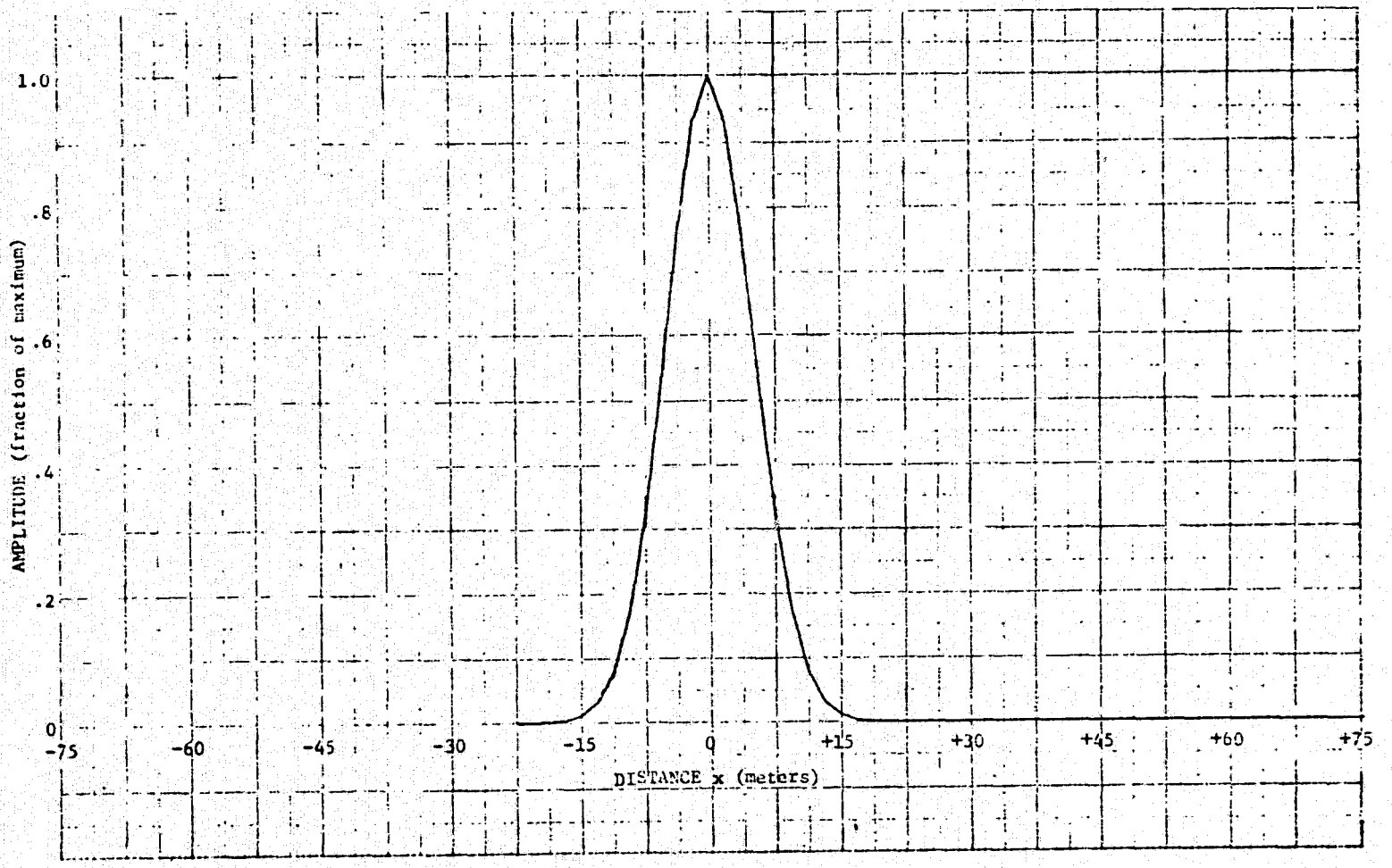

FIGURE II-7 INITIAL AND FINAL LANDSAT FOLLOW-ON TM SIMULATION GAUSSIAN BLUR SPATIAL WEIGHTING COMPONENT STANDARD DEVIATION (σ) = 5 meters

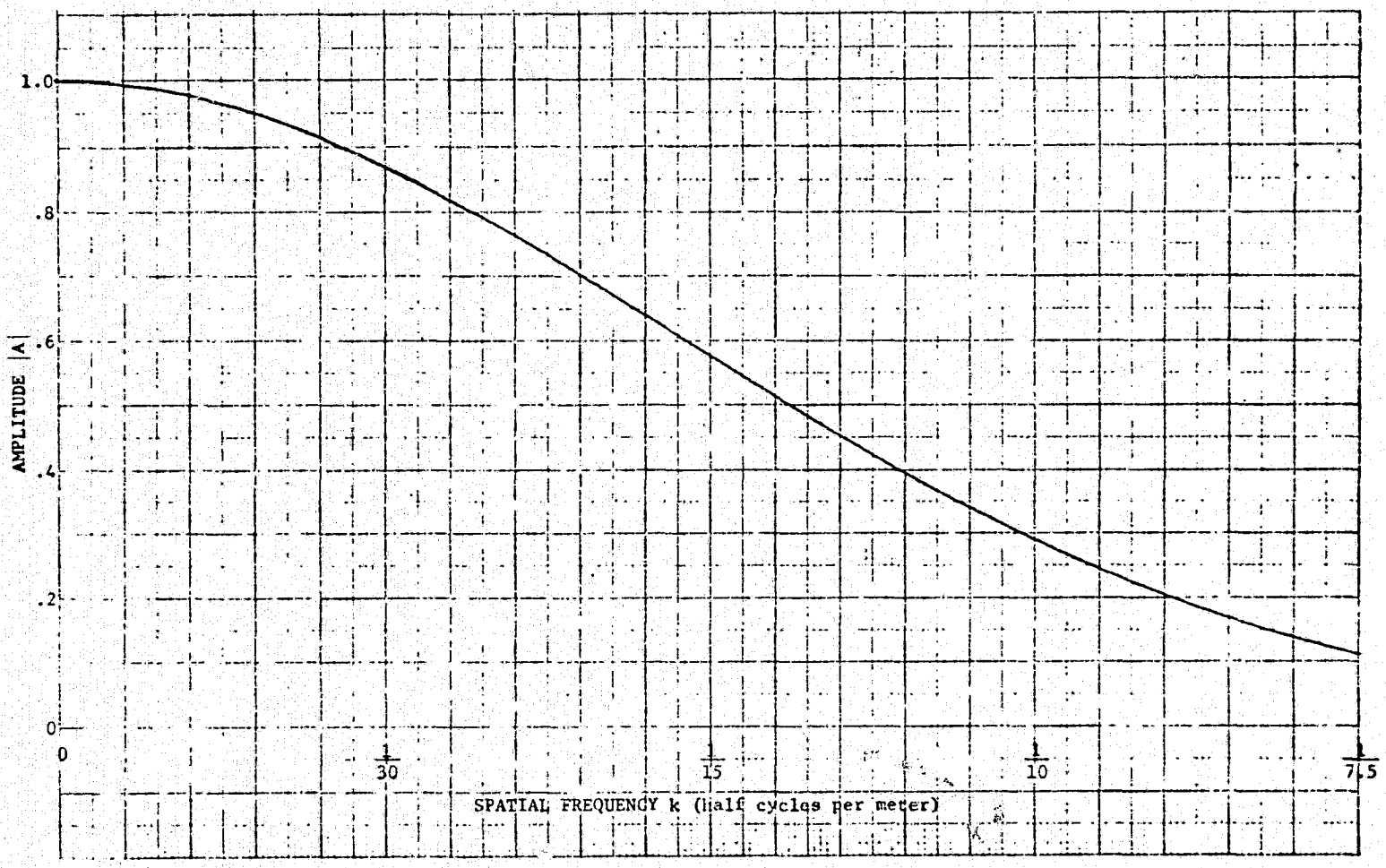

FIGURE II-8 INITIAL AND FINAL LANDSAT FOLLOW-ON TM SIMULATION GAUSSIAN BLUR MODULATION TRANSFER COMPONENT SPATIAL STANDARD DEVIATION (σ) = 5 meters

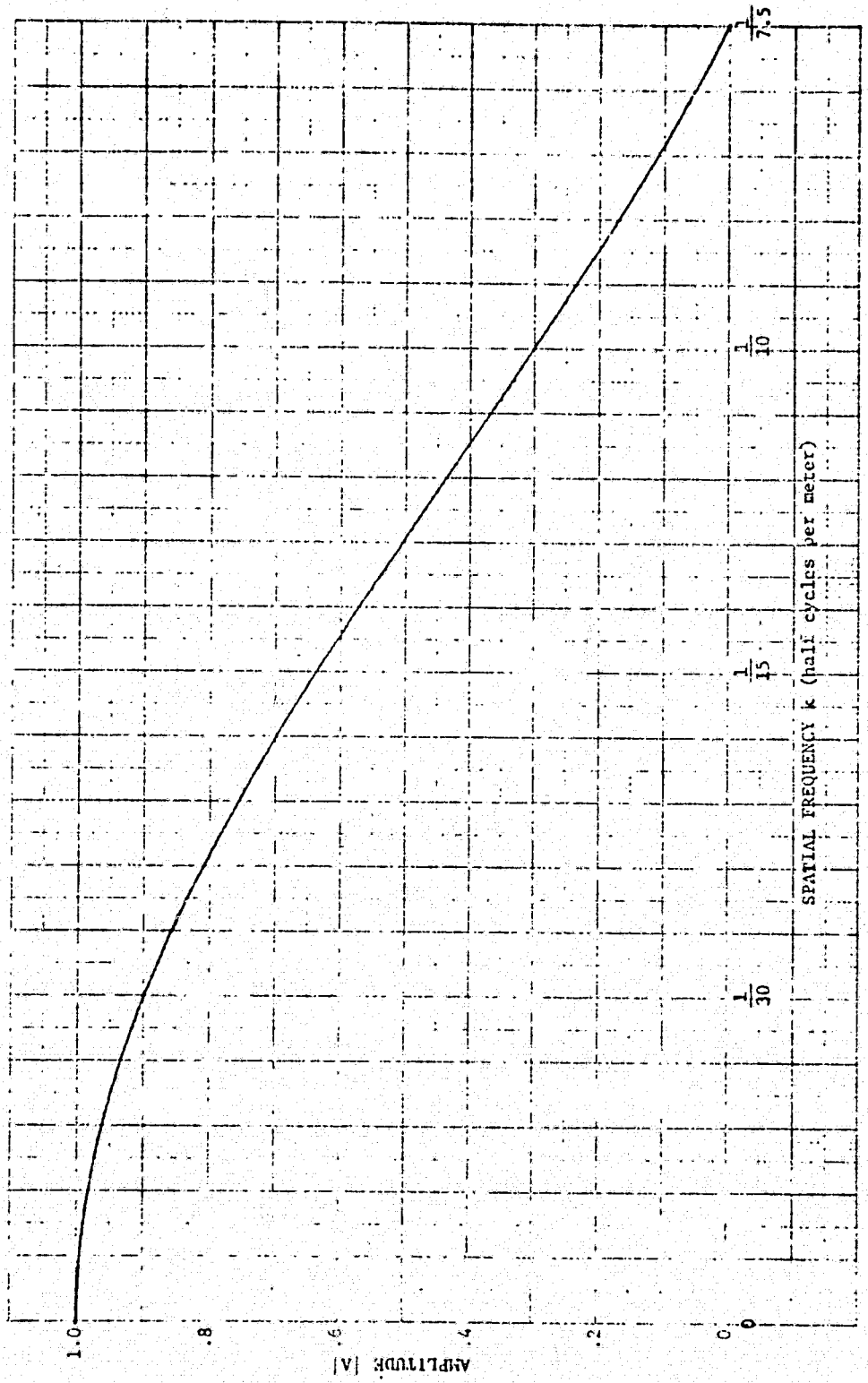

FIGURE II-9 SECOND LANDSAT FOLLOW-ON TM SIMULATION [OPTION #1] 15-METER IFOV MODULATION TRANSFER COMPONENT OF WITHIN-SCAN SYSTEM RESPONSE

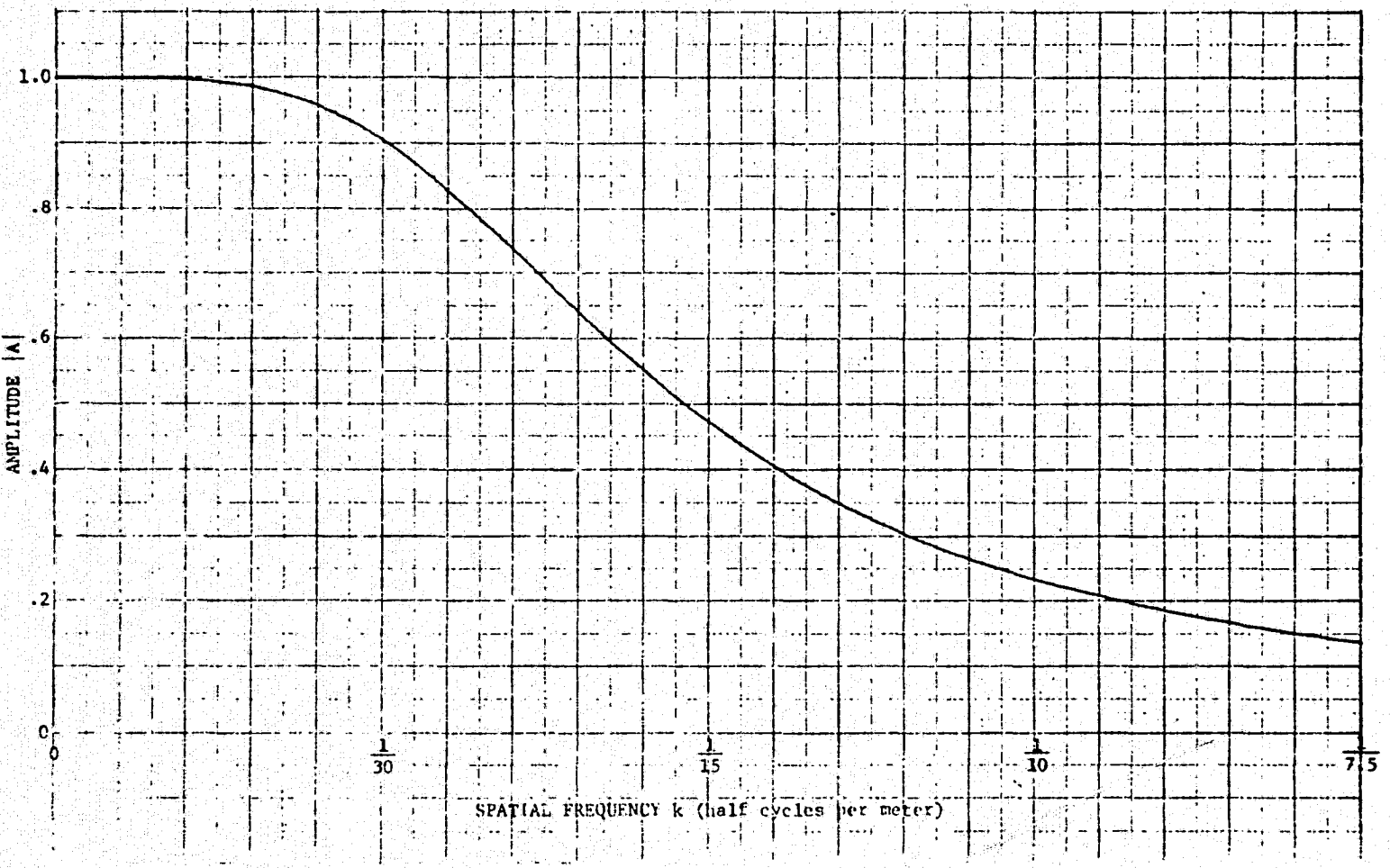

FIGURE II-10 FINAL LANDSAT FOLLOW-ON TM SIMULATION: 2 POLE BUTTERWORTH MODULATION TRANSFER COMPONENT OF WITHIN-SCAN SYSTEM RESPONSE

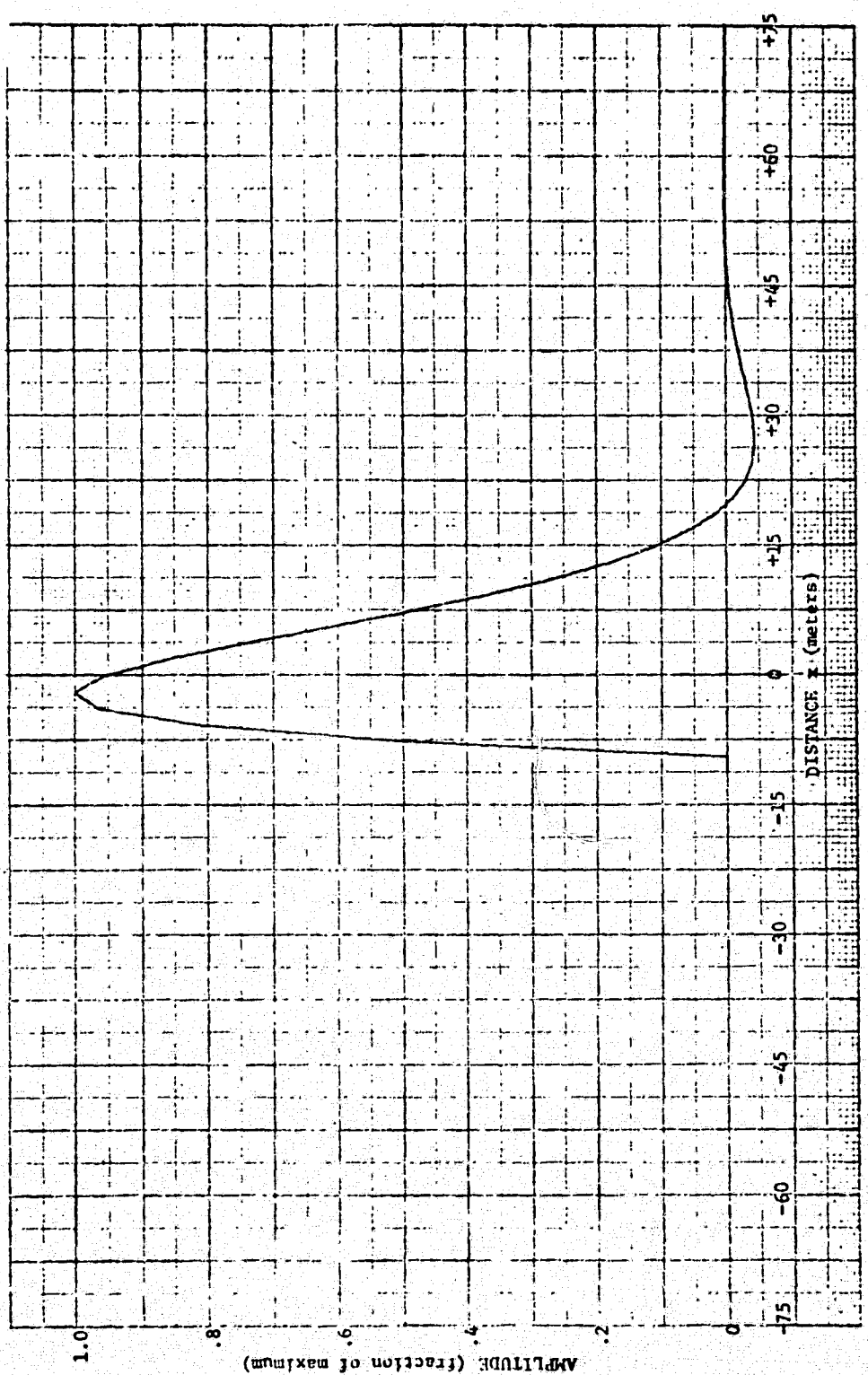

FIGURE II-11 FINAL LANDSAT FOLLOW-ON TM SIMULATION: 2 POLE BUTTERWORTH SPATIAL WEIGHTING COMPONENT OF WITHIN-SCAN SYSTEM RESPONSE

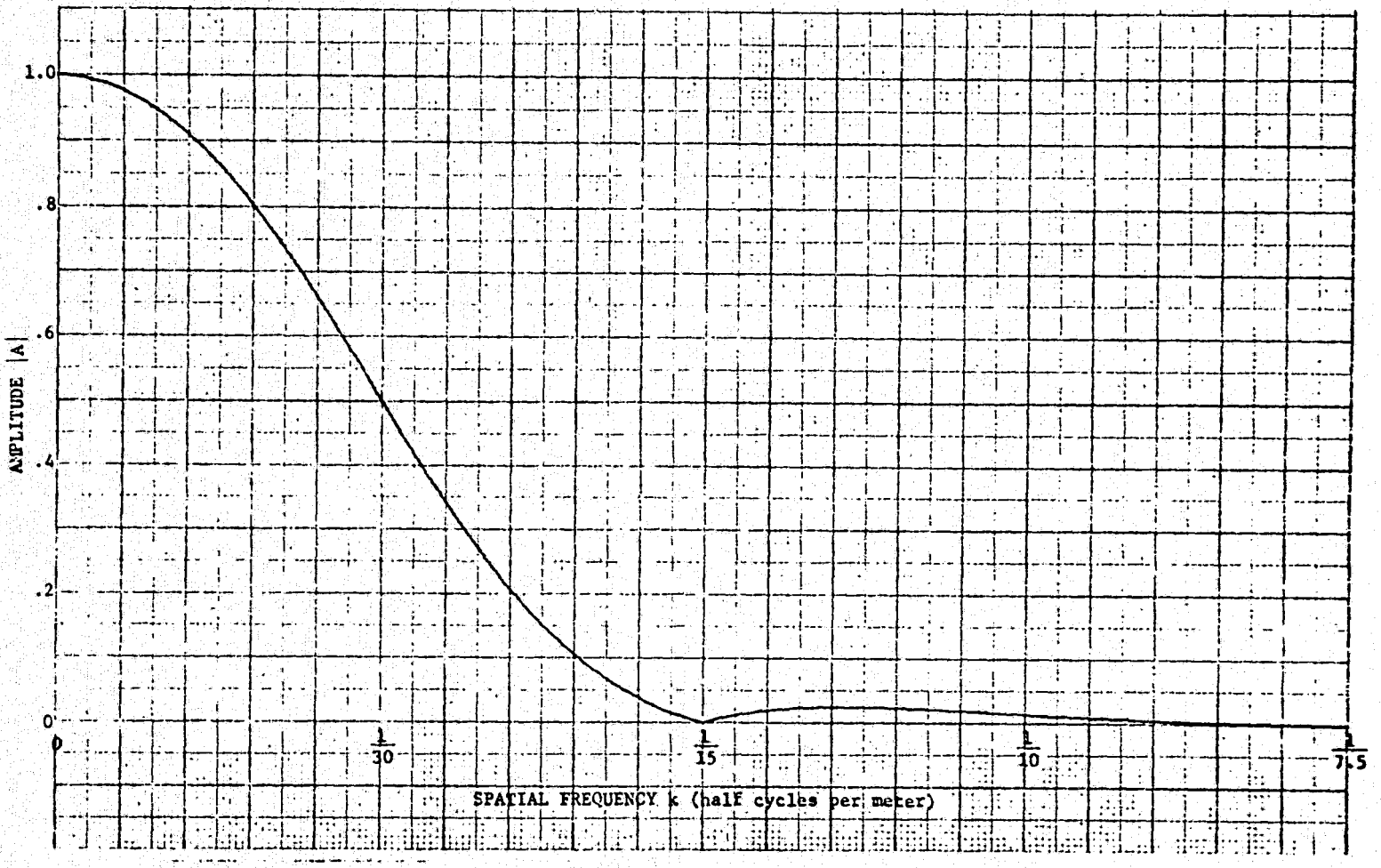

FIGURE II-12 FINAL LANDSAT FOLLOW-ON TM SIMULATION WITHIN-SCAN MODULATION TRANSFER FUNCTION 30 METER RESOLUTION

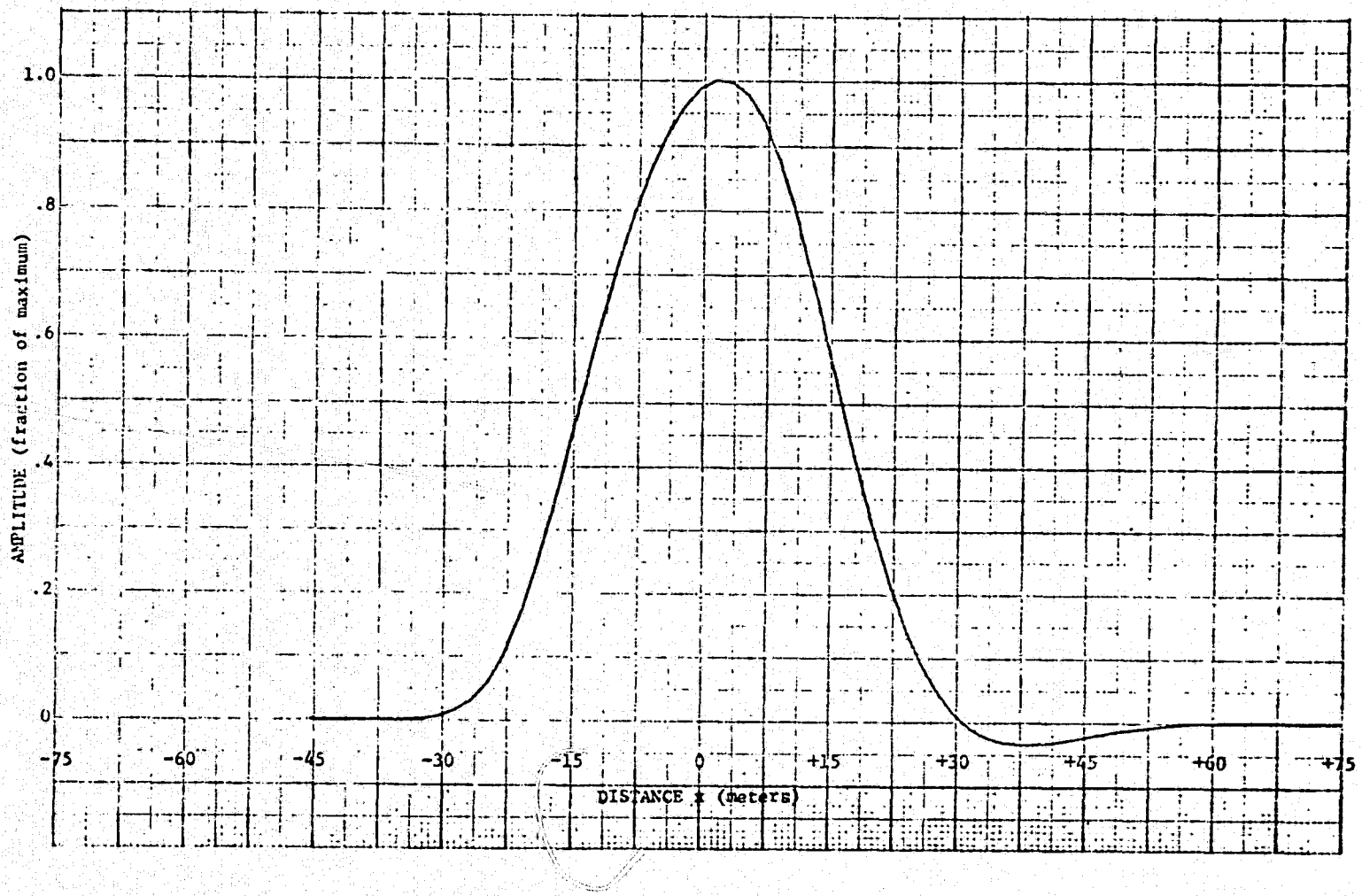

FIGURE II-13 FINAL LANDSAT FOLLOW-ON TM SIMULATION WITHIN-SCAN SPATIAL WEIGHTING FUNCTION
30 METER RESOLUTION

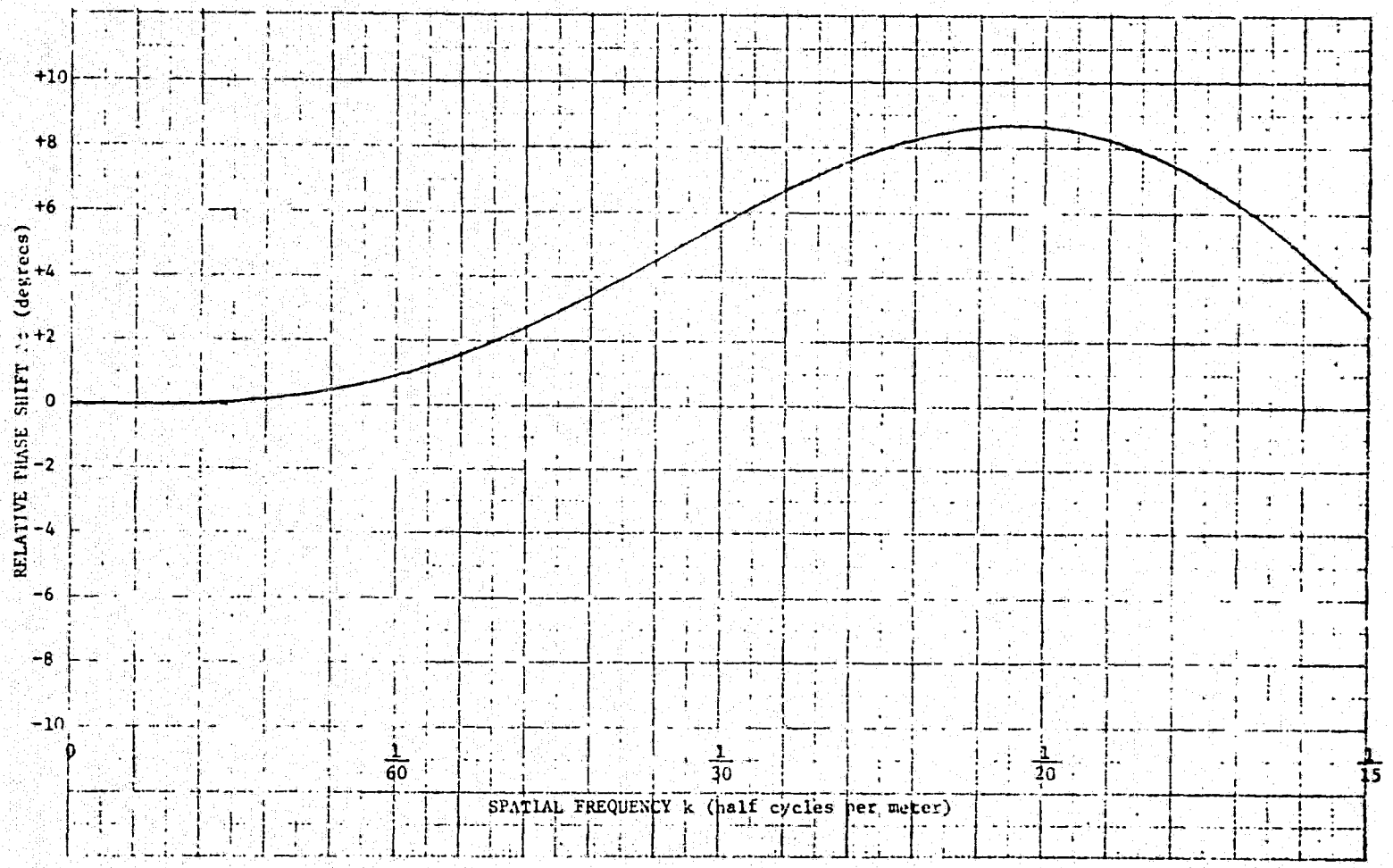

FIGURE II-14 FINAL LANDSAT FOLLOW-ON TM SIMULATION WITHIN-SCAN RELATIVE PHASE SHIFT 30 METER RESOLUTION

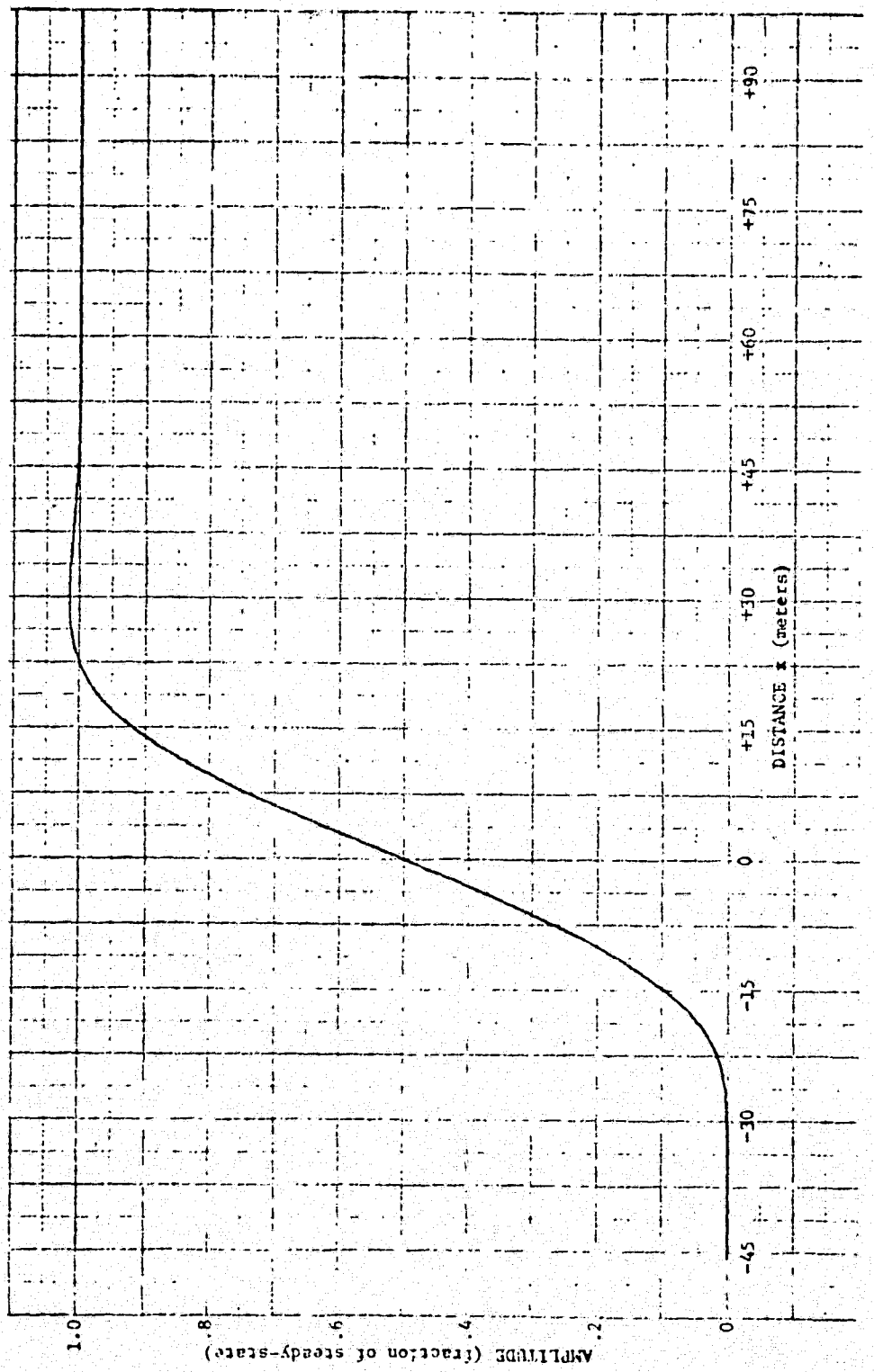

FIGURE II-15. FINAL LANDSAT FOLLOW-ON TM SIMULATION WITHIN-SCAN SPATIAL EDGE RESPONSE 30 METER RESOLUTION

II.2 NOISE ADDITION

The process of averaging many pixels together to obtain the simulated data pixel results in data which is essentially noiseless. To simulate the expected radiometric quality of the LANDSAT-D data, it is necessary to add noise to the data. This is accomplished in digital computer processing by adding the output of a Gaussian distribution random number generator subroutine to each channel of the simulated data. The generator is set up so that the mean of the resulting population is zero and the standard deviation is equal to $DE\Delta\rho$, the number of data quantization levels corresponding to the specified $NE\Delta\rho$ ($NE\Delta T$) for each channel(band) of data. The set of $DE\Delta\rho$ for each data set is given in Appendix I, Section I.3 along with a discussion of their derivation.

II.3 SPECTRAL SIMULATION

Spectral simulations also are carried out as part of this study so as to accurately simulate thematic mapper data. The seven spectral bands recommended by the Landsat Follow-on Thematic Mapper Technical Working Group are listed below with the M7 bands which were used to simulate them.

TABLE II.2
THEMATIC MAPPER SPECTRAL BANDS

SPECIFIED	SIMULATED VIA M-7
0.45-0.52 μm	(0.46-0.49μm) + (0.48-0.51μm)
0.52-0.60 μm	(0.52-0.57μm) + (0.54-0.60μm)
0.63-0.69 μm	0.61-0.70 μm
0.74-0.80 μm 0.80-0.91 μm	0.72-0.92 μm
1.55-1.75 μm	1.5-1.8 μm
10.4-12.5 μm	9.3-11.7 μm

As indicated above, the simulation of the Thematic Mapper bands using M7 scanner bands was accomplished for four of the bands by simply using the most similar M7 bands. For the other two TM bands, 1 and 2, a simple average was done to combine the two M7 bands to simulate each of the TM bands in those regions.

II.4 IMPLEMENTATION OF SPATIAL RESOLUTION SIMULATION MODEL

The implementation of the Spatial Resolution Simulation Model to generate data for spatial resolutions of 30,40,50,60, and 90 meters was carried out according to the flow in Fig. II.1. First the point-spread functions were applied on a pixel-by-pixel basis within each discrete window. Then the output pixel was perturbed by the addition of noise to each channel of data, as described above. Finally, the spectral simulation was carried out to yield the simulated Landsat Follow-on Thematic Mapper data.

APPENDIX III

TRAINING PROCEDURES

This discussion outlines the training procedures used. It should be kept in mind that the spatially simulated data had the same IFOV in each band.

Two training procedures were carried out for this study. The first used only pixels from a certain subset of fields which, for each of the four data sets, yielded field signatures at all resolutions. In this manner differences in classification which might have resulted from using different training data at each resolution were negated. The second procedure utilized all available information at each resolution, thus more realistically depicting expected processing results for each resolution. All training procedures were carried out using only field center pixels, as defined below.

III.1 DEFINITION OF FIELD CENTER PIXELS

It is important when carrying out multivariate pattern recognition, that the data used to train the algorithms represent pure instances of the classes of interest. To this end, it is therefore important in processing multispectral scanner data to use for training only those pixels which are known with certainty to represent pure samples of the classes of interest. Such samples are known as field center pixels, for obvious reasons.

The first step in identifying field center pixels is to identify the locations of the fields. This was accomplished using gray scale maps of the 10 meter data for each of the four data sets. At ERIM, we have developed a philosophy of describing fields as polygons (not necessarily convex) with n vertices. Thus by identifying the line and point coordinates of all the vertices of each field, the fields were defined.

To identify with confidence those pixels inside a field which lie entirely within the borders of the field (and are therefore to be considered pure or field center pixels) a smaller, similar polygon is inscribed within the one being considered. A pixel is identified as being a field center pixel if its center is within the inscribed, inset polygon. The amount the inscribed polygon is inset is calculated so that in the worst case a field center pixel will be resolving only an area entirely within the field.

Since we want to train (and later evaluate classification performance) on field center pixels, the first step was to identify the inset to be used. In general, different insets can be specified for the along-scan and the along-track direction. The formula can be written as

INSET = RESOLUTION * 0.5 + ERROR IN LOCATION

For these data, the error in field vertex location was less than one-half pixel or about 3.8 and 5m in the two directions. The value used for resolution was the distance between the zero response points of the digital point-spread functions used. The resulting insets calculated for each case are given in Table III.1.

A tabulation of the number of such pure pixels available at each resolution was conducted and is presented in Figs. III.1 and III.2 for the two study segments. Roughly speaking, the general trend is to lose 60% of the field center pixels when degrading resolution by 10m. Obviously, this result is specific to the field-size distribution studied and also to the shape (aspect ratio) of the fields.

TABLE III.1

POLYGON INSETS FOR IDENTIFYING FIELD CENTER PIXELS

SIMULATED RESOLUTION	DIRECTION	RESOLVING DISTANCE	* 0.5	+ ERROR IN LOCATION	= TOTAL INSET
10M	Along Scan	7.6 meters	* 0.5	+ 3.8 meters	= 7.6 meters
10M	Along Track	10		5.0	10.0
30M	Along Scan	46		3.8	27.0
30M	Along Track	50		5.0	30.0
40M	Along Scan	68		3.8	38.0
40M	Along Track	60		5.0	35.0
50M	Along Scan	76		3.8	42.0
50M	Along Track	70		5.0	40.0
60M	Along Scan	99		3.8	53.0
60M	Along Track	80		5.0	45.0
90M	Along Scan	160		3.8	84.0
90M	Along Track	130		5.0	70.0

III.2 COMMON-FIELD SIGNATURE TRAINING PROCEDURE

It was desired to design an initial training procedure for which any changes noted in classification results could be attributed with certainty to effects of changing spatial resolution and not to anomalies in fields or inconsistancies in the training process. Therefore, the procedure defined used only those fields and those areas from which field center pixels were available at all resolutions.

Thus signatures at all resolutions were calculated for the same set of fields, where the fields were defined as those which had a minimum of six field center pixels* at the coarsest resolution (90 meters). For the set of fields identified, signatures for each field were calculated using the standard ERIM statistics program, which includes an editing capability to detect and reject outliers -- pixels which are not from the same distribution as the majority of the pixels from the specified field. At no time were the signatures combined. This meant that there was some within-class overlap between signatures, but this did not impact the classification performance.

III.3 ALL-FIELD SIGNATURE TRAINING PROCEDURE

The field signature extraction procedure defined above used only the same common set of fields at all resolutions. There is also the consideration of having more training information available at 30 meters than at 90 meters and a need to understand what the effects are of using the increased information available. A study of the number of field center pixels at each simulated resolution for the two sites was carried out. As seen in Figs. III.1 and III.2, the number available goes from tens of thousands at 10-meter resolution to tens at 90-meter resolution. The number of fields from which field center pixels can be found also decreases substantially with coarsening resolution. Training on all available data is important, especially as regards the radiometric simulation where it is important to simulate as closely as possible all the expected spectral variation in the scene.

Thus, a training procedure, here called the all-field training procedure, was defined and implemented to utilize as much of the available information for training as possible. The procedure used was to first extract signatures from all individual fields; signatures with singular covariance matrices (i.e., which were calculated using fewer independent samples than there were channels of information) were discarded. The signatures, were then grouped using an algorithm based solely on clusters of means of the signatures, thus taking advantage of spectral similarities between many of the signatures to reduce the number of signatures for training the computer from 120-140 to around 20. The algorithm to group the signatures was unsupervised -- i.e., signatures could be grouped irrespective of their class -- but in practice only groups of signatures of common class resulted.

*A minimum of six pixels in a field is required because, for this procedure, individual field signatures were calculated and a minimum of six independent samples is required in order to have a positive definite covariance matrix of order six (because here, there are six channels of data being processed).

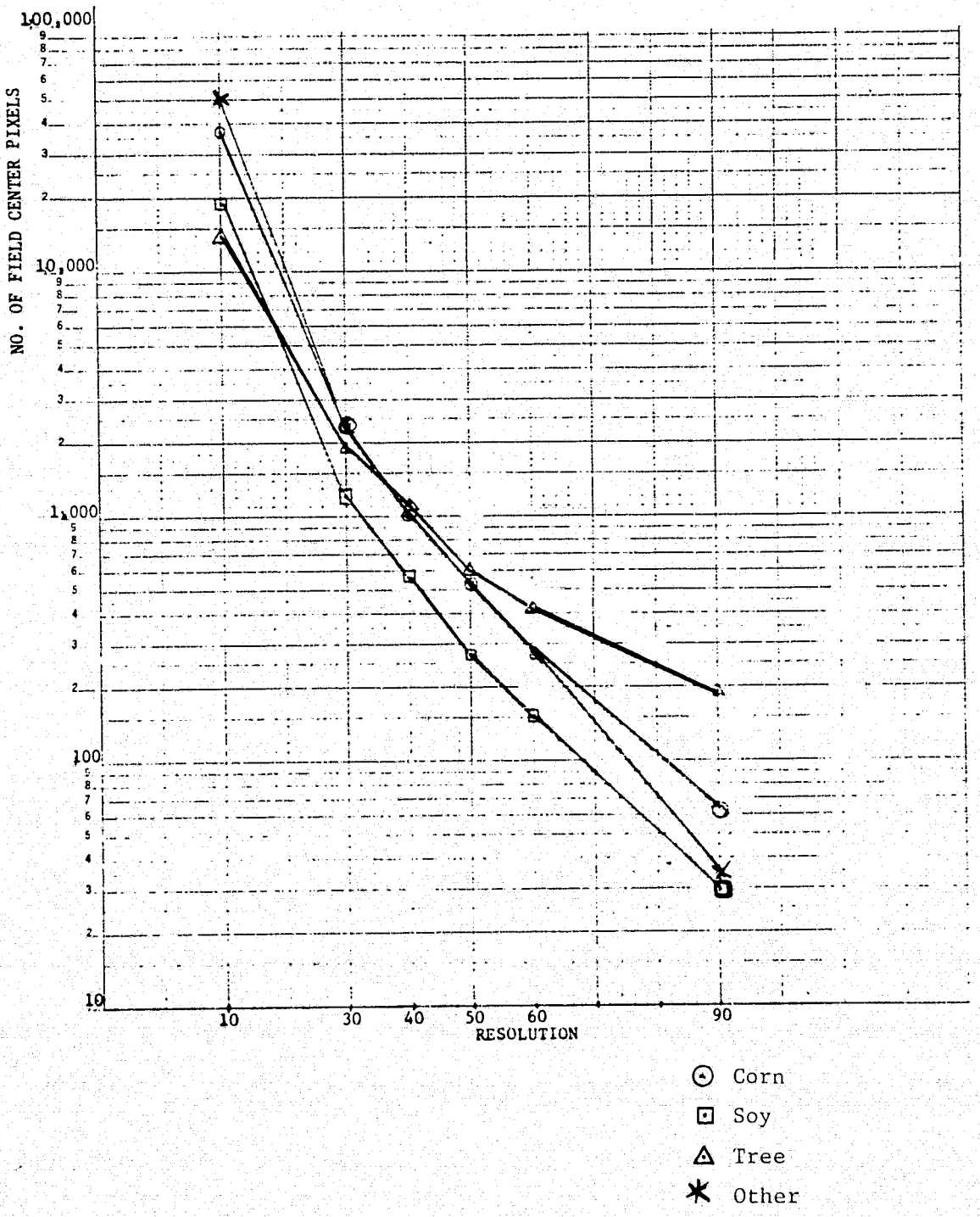

FIGURE III-1. NUMBER OF FIELD CENTER PIXELS BY CLASS AS A FUNCTION OF SPATIAL RESOLUTION, SEGMENT 212

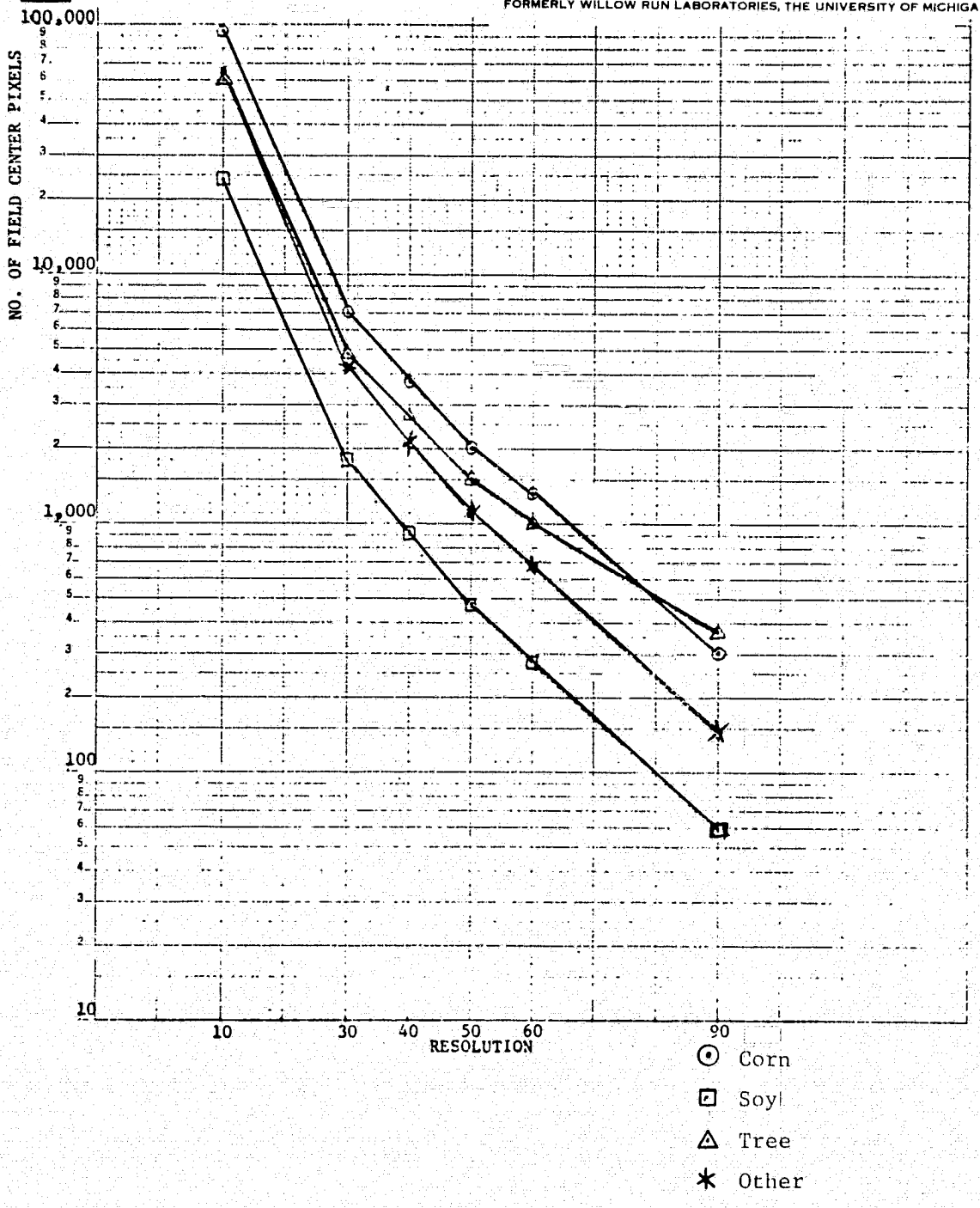

FIGURE III-2. NUMBER OF FIELD CENTER PIXELS BY CLASS AS A FUNCTION OF SPATIAL RESOLUTION, SEGMENT 204

APPENDIX IV

TABULAR RESULTS FOR SPATIAL RESOLUTION STUDY

This appendix presents the complete tabular results obtained for the spatial resolution study. At the end, several relevant graphs of the tabular data are included.

The results reported herein include data of spatial resolutions 10, 30, 40, 50, 60 and 90 meter. The results of the processing of the 10 meter data (original M-7 resolution) were not included in the analyses presented in the text because the noise level inherent in the 10 meter data (approximately 1.0 per cent NE$\Delta\rho$) does not match that in the coarser resolution data, and hence direct comparisons between the 10 meter results and those obtained for the other resolutions could not be accomplished in a meaningful way. The 10 meter results are included here for completeness.

TABLE IV.1

FIELD CENTER CLASSIFICATION RESULTS
(Common Field Signature Training Procedure)
S-212 Aug 17 (43M)

10 METER

	CORN	SOY	TREE	OTHER	UNCLAS.
CORN	94	1	1	1	3
SOY	0	90	0	3	7
TREE	0	0	99	1	0
OTHER	3	1	1	87	8

OVERALL = 92.82%

30 METER

	CORN	SOY	TREE	OTHER	UNCLAS.
CORN	95	0	0	2	3
SOY	0	90	0	3	7
TREE	0	0	100	0	0
OTHER	2	1	0	94	3

OVERALL = 94.59%

40 METER

	CORN	SOY	TREE	OTHER	UNCLAS.
CORN	96	0	0	1	3
SOY	0	91	0	2	7
TREE	0	0	100	0	0
OTHER	2	2	0	96	0

OVERALL = 95.62%

50 METER

	CORN	SOY	TREE	OTHER	UNCLAS.
CORN	92	0	1	2	5
SOY	0	89	0	3	8
TREE	0	0	99	0	1
OTHER	0	1	0	98	1

OVERALL = 93.09%

TABLE IV.1 (Continued)

S-212 Aug 17 (43M)

60 METER

	CORN	SOY	TREE	OTHER	UNCLAS.
CORN	92	0	0	1	7
SOY	0	88	0	2	10
TREE	0	0	100	0	0
OTHER	2	0	0	95	3

OVERALL = 92.39%

90 METER

	CORN	SOY	TREE	OTHER	UNCLAS.
CORN	75	1	0	1	23
SOY	0	81	0	4	15
TREE	0	0	80	0	20
OTHER	0	0	0	94	6

OVERALL = 78.85%

TABLE IV.2

FIELD CENTER CLASSIFICATION RESULTS
(Common Field Signature Training Procedure)
S-204 Aug 13 (43M)

10 METER

	CORN	SOY	TREE	OTHER	UNCLAS.
CORN	98	0	0	1	1
SOY	0	91	1	2	6
TREE	0	0	93	0	7
OTHER	0	0	0	96	4

OVERALL = 95.95%

30 METER

	CORN	SOY	TREE	OTHER	UNCLAS.
CORN	98	1	0	0	1
SOY	1	97	0	0	2
TREE	1	0	95	0	4
OTHER	0	0	0	98	2

OVERALL = 97.47%

40 METER

	CORN	SOY	TREE	OTHER	UNCLAS.
CORN	97	1	0	0	2
SOY	0	98	0	0	2
TREE	1	1	94	0	4
OTHER	0	0	0	98	2

OVERALL = 96.94%

50 METER

	CORN	SOY	TREE	OTHER	UNCLAS.
CORN	99	1	0	0	0
SOY	1	97	0	0	2
TREE	0	0	91	0	9
OTHER	0	0	0	95	5

OVERALL = 97.24%

TABLE IV.2 (Continued)

S-204 Aug 13 (43M)

60 METER

	CORN	SOY	TREE	OTHER	UNCLAS.
CORN	95	1	0	0	4
SOY	0	98	0	0	2
TREE	0	0	95	0	5
OTHER	0	0	0	95	5

OVERALL = 95.48%

90 METER

	CORN	SOY	TREE	OTHER	UNCLAS.
CORN	97	0	0	0	3
SOY	0	82	0	0	18
TREE	0	0	90	0	10
OTHER	0	0	0	96	4

OVERALL = 93.85%

TABLE IV.3

FIELD CENTER CLASSIFICATION RESULTS
(Common Field Signature Training Procedure)
S-204 Aug 5 (42M)

10 METER

	CORN	SOY	TREE	OTHER	UNCLAS.
CORN	98	0	0	0	2
SOY	6	80	0	0	14
TREE	0	0	92	0	8
OTHER	0	0	0	97	3

OVERALL = 94.23%

30 METER

	CORN	SOY	TREE	OTHER	UNCLAS.
CORN	97	2	0	0	1
SOY	7	89	0	0	4
TREE	0	0	97	0	3
OTHER	0	0	0	99	1

OVERALL = 96.40%

40 METER

	CORN	SOY	TREE	OTHER	UNCLAS.
CORN	97	1	0	0	2
SOY	7	90	0	0	3
TREE	0	0	97	0	3
OTHER	0	0	0	100	0

OVERALL = 96.64%

50 METER

	CORN	SOY	TREE	OTHER	UNCLAS.
CORN	98	1	0	0	1
SOY	6	91	0	0	3
TREE	0	0	96	0	4
OTHER	0	0	0	100	0

OVERALL = 96.99%

TABLE IV.3 (Continued)

S-204 Aug 5 (42M)

60 METER

	CORN	SOY	TREE	OTHER	UNCLAS.
CORN	98	1	0	0	1
SOY	5.5	88.5	0	3	3
TREE	0	0	91	0	9
OTHER	0	0	0	99	1

OVERALL = 95.18%

90 METER

	CORN	SOY	TREE	OTHER	UNCLAS.
CORN	93	0	0	0	7
SOY	5	90	0	0	5
TREE	0	0	74	0	26
OTHER	0	0	0	100	0

OVERALL = 87.99%

TABLE IV.4

FIELD CENTER CLASSIFICATION RESULTS
(Common Field Signature Training Procedure)
S-204 Jul 12 (41M)

10 METER

	CORN	SOY	TREE	OTHER	UNCLAS.
CORN	93	0	1	.5	5.5
SOY	0	89	0	1	10
TREE	1	0	91	0	8
OTHER	0	0	0	89	11

OVERALL = 91.16%

30 METER

	CORN	SOY	TREE	OTHER	UNCLAS.
CORN	96	0	1	0	3
SOY	0	96	0	2	2
TREE	1	0	94	1	4
OTHER	0	0	0	98	2

OVERALL = 95.78%

40 METER

	CORN	SOY	TREE	OTHER	UNCLAS.
CORN	97	0	1	0	2
SOY	0	97	0	1	2
TREE	1	0	97	0	2
OTHER	0	0	0	98	2

OVERALL = 97.19%

50 METER

	CORN	SOY	TREE	OTHER	UNCLAS.
CORN	98	0	1	0	1
SOY	0	96	0	1	3
TREE	0	0	98	0	2
OTHER	0	0	0	99	1

OVERALL = 97.98%

TABLE IV.4 (Continued)

S-204 Jul 12 (41M)

60 METER

	CORN	SOY	TREE	OTHER	UNCLAS.
CORN	98	0	1	0	1
SOY	0	94	0	2	4
TREE	1	0	98	0	1
OTHER	0	0	0	100	0

OVERALL = 97.97%

90 METER

	CORN	SOY	TREE	OTHER	UNCLAS.
CORN	93	0	1	0	6
SOY	0	96	0	0	4
TREE	0	0	95	0	5
OTHER	0	0	0	70	30

OVERALL = 90.33%

TABLE IV.5

ESTIMATED PROPORTIONS OF CLASSES OVER THE ENTIRE SCENE
(Common Field Signature Training Procedure)
S-212 Aug 17 (43M)

RESOLUTION	CORN	SOY	TREE	TOTAL OTHER =	(OTHER + UNCLAS.)		E_{RMS} (%)
10	27.18	15.55	9.07	48.20	30.70	17.50	.052
30	29.22	15.53	8.37	46.88	31.35	15.53	.048
40	28.88	15.19	7.86	48.07	29.55	18.52	.055
50	28.24	12.51	7.17	52.08	27.18	24.90	.074
60	26.46	11.40	3.67	58.47	23.53	34.90	.110
90	14.23	6.38	.89	78.50	14.10	64.40	.224
REAL	.30	15	15	.40			

$$E_{RMS} = \left(\frac{1}{n} \sum_{i=1}^{n} (\hat{P} - P)^2 \right)^{1/2}$$

P = true proportion

n = 4

$\hat{P}$ = estimate proportion

TABLE IV.6

ESTIMATED PROPORTIONS OF CLASSES OVER THE ENTIRE SCENE
(Common Field Signature Training Procedure)
S-204 Aug 13 (43M)

RESOLUTION	CORN	SOY	TREE	TOTAL OTHER	=	(OTHER + UNCLAS.)		E_{RMS} (%)
10	29.71	8.03	14.02	48.24		15.72	32.52	.0478
30	32.24	12.58	14.10	41.07		12.12	28.95	.0140
40	31.68	13.25	13.46	41.60		10.07	31.53	.0199
50	33.96	13.55	12.84	39.64		8.67	30.97	.0209
60	30.96	11.50	13.77	43.77		6.60	37.17	.0243
90	23.63	3.60	7.24	65.52		2.21	63.31	.1475
REAL	33	11	16	40				

TABLE IV.7

ESTIMATED PROPORTIONS OF CLASSES OVER THE ENTIRE SCENE
(Common Field Signature Training Procedure)
S-204 Aug 5 (42M)

RESOLUTION	CORN	SOY	TREE	TOTAL OTHER =	(OTHER + UNCLAS.)		$E_{(RMS)}$ (%)
10	30.19	5.00	9.53	55.27	7.94	47.33	8.93
30	27.34	12.65	12.10	47.91	5.47	42.44	5.30
40	25.84	10.92	11.89	51.35	4.73	46.61	7.02
50	25.00	9.98	10.61	54.71	4.39	49.98	8.81
60	22.06	13.38	9.35	53.05	3.53	48.32	9.22
90	13.37	4.16	6.54	79.45	1.21	74.72	22.79
REAL	33	11	16	40			

$$E_{RMS} = \left(\frac{1}{n} \sum_{n=1}^{n} (\hat{P} - P)^2 \right)^{1/2}$$

where

P = true proportions

$\hat{P}$ = estimate proportions

$n = 4$.

TABLE IV.8

ESTIMATED PROPORTIONS OF CLASSES OVER THE ENTIRE SCENE
(Common Field Signature Training Procedure)
S-204 Jul 12 (41M)

RESOLUTION	CORN	SOY	TREE	TOTAL OTHER =	(OTHER + UNCLAS.)		E_{RMS} (%)
10	19.93	6.77	9.99	63.30	16.49	46.81	13.21
30	26.84	10.02	8.84	54.30	25.76	28.54	7.90
40	23.78	9.45	8.22	58.55	22.12	36.43	10.42
50	24.21	10.26	8.11	57.42	20.61	36.81	9.86
60	22.52	7.10	7.40	62.99	17.98	45.01	12.80
90	10.99	4.17	5.64	79.20	2.08	77.12	22.67
REAL	33.0	11.0	15.0	41.0			

$$E_{RMS} = \left[\frac{1}{N} \sum_{n=1}^{n} (\hat{P} - P)^2 \right]^{1/2}$$

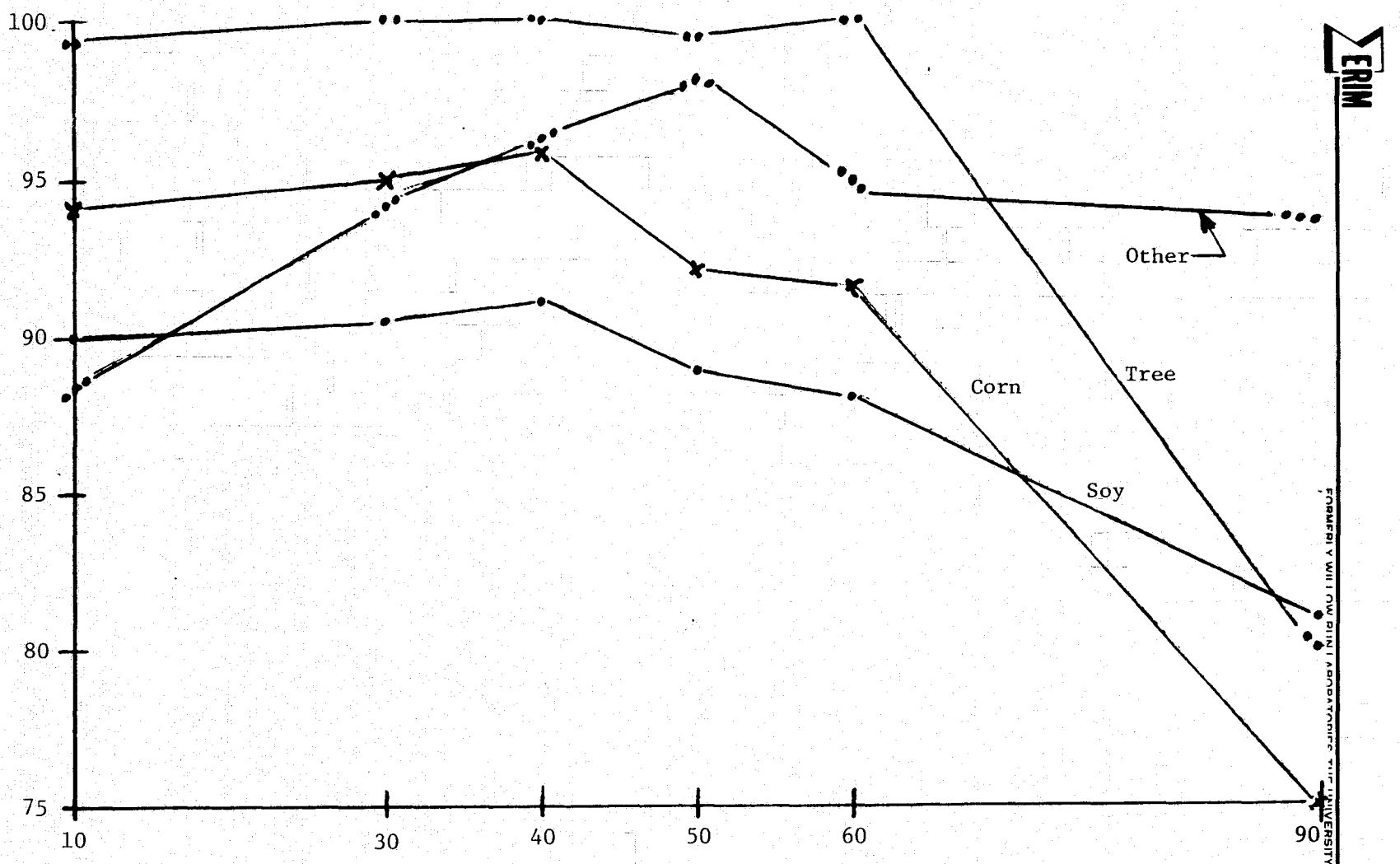

FIGURE IV-1. FIELD CENTER CLASSIFICATION RESULTS AS A FUNCTION OF SPATIAL RESOLUTION
S212, August 17 (43M)
(Common Field Signature Training Procedure)

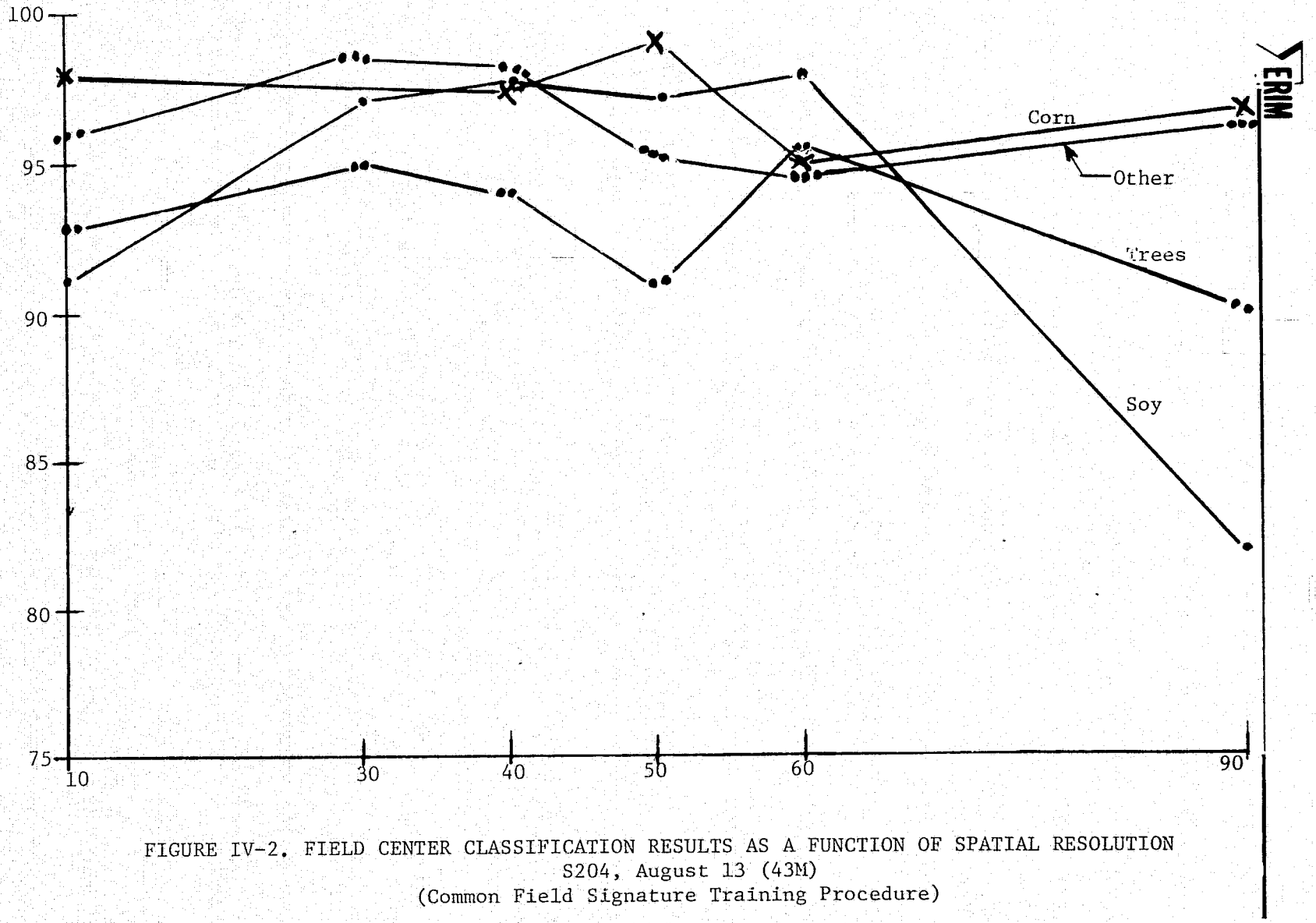

FIGURE IV-2. FIELD CENTER CLASSIFICATION RESULTS AS A FUNCTION OF SPATIAL RESOLUTION
S204, August 13 (43M)
(Common Field Signature Training Procedure)

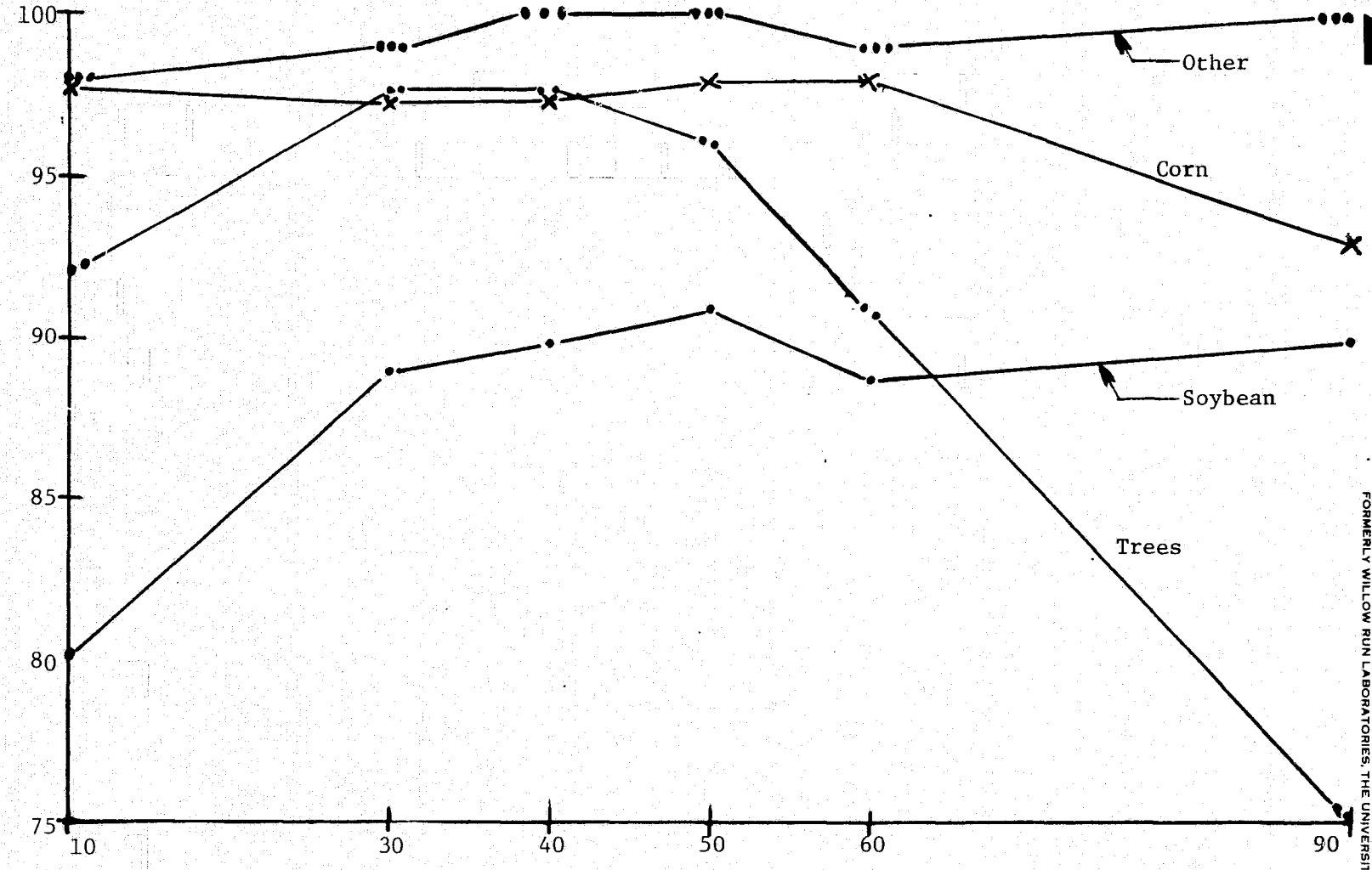

FIGURE IV-3. FIELD CENTER CLASSIFICATION RESULTS AS A FUNCTION OF SPATIAL RESOLUTION
S204, August 5 (42M)
(Common Field Signature Training Procedure)

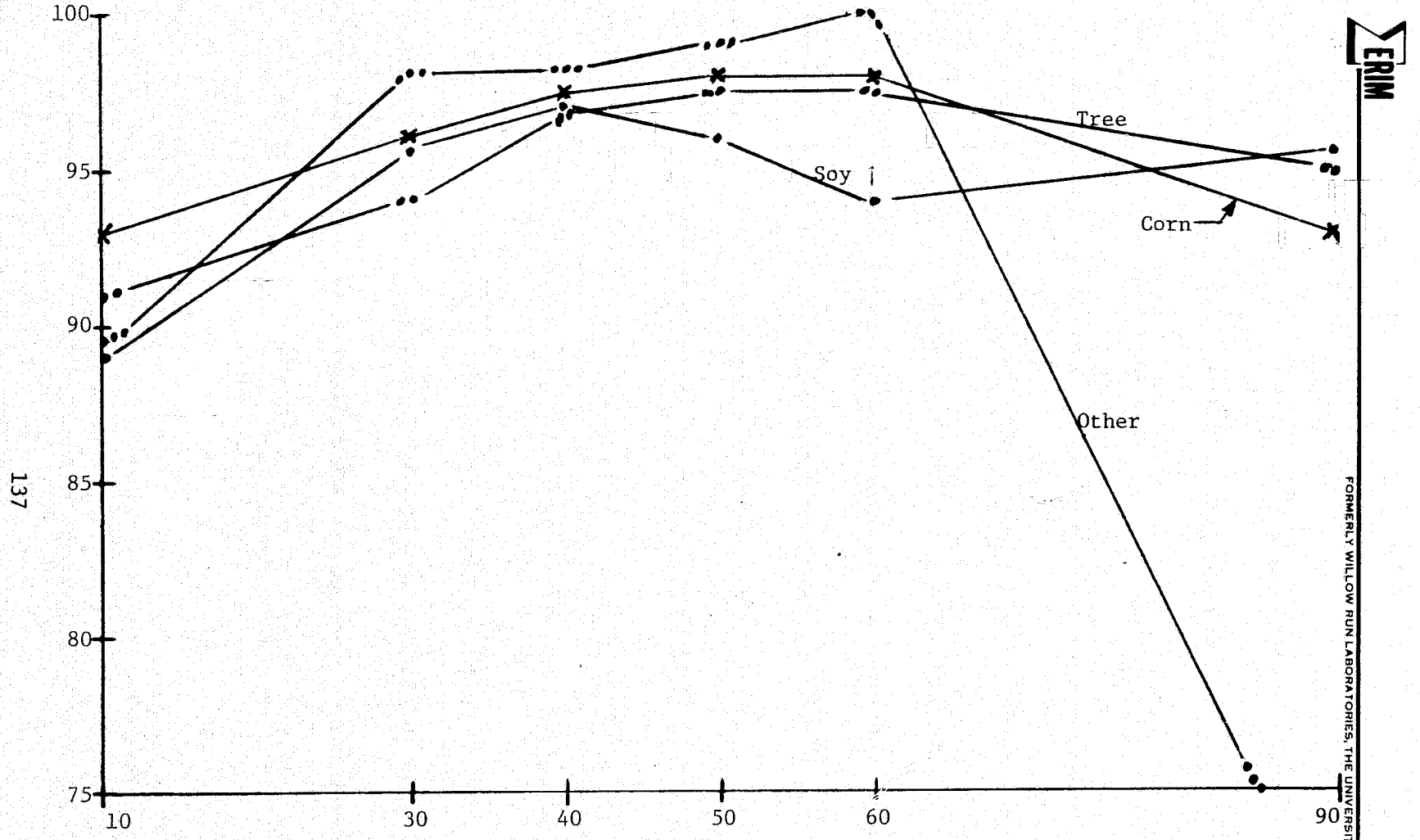

FIGURE IV-4. FIELD CENTER CLASSIFICATION RESULTS AS A FUNCTION OF SPATIAL RESOLUTION
S204, July 12 (41M)
(Common Field Signature Training Procedure

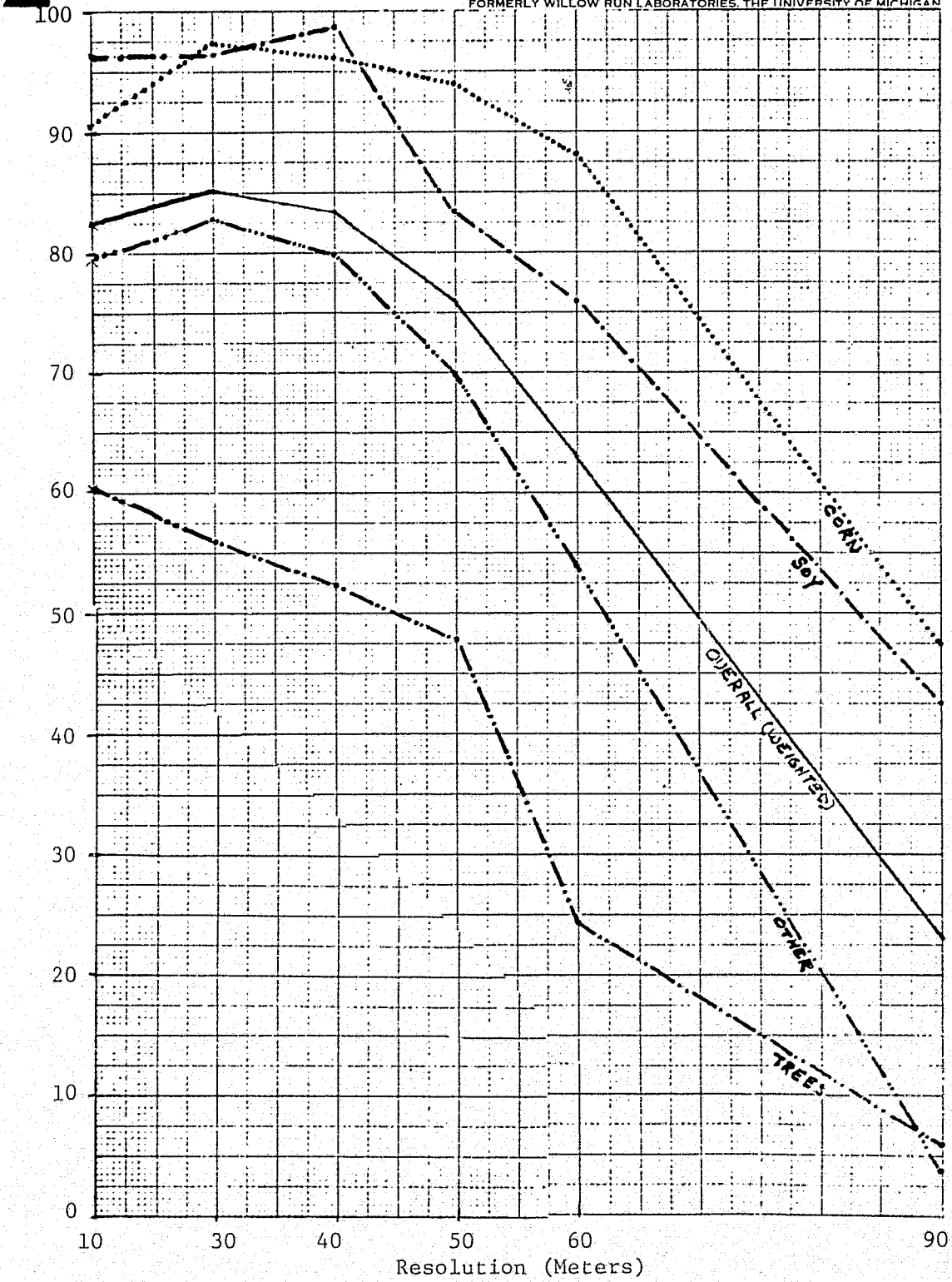

FIGURE IV-5. RELATIVE PROPORTION ESTIMATION BY CLASS
S212, August 17 (43M)
(Common Field Signature Training Procedure)

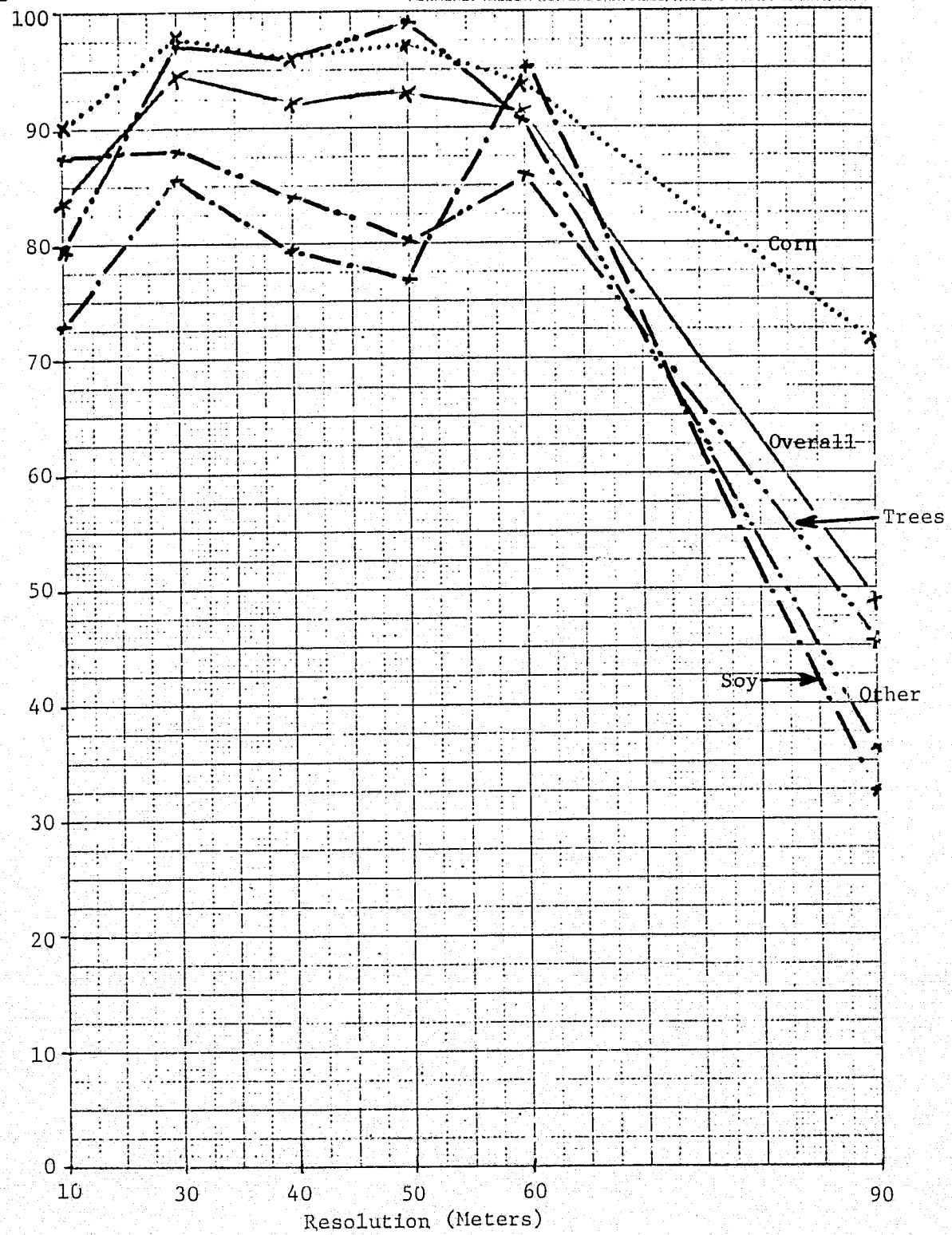

FIGURE IV-6. RELATIVE PROPORTION ESTIMATION BY CLASS
S204, August 13 (43M)
(Common Field Signature Training Procedure)

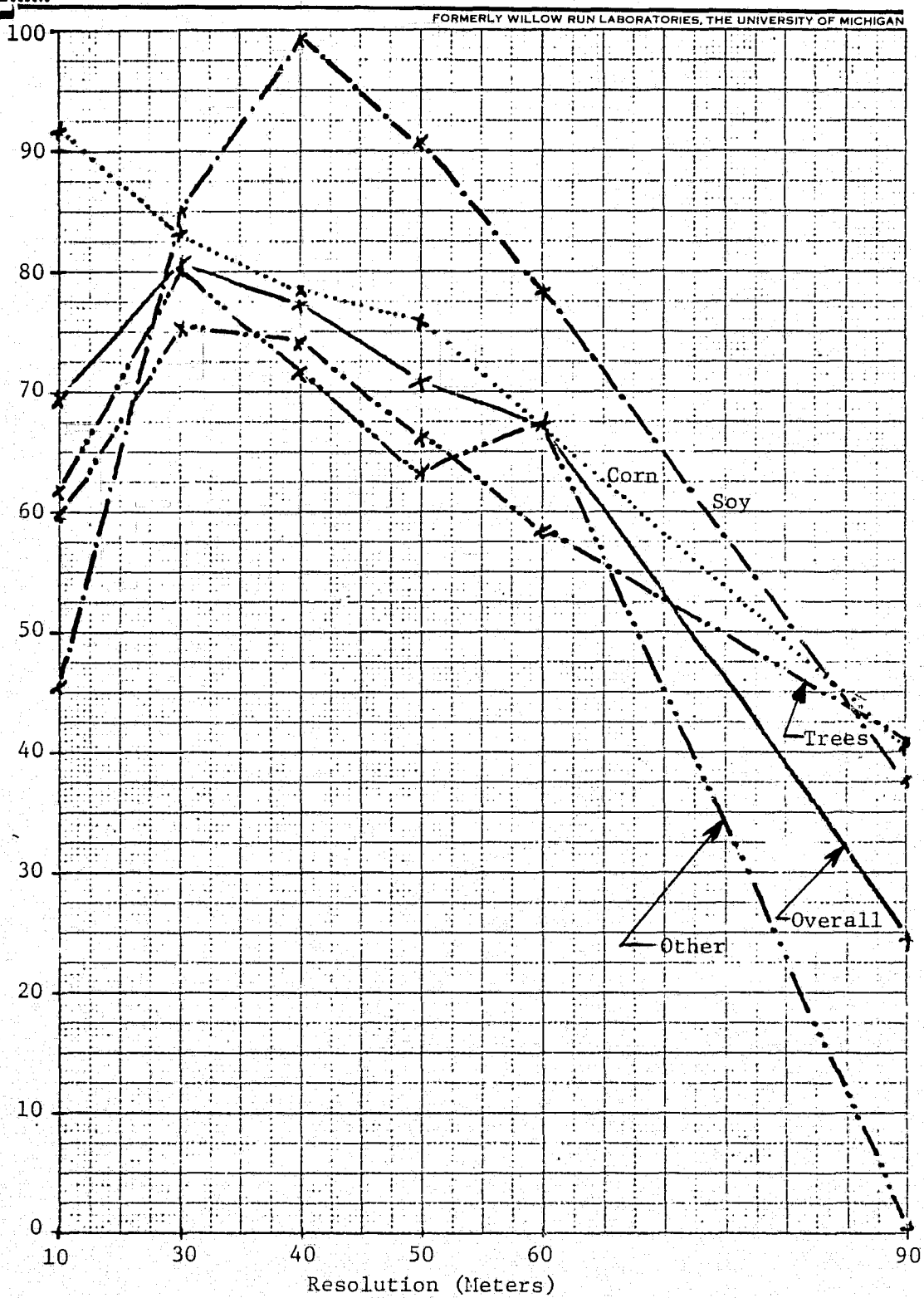

FIGURE IV-7. RELATIVE PROPORTION ESTIMATION BY CLASS
S204, August 5 (42M)
(Common Field Signature Training Procedure)

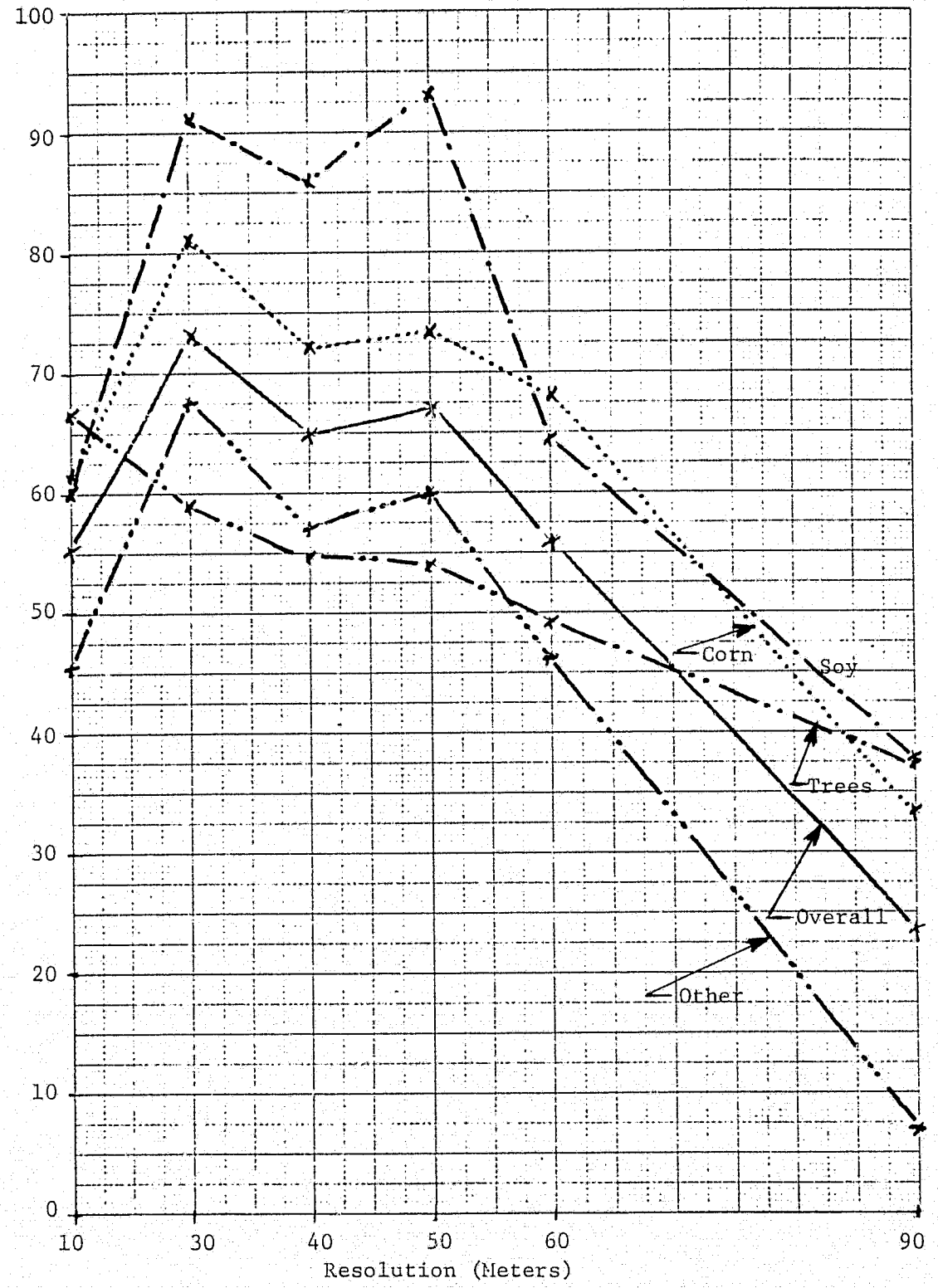

FIGURE IV-8. RELATIVE PROPORTION ESTIMATION BY CLASS
S204, July 12 (41M)
(Common Field Signature Training Procedure)

APPENDIX V

ANALYSIS OF EFFECTS ON CLASSIFICATION ACCURACY OF AGRICULTURAL FIELD SIZE AND SCANNER SPATIAL RESOLUTION

V.1 INTRODUCTION

In this section we report the results of a study carried out to determine the effects of various multispectral scanner spatial resolutions on area mensuration accuracy for various field size distributions. The study, which used simulation techniques, sought to generalize classification accuracy calculated for particular sets of Landsat Follow-on simulated multispectral scanner data gathered over the Indiana corn belt to other field-size distributions. The measure used for this effort was that of area mensuration which takes into account classifications for both pure (field center) pixels and mixture (boundary) pixels for the classes in the scene. Obviously, for different combinations of spatial resolutions and field sizes, the scene may yield mostly pure pixels, mostly mixture pixels or any combination in between. Area mensuration results are an accurate measure of classification results over all such scenes and offers a good basis for comparisons.

V.2 PROCEDURES

In general, the procedure followed was to simulate a variety of scenes scanned using several resolutions and then determining the resulting area mensuration results as a function of the proportions of the scene which were pure pixels and mixture pixels, using the classification rates for such pure and mixture pixels. Each scene was designed as a grid of fields of the same size and shape; for this study, 1,2,4,8, and 16 hectare field sizes were used (approximately 2.5,5,10,20,40 acres). All simulated scenes used an aspect ratio of 2:1, this ratio, according to available information is apparently most typical of worldwide agricultural practices. The scanning was assumed done in a manner square to the fields; i.e., if the fields were laid out on a strictly north-south-east-west grid, then the scan plane would be east-west. In general, this produces fewer boundary pixels than an oblique scan would.

The basis for the classification results for the study came from employing the ERIM classification simulator (Appendix IX) for pure pixels and for mixture pixels. As inputs to the simulator, we used the 30 meter data signature sets acquired having used all fields in the scene to calculate the signatures. The signature sets from all three segment 204 data sets were used for this study, affording a chance to study the effects of field size and spatial resolution as a function of time during the growing season.

The classification results used for the field center simulation were taken from the simulation results of the radiometric study (using the nominal noise case). For the classification of mixture pixels, the simulated classifier was modified to produce mixture pixels as follows:

$$M_i = \alpha R_{A,i} + (1-\alpha) R_{B,i} \qquad \text{(V.1)}$$

where

i is the channel index

M is the output pixel

R_A and R_B are the randomly generated pixels from signatures A and B

α is the proportion of the mixture calculated.

For this study 11 different mixtures were calculated: $\alpha = \{0, 0.1, 0.2, 0.3, 0.4, 0.5, 0.6, 0.7, 0.8, 0.9, 1.0\}$. For each α and each pair of signatures A and B, 100 mixture pixels were generated and classified by the simulator. Mixture combinations were calculated for all pairs of signatures of the major classes (corn, soybeans, trees) and for many of the particular other classes in the scene (water, winter wheat, oats, hay, pasture, and diverted). Figures V-1 to V-8 present results. Note Figures V-1 to V-3 where the graphs of mixtures (soy-corn, corn-trees, and trees-soy) indicate a definite skewed shape, which implies unequal classification probabilities between the two classes. As a matter of fact, Figure V-2 indicates the probability that a mixture of corn-trees (for data set: S204, August 13 (43M)) will result in a pixel being classified as

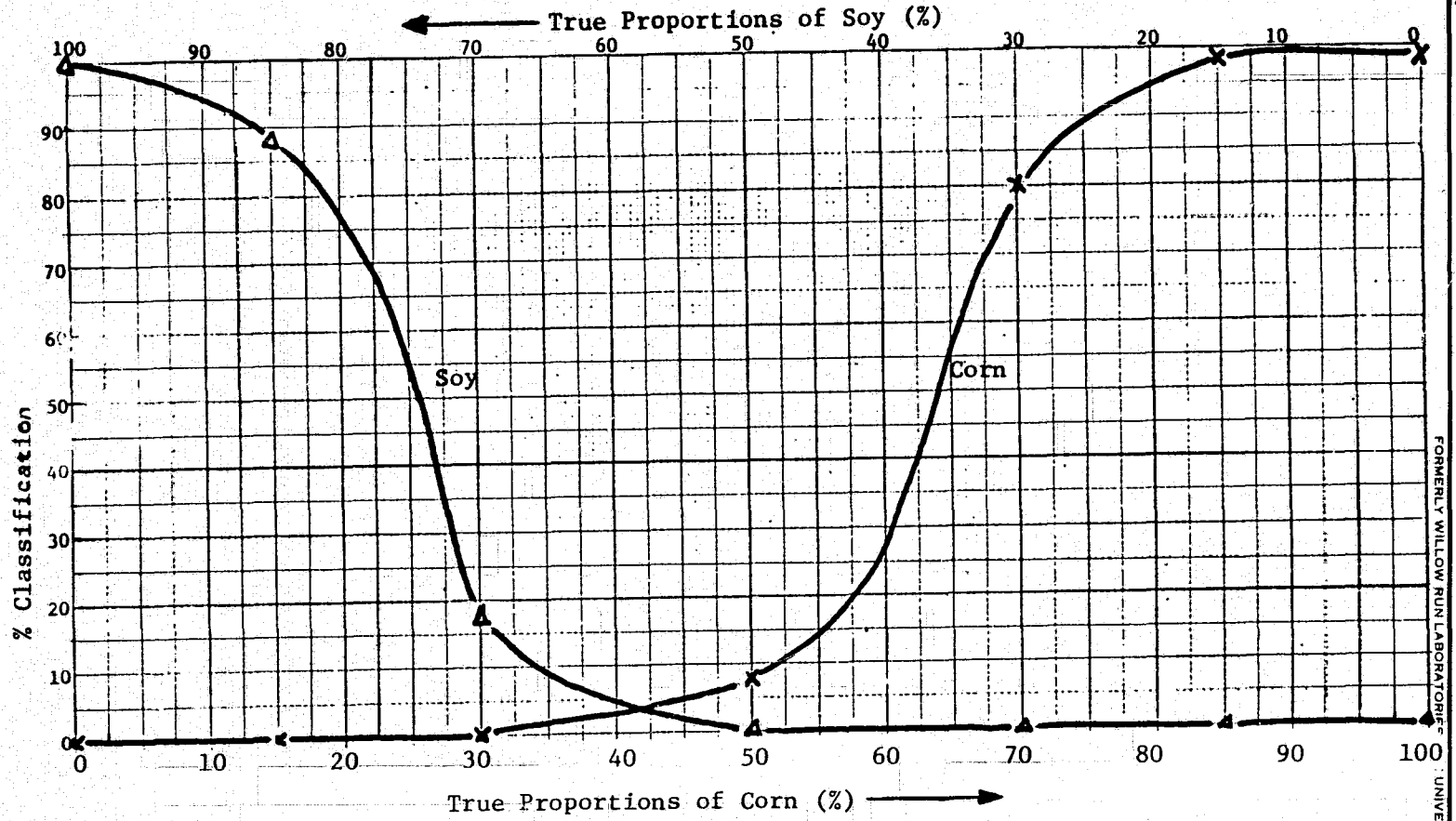

FIGURE V-1. MIXTURE PIXEL CLASSIFICATION RESULTS -- Corn-Soy Mixture
Data Set: S204, 43M

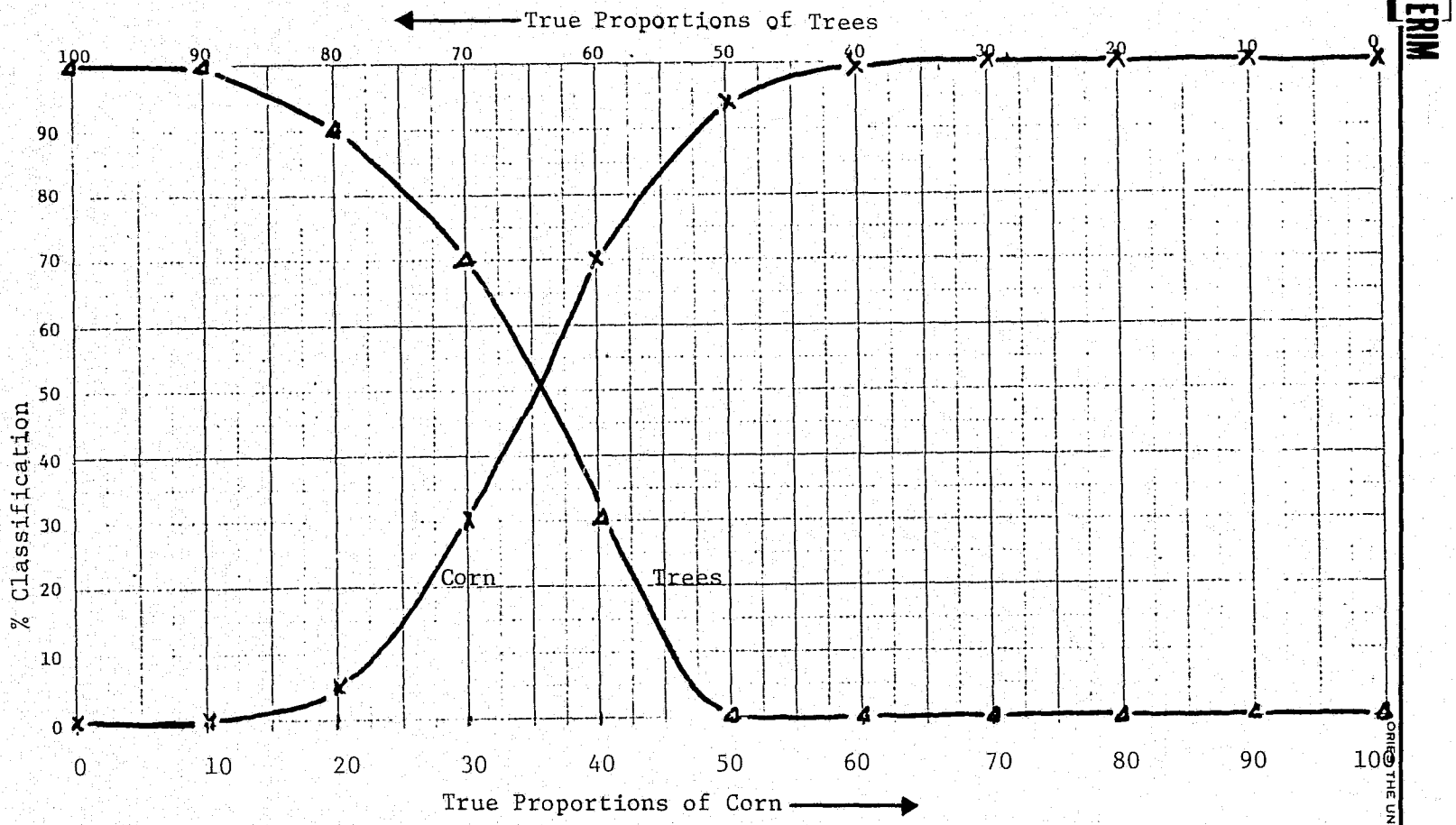

FIGURE V-2. MIXTURE PIXEL CLASSIFICATION RESULTS -- Corn-Trees Mixture
Data Set: S204, 43M

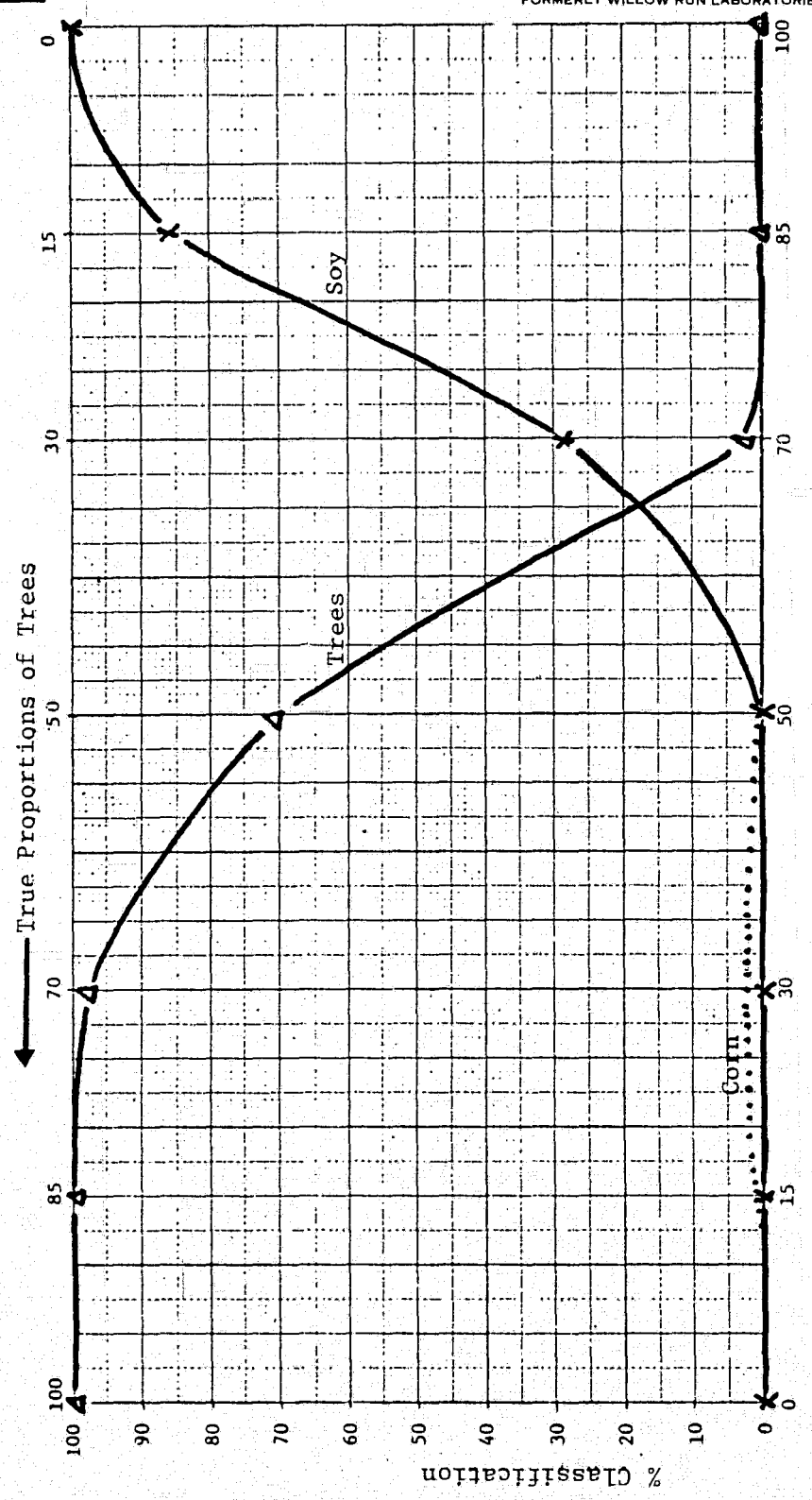

FIGURE V-3. MIXTURE PIXEL CLASSIFICATION RESULTS -- Trees-Soy Mixture
Data Set: S204, 43M

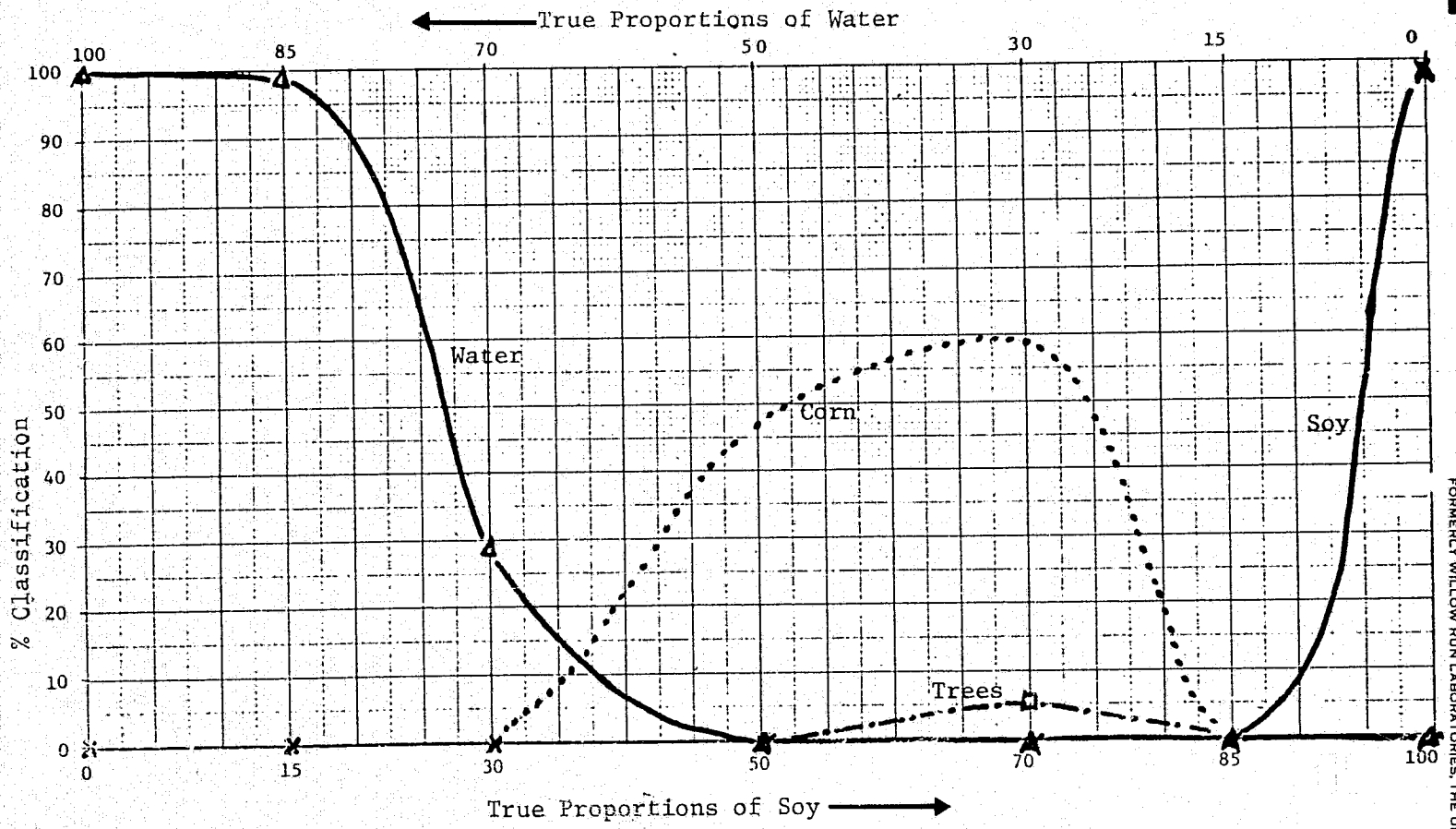

FIGURE V-4. MIXTURE PIXEL CLASSIFICATION RESULTS -- Water-Soy Mixture

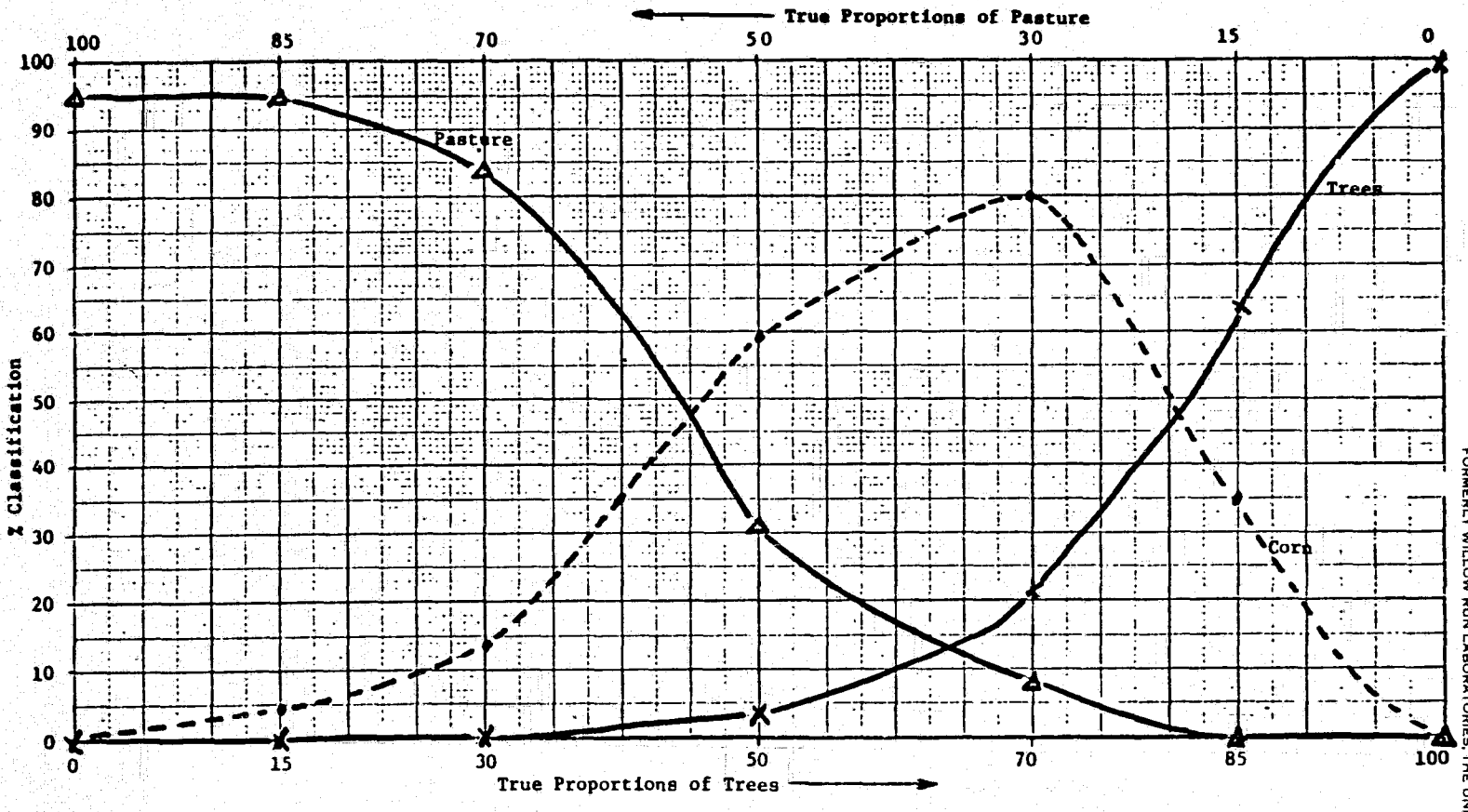

FIGURE V-5. MIXTURE PIXEL CLASSIFICATION RESULTS -- Pasture-Tree Mixture
Data Set: S204, 43M

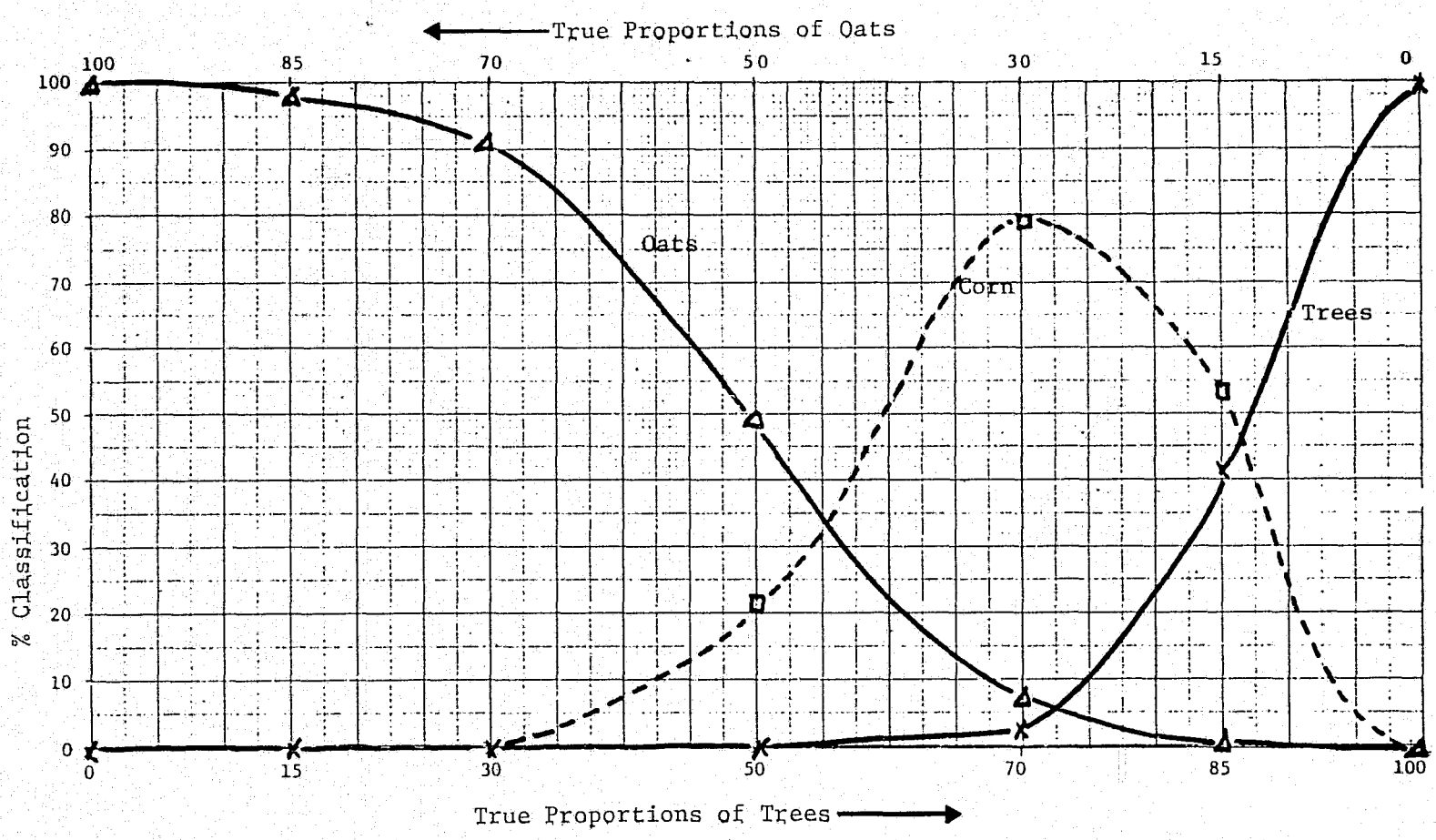

FIGURE V-6. MIXTURE PIXEL CLASSIFICATION RESULTS -- Oats-Trees Mixture
Data Set: S204, 43M

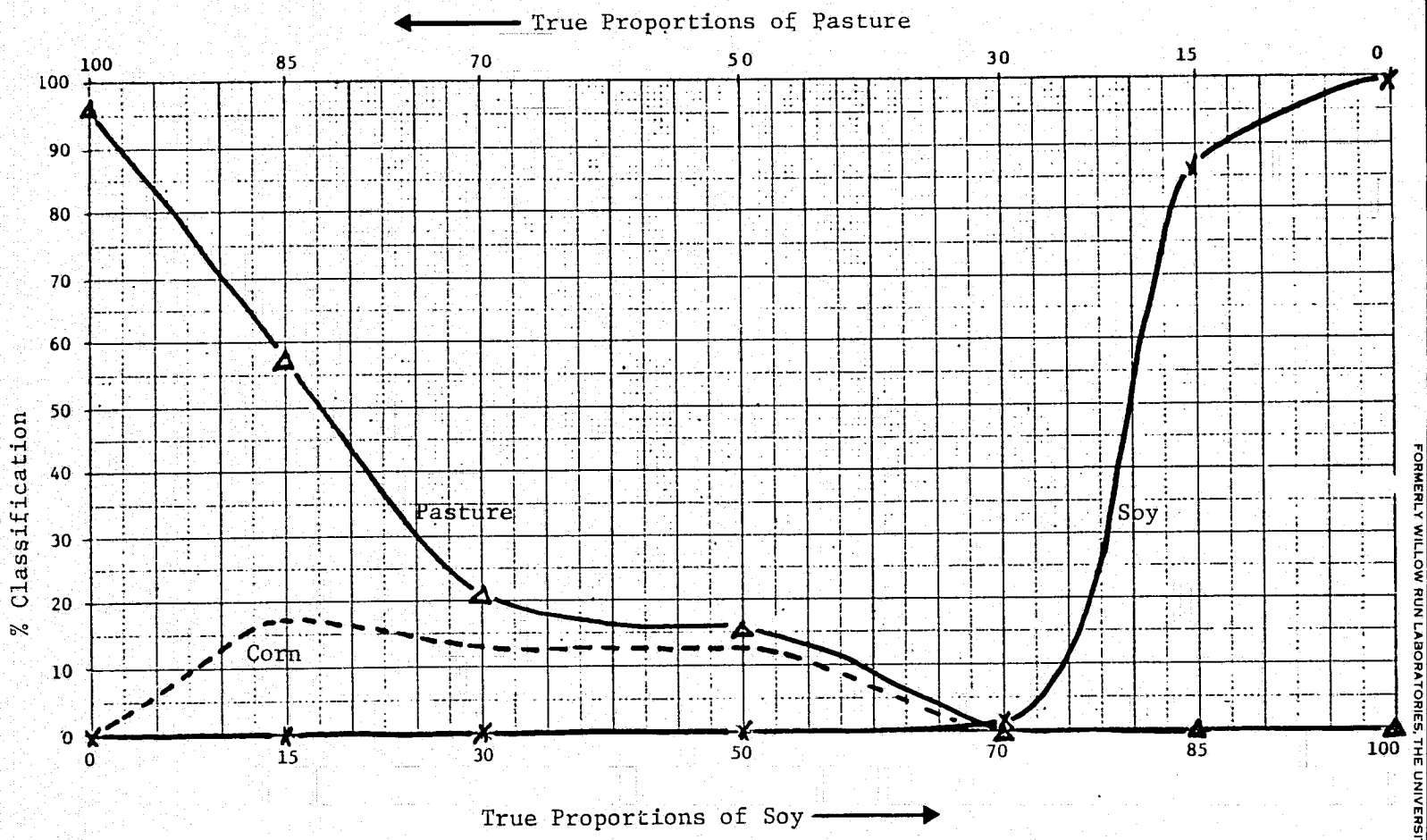

FIGURE V-7. MIXTURE PIXEL CLASSIFICATION RESULTS -- Pasture-Soy Mixture
Data Set: S204, 43M

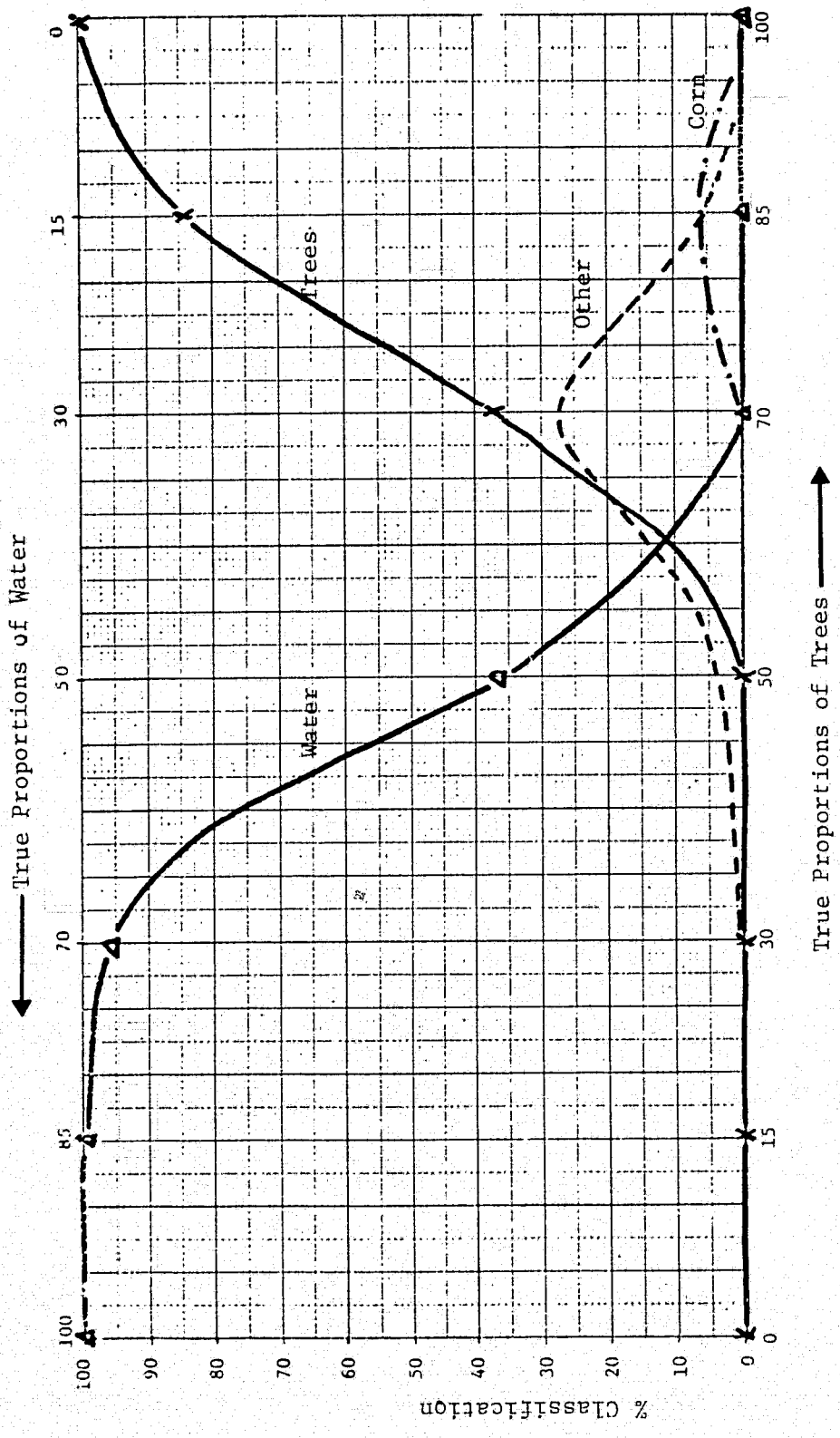

FIGURE V-8. MIXTURE PIXEL CLASSIFICATION RESULTS -- Water-Trees Mixture
Data Set: S204-43M

corn is twice as great as the probability of calling the mixture pixel a tree. Similar effects are also noted in Figures V-1 and V-3. Note that in Figure V-1, for mixture pixels of approximately 25-65% corn, the proportion of unclassified (one minus the sum of the areas under the two curves) is very high.

These three mixtures are examples of relatively "clean" mixtures -- that is, no classifications of a third class occur. Figures V-4 through V-8 are examples of "contaminated" mixtures -- that is, a third, and sometimes additional, classes are being classified from two-class mixture pixels. Upon close observation of Figures V-4, V-5, and V-6, it is noted that the probability of classifying a third class is greater than that of of classifying one of the original two classes. These examples of "contaminated" mixtures indicate a trend that overestimates are highly probable for a third-class type while underestimating the original two classes. In particular, these figures indicate a possibly serious overestimate of corn for the area being tested.

The results of analyzing mixture pixel classifications are:

1. the classification of a set of two-class mixture pixels does not result in an equal probability of classification for the two classes considered
2. classification of a third class, and at times additional classes, are highly probable
3. in studying possible effects on area mensuration, the errors of commission apparently do not compensate.

These inputs were then used to enable the computation of mensuration accuracy for a set of artificial scenes of varying field size. In order to add realism, each scene did not contain an equal number of scene classes. Instead, proportions roughly equivalent to those in the original Segment 204 data were used, and these proportions are shown in Table V.1. In carrying out the calculations, each scene was assumed to be made up of these proportions and furthermore, for purposes of these calculations, it was assumed that only two-class mixtures existed in each scene.

TABLE V.1

ACTUAL PROPORTIONS OF CLASSES IN SIMULATED SCENE

CLASS	PROPORTION (λ)
Corn	.30
Soy	.10
Trees	.20
Water	.01
Winter Wheat	.04
Oats	.05
Hay	.10
Pasture	.10
Diverted	.10
	1.00

To begin the calculations, the first thing to find is the proportion of the scene which is field center and that which is boundaries. There have been reported some generalized methods to do this. Unfortunately, they all assume that the field dimensions are much larger than the pixel dimensions and for this study, such an assumption is not valid. We therefore developed the following procedure which is specifically geared toward the scene we established. We introduce the notation:

n	Size of field in hectares (10^4 meter^2)
ASPECT	Aspect Ratio of length of field to width
A	Width of a field
B	Length of field
TRUNC	Is the TRUNCATION function
MOD	Is the MODULO function
R	Spatial resolution in meters

and recalling that each scene is composed of rectangular fields of same size and shape then

$$A = (n/ASPECT)^{1/2} \quad 10^2 \text{ Meters} \tag{V.2}$$

$$B = ASPECT * A \tag{V.3}$$

let

$$C = TRUNC(A/R) \quad ; \quad D = TRUNC(B/R) \tag{V.4}$$

$$\beta_w = \frac{(C+1)}{A} A \text{ MOD } R \; ; \quad \beta_\ell = \frac{(D+1)}{B} B \text{ MOD } R \tag{V.5}$$

Then the expected value of the number of field center pixels in one field (E(F)) is equal to the product of the expected number of pixels in the length and width of the field or:

$$\begin{aligned} E(F) &= E(F \text{ in length}) \cdot E(F \text{ in width}) \\ &= [C\beta_w + (1-\beta_w)(C-1)] \cdot [D\beta_\ell + (1-\beta_\ell)(D-1)] \end{aligned} \tag{V.6}$$

To explain this equation, we note that, in each dimension of the field, there is some portion of the time (β) when the scan of pixels will be such that some number of pixels (TRUNC(A/R)) will be field center. The rest of the time ($1-\beta$) one less than (TRUNC(A/R)) will be field center. The value for β is as given in Eq. (V.5). The use of the functions TRUNC and MOD arise because of working with integral units (whole pixels). Finally, the proportion of the scene which is field center and boundaries is:

$$P(FCP) = \frac{E(F) \cdot R^2}{A \cdot B} \tag{V.7}$$

$$P(B) = 1.0 - P(FCP) \tag{V.8}$$

Now, the area mensuration for class i in the scene is the field center classification of that class for the field portion of the scene plus the boundary pixel classification rate for class i for the boundary portion of the scene, or:

$$P(\text{CLASS } i) = P(\text{FCP}) \cdot P(\text{CLASS } i \text{ in field center}) + P(B) \cdot P(\text{CLASS } i \text{ in boundaries}) \tag{V.9}$$

$$= P(\text{FCP}) \cdot \sum_{j=1}^{\text{CLASS}} \lambda_j \, P(\text{Crop } i \,|\, \text{Crop } j)$$

$$+ P(B) \cdot \sum_{j=1}^{\text{CLASS}} \sum_{k=1}^{\text{CLASS}} P(\text{Mixture of } j,k) \, P(\text{Crop } i \,|\, \text{Mixture } j,k) \tag{V.10}$$

where λ_i are as given in Table V.1 and P is for probability.

For this study, the scene was constrained so that there would not be two fields of the same class next to each other, i.e.,

$$P(\text{Mixture of } j,k) = 0 \qquad \text{for } j = k$$

$$\text{Thus} \qquad P(\text{Mixture of } j,k) = \frac{\lambda_j \lambda_k}{2 \sum_{\ell=1}^{\text{CLASS}} \sum_{m=\ell+1}^{\text{CLASS}} \lambda_\ell \lambda_m} \qquad \text{for } j \neq k \tag{V.11}$$

Finally, in calculating the P(Class i|Mixture j,k) all mixtures (α in Eq. (V.1)) were considered equally likely and all mixtures were considered to be two class mixtures. Also, where there were several signatures per class, all mixtures of the signatures (cases) for that class were considered equally likely. Thus

$$P(\text{Class } i \,|\, \text{Mixture } j,k) = \frac{1}{\text{Case}} \sum_{\ell=1}^{\text{Case}} \left(\int_0^{1.0} p(\text{Class } i \,|\, \text{Mixture } j,k) \alpha \, d\alpha \right) \tag{V.12}$$

Thus, evaluation of Eq. (V.10) for each class for different field sizes and scanning resolution yields the results given in the next appendix.

APPENDIX VI

TABULAR RESULTS FOR SIMULATION OF AREA MENSURATION AS A FUNCTION OF FIELD SIZE DISTRIBUTION

This appendix contains complete tabular results for the study of expected area mensuration accuracy as a function of field size distribution carried out using the scene simulations which were described in Appendix V.

TABLE VI.1

PROPORTION OF SCENE REPRESENTED BY FIELD CENTER PIXELS AS A FUNCTION OF FIELD SIZE AND SPATIAL RESOLUTION

FIELD SIZE (Hectares)	(Acres)	RESOLUTION (Meters) 30	40	50	60	90
1	2.5	.480	.352	.264	.147	0
2	5.0	.616	.512	.375	.346	.105
4	10.0	.709	.628	.547	.487	.317
8	20.0	.792	.720	.656	.616	.461
16	40.0	.845	.795	.754	.711	.583

TABLE VI.2

SIMULATION BASED ON SIGNATURES FROM SEGMENT S-204, 41M
DATA PROPORTION (%) OF CROP i AS A FUNCTION OF FIELD SIZE
AND SCANNER RESOLUTION

FIELD SIZE (Hectares)	RESOLUTION (Meters) 30	40	50	60	90	CROP	TRUE PROPORTION
1	27.69	27.87	27.99	28.16	28.39		
2	27.50	27.65	27.84	27.88	28.23		
4	27.36	27.47	27.60	27.69	27.93	Corn	30%
8	27.25	27.35	27.44	27.50	27.73		
16	27.17	27.24	27.29	27.36	27.54		
1	8.89	8.08	7.58	6.82	5.82		
2	9.71	9.02	8.20	8.02	6.51		
4	10.27	9.84	9.27	9.89	7.83	Soy	10%
8	10.77	10.33	9.96	9.71	8.70		
16	11.15	10.83	10.59	10.27	9.52		
1	14.72	13.38	12.55	11.32	9.66		
2	16.05	14.92	13.58	13.27	10.80		
4	16.98	16.26	15.33	14.72	12.96	Trees	20%
8	17.81	17.09	16.47	16.05	14.41		
16	18.42	17.91	17.50	16.98	15.74		
1	48.70	50.67	51.88	53.70	56.30		
2	46.74	48.41	50.38	50.83	54.46		
4	45.39	46.43	47.80	48.70	51.28	Other	40%
8	44.17	45.23	46.13	47.56	49.16		
16	43.26	44.02	44.62	45.39	47.20		

TABLE VI.3

SIMULATION BASED ON SIGNATURES FROM SEGMENT S-204, 42M
DATA PROPORTION (%) OF CROP i AS A FUNCTION OF FIELD SIZE
AND SCANNER RESOLUTION

FIELD SIZE (Hectares)	RESOLUTION (Meters) 30	40	50	60	90	CROP	TRUE PROPORTION
1	24.65	23.45	22.62	21.52	20.07		
2	25.93	24.95	23.66	23.39	21.12		
4	26.81	26.05	25.28	24.72	23.12	Corn	30%
8	27.59	26.91	26.31	25.93	24.47		
16	28.09	27.62	27.24	26.83	25.62		
1	7.46	6.87	6.46	5.91	5.19		
2	8.10	7.62	6.97	6.84	5.71		
4	8.54	8.16	7.78	7.50	6.70	Soy	10%
8	8.93	8.59	8.29	8.10	7.37		
16	9.18	8.94	8.75	8.55	7.95		
1	14.71	13.42	12.53	11.33	9.78		
2	16.09	15.04	13.65	13.35	10.91		
4	17.05	16.22	15.39	14.79	13.06	Trees	20%
8	17.89	17.15	16.51	16.09	14.52		
16	18.43	17.92	17.50	17.06	15.76		
1	53.18	56.26	58.39	61.24	64.96		
2	49.88	52.39	55.72	56.42	62.26		
4	47.60	49.57	51.55	52.99	57.12	Other	40%
8	45.59	47.35	48.89	49.88	53.64		
16	44.30	45.52	46.51	47.56	50.67		

TABLE VI.4

SIMULATION BASED ON SIGNATURES FROM SEGMENT S-204, 43M
DATA PROPORTION (%) OF CROP i AS A FUNCTION OF FIELD SIZE
AND SCANNER RESOLUTION

FIELD SIZE (Hectares)	RESOLUTION (Meters) 30	40	50	60	90	CROP	TRUE PROPORTION
1	25.06	23.74	23.24	22.20	20.82		
2	26.18	25.22	24.10	23.84	21.77		
4	26.96	26.35	25.57	25.06	23.59	Corn	30%
8	27.64	27.04	26.52	26.18	24.79		
16	28.16	27.73	27.39	26.96	25.92		
1	6.62	5.71	5.26	4.48	3.44		
2	7.47	6.75	5.90	5.72	4.15		
4	8.05	7.60	7.01	6.62	5.52	Soy	10%
8	8.56	8.10	7.72	7.47	6.43		
16	8.96	8.63	8.38	8.05	7.27		
1	13.80	12.22	11.24	9.77	7.82		
2	15.38	14.04	12.46	12.09	9.16		
4	16.48	15.63	14.53	13.80	11.73	Trees	20%
8	17.46	16.60	15.40	15.38	13.43		
16	18.19	17.58	17.10	16.48	15.02		
1	54.52	58.07	60.26	63.55	67.92		
2	50.97	53.99	57.54	58.35	64.92		
4	48.51	50.42	52.89	54.52	59.16	Other	40%
8	46.34	48.25	50.36	50.97	55.35		
16	44.69	46.06	47.13	48.51	51.79		

TABLE VI.5

SIMULATION BASED ON SIGNATURES FROM SEGMENT S-212, 43M
DATA PROPORTION (%) OF CROP i AS A FUNCTION OF FIELD SIZE
AND SCANNER RESOLUTION

FIELD SIZE (Hectares)	RESOLUTION (Meters) 30	40	50	60	90	CROP	TRUE PROPORTION
1	.2403	.2205	.2069	.1887	.1649		
2	.2614	.2453	.2240	.2195	.1822		
4	.2759	.2633	.2507	.2414	.2150	Corn	30%
8	.2887	.2776	.2677	.2614	.2373		
16	.2970	.2893	.2829	.2761	.2563		
1	.1351	.1395	.1426	.1467	.1520		
2	.1304	.1340	.1388	.1398	.1481		
4	.1271	.1299	.1328	.1349	.1408	Soybeans	10%
8	.1242	.1267	.1290	.1304	.1358		
16	.1224	.1241	.1256	.1271	.1315		
1	.1359	.1202	.1093	.0949	.0760		
2	.1527	.1399	.1230	.1194	.0897		
4	.1643	.1543	.1442	.1368	.1158	Trees	20%
8	.1745	.1656	.1577	.1527	.1336		
16	.1811	.1749	.1699	.1645	.1487		
1	48.87	51.98	54.12	56.97	60.71		
2	45.55	48.08	51.36	52.13	58.00		
4	43.27	45.25	47.23	48.69	52.84	Other	40%
8	41.26	43.01	44.56	45.55	49.33		
16	39.95	41.17	42.16	43.23	46.35		

APPENDIX VII

RADIOMETRIC SENSITIVITY STUDY PROCEDURES

VII.1 APPROACH

The purpose of the radiometric sensitivity study was to identify and quantify the degradation in classification results which occurs as the radiometric sensitivity of the system is reduced (as more noise enters the system). This study was carried out using simulation techniques because of the efficiency provided by this approach compared to that needed to actually degrade and classify data for all the cases simulated.

The general processing flow for the radiometric sensitivity simulation is given in Fig. VII.1. Briefly, the set of signatures extracted from the data for each data set and resolution which represents the nominal radiometric case, were used as the basis for the simulation. In all, we tested nine different levels of radiometric sensitivity: One-half the nominal case, nominal,1.3,1.6,2.0,3.0,6.0,10.0 and 20.0 times the nominal case. The simulation was run only for the 30m and 40m data sets. To evaluate results of each of the simulated noise levels, as the chart shows, all signatures in the set being processed were first modified according to the model (description follows below), and were then input to the simulated classifier, PEC (Appendix IX), which first uses Monte-Carlo methods to generate a set of pixels from each of the training distributions, and then classifies them. The number, N, which is the number of pixels generated for each signature, varies from signature to signature to reflect the proportion of the scene which is represented by that signature. In general, n is on the order of 1000 pixels.

The results from this procedure are expected performance matrices, which may then be analyzed for trends in the classification as a function of radiometric resolution.

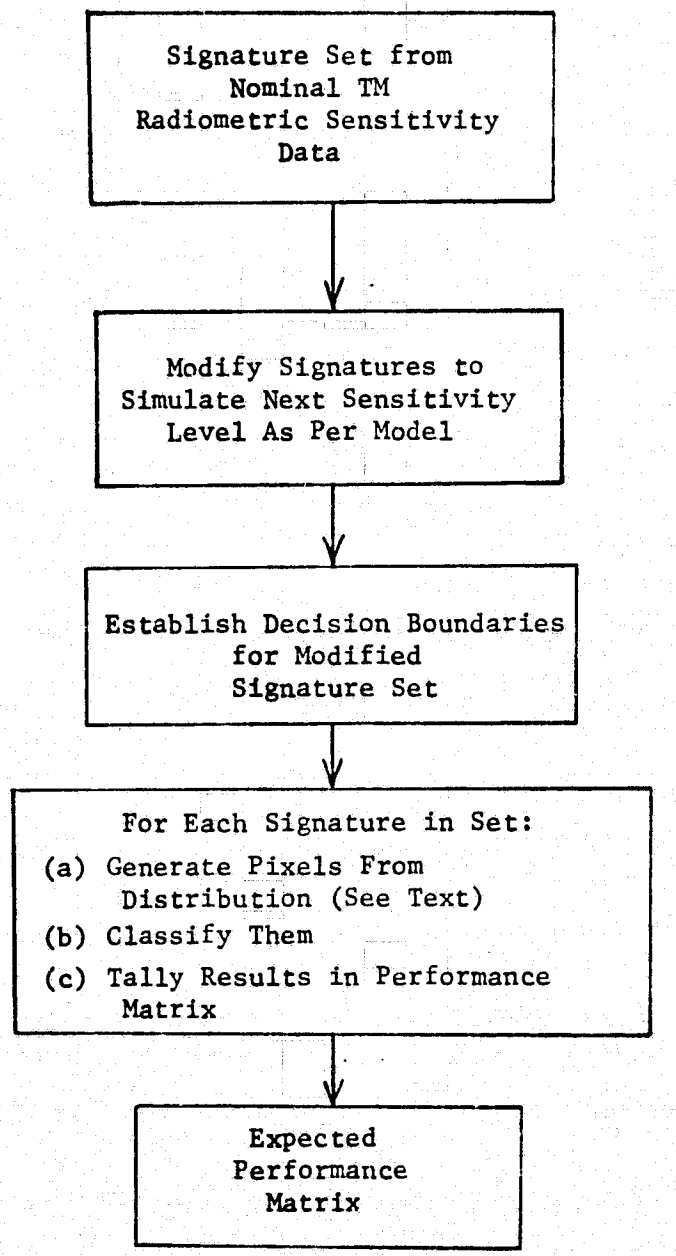

FIGURE VII-1. FLOW CHART FOR RADIOMETRIC SIMULATION

VII.2 SIMULATION MODEL FOR RADIOMETRIC SENSITIVITY STUDY

The model for adding noise to the data is: DATA + NOISE where NOISE is a Gaussian function with $\mu = 0$, σ = counts equivalent change in reflectance. Also, note that the noise functions for each of the channels are independent and uncorrelated.

To modify a signature which initially is "noise free," we note the following:

(for each channel i, data values x_i)

The noisy data can be represented as

$$x_i' = x_i + \varepsilon$$

where ε is the same as the NOISE function above.

Then $\bar{x}_i' = E(x_i + \varepsilon) = \bar{x}_i$

and $\sigma^2_{x_i'} = E((x_i + \varepsilon)^2) - [E(x_i + \varepsilon)]^2$

$$= \sigma^2_{x_i} + \sigma^2_\varepsilon$$

In the case where the signatures already have had some other noise function, δ, added to it, we find that to get $\sigma^2_{x_i'}$ we start at:

$$\sigma^2_{IN} = \sigma^2_X + \sigma^2_\delta$$

or

$$\sigma^2_X = \sigma^2_{IN} - \sigma^2_\delta$$

where σ^2_{IN} is the initial variance of the signature. So

$$\sigma^2_{X'} = \sigma^2_{IN} + [\sigma^2_{\varepsilon} - \sigma^2_{\delta}]$$

Further, the covariance of the signatures does not change since

$$\begin{aligned} &COV(X_i + \varepsilon_i, X_j + \varepsilon_j) \\ &= COV(X_i, X_j) + COV(X_i \varepsilon_j) + COV(X_j \varepsilon_i) + COV(\varepsilon_i \varepsilon_j) \\ &= COV(X_i, X_j) \end{aligned}$$

(since the covariance between independent random variables is zero)

Thus to change the noise characteristic of the signatures we implement the following algorithm:

(1) Calculate $T = \sigma^2_{\varepsilon} - \sigma^2_{\delta} = (z^2 - 1^2)\, S^2$

where S is the number of data counts equivalent to the change in reflection ($DE_{\Delta\rho}$) at the nominal case and z is the multiplier for the case being processed (0.5,1.0,1.3,1.6,2.0,3.0,6.0,10.0 or 70.0).

(2) Modify the diagonal elements of each of the covariance matrices by

$$\sigma^2_{Final} = \sigma^2_{IN} + T$$

Thus T is the amount to be added to the variance to simulate a signature of variance $\sigma^2_{IN} + \sigma^2_{\varepsilon}$. In the instance of the half nominal simulation, T will be negative but this poses no problems as σ^2_{IN} is always greater than T. At the limit, when z is zero, then σ^2_{Final} is nearly σ^2_X which is the noiseless case.

VII.3 RADIOMETRIC SIMULATION MODEL VALIDATION

Before actually using the radiometric simulation, it was necessary to validate both the signature adaptation model and the simulation procedure. We began by adding noise to the 30 meter and 40 meter data for Segment 204, 43M to simulate a data set gathered with a radiometric sensitivity three times noisier than the nominal TM values.

Sets of signatures were extracted from this data using the field signature training procedure outlined earlier in this report. These signatures were then compared, one by one, to a set of signatures which had been modified to the three times specification level according to the signature-simulation model. As expected there was no change in the means. The standard deviations were compared and while not exact, were nevertheless found to be very close.

To test the rest of the simulation procedure, the extracted "noisy" signatures were used to classify the "noisy" data and then, evaluation of field center pixels was carried out. These results were compared to those obtained using the modified signatures as input to the simulated classifier. The results for the two resolutions studied given in Tables VII.1 and VII.2 show good agreement between the two sets of results. This, along with the similarity of the two signature sets, validated the model.

TABLE VII.1

COMPARISON OF "NOISY" DATA CLASSIFICATION RESULTS VERSUS SIMULATION RESULTS, S-204, 30 METER

(First numbers are from data classification, second are from Simulation Method)

%

	CORN	SOY	TREES	OTHER	UNCLASSIFIED
CORN	96.5/96	.5/.8	2.0/2.2	1./.5	0/.5
SOY	2.6/2.7	95./96.5	.6/0	1.6/.5	.6/.3
TREES	5./4.3	0/0	94/95.4	.5/0	.5/.3
OTHER	1.5/2.5	.8/.6	0/0	97.6/96.5	.1/.4

TABLE VII.2

COMPARISON OF "NOISY" DATA CLASSIFICATION RESULTS VERSUS SIMULATION RESULTS, S-204, 40 METER

(First numbers are from data classification, second are from Simulation Method)

%

	CORN	SOY	TREES	OTHER	UNCLASSIFIED
CORN	96.1/96.9	1.1/1.0	1.7/2.	1/0	0.1/.1
SOY	2.9/4.	94.7/95.	0.2/0	2./.5	0.2/.5
TREES	9/4.	/0	91/96	/0	/.0
OTHER	2.7/3	.2/0	0/0	96.7/96	.4/1

APPENDIX VIII

RESULTS FOR RADIOMETRIC SENSITIVITY STUDY

This appendix contains the results -- both tabular and graphic -- for the radiometric simulations carried out in accordance with the procedures described in Appendix VII.

TABLE VIII.1

EXPECTED PERFORMANCE MATRICES, 30 METER RESOLUTION,
RADIOMETRIC SENSITIVITY TIMES THE NOMINAL CASE

STUDY SEGMENT S-204, 43M

Radiometric Sensitivity: 0.5

	CORN	SOYBEANS	TREE	OTHER	UNCLAS.
CORN	.9924	.0003	.0000	.0027	.0045
SOYBEANS	.0006	.9877	.0000	.0039	.0077
TREES	.0000	.0000	.9991	.0000	.0009
OTHER	.0000	.0000	.9991	.0000	.0009

OVERALL CORRECT CLASSIFICATION = .966

Radiometric Sensitivity: 1.0

	CORN	SOYBEANS	TREE	OTHER	UNCLAS.
CORN	.9763	.0011	.0006	.0179	.0041
SOYBEANS	.0023	.9872	.0000	.0087	.0017
TREES	.0000	.0000	1.0000	.0000	.0000
OTHER	.0037	.0050	.0000	.9620	.0293

OVERALL CORRECT CLASSIFICATION = .977

Radiometric Sensitivity: 1.3

	CORN	SOYBEANS	TREE	OTHER	UNCLAS.
CORN	.9638	.0028	.0007	.0295	.0032
SOYBEANS	.0029	.9837	.0000	.0116	.0017
TREES	.0000	.0000	1.0000	.0000	.0000
OTHER	.0046	.0087	.0000	.9680	.0188

OVERALL CORRECT CLASSIFICATION = .97

TABLE VIII.1 (Continued)

STUDY SEGMENT S-204, 43M

Radiometric Sensitivity: 1.6

	CORN	SOYBEANS	TREE	OTHER	UNCLAS.
CORN	.9520	.0058	.0013	.0392	.0017
SOYBEANS	.0041	.9808	.0000	.0151	.0000
TREES	.0037	.0000	.9962	.0000	.0000
OTHER	.0000	.0000	.9962	.0000	.0000

OVERALL CORRECT CLASSIFICATION = .964

Radiometric Sensitivity: 2.0

	CORN	SOYBEANS	TREE	OTHER	UNCLAS.
CORN	.9365	.0093	.0030	.0501	.0011
SOYBEANS	.0047	.9750	.0000	.0204	.0000
TREES	.0075	.0000	.9925	.0000	.0000
OTHER	.0114	.0128	.0000	.9634	.0124

OVERALL CORRECT CLASSIFICATION = .953

Radiometric Sensitivity: 3.0

	CORN	SOYBEANS	TREE	OTHER	UNCLAS.
CORN	.8935	.0191	.0077	.0794	.0004
SOYBEANS	.0093	.9610	.0000	.0297	.0000
TREES	.0237	.0012	.9750	.0000	.0000
OTHER	.0261	.0169	.0000	.9510	.0059

OVERALL CORRECT CLASSIFICATION = .924

TABLE VIII.1 (Continued)

STUDY SEGMENT S-204, 43M

Radiometric Sensitivity: 6.0

	CORN	SOYBEANS	TREES	OTHER	UNCLAS.
CORN	.7459	.0529	.0318	.1691	.0004
SOYBEANS	.0338	.8783	.0041	.0839	.0000
TREES	.1037	.0062	.8887	.0012	.0000
OTHER	.0449	.0494	.0005	.9048	.0005

OVERALL CORRECT CLASSIFICATION = .810

Radiometric Sensitivity: 10.0

	CORN	SOYBEANS	TREES	OTHER	UNCLAS.
CORN	.5432	.0998	.0923	.2644	.0004
SOYBEANS	.0670	.7146	.0384	.1800	.0000
TREES	.1775	.0500	.7612	.0112	.0000
OTHER	.0673	.1249	.0059	.8018	.0000

OVERALL CORRECT CLASSIFICATION = .646

Radiometric Sensitivity: 20.0

	CORN	SOYBEANS	TREES	OTHER	UNCLAS.
CORN	.2549	.1947	.1913	.3589	.0002
SOYBEANS	.0897	.4945	.1153	.3005	.0000
TREES	.1562	.1937	.5700	.0800	.0000
OTHER	.0929	.2215	.0311	.6545	.0000

OVERALL CORRECT CLASSIFICATION = .408

TABLE VIII.2

EXPECTED PERFORMANCE MATRICES, 40 METER RESOLUTION,
RADIOMETRIC SENSITIVITY TIMES THE NOMINAL CASE

STUDY SEGMENT S-204, 43M

Radiometric Sensitivity: 0.5

	CORN	SOYBEANS	TREES	OTHER	UNCLAS.
CORN	.9926	.0003	.0000	.0016	.0000
SOYBEANS	.0000	.9911	.0000	.0000	.0000
TREES	.0000	.0008	.9983	.0000	.0000
OTHER	.0000	.0000	.0000	.9272	.0144

OVERALL CORRECT CLASSIFICATION = .980

Radiometric Sensitivity: 1.0

	CORN	SOYBEANS	TREES	OTHER	UNCLAS.
CORN	.9905	.0003	.0012	.0069	.0000
SOYBEANS	.0022	.9978	.0000	.0000	.0000
TREES	.0008	.0017	.9967	.0000	.0000
OTHER	.0005	.0000	.0000	.9533	.0138

OVERALL CORRECT CLASSIFICATION = .984

Radiometric Sensitivity: 1.3

	CORN	SOYBEANS	TREES	OTHER	UNCLAS.
CORN	.9836	.0010	.0022	.0121	.0000
SOYBEANS	.0022	.9956	.0000	.0000	.0000
TREES	.0008	.0017	.9958	.0008	.0000
OTHER	.0041	.0005	.0005	.9492	.0133

OVERALL CORRECT CLASSIFICATION = .979

TABLE VIII.2 (Continued)

STUDY SEGMENT S-204, 43M

Radiometric Sensitivity: 1.6

	CORN	SOYBEANS	TREES	OTHER	UNCLAS.
CORN	.9753	.0019	.0034	.0183	.0000
SOYBEANS	.0022	.9956	.0000	.0022	.0000
TREES	.0025	.0017	.9942	.0017	.0000
OTHER	.0056	.0005	.0010	.9477	.0154

OVERALL CORRECT CLASSIFICATION = .973

Radiometric Sensitivity: 2.0

	CORN	SOYBEANS	TREES	OTHER	UNCLAS.
CORN	.9588	.0021	.0076	.0297	.0000
SOYBEANS	.0022	.9933	.0000	.0022	.0000
TREES	.0067	.0025	.9875	.0033	.0000
OTHER	.0067	.0005	.0026	.9467	.0159

OVERALL CORRECT CLASSIFICATION = .962

Radiometric Sensitivity: 3.0

	CORN	SOYBEANS	TREES	OTHER	UNCLAS.
CORN	.9229	.0024	.0198	.0529	.0000
SOYBEANS	.0022	.9844	.0000	.0111	.0000
TREES	.0208	.0008	.9742	.0000	.0000
OTHER	.0308	.0036	.0041	.9287	.0185

OVERALL CORRECT CLASSIFICATION = .934

TABLE VIII.2 (Continued)

STUDY SEGMENT S-204, 43M

Radiometric Sensitivity: 6.0

	CORN	SOYBEANS	TREES	OTHER	UNCLAS.
CORN	.7897	.0026	.0841	.1234	.0000
SOYBEANS	.0089	.9489	.0000	.0422	.0000
TREES	.0992	.0017	.8933	.0050	.0000
OTHER	.0713	.0082	.0154	.8810	.0226

OVERALL CORRECT CLASSIFICATION = .829

Radiometric Sensitivity: 10.0

	CORN	SOYBEANS	TREES	OTHER	UNCLAS.
CORN	.5805	.0059	.1693	.2441	.0000
SOYBEANS	.0089	.8689	.0022	.1200	.0000
TREES	.1842	.0033	.7750	.0375	.0000
OTHER	.1144	.0231	.0231	.8138	.0256

OVERALL CORRECT CLASSIFICATION = .668

Radiometric Sensitivity: 20.0

	CORN	SOYBEANS	TREES	OTHER	UNCLAS.
CORN	.2738	.0459	.2779	.4010	.0010
SOYBEANS	.0244	.7489	.0133	.2133	.0000
TREES	.1725	.0317	.6383	.1575	.0000
OTHER	.1231	.0549	.0831	.6872	.0518

OVERALL CORRECT CLASSIFICATION - .429

TABLE VIII.3

EXPECTED PERFORMANCE MATRICES, 30 METER RESOLUTION,
RADIOMETRIC SENSITIVITY TIMES THE NOMINAL CASE

STUDY SEGMENT S-204, 42M

Radiometric Sensitivity: 0.5

	CORN	SOYBEANS	TREES	OTHER	UNCLAS.
CORN	.9818	.0006	.0000	.0014	.0163
SOYBEANS	.0028	.9792	.0000	.0009	.0170
TREES	.0000	.0000	1.0000	.0000	.0000
OTHER	.0005	.0011	.0000	.9304	.0680

OVERALL CORRECT CLASSIFICATION = .969

Radiometric Sensitivity: 1.0

	CORN	SOYBEANS	TREES	OTHER	UNCLAS.
CORN	.9818	.0025	.0000	.0019	.0138
SOYBEANS	.0047	.9698	.0000	.0066	.0189
TREES	.0000	.0000	1.0000	.0000	.0000
OTHER	.0011	.0032	.0000	.9433	.0523

OVERALL CORRECT CLASSIFICATION = .971

Radiometric Sensitivity: 1.3

	CORN	SOYBEANS	TREES	OTHER	UNCLAS.
CORN	.9834	.0061	.0000	.0028	.0077
SOYBEANS	.0094	.9547	.0000	.0142	.0217
TREES	.0000	.0000	1.0000	.0000	.0000
OTHER	.0005	.0054	.0000	.9514	.0426

OVERALL CORRECT CLASSIFICATION = .972

TABLE VIII.3 (Continued)

STUDY SEGMENT S-204, 42M

Radiometric Sensitivity: 1.6

	CORN	SOYBEANS	TREES	OTHER	UNCLAS.
CORN	.9815	.0099	.0000	.0039	.0047
SOYBEANS	.0123	.9443	.0000	.0236	.0198
TREES	.0000	.0000	1.0000	.0000	.0000
OTHER	.0027	.0070	.0000	.9530	.0372

OVERALL CORRECT CLASSIFICATION = .970

Radiometric Sensitivity: 2.0

	CORN	SOYBEANS	TREES	OTHER	UNCLAS.
CORN	.9699	.0199	.0008	.0052	.0041
SOYBEANS	.0170	.9264	.0000	.0377	.0189
TREES	.0000	.0000	1.0000	.0000	.0000
OTHER	.0043	.0103	.0000	.9530	.0324

OVERALL CORRECT CLASSIFICATION = .961

Radiometric Sensitivity: 3.0

	CORN	SOYBEANS	TREES	OTHER	UNCLAS.
CORN	.9365	.0461	.0030	.0110	.0033
SOYBEANS	.0330	.8726	.0000	.0736	.0208
TREES	.0020	.0000	.9980	.0000	.0000
OTHER	.0059	.0124	.0000	.9563	.0254

OVERALL CORRECT CLASSIFICATION = .936

TABLE VIII.3 (Continued)

STUDY SEGMENT S-204, 42M

Radiometric Sensitivity: 6.0

	CORN	SOYBEANS	TREES	OTHER	UNCLAS.
CORN	.8401	.1108	.0144	.0348	.0000
SOYBEANS	.0585	.7764	.0019	.1604	.0028
TREES	.0560	.0000	.9440	.0000	.0000
OTHER	.0167	.0259	.0000	.9482	.0092

OVERALL CORRECT CLASSIFICATION = .866

Radiometric Sensitivity: 10.0

	CORN	SOYBEANS	TREES	OTHER	UNCLAS.
CORN	.7155	.1627	.0464	.0754	.0000
SOYBEANS	.0896	.7066	.0019	.2009	.0009
TREES	.1240	.0160	.8580	.0020	.0000
OTHER	.0389	.0405	.0000	.9131	.0076

OVERALL CORRECT CLASSIFICATION = .776

Radiometric Sensitivity: 20.0

	CORN	SOYBEANS	TREES	OTHER	UNCLAS.
CORN	.4754	.1840	.1323	.2083	.0000
SOYBEANS	.1189	.6038	.0321	.2434	.0019
TREES	.2540	.0660	.6580	.0220	.0000
OTHER	.0745	.0820	.0038	.8343	.0054

OVERALL CORRECT CLASSIFICATION = .602

TABLE VIII.4

EXPECTED PERFORMANCE MATRICES, 40 METER RESOLUTION,
RADIOMETRIC SENSITIVITY TIMES THE NOMINAL CASE

STUDY SEGMENT S-204, 42M

Radiometric Sensitivity: 0.5

	CORN	SOYBEANS	TREES	OTHER	UNCLAS.
CORN	.9564	.0000	.0000	.0002	.0000
SOYBEANS	.0000	.9565	.0000	.0000	.0000
TREES	.0000	.0000	1.0000	.0000	.0000
OTHER	.0000	.0007	.0000	.9366	.0000

OVERALL CORRECT CLASSIFICATION = .955

Radiometric Sensitivity: 1.0

	CORN	SOYBEANS	TREES	OTHER	UNCLAS.
CORN	.9786	.0014	.0000	.0005	.0000
SOYBEANS	.0019	.9704	.0000	.0009	.0000
TREES	.0000	.0000	1.0000	.0000	.0000
OTHER	.0000	.0046	.0000	.9490	.0000

OVERALL CORRECT CLASSIFICATION = .973

Radiometric Sensitivity: 1.3

	CORN	SOYBEANS	TREES	OTHER	UNCLAS.
CORN	.9753	.0077	.0000	.0007	.0000
SOYBEANS	.0019	.9722	.0000	.0056	.0000
TREES	.0000	.0000	1.0000	.0000	.0000
OTHER	.0000	.0065	.0000	.9523	.0000

OVERALL CORRECT CLASSIFICATION = .972

TABLE VIII.4 (Continued)

STUDY SEGMENT S-204, 42M

Radiometric Sensitivity: 1.6

	CORN	SOYBEANS	TREES	OTHER	UNCLAS.
CORN	.9753	.0149	.0000	.0014	.0000
SOYBEANS	.0037	.9620	.0000	.0130	.0000
TREES	.0000	.0000	1.0000	.0000	.0000
OTHER	.0000	.0092	.0000	.9536	.0000

OVERALL CORRECT CLASSIFICATION = .970

Radiometric Sensitivity: 2.0

	CORN	SOYBEANS	TREES	OTHER	UNCLAS.
CORN	.9620	.0291	.0000	.0021	.0000
SOYBEANS	.0074	.9537	.0000	.0259	.0000
TREES	.0000	.0000	1.0000	.0000	.0000
OTHER	.0000	.0111	.0000	.9542	.0000

OVERALL CORRECT CLASSIFICATION = .961

Radiometric Sensitivity: 3.0

	CORN	SOYBEANS	TREES	OTHER	UNCLAS.
CORN	.9252	.0613	.0009	.0091	.0000
SOYBEANS	.0194	.9176	.0000	.0519	.0000
TREES	.0067	.0000	.9933	.0000	.0000
OTHER	.0046	.0183	.0000	.9588	.0000

OVERALL CORRECT CLASSIFICATION = .935

TABLE VIII.4 (Continued)

STUDY SEGMENT S-204, 42M

Radiometric Sensitivity: 6.0

	CORN	SOYBEANS	TREES	OTHER	UNCLAS.
CORN	.8228	.1441	.0068	.0261	.0000
SOYBEANS	.0537	.8287	.0009	.1148	.0000
TREES	.0422	.0000	.9578	.0000	.0000
OTHER	.0255	.0340	.0000	.9320	.0000

OVERALL CORRECT CLASSIFICATION = .855

Radiometric Sensitivity: 10.0

	CORN	SOYBEANS	TREES	OTHER	UNCLAS.
CORN	.7154	.1946	.0270	.0629	.0000
SOYBEANS	.0778	.7509	.0019	.1694	.0000
TREES	.1200	.0156	.8622	.0022	.0000
OTHER	.0405	.0497	.0000	.9052	.0000

OVERALL CORRECT CLASSIFICATION = .769

Radiometric Sensitivity: 20.0

	CORN	SOYBEANS	TREES	OTHER	UNCLAS.
CORN	.4916	.2112	.1082	.1890	.0000
SOYBEANS	.1194	.6565	.0213	.2028	.0000
TREES	.2044	.0711	.6956	.0289	.0000
OTHER	.0641	.0863	.0039	.8458	.0000

OVERALL CORRECT CLASSIFICATION = .602

TABLE VIII.5

EXPECTED PERFORMANCE MATRICES, 30 METER RESOLUTION
RADIOMETRIC SENSITIVITY TIMES THE NOMINAL CASE

STUDY SEGMENT S-204, 41M

Radiometric Sensitivity: 0.5

	CORN	SOYBEANS	TREES	OTHER	UNCLAS.
CORN	.8629	.0316	.0003	.0588	.0465
SOYBEANS	.0283	.9345	.0000	.0262	.0110
TREES	.0000	.0000	.9986	.0000	.0014
OTHER	.0126	.0233	.0000	.8986	.0656

OVERALL CORRECT CLASSIFICATION = .896

Radiometric Sensitivity: 1.0

	CORN	SOYBEANS	TREES	OTHER	UNCLAS.
CORN	.8588	.0513	.0035	.0649	.0215
SOYBEANS	.0393	.9207	.0007	.0324	.0069
TREES	.0071	.0000	.9929	.0000	.0000
OTHER	.0163	.0335	.0000	.8893	.0609

OVERALL CORRECT CLASSIFICATION = .889

Radiometric Sensitivity: 1.3

	CORN	SOYBEANS	TREES	OTHER	UNCLAS.
CORN	.8389	.0654	.0088	.0694	.0174
SOYBEANS	.0490	.9062	.0007	.0393	.0048
TREES	.0129	.0000	.9871	.0000	.0000
OTHER	.0191	.0465	.0000	.8735	.0609

OVERALL CORRECT CLASSIFICAITON = .872

TABLE VIII.5 (Continued)

STUDY SEGMENT S-204, 41M

Radiometric Sensitivity: 1.6

	CORN	SOYBEANS	TREES	OTHER	UNCLAS.
CORN	.8184	.0780	.0149	.0760	.0126
SOYBEANS	.0593	.8855	.0007	.0531	.0014
TREES	.0229	.0043	.9729	.0000	.0000
OTHER	.0233	.0572	.0000	.3609	.0586

OVERALL CORRECT CLASSIFICATION = .854

Radiometric Sensitivity: 2.0

	CORN	SOYBEANS	TREES	OTHER	UNCLAS.
CORN	.7717	.0987	.0278	.0932	.0086
SOYBEANS	.0786	.8559	.0014	.0621	.0021
TREES	.0343	.0071	.9586	.0000	.0000
OTHER	.0288	.0688	.0000	.8451	.0572

OVERALL CORRECT CLASSIFICATION = .821

Radiometric Sensitivity: 3.0

	CORN	SOYBEANS	TREES	OTHER	UNCLAS.
CORN	.6712	.1407	.0631	.1205	.0045
SOYBEANS	.1138	.7779	.0069	.0979	.0034
TREES	.0586	.0143	.9271	.0000	.0000
OTHER	.0377	.1084	.0000	.8060	.0479

OVERALL CORRECT CLASSIFICATION = .747

TABLE VIII.5 (Continued)

STUDY SEGMENT S-204, 41M

Radiometric Sensitivity: 6.0

	CORN	SOYBEANS	TREES	OTHER	UNCLAS.
CORN	.4242	.2101	.1402	.2245	.0010
SOYBEANS	.1503	.6421	.0262	.1814	.0000
TREES	.0535	.1916	.0019	.7367	.0163
OTHER	.0535	.1916	.0019	.7367	.0163

OVERALL CORRECT CLASSIFICATION = .574

Radiometric Sensitivity: 10.0

	CORN	SOYBEANS	TREES	OTHER	UNCLAS.
CORN	.2697	.2503	.1909	.2886	.0005
SOYBEANS	.1393	.5510	.0497	.2600	.0000
TREES	.2000	.1029	.6386	.0586	.0000
OTHER	.0595	.2600	.0120	.6679	.0023

OVERALL CORRECT CLASSIFICATION = 454

Radiometric Sensitivity: 20.0

	CORN	SOYBEANS	TREES	OTHER	UNCLAS.
CORN	.1535	.3086	.2045	.3331	.0003
SOYBEANS	.1090	.4772	.0890	.3248	.0000
TREES	.1943	.2000	.4414	.1643	.0000
OTHER	.0749	.3344	.0353	.5549	.0005

OVERALL CORRECT CLASSIFICATION = .339

TABLE VIII.6

EXPECTED PERFORMANCE MATRICES, 40 METER RESOLUTION
RADIOMETRIC SENSITIVITY VERSUS THE NOMINAL CASE

STUDY SEGMENT S-204, 41M

Radiometric Sensitivity: 0.5

	CORN	SOYBEANS	TREES	OTHER	UNCLAS.
CORN	.9217	.0142	.0000	.0348	.0293
SOYBEANS	.0236	.9559	.0000	.0063	.0142
TREES	.0000	.0000	.9986	.0000	.0014
OTHER	.0194	.0065	.0000	.8682	.1059

OVERALL CORRECT CLASSIFICATION = .923

Radiometric Sensitivity: 1.0

	CORN	SOYBEANS	TREES	OTHER	UNCLAS.
CORN	.9110	.0264	.0020	.0374	.0232
SOYBEANS	.0457	.9394	.0000	.0087	.0063
TREES	.0014	.0000	.9986	.0000	.0000
OTHER	.0329	.0147	.0000	.8576	.0947

OVERALL CORRECT CLASSIFICATION = .912

Radiometric Sensitivity: 1.3

	CORN	SOYBEANS	TREES	OTHER	UNCLAS.
CORN	.8974	.0359	.0061	.0409	.0197
SOYBEANS	.0606	.9236	.0000	.0118	.0039
TREES	.0114	.0000	.9886	.0000	.0000
OTHER	.0394	.0288	.0000	.8353	.0965

OVERALL CORRECT CLASSIFICATION = .896

TABLE VIII.6 (Continued)

STUDY SEGMENT S-204, 41M

Radiometric Sensitivity: 1.6

	CORN	SOYBEANS	TREES	OTHER	UNCLAS.
CORN	.8791	.0452	.0110	.0455	.0191
SOYBEANS	.0827	.8969	.0008	.0181	.0016
TREES	.0214	.0014	.9771	.0000	.0000
OTHER	.0412	.0365	.0000	.8247	.0976

OVERALL CORRECT CLASSIFICATION = .879

Radiometric Sensitivity: 2.0

	CORN	SOYBEANS	TREES	OTHER	UNCLAS.
CORN	.8455	.0609	.0246	.0522	.0168
SOYBEANS	.1039	.8685	.0008	.0252	.0016
TREES	.0357	.0071	.9571	.0000	.0000
OTHER	.0494	.0559	.0000	.7976	.0971

OVERALL CORRECT CLASSIFICATION = .849

Radiometric Sensitivity: 3.0

	CORN	SOYBEANS	TREES	OTHER	UNCLAS.
CORN	.7545	.1014	.0603	.0728	.0110
SOYBEANS	.1252	.8181	.0071	.0480	.0016
TREES	.0686	.0129	.9186	.0000	.0000
OTHER	.0565	.1088	.0000	.7624	.0724

OVERALL CORRECT CLASSIFICATION = .784

TABLE VIII.6 (Continued)

STUDY SEGMENT S-204, 41M

Radiometric Sensitivity: 6.0

	CORN	SOYBEANS	TREES	OTHER	UNCLAS.
CORN	.5119	.1786	.1559	.1504	.0032
SOYBEANS	.1559	.6709	.0291	.1441	.0000
TREES	.1514	.0500	.7943	.0043	.0000
OTHER	.0676	.2071	.0053	.6888	.0312

OVERALL CORRECT CLASSIFICATION = .610

Radiometric Sensitivity: 10.0

	CORN	SOYBEANS	TREES	OTHER	UNCLAS.
CORN	.3528	.2206	.2081	.2183	.0003
SOYBEANS	.1441	.5811	.0669	.2079	.0000
TREES	.1714	.1000	.6657	.0629	.0000
OTHER	.0676	.2935	.0182	.6147	.0059

OVERALL CORRECT CLASSIFICATION = .487

Radiometric Sensitivity: 20.0

	CORN	SOYBEANS	TREES	OTHER	UNCLAS.
CORN	.2267	.2849	.2441	.2443	.0000
SOYBEANS	.1252	.5079	.1268	.2402	.0000
TREES	.1671	.1957	.4886	.1486	.0000
OTHER	.0700	.3994	.0565	.4741	.0000

OVERALL CORRECT CLASSIFICATION = .362

TABLE VIII.7

EXPECTED PERFORMANCE MATRICES, 40 METER RESOLUTION, RADIOMETRIC SENSITIVITY TIMES THE NOMINAL CASE

STUDY SEGMENT S-212, 43M

Radiometric Sensitivity: 0.5

	LIGHTLY STRESSED CORN	HEAVILY STRESSED CORN	SOYBEANS	TREES	OTHER	UNCLAS.
CORN (LIGHTLY STRESSED)	.6260	.0490	.0330	.0000	.2920	.0000
CORN (HEAVILY STRESSED)	.0870	.8770	.0000	.0000	.0360	.0000
SOYBEANS	.0014	.0000	.9521	.0000	.0464	.0000
TREES	.0000	.0000	.0000	1.0000	.0000	.0000
OTHER	.0018	.0014	.0041	.0000	.9927	.0000

OVERALL CORRECT CLASSIFICATION = 91.212

Radiometric Sensitivity: 1.0

	LIGHTLY STRESSED CORN	HEAVILY STRESSED CORN	SOYBEANS	TREES	OTHER	UNCLAS.
CORN (LIGHTLY STRESSED)	.6440	.1070	.0280	.0000	.2210	.0000
CORN (HEAVILY STRESSED)	.1110	.8030	.0000	.0000	.0860	.0000
SOYBEANS	.0014	.0000	.9464	.0000	.0521	.0000
TREES	.0000	.0000	.0010	.9990	.0000	.0000
OTHER	.0023	.0027	.0068	.0000	.9882	.0000

OVERALL CORRECT CLASSIFICATION = 90.076

TABLE VIII.7 (Continued)

STUDY SEGMENT S-212, 43M

Radiometric Sensitivity: 1.3

	LIGHTLY STRESSED CORN	HEAVILY STRESSED CORN	SOYBEANS	TREES	OTHER	UNCLAS.
CORN (LIGHTLY STRESSED)	.5540	.1260	.0360	.0010	.2830	.0000
CORN (HEAVILY STRESSED)	.1220	.7630	.0000	.0000	.1150	.0000
SOYBEANS	.0014	.0000	.9229	.0000	.0757	.0000
TREES	.0000	.0000	.0020	.9980	.0000	.0000
OTHER	.0032	.0045	.0150	.0000	.9773	.0000

OVERALL CORRECT CLASSIFICATION = 87.2

Radiometric Sensitivity: 1.6

	LIGHTLY STRESSED CORN	HEAVILY STRESSED CORN	SOYBEANS	TREES	OTHER	UNCLAS.
CORN (LIGHTLY STRESSED)	.5050	.1280	.0430	.0030	.3210	.0000
CORN (HEAVILY STRESSED)	.1330	.7190	.0000	.0000	.1480	.0000
SOYBEANS	.0014	.0000	.9021	.0000	.0964	.0000
TREES	.0000	.0000	.0030	.9960	.0010	.0000
OTHER	.0045	.0077	.0250	.0000	.9627	.0000

OVERALL CORRECT CLASSIFICATION = 84.864

TABLE VIII.7 (Continued)

STUDY SEGMENT S-212, 43M

Radiometric Sensitivity: 2.0

	LIGHTLY STRESSED CORN	HEAVILY STRESSED CORN	SOYBEANS	TREES	OTHER	UNCLAS.
CORN (LIGHTLY STRESSED)	.4410	.1270	.0520	.0070	.3730	.0000
CORN (HEAVILY STRESSED)	.1350	.6610	.0000	.0000	.2040	.0000
SOYBEANS	.0014	.0000	.8614	.0000	.1371	.0000
TREES	.0000	.0000	.0050	.9910	.0040	.0000
OTHER	.0064	.0123	.0391	.0000	.9423	.0000

OVERALL CORRECT CLASSIFICATION = 81.394

Radiometric Sensitivity: 3.0

	LIGHTLY STRESSED CORN	HEAVILY STRESSED CORN	SOYBEANS	TREES	OTHER	UNCLAS.
CORN (LIGHTLY STRESSED)	.3190	.1190	.0660	.0230	.4730	.0000
CORN (HEAVILY STRESSED)	.1350	.5690	.0000	.0000	.2960	.0000
SOYBEANS	.0014	.0000	.7957	.0021	.2007	.0000
TREES	.0010	.0000	.0090	.9660	.0240	.0000
OTHER	.0150	.0182	.0814	.0009	.8845	.0000

OVERALL CORRECT CLASSIFICATION = 74.455

TABLE VIII.7 (Continued)

STUDY SEGMENT S-212, 43M

Radiometric Sensitivity: 6.0

	LIGHTLY STRESSED CORN	HEAVILY STRESSED CORN	SOYBEANS	TREES	OTHER	UNCLAS.
CORN (LIGHTLY STRESSED)	.1650	.1130	.0880	.0710	.5630	.0000
CORN (HEAVILY STRESSED)	.0840	.4110	.0030	.0080	.4940	.0000
SOYBEANS	.0021	.0000	.6779	.0064	.3136	.0000
TREES	.0110	.0010	.0500	.7910	.1470	.0000
OTHER	.0205	.0282	.1300	.0086	.8127	.0000

OVERALL CORRECT CLASSIFICATION = 62.182

Radiometric Sensitivity: 10.0

	LIGHTLY STRESSED CORN	HEAVILY STRESSED CORN	SOYBEANS	TREES	OTHER	UNCLAS.
CORN (LIGHTLY STRESSED)	.0790	.1090	.1060	.1420	.5640	.0000
CORN (HEAVILY STRESSED)	.0560	.2840	.0160	.0570	.5870	.0000
SOYBEANS	.0050	.0014	.5807	.0300	.3829	.0000
TREES	.0160	.0190	.1120	.6120	.2410	.0000
OTHER	.0191	.0409	.1709	.0273	.7418	.0000

OVERALL CORRECT CLASSIFICATION = 51.818

TABLE VIII.7 (Continued)

STUDY SEGMENT S-212, 43M

Radiometric Sensitivity: 20.0

	LIGHTLY STRESSED CORN	HEAVILY STRESSED CORN	SOYBEANS	TREES	OTHER	UNCLAS.
CORN (LIGHTLY STRESSED)	.0260	.0960	.1510	.1890	.5380	.0000
CORN (HEAVILY STRESSED)	.0180	.1620	.0620	.1350	.6230	.0000
SOYBEANS	.0029	.0157	.4479	.0729	.4607	.0000
TREES	.0150	.0600	.1520	.3980	.3750	.0000
OTHER	.0105	.0527	.2118	.0764	.6486	.0000

OVERALL CORRECT CLASSIFICATION = 40.000

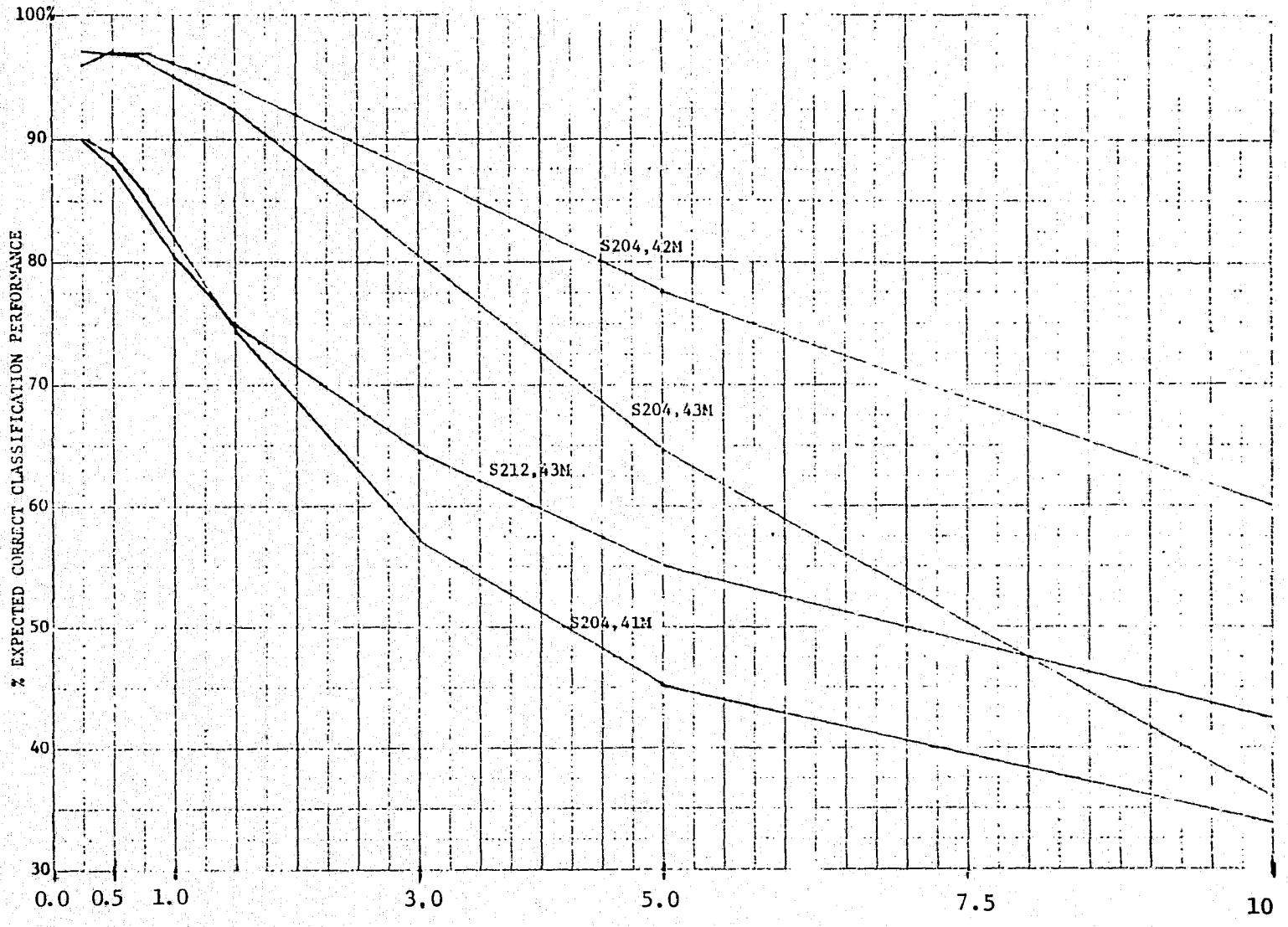

FIGURE VIII-1. RADIOMETRIC SIMULATION -- 30 METER RESOLUTION -- PERFORMANCE OVER ALL CLASSES
(All Available Fields In Scene Utilized In Training Procedure)

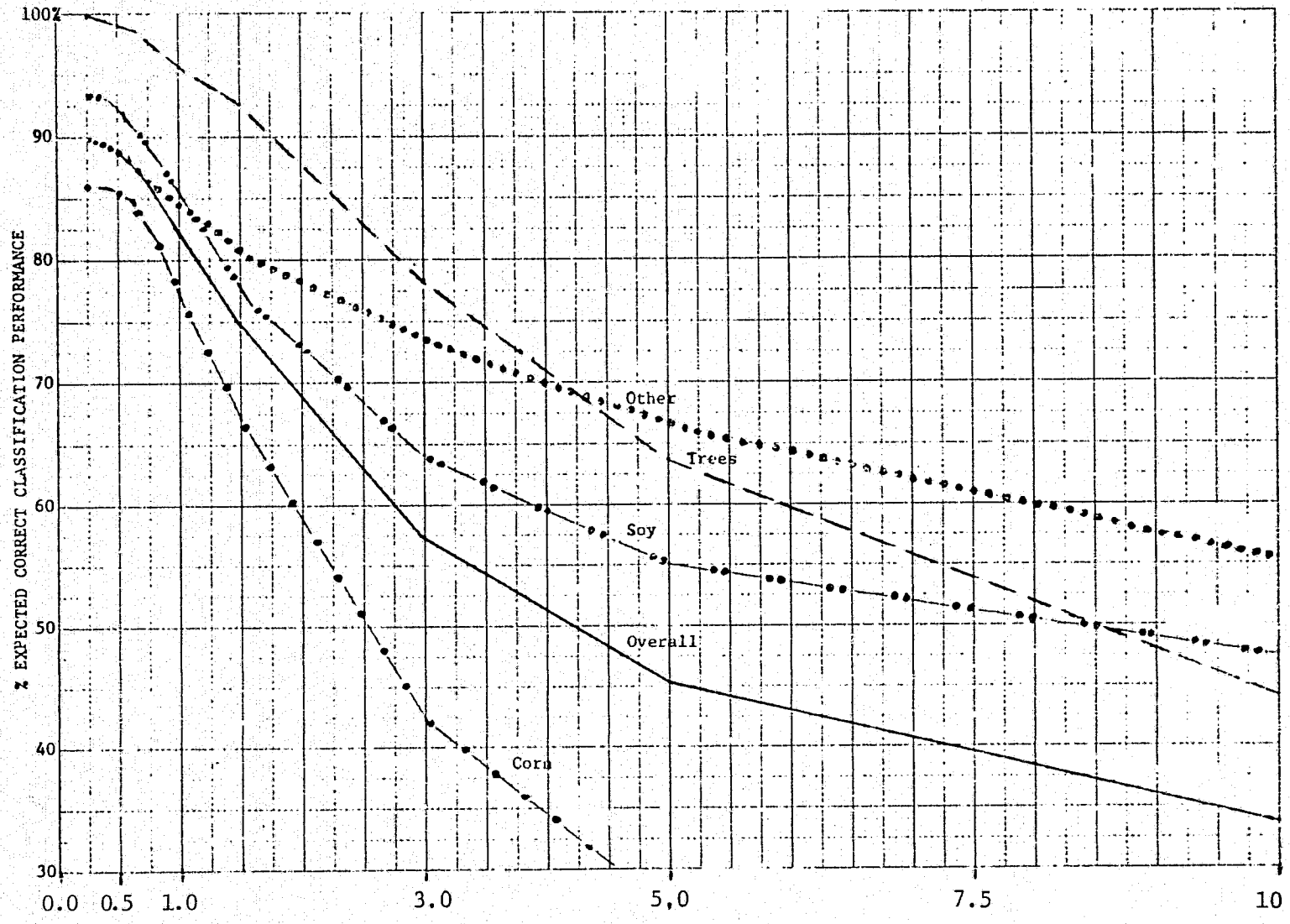

FIGURE VIII-2. RADIOMETRIC SIMULATION -- Segment 204, July 12 (41M) -- 30 METER RESOLUTION
(121 Fields In Scene Utilized In Training Procedure)

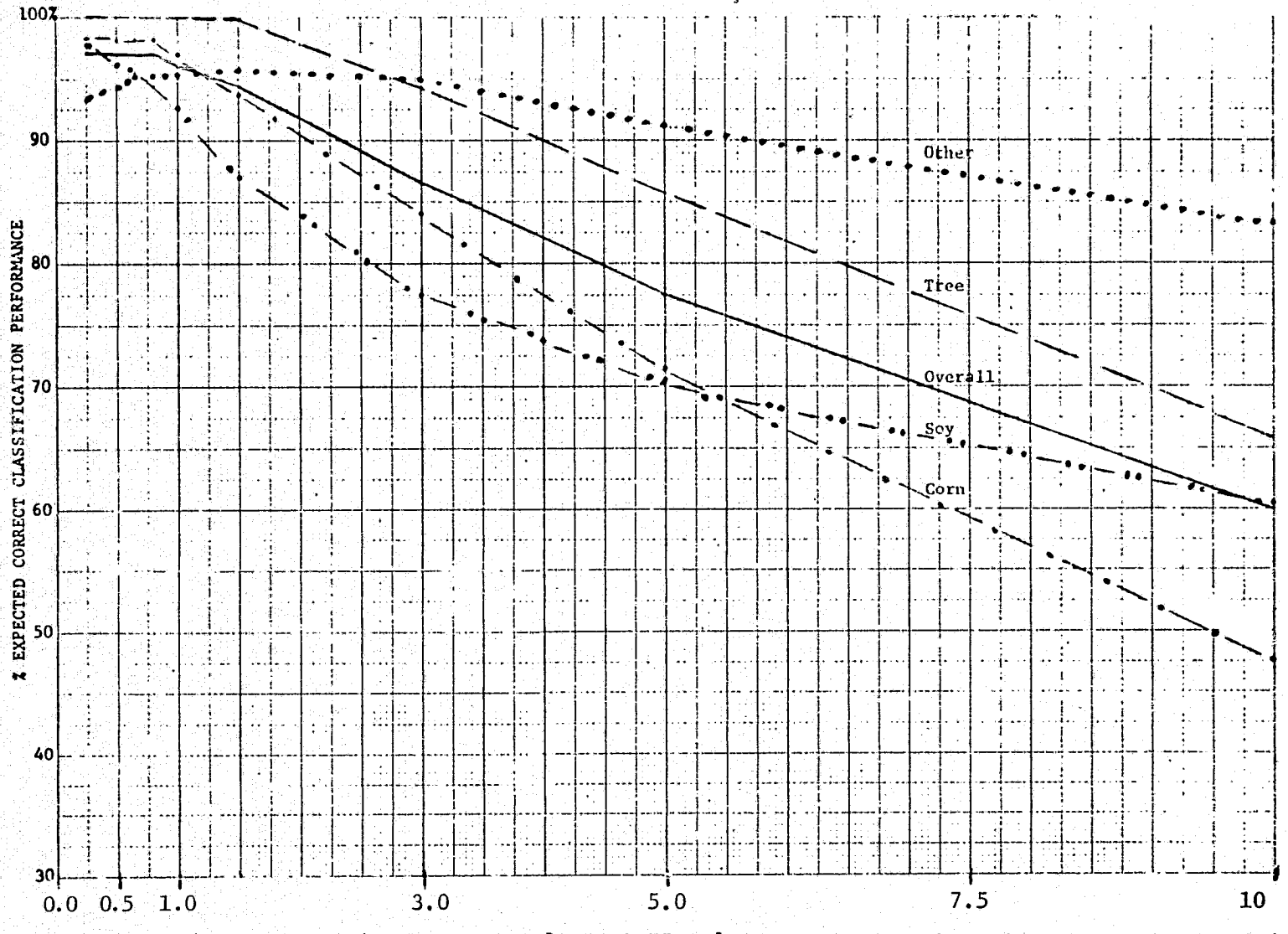

FIGURE VIII-3. RADIOMETRIC SIMULATION -- Segment 204, August 5 (42M) -- 30 METER RESOLUTION (120 Fields In Scene Utilized In Training Procedure)

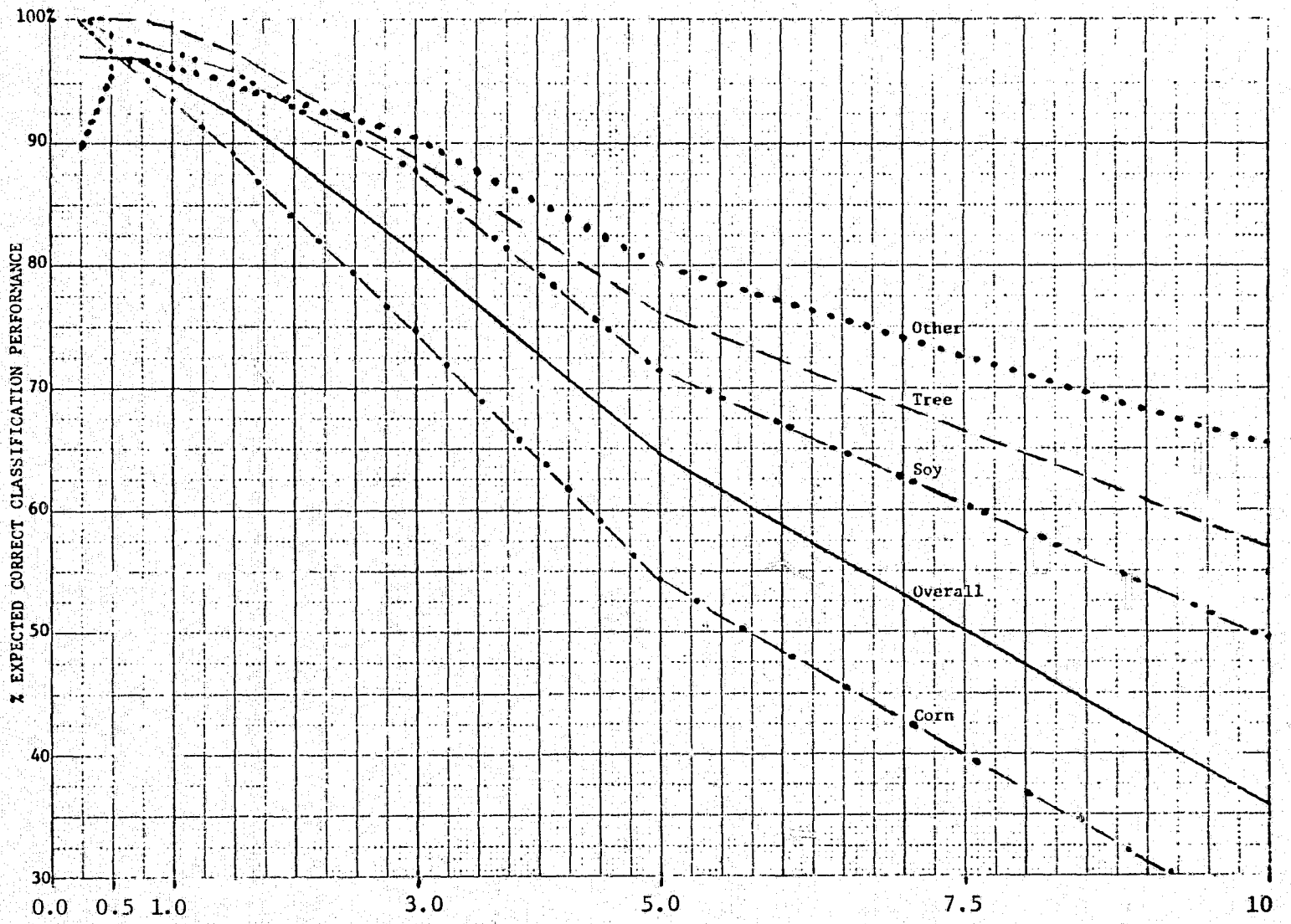

FIGURE VIII-4. RADIOMETRIC SIMULATION -- Segment 204, August 13 (43M) -- 30 METER RESOLUTION
(143 Fields In Scene Utilized In Training Procedure)

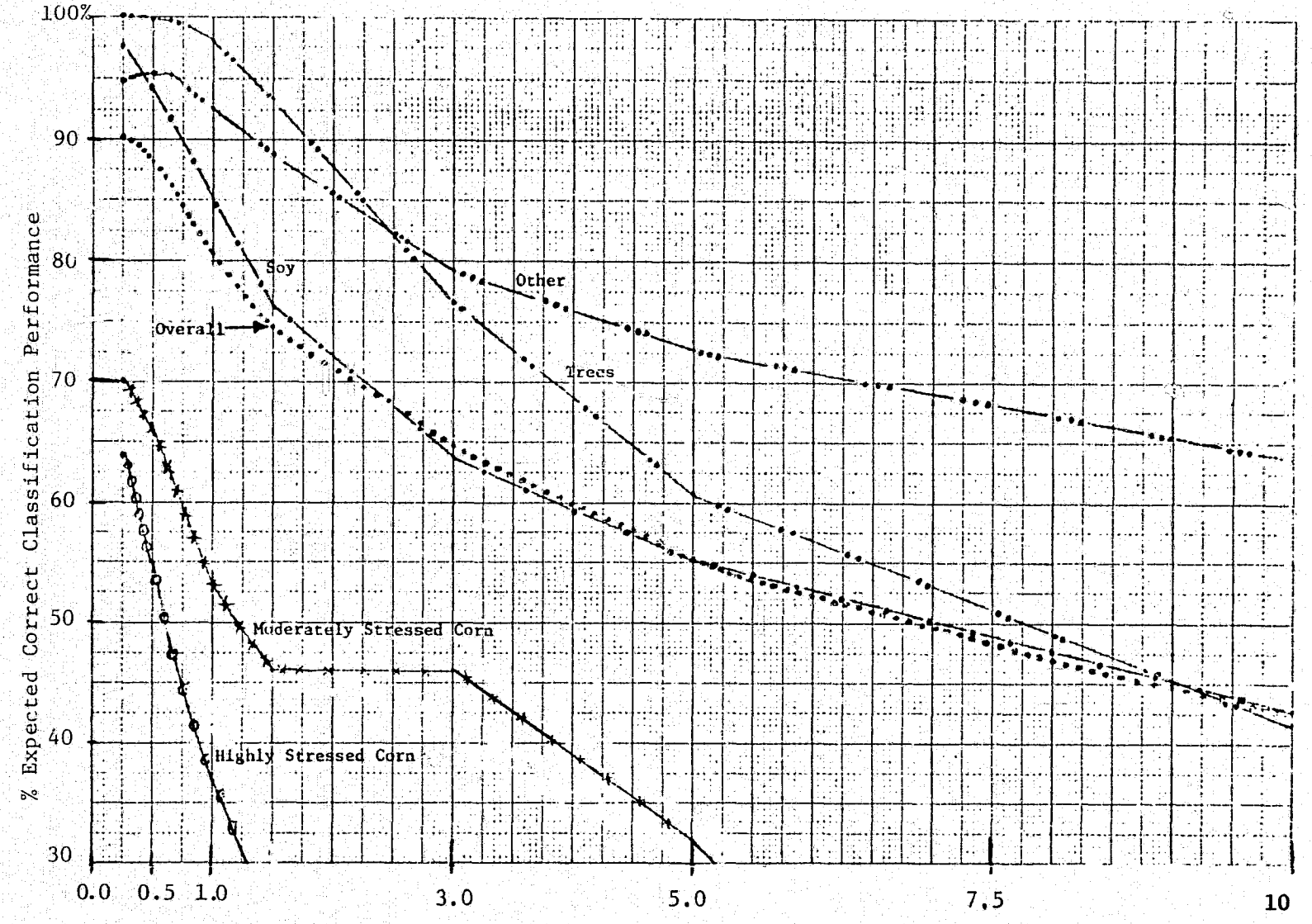

FIGURE VIII-5. RADIOMETRIC SIMULATION -- Segment 212, August 18 (43M) -- 30 METER RESOLUTION (186 Fields In Scene Utilized In Training Procedure)

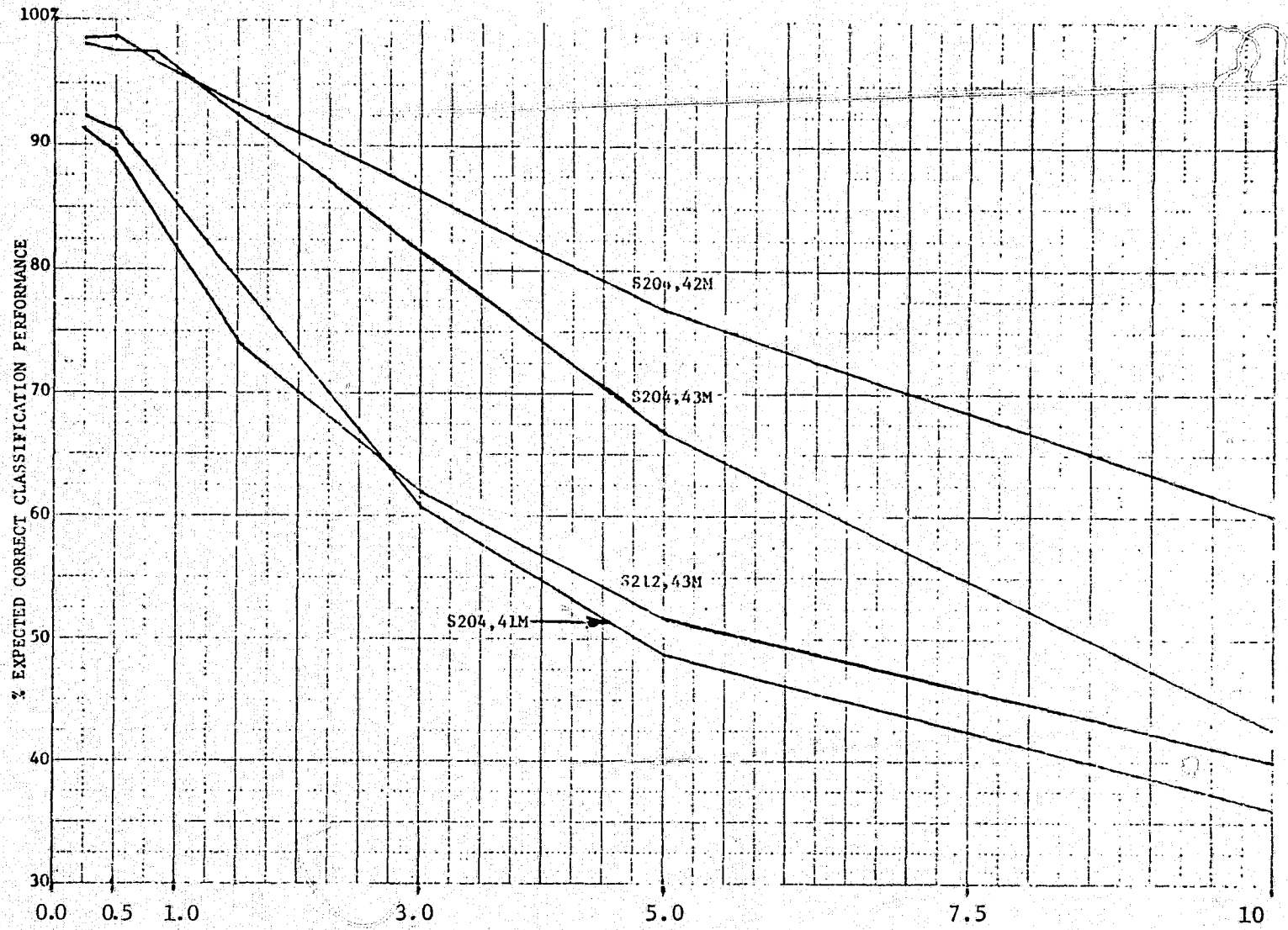

FIGURE VIII-6. RADIOMETRIC SIMULATION -- 40 METER RESOLUTION -- PERFORMANCE OVER ALL CLASSES (All Available Fields In Scene Utilized In Training -- This Is About 80% Of The Fields Used In The Corresponding 30 Meter Results)

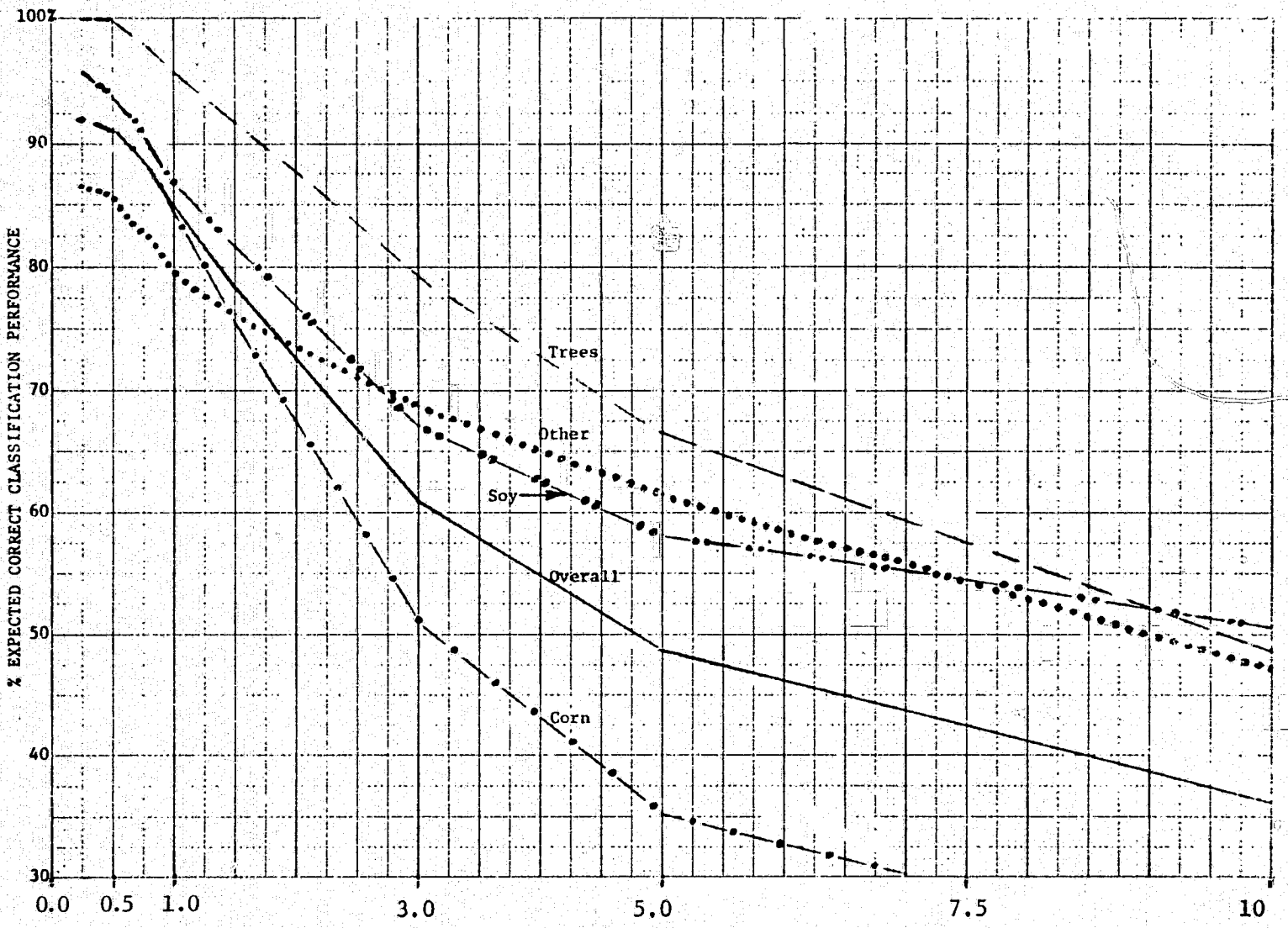

FIGURE VIII-7. RADIOMETRIC SIMULATION -- Segment 204, July 12 (41M) -- 40 METER RESOLUTION
(83 Fields In Scene Utilized In Training Procedure)

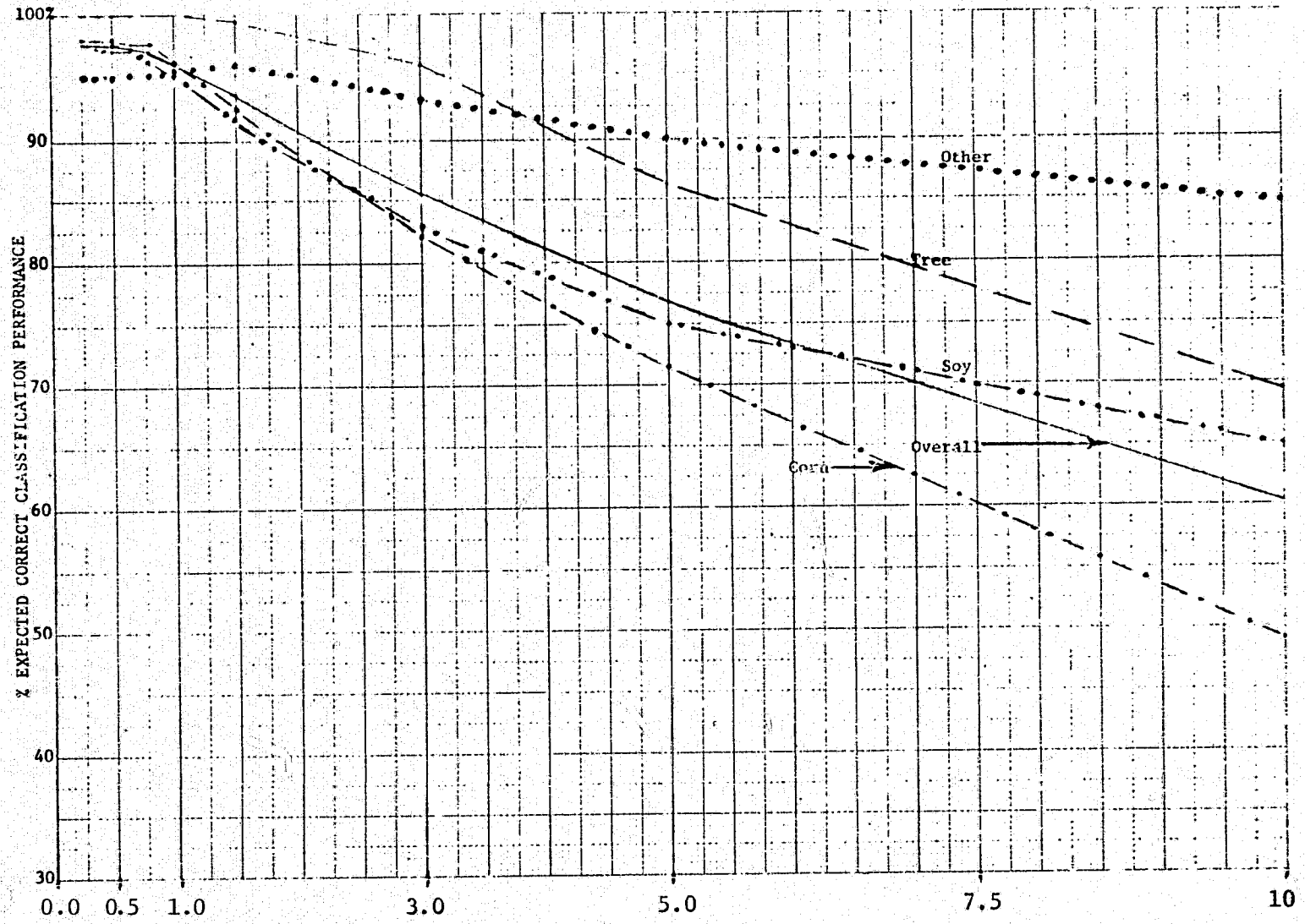

FIGURE VIII-8. RADIOMETRIC SIMULATION -- Segment 204, August 5 (42M) -- 40 METER RESOLUTION
(93 Fields In Scene Utilized In Training Procedure)

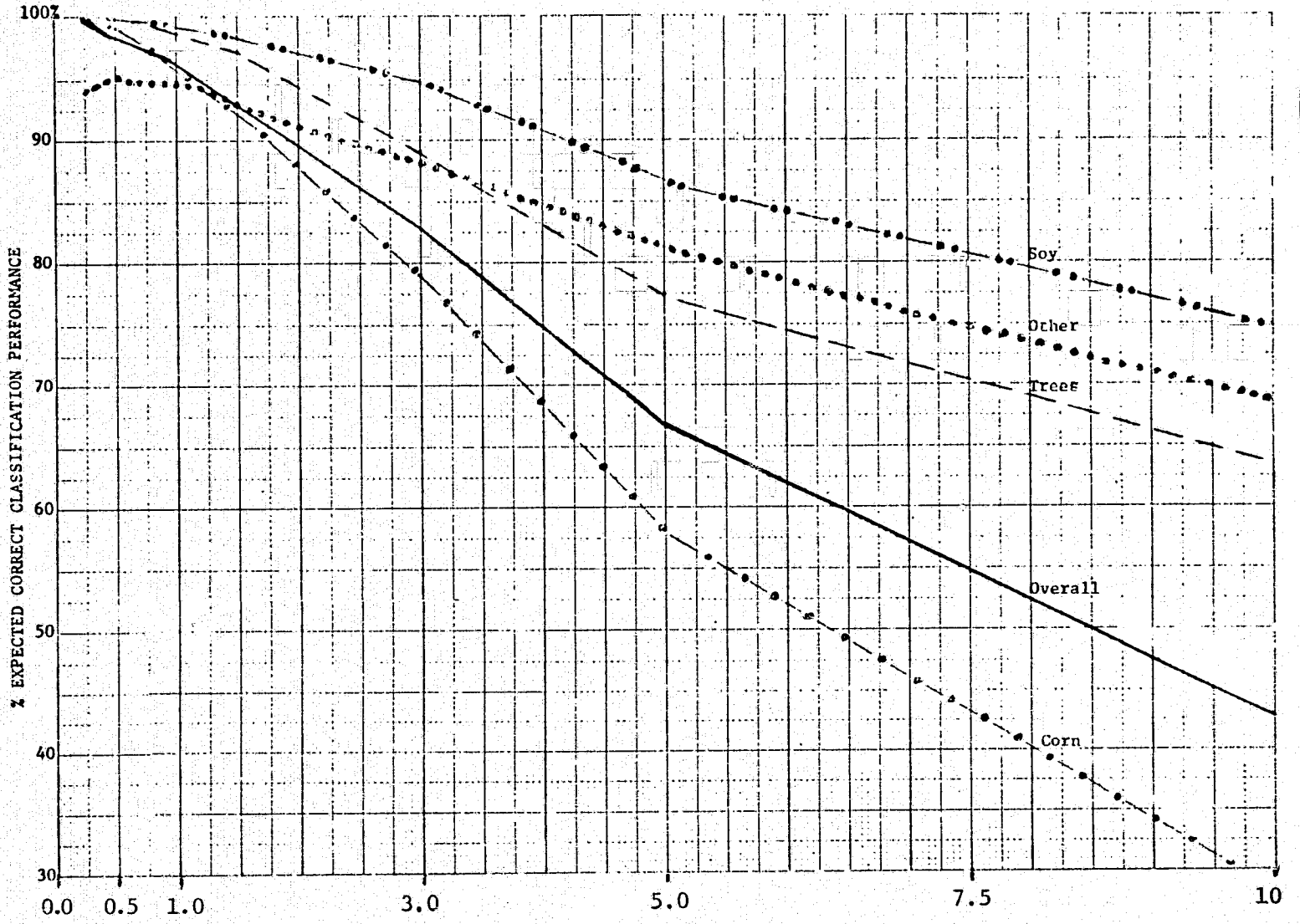

FIGURE VIII-9. RADIOMETRIC SIMULATION -- Segment 204, August 13 (43M) -- 40 METER RESOLUTION (110 Fields In Scene Utilized In Training Procedure)

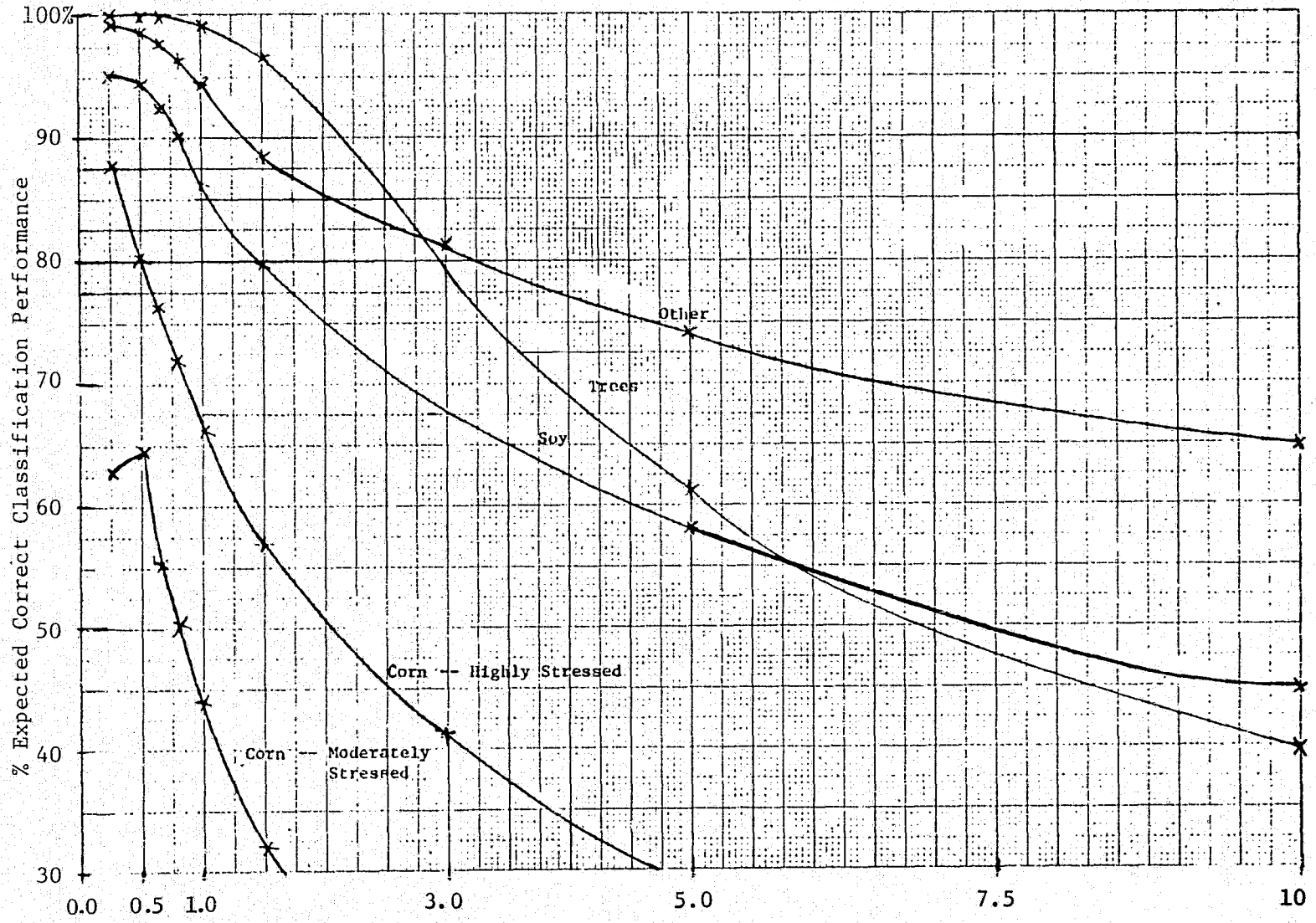

Percent NEΔρ (For Bands 1-4. In Band 5 [1.55-1.75 μm] NEΔρ Is Twice the Value Shown; For Band 6, the NEΔTValue Is as Shown on the Axis)

FIGURE VIII-10. RADIOMETRIC SIMULATION -- Segment 212, August 17 (43M) -- 40 METER RESOLUTION (152 Fields In Scene Utilized In Training Procedure)

APPENDIX IX

ALGORITHM DOCUMENTATION

This appendix contains descriptions of the important algorithms used in the processing of multispectral data for this experiment. There are six basic algorithms which are described here. First, the multispectral data were prepared to satisfy the experimental design requirements -- spatial degradation of the data to meet specific resolution requirements and noise addition for the radiometric aspect of the experiment. Next, signatures were computed (mean and covariance matrix) for many fields or areas of each class only from field center pixels. A clustering algorithm [24] was then used to identify and combine spectrally similar signatures. For the radiometric study, these signatures were then processed through ERIM's simulation classifier. For the spatial resolution study, the multispectral data was classified using ERIM's "best" linear classifier. In the spectral band study an optimum subset of channels was identified which minimized the average pairwise linear approximation of the probability of misclassification after an exhaustive search of all possible sextuples. Then, spectral band ranking was achieved using a similar program which computes the optimum sextuple using a without replacement algorithm.

The spatial degradation algorithm performs the required spatial degradation for the spatial resolution study (refer to Figure IX.1). The degradation is the result of a weighted average over a grid of pixels; this calculation is performed throughout an entire scene comprised of a set of overlapping grids.

After the spatial degradation, noise was added for simulation of TM data with specified radiometric sensitivity. The noise addition model is: $DATA_i + NOISE_i$ (for the i^{th} channel) where NOISE is a Gaussian function with a mean zero and standard deviation equal to the counts equivalent change in reflectance, $DE\Delta\rho$, corresponding to the specific $NE\Delta\rho$ ($NE\Delta T$) for each channel (band) of data. These noise

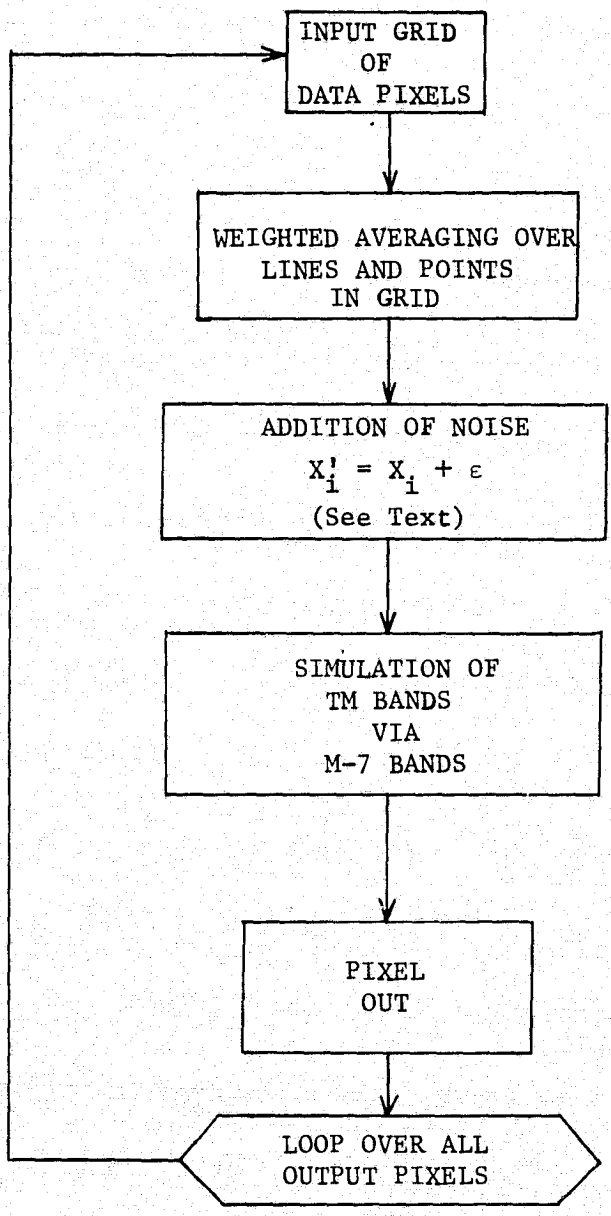

FIGURE IX-1. SPATIAL DEGRADATION FLOW CHART

functions are independent and uncorrelated for each channel.

For initially "noise free" data, noise transformed data can be represented by:

$$x_i' = x_i + \varepsilon$$

where

x_i' is the output data value

x_i is the input data value

i is the channel being referred

ε is the amount of noise added

so that the resulting data has the following characteristics:

$$E(x') = E(x)$$

and

$$\sigma^2_{x'} = \sigma^2_x + \sigma^2_\varepsilon$$

where

$E(\ )$ . . . denotes the expected value function

σ^2_x . . . is the variance of the input data

$\sigma^2_{x'}$ . . . is the variance of the output data

σ^2_ε . . . is the variance of the noise added

where: $\sigma^2_\varepsilon = (DE\Delta\rho)^2$

For the required spectral simulation of the seven recommended TM bands, four of the M-7 bands were used without modification. A simple average was done to combine two M-7 bands to simulate two of the TM bands as indicated:

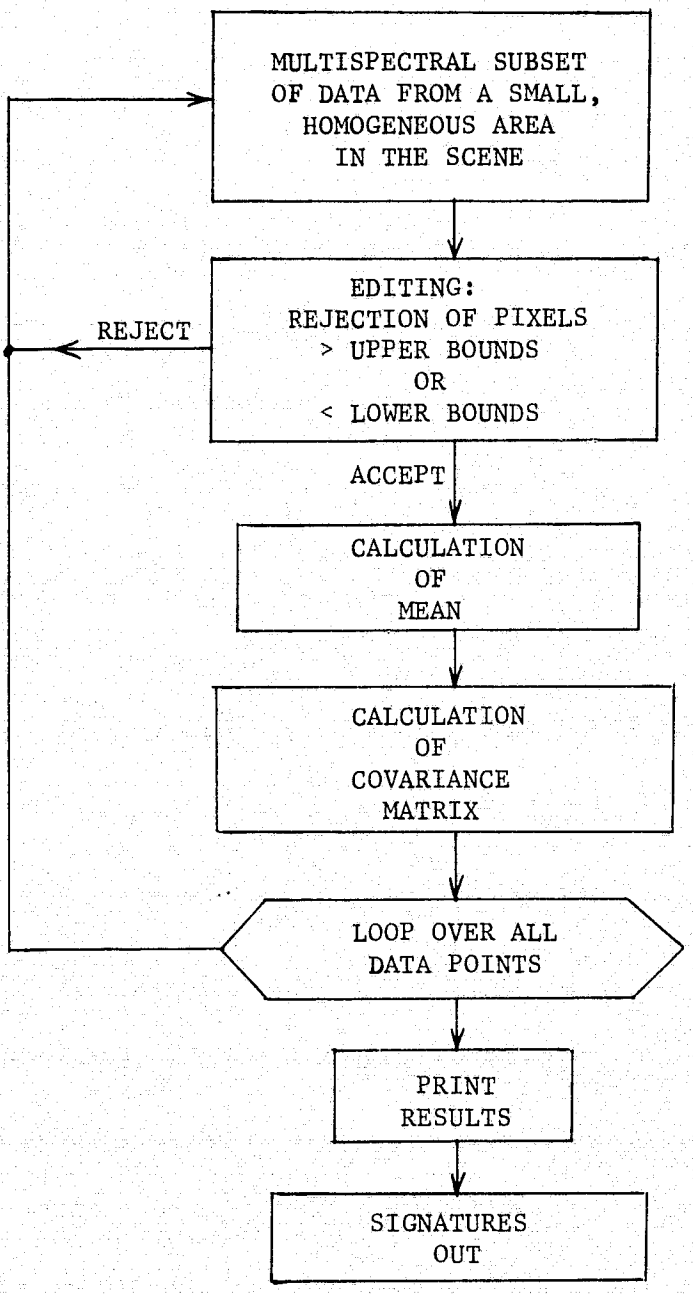

FIGURE IX-2. SIGNATURE EXTRACTION FLOW CHART

for the standard deviation:

$$\sigma(I) = (COV(I,J))^{1/2}$$

and for the correlation:

$$COR.(I,J) = \frac{COV(I,J)}{\sigma_i \sigma_j}$$

The editing procedure is utilized to reject all pixels which are not normal to the distribution (outliers). To do this, the pixels are sorted, the median is calculated, and Q, the average of the quartile deviations, is determined. Then, the upper and lower bounds are determined from the median plus/minus 5.6 times the quartile.

$$\text{edit bounds} = M \pm 5.6\ Q$$

where: M...is the median
Q...is the quartile deviation

In utilizing this procedure, most, if not all, outliers are rejected along with only 0.1% of all good pixels -- assuming a multivariate, normal distribution.

ERIM's simulation classifier (refer to Figure IX.3) computes the expected performance matrix for a given set of signatures and classifier parameters, generating many random pixels for simulation of a scene with classes represented by the signatures. The number of pixels generated for the simulation of each class is generally on the order of a thousand. The matrix gives the probability that pixels from each given distribution, as represented by the signature, will be classified into each given recognition class, based on the best linear decision boundaries between recognition classes. Once boundaries between all pairs of signatures are established, each pixel will then be classified and for the "winning" signature, the exponent value will be calculated.

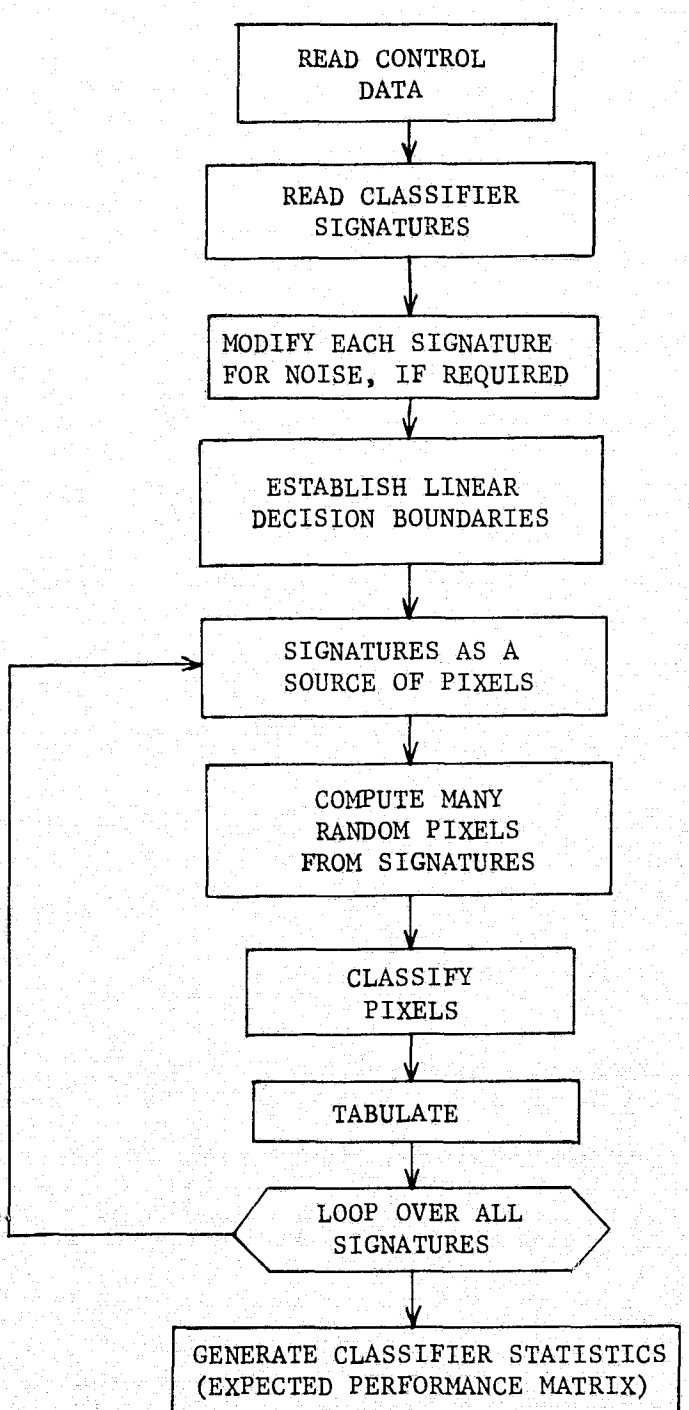

FIGURE IX-3. SIMULATION CLASSIFIER FLOW CHART

If the exponent is less than the specified threshold (based on a level of significance for the chi-square test), the pixel will be tabulated as belonging to the "winning" signature class; otherwise, it will be tabulated as being unclassified.

The production of a random pixel for a given scene class is accomplished as follows: We want a pixel, $\vec{y}$, such that the set of all $\vec{y}$, $\{\vec{y}\}$, is normally distributed with a signature mean, $\vec{b}$, and a covariance, R. First, a vector of random numbers, $\vec{x}$, is produced with each element belonging to a normal distribution, so that, it has a mean equal to zero (0) and a covariance of I (the identity -- that is, the channels are uncorrelated and a variance of unity). The equation

$$\vec{y} = P\vec{x} + \vec{b} \qquad \text{(IX.1)}$$

gives the transformation to $\vec{y}$ from every $\vec{x}$. To arrive at P, by definition, the covariance, R, can be written:

$$R = E\{(\vec{y}-\vec{b})(\vec{y}-\vec{b})^T\} \qquad \text{(IX.2)}$$

where

$E\{\ \}$ denotes the expected value of the enclosed terms

From this we get:

$$R = E\{(Px)(Px)^T\} = E\{Pxx^TP^T\}$$
$$= PP^T$$

By definition, P is the Cholesky decomposition of R. After computing P, each $\vec{y}$ can be calculated from Equation (IX.1).

A subroutine was used with the simulation classifier to modify the individual covariance matrices to allow for noise addition in the radiometric phase of this experiment. This subroutine would take the given matrix and add a vector, representing a specified noise level, to the diagonal elements of that matrix.

The linear classifier (refer to Figure IX.4) is an algorithm whose function is to classify multispectral data using ERIM's "best" linear rule [25]. This classifier utilizes successive applications of a pairwise linear rule which best classifies data from two multivariate, normal distirbutions. Assuming two signatures, H_0 and H_1, from a set of signatures ($H_0 \cdots H_n$) with a mean and covariance matrix of (μ_0,R_0) and (μ_1,R_1) respectively; the decision rule to determine if data pixel x belongs to H_0 is:

$$(x-\mu_o)^T \vec{C} < 1$$

where

C is a vector normal to the hyperplane which is the decision boundary between H_0 and H_1

Otherwise it will be determined to belong to H_1. The winning signature (H_0 or H_1) is then paired with the next signature, H_2, and the decision rule is again implemented. This process continues until all signatures are tested and a final likeliest signature, H_ℓ, is identified. After determining the likeliest signature for x, the null test is employed by calculating the exponent value:

$$E = (\vec{x} - \vec{\mu_\ell})^T (R_\ell)^{-1} (\vec{x} - \vec{\mu_\ell})$$

If this exponent is less than a specified threshold (from the chi-square test), the pixel will be tabulated as belonging to the "winning" signature. Otherwise, it will be tabulated as being "unclassified".

The feature selection (without replacement) algorithm (refer to Figure IX.5) selects the optimum channels according to the probability of misclassification (p.m.) criterion, which is based minimizing the average pairwise linear approximation of the probability of misclassification.

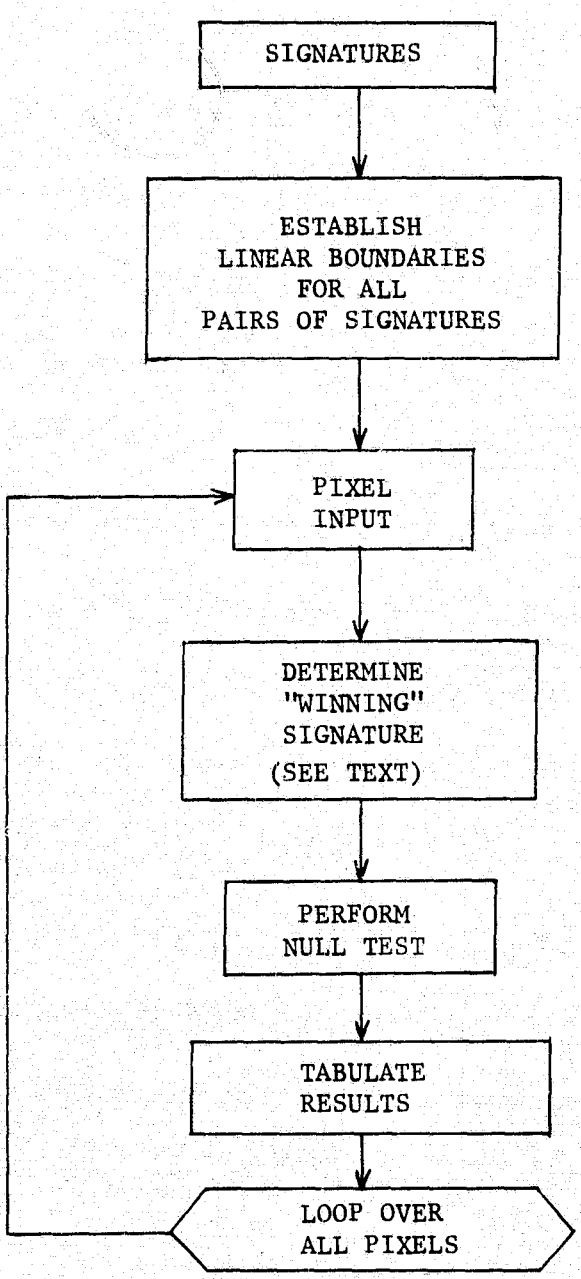

FIGURE IX-4. LINEAR RULE CLASSIFIER FLOW CHART

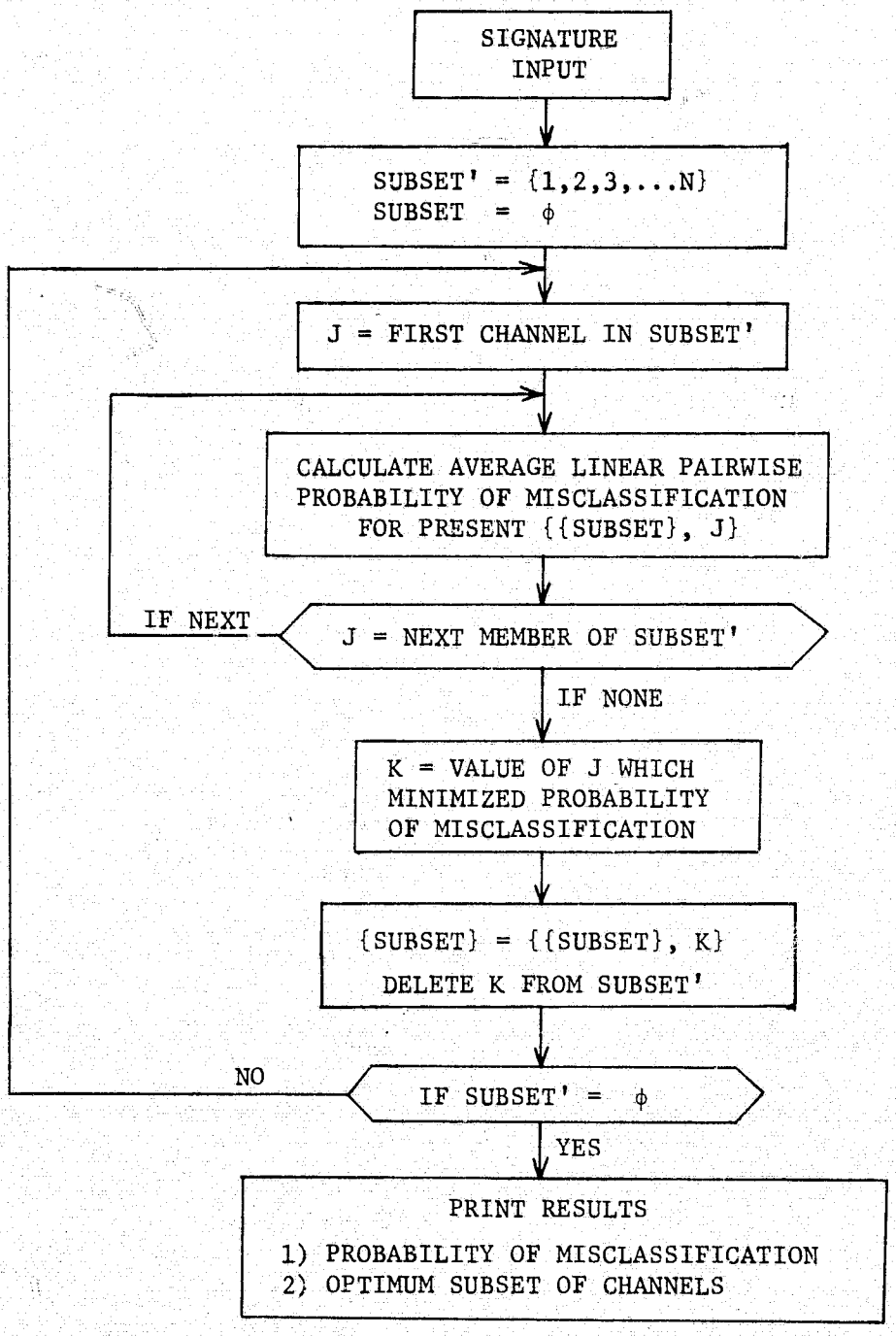

FIGURE IX-5. FEATURE SELECTION (WITHOUT REPLACEMENT) FLOW CHART

Using the p.m. criterion, the best channel is selected out of a set of channels; next, a second channel is selected which along with the first are the two best channels; then, a third best channel is selected which along with the first and second as being the best set of three channels, and so on. The result of this program is a table showing a decrease in the average pairwise p.m. with an increase in the number of channels.

The linear approximation to the p.m. is the p.m. that would be obtained if each covariance matrix of a pair is replaced by the average of the two covariance matrices. The approximate p.m. is computed in the following manner:

$$\text{prob}\{\text{choose sig 2} \mid \text{sig 1}\} = \phi(-D/2)$$

$$\text{prob}\{\text{choose sig 1} \mid \text{sig 2}\} = \phi(-D/2)$$

where

sig · · · is signature

$\phi(x)$ · · · is defined as $\int_{-\infty}^{x} \frac{1}{\sqrt{2\pi}} e^{-t^2/2}\, dt$

$D = (\mu^T R^{-1} \mu)^{1/2}$

R · · · is the average of the two covariance matrices

μ · · · is the second mean minus the first

The feature selection with replacement algorithm (see Figure IX.6) is similar to the above algorithm, except, in choosing the subset of n optimum channels, it tests all possible n-tuples and selects the best set of channels from all possible combinations. This algorithm tends to be more precise in selecting optimum subsets of channels; but, it is a much more lengthy process.

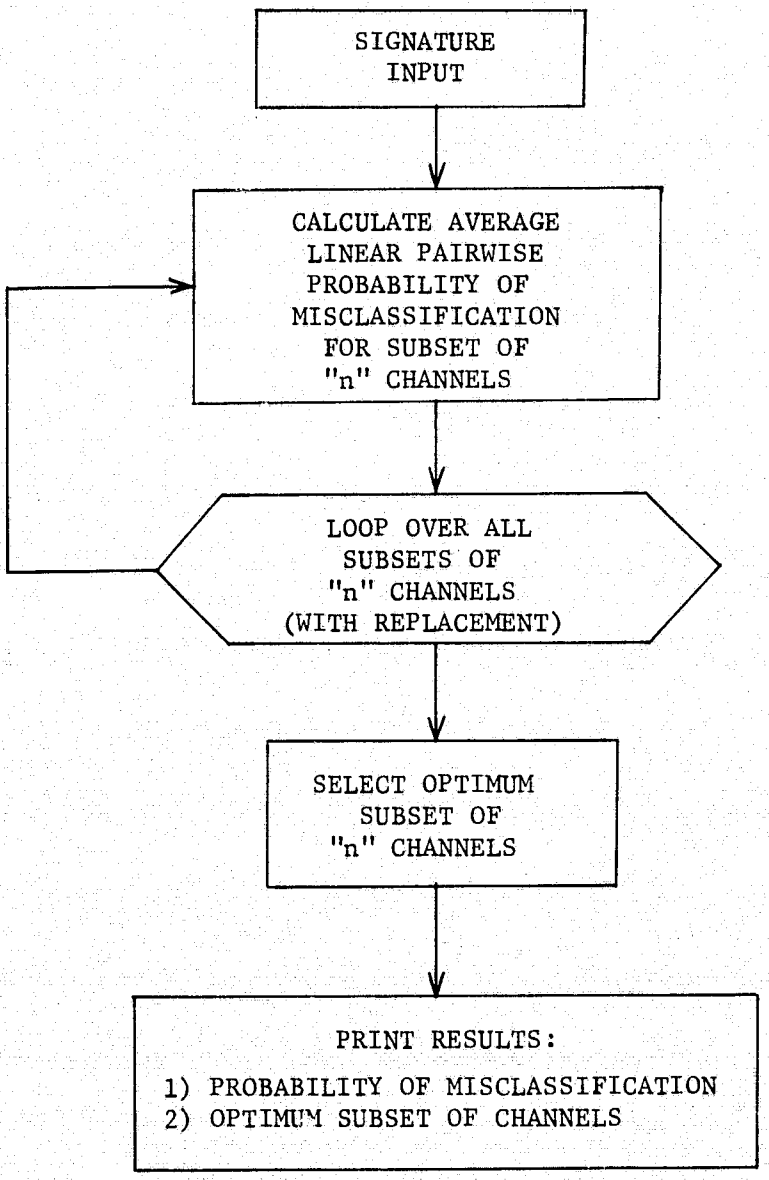

FIGURE IX-6. FEATURE SELECTION (WITH REPLACEMENT) FLOW CHART

REFERENCES

1. F. J. Thomson, J. D. Erickson, R. F. Nalepka, J. D. Weber, Multispectral Scanner Data Applications Study, Volume 1, Report 102800-40-F, Environmental Research Institute of Michigan, Ann Arbor, Michigan, December 1974.

2. Advanced Scanners and Imaging Systems for Earth Observations, NASA/GSFC Report No. NASA SP-335, Washington, D.C., 1973.

3. D. Lowe, J. Cook, et al., Earth Resources Applications of the Synchronous Earth Observatory Satellite (SEOS), Environmental Research Institute of Michigan, Ann Arbor, Michigan, 1973.

4. TERSSE: Total Earth Resources System for the Shuttle Era, (10 volumes) General Electric and Environmental Research Institute of Michigan, NASA Contract NAS9-13401, March 1975.

5. National Aeronautics and Space Administration, Earth Observatory Satellite Payload Discussion Group (EOSPDG), Final Report, Goddard Space Flight Center, Greenbelt, Maryland, 1973.

6. LANDSAT-D Thematic Mapper Technical Working Group, NASA Johnson Space Center, JSC-09797, Houston, Texas, June 1975.

7. TOSS -- TERSSE Operational Systems Study, General Electric, Philadelphia, Pennsylvania, Preliminary Draft.

8. Corn Blight Watch Final Report, Volume III, NASA Johnson Space Center, Houston, Texas, 1973.

9. R. F. Nalepka, J. P. Morgenstern, Signature Extension Techniques Applied to Multispectral Scanner Data, 8th International Symposium on Remote Sensing of Environment, Ann Arbor, October 1972.

10. R. Crane, W. Richardson, Rapid Processing of Multispectral Scanner Data Using Linear Techniques, Remote Sensing of Earth Resources, Vol. I, Selected Papers from Earth Resources Observation and Information Analysis Systems Conference, 13-14 March 1972, May 1972.

11. M. M. Podwysocki, An Estimate of Field Size Distributions for Selected Sites in the Major Grain Producing Countries, NASA/GSFC, Preliminary Draft.

12. P. Hasell, et al, Michigan Experimental Mapping System -- A Description of the M7 Airborne Sensor and Its Performance, Report No. 190900-10-T, Environmental Research Institute of Michigan, Ann Arbor, January 1974.

13. R. F. Nalepka, J. P. Morgenstern and W. L. Brown, Detailed Interpretation and Analysis of Selected Corn Blight Watch Data Sets. Presented at the 4th Annual Earth Resources Program Review, NASA/MSC, Houston, January 17, 1972, and published in Proceedings.

14. G. H. Suits, G. R. Safir, Verification of a Reflectance Model for Mature Corn with Applications to Corn Blight Detection, Remote Sensing of Environment, 2, pp. 183-92, 1972.

15. V. Leeman, D. Earing, R. K. Vincent, S. Ladd, The NASA Earth Resources Spectral Information System: A Data Compilation, The University of Michigan (WRL), Ann Arbor, Report 31650-24-T, May 1971.

16. D. Earing, ed., Target Signatures Analysis Center: Data Compilation, 2nd Supplement, Air Force Avionics Laboratory, Wright-Patterson Air Force Base, Ohio, July 1967.

17. V. Kourganoff, Introduction to the General Theory of Particle Transfer, Gordon and Breach, N. Y., 1969.

18. W. A. Malila, R. B. Crane and R. E. Turner, Information Extraction Techniques for Multispectral Scanner Data, Report No. 31650-74-T, Willow Run Laboratories of the Institute of Science and Technology, The University of Michigan, Ann Arbor, 1972.

19. A. J. LaRocca and R. E. Turner, Atmospheric Transmittance and Radiance: Methods of Calculation, Environmental Research Institute of Michigan, Ann Arbor, Michigan, Report No. 107600-10-T, June 1975.

20. K. L. Coulson, G. M. B. Bouricius, and E. L. Gray, Effects of Surface Reflection on Radiation Emerging from the Top of a Planetary Atmosphere, NASA Contract NAS5-3925, December 1965. Missile and Space Division, General Electric Co.; available from the National Technical Information Service, U.S. Commerce Dept., Springfield, Virginia 22151.

21. R. E. Hufnagel and N. R. Stanley, Modulation Transfer Function Associated with Image Transmission through Turbulent Media, J. Opt. Soc. America 54, 52 (1964).

22. R. M. Bizzell, A. H. Feiveson, F. G. Hall, M. E. Bauer, B. J. Davis, W. A. Malila and D. P. Rice, Crop Identification Technology Assessment for Remote Sensing (CITARS), Volume X, Interpretation of Results, Johnson Space Center, Houston, Texas, Report JSC-09393, December 1975.

23. M. J. Duggan, et al., Factors Controlling the Application in Agriculture of Multi-Channel Remote Sensing Surveys, Proceedings of Fourth Annual Symposium on Remote Sensing of Earth Resources, University of Tennessee, Knoxville, Tennessee, 1975.

24. H. Horwitz, J. Lewis, A. Pentland, Estimating Proportions of Objects from Multispectral Scanner Data, Appendix E, Report 109600-13-F, Environmental Research Institute of Michigan, Ann Arbor, Michigan, May 1975.

25. T. W. Anderson and R. R. Bahadur, Classification into Two Multivariate Normal Distributions With Different Covariance Matrices, Annals of Mathematical Statistics, Vol. 33, 1962, p. 420.